

REPORT DOCUMENTATION PAGE			Form Approved OMB No. 0704-0188	
Public reporting burden for this collection of information is estimated to average 1 hour per response, including the time for reviewing instructions, searching existing data sources, gathering and maintaining the data needed, and completing and reviewing the collection of information. Send comments regarding this burden estimate or any other aspect of this collection of information, including suggestions for reducing this burden, to Washington Headquarters Services, Directorate for Information Operations and Reports, 1215 Jefferson Davis Highway, Suite 1204, Arlington, VA 22202-4302, and to the Office of Management and Budget, Paperwork Reduction Project (0704-0188), Washington, DC 20503.				
1. AGENCY USE ONLY (Leave blank)	2. REPORT DATE 8.Sep.05	3. REPORT TYPE AND DATES COVERED DISSERTATION		
4. TITLE AND SUBTITLE PHAGE-COUPLED PIEZOELECTRIC BIODETECTOR FOR SALMONELLA TYPHIMURIUM.		5. FUNDING NUMBERS		
6. AUTHOR(S) MAJ OLSEN ERIC V				
7. PERFORMING ORGANIZATION NAME(S) AND ADDRESS(ES) AUBURN UNIVERSITY MAIN CAMPUS		8. PERFORMING ORGANIZATION REPORT NUMBER  CI04-1238		
9. SPONSORING/MONITORING AGENCY NAME(S) AND ADDRESS(ES) THE DEPARTMENT OF THE AIR FORCE AFIT/CIA, BLDG 125 2950 P STREET WPAFB OH 45433		10. SPONSORING/MONITORING AGENCY REPORT NUMBER		
11. SUPPLEMENTARY NOTES				
12a. DISTRIBUTION AVAILABILITY STATEMENT Unlimited distribution In Accordance With AFI 35-205/AFIT Sup 1 <b>DISTRIBUTION STATEMENT A</b> Approved for Public Release Distribution Unlimited			12b. DISTRIBUTION CODE	
13. ABSTRACT (Maximum 200 words)				
14. SUBJECT TERMS			15. NUMBER OF PAGES 319	
			16. PRICE CODE	
17. SECURITY CLASSIFICATION OF REPORT	18. SECURITY CLASSIFICATION OF THIS PAGE	19. SECURITY CLASSIFICATION OF ABSTRACT	20. LIMITATION OF ABSTRACT	

**THE VIEWS EXPRESSED IN THIS ARTICLE ARE  
THOSE OF THE AUTHOR AND DO NOT REFLECT  
THE OFFICIAL POLICY OR POSITION OF THE  
UNITED STATES AIR FORCE, DEPARTMENT OF  
DEFENSE, OR THE U.S. GOVERNMENT.**

DISSERTATION ABSTRACT  
PHAGE-COUPLED PIEZOELECTRIC BIODETECTOR FOR *SALMONELLA*  
*TYPHIMURIUM*

Eric Vincent Olsen

Doctor of Philosophy, August 8, 2005  
(M.S., Auburn University, 2000)  
(M.S., University of Southern Mississippi, 1997)  
(B.S.M.T., University of Texas, 1993)  
(A.S., Galveston College, 1989)

319 Typed Pages

Directed by Dr. James Barbaree and Dr. Valery Petrenko

*Salmonella typhimurium* is a leading cause of foodborne illness and a critical threat agent for potential bioterrorism. Current rapid detection initiatives include biosensors that routinely incorporate antibodies for biorecognition. However, antibodies are costly and may degrade under unfavorable environmental conditions. A stable, inexpensive substitute may be filamentous bacteriophage affinity selected from a phage display library for specificity to *S. typhimurium*. We immobilized affinity-selected phage to a quartz crystal microbalance for detection of *S. typhimurium* in solution. An ELISA procedure, precipitation assay, and flow cytometry were employed to confirm phage specificity and selectivity. The phage was up to 22,000 times more specific for *S.*

**DISTRIBUTION STATEMENT A**  
Approved for Public Release  
Distribution Unlimited

iv

20050919 000

*typhimurium* than controls and up to 1,000 times more selective in comparison to other bacteria. For recognition of the phage targeted bacterial outer membrane structure, biotinylated *S. typhimurium* surface proteins from lysate were reacted with phage cross-linked to water-soluble resin to prepare a protein eluate for Western blot, which revealed a single 60-70 kD band. Three immobilization methods (physical adsorption, biotin-streptavidin-phage self-assembly, and Langmuir-Blodgett) using two phage forms (filamentous and phage coat proteins) were evaluated for proof of concept sensor preparation. Specific binding between phage and target on the biosensor resulted in concentration dependent resonance frequency changes. Best results were obtained when  $10^{10} - 10^{11}$  filamentous phage particles converted to spherical forms (spheroids) by chloroform denaturation were immobilized as phage coat proteins using Langmuir-Blodgett technique. The sensors had an average rapid response time of <180 s, lower threshold of  $10 - 10^2$  cells/ml, linear response from  $10 - 10^7$  cells/ml, and a sensitivity of 2 Hz/mV per order of magnitude of bacterial concentration. Fluorescent, optical, and scanning electron microscopy confirmed binding of bacteria to filamentous phage-coated sensors, while transmission electron microscopy verified spheroid-bacteria binding in solution. In summary, filamentous phage selected from a phage library can be used for the preparation of rapid, specific, and selective biodetectors that may ultimately be suitable for continuous food and environmental monitoring devices, diagnostic assays, and biosorbents.



PHAGE-COUPLED PIEZOELECTRIC BIODETECTOR FOR *SALMONELLA*  
*TYPHIMURIUM*

Except where reference is made to the work of others, the work described in this dissertation is my own or was done in collaboration with my advisory committee. This dissertation does not include proprietary or classified information.

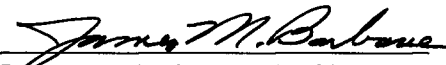


Eric Vincent Olsen

Certificate of Approval:



Valery Petrenko, Co-Chair  
Professor  
Pathobiology



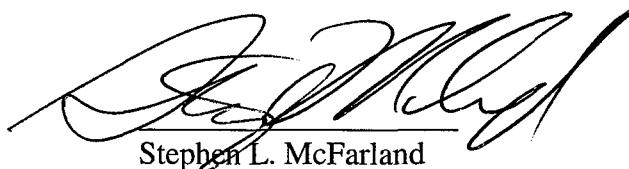
James M. Barbaree, Co-Chair  
Professor  
Biological Sciences



Vitaly Vodyanoy  
Professor  
Anatomy, Physiology and  
Pharmacology



Iryna Sbrokulova  
Visiting Professor  
Anatomy, Physiology and  
Pharmacology



Stephen L. McFarland  
Acting Dean  
Graduate School

PHAGE-COUPLED PIEZOELECTRIC BIODETECTOR FOR *SALMONELLA*  
*TYPHIMURIUM*

Eric Vincent Olsen

A Dissertation  
Submitted to  
the Graduate Faculty of  
Auburn University  
in Partial Fulfillment of the  
Requirements for the  
Degree of  
Doctor of Philosophy

Auburn, Alabama

August 8, 2005

## VITA

Eric Vincent Olsen, [REDACTED], was born [REDACTED] in Juneau, Alaska. Upon graduating from high school in Brandon, Florida in 1981, he enlisted in the United States Coast Guard for six years. In 1989, he completed an Associate of Science at Galveston College, Galveston, Texas. While working for the University of Texas Medical Branch in Galveston, Texas, he completed a Bachelor of Science in Medical Technology in 1993 with highest honors. He was subsequently inducted into The Alpha Eta Honor Society for Healthcare Professionals and listed in Who's Who Among Students in American Universities and Colleges for his scholastic achievements. In 1995, he received a commission in the United States Air Force as a Laboratory Officer in the Biomedical Science Corps and currently holds the rank of Major. He graduated from the University of Southern Mississippi in Long Beach, Mississippi with a Master of Science in Technical and Occupational Education in 1997, and in 1998 was awarded a prestigious Air Force Institute of Technology (AFIT) scholarship to attend Auburn University, where he completed a Master of Science in Microbiology. He was subsequently inducted into Sigma Xi and Phi Kappa Phi honor societies for scholastic achievements. In 2002, he was awarded a second AFIT scholarship to attend Auburn University to complete the Doctor of Philosophy degree in Biological Sciences. He is married [REDACTED]. [REDACTED] has two children, [REDACTED].

DISSERTATION ABSTRACT

PHAGE-COUPLED PIEZOELECTRIC BIODETECTOR FOR *SALMONELLA*  
*TYPHIMURIUM*

Eric Vincent Olsen

Doctor of Philosophy, August 8, 2005  
(M.S., Auburn University, 2000)  
(M.S., University of Southern Mississippi, 1997)  
(B.S.M.T., University of Texas, 1993)  
(A.S., Galveston College, 1989)

319 Typed Pages

Directed by Dr. James Barbaree and Dr. Valery Petrenko

*Salmonella typhimurium* is a leading cause of foodborne illness and a critical threat agent for potential bioterrorism. Current rapid detection initiatives include biosensors that routinely incorporate antibodies for biorecognition. However, antibodies are costly and may degrade under unfavorable environmental conditions. A stable, inexpensive substitute may be filamentous bacteriophage affinity selected from a phage display library for specificity to *S. typhimurium*. We immobilized affinity-selected phage to a quartz crystal microbalance for detection of *S. typhimurium* in solution. An ELISA procedure, precipitation assay, and flow cytometry were employed to confirm phage specificity and selectivity. The phage was up to 22,000 times more specific for *S.*

*typhimurium* than controls and up to 1,000 times more selective in comparison to other bacteria. For recognition of the phage targeted bacterial outer membrane structure, biotinylated *S. typhimurium* surface proteins from lysate were reacted with phage cross-linked to water-soluble resin to prepare a protein eluate for Western blot, which revealed a single 60-70 kD band. Three immobilization methods (physical adsorption, biotin-streptavidin-phage self-assembly, and Langmuir-Blodgett) using two phage forms (filamentous and phage coat proteins) were evaluated for proof of concept sensor preparation. Specific binding between phage and target on the biosensor resulted in concentration dependent resonance frequency changes. Best results were obtained when  $10^{10} - 10^{11}$  filamentous phage particles converted to spherical forms (spheroids) by chloroform denaturation were immobilized as phage coat proteins using Langmuir-Blodgett technique. The sensors had an average rapid response time of <180 s, lower threshold of  $10 - 10^2$  cells/ml, linear response from  $10 - 10^7$  cells/ml, and a sensitivity of 2 Hz/mV per order of magnitude of bacterial concentration. Fluorescent, optical, and scanning electron microscopy confirmed binding of bacteria to filamentous phage-coated sensors, while transmission electron microscopy verified spheroid-bacteria binding in solution. In summary, filamentous phage selected from a phage library can be used for the preparation of rapid, specific, and selective biodetectors that may ultimately be suitable for continuous food and environmental monitoring devices, diagnostic assays, and biosorbents.

## ACKNOWLEDGEMENTS

The author is deeply indebted to his advisory committee: Drs. James Barbaree, Valery Petrenko, Vitaly Vodyanoy, and Iryna Sorokulova – their wisdom, training, patience and encouragement were vital to the conduct and completion of this research. The author wishes to gratefully acknowledge the United States Air Force, which provided the scholarship to attend Auburn University, and would also like to recognize the insightful collaboration, support, and assistance of co-authors: I-Hsuan Chen, Dr. Bryan Chin, Dr. Ben Fiebor, Dr. William Neely, Dr. Suram Pathirana, Dr. Alexandre Samoylov, and Dr. Arnold Vainrub. The author would like to thank Dr. Aleksandr Simonian for serving as outside reader for the dissertation, and the following individuals and groups for their valuable assistance, logistic support, and training in the conduct of this investigation: Dr. Jennifer Brigati, Ludmila Globa, Dr. Galina Kouzmitcheva, Dr. Jane Mount, Nancy Morrison, Natasha Petrenko, Oleg Pustovyy, Alexey Samoylov, Dr. Tatiana Samoylova, Dr. Jennifer Sykora, Dr. Maria Toivio-Kinnucan, Viswaprakash Nanduri, Dr. Tetyana Voloshenyuk, Soloman Yilma, Randy Young-White, Sigma Xi Grants-in-Aid of Research, and the departmental staff of Biological Sciences; Pathobiology; and Anatomy, Physiology and Pharmacology at Auburn University. A special thanks goes out to the author's family for the love, understanding, and support they provided during graduate studies. The author dedicates this work to his greatest supporter and best friend [REDACTED]

Style manual or journals used: MLA Handbook for Writers, Journal of Microbiological Methods.

Computer software used: Adobe® Photoshop® ver. 4.0 and 5.0LE, Kodak 1D software ver. 3.5.3, Microcal™ Origin® ver. 6.0, Microsoft® Office Word 2003, Microsoft® Office Excel 2003, locally developed microscale data acquisition software, Radio Shack Scopeview, SPOT Advanced software ver. 3.5.9.

## TABLE OF CONTENTS

LIST OF TABLES.....	xiii
LIST OF FIGURES.....	xiv
I. INTRODUCTION.....	1
Dissertation organization.....	4
II. REVIEW OF LITERATURE.....	5
Salmonellosis.....	5
<i>Salmonella</i> as a weapon.....	8
<i>Salmonella</i> and poultry processing.....	11
<i>Salmonella</i> detection in poultry.....	14
QCM-based biodetection.....	17
Acoustic wave immunosensors for <i>Salmonella</i> detection.....	20
Bacteriophage – a novel biorecognition component.....	23
III. SPECIFIC AND SELECTIVE BIOSENSOR FOR <i>SALMONELLA</i> <i>TYPHIMURIUM</i> AND ITS DETECTION IN THE ENVIRONMENT.....	29
Abstract.....	29
1. Introduction.....	30
2. Materials and methods.....	32
2.1. Cultures.....	32
2.2. Growth of cultures and preparation of test suspensions.....	32
2.3. Colony forming unit (CFU) determinations.....	33
2.4. Antibodies.....	33
2.5. Acoustic Wave Device (AWD).....	34
2.5.1. Substrate.....	34
2.5.2. Frequency monitor.....	34
2.6. Monolayer preparation.....	35
2.6.1. Surface film balance.....	35



2.6.2. Monolayer formation and deposition.....	35
2.6.2.1. Phospholipid monolayers.....	35
2.6.2.2. Monolayers with immobilized antibodies.....	36
2.7. Bacteria binding measurements.....	36
2.8. Dark-field microscopy.....	37
2.9. Scanning electron microscopy.....	37
2.10. Environmental aging of sensors.....	38
3. Results and discussion.....	39
3.1. Rigid versus flexible positioning of bacteria at the sensor surface.....	39
3.2. Validation of mass measurements of monolayers.....	40
3.3. Specificity and selectivity of bacterial binding.....	40
3.4. Effects of rigid and flexible positioning of bacteria on the apparent mass measured by AWD.....	42
4. Conclusions.....	46
Appendix: Simplified analysis of the thickness-shear mode acoustic resonator.....	48
IV. LANDSCAPE PHAGE PROBES FOR <i>SALMONELLA</i> <i>TYPHIMURIM</i> .....	62
Abstract.....	62
1. Introduction.....	63
2. Materials and methods.....	66
2.1. Organisms.....	66
2.1.1. Bacterial cultures.....	66
2.1.2. Bacterial suspensions.....	67
2.1.3. Starved cells.....	67
2.2. Phage growth, purification, and titering.....	68
2.3. Selection of <i>Salmonella</i> -binding phage clones.....	69
2.3.1. Selection procedure A.....	70
2.3.2. Selection procedure B.....	71
2.3.3. Selection procedure C.....	71
2.4. Confirming specificity of <i>Salmonella</i> -binding phage clones....	72
2.4.1. Phage capture ELISA.....	72
2.4.2. <i>Salmonella</i> capture ELISA.....	73
2.5. Co-precipitation assay to determine phage E2 selectivity.....	74
2.6. Dose-dependent binding of E2 to <i>S. typhimurium</i> .....	75
2.7. Calculations.....	75
2.8. Flow cytometry studies.....	76
2.9. Peptide insert sequence analysis.....	78

2.10. <i>Salmonella</i> interaction with phage adsorbed to Au.....	79
2.11. Fluorescence microscopy.....	80
2.12. Molecular characterization of phage receptor.....	81
2.12.1. Affinity matrix.....	81
2.12.2. <i>S. typhimurium</i> biotinylation.....	81
2.12.3. Cell lysate preparation.....	82
2.12.4. Isolation of phage-targeted bacterial outer membrane receptors.....	82
2.12.5. Eluate analysis.....	82
2.12.5.1. SDS PAGE.....	82
2.12.5.2. Western blot.....	83
2.12.5.3. Protein sequencing.....	84
3. Results.....	84
3.1. Selection of phage clones binding to <i>S. typhimurium</i> .....	84
3.2. Specificity of phage binding to <i>S. typhimurium</i> .....	87
3.3. Selective binding of phage E2 to <i>S. typhimurium</i> .....	88
3.4. Dose-dependent binding of phage E2 to <i>S. typhimurium</i> .....	89
3.5. Molecular characterization of phage receptor.....	91
4. Discussion.....	92
Appendix: Binding equations.....	99
 V. PHAGE-COUPLED PIEZOELECTRIC BIODETECTOR FOR <i>SALMONELLA TYPHIMURIUM</i> .....	 123
Abstract.....	123
1. Introduction.....	124
2. Materials and methods.....	126
2.1. Microorganisms.....	126
2.1.1. Bacteria.....	126
2.1.2. Bacteriophage.....	128
2.2. QCM-based phage biosensor preparation.....	128
2.2.1. Biosensors prepared by physical adsorption.....	129
2.2.1.1. Filamentous phage deposition study.....	129
2.2.1.1.1. Substrate.....	129
2.2.1.1.2. Measurement apparatus.....	130
2.2.1.1.3. Procedure.....	131
2.2.1.1.4. Data analysis.....	132
2.2.1.1.5. Visual confirmation of phage deposition.....	132
2.2.1.2. Biosensor preparation and testing.....	134
2.2.1.2.1. Substrate.....	134
2.2.1.2.2. Preparation.....	134

2.2.1.2.3. Measurement apparatus.....	134
2.2.1.2.4. Assay procedure.....	136
2.2.1.2.5. Biosensor data analysis.....	137
2.2.1.2.6. Fluorescence microscopy.....	138
2.2.1.2.7. Scanning electron microscopy.....	140
2.2.2. Biosensors prepared by biotin-streptavidin-phage self-assembly.....	140
2.2.2.1. Preparation.....	140
2.2.2.2. Assay procedure.....	141
2.2.3. Biosensors prepared by Langmuir-Blodgett method.....	141
2.2.3.1. Spheroid preparation.....	141
2.2.3.2. Spheroids in phospholipid base.....	142
2.2.3.3. Spheroid electrophoresis.....	143
2.2.3.3.1. Timed chloroform exposure studies.....	143
2.2.3.3.2. Phage-chloroform concentration studies.....	144
2.2.3.4. Visualization of spheroids.....	144
2.2.3.5. <i>Salmonella</i> antibodies.....	145
2.2.3.6. Apparatus for $\Pi$ -A isotherm and biosensor preparation.....	145
2.2.3.7. Isotherm procedure.....	146
2.2.3.8. Isotherm data analysis.....	147
2.2.3.9. Phage coat biosensor preparation.....	147
2.2.3.10. Biosensor assay procedure.....	148
3. Results and Discussion.....	149
3.1. Filamentous phage deposition to resonators.....	149
3.2. Evaluation of biosensors.....	153
3.2.1. Biosensors prepared by physical adsorption.....	154
3.2.1.1. Platform evaluation.....	154
3.2.1.2. Biosensor results.....	160
3.2.2. Biosensors prepared by biotin-streptavidin-phage self-assembled layers.....	166
3.2.3. Biosensors prepared with phage coat proteins.....	170
3.2.3.1. Spheroid preparation.....	171
3.2.3.2. Isotherm analysis.....	173
3.2.3.3. Biosensor preparation.....	175
3.2.3.4. Biosensor results.....	176
3.2.4. Biosensors prepared with phage coat proteins in phosphocholine.....	177
3.2.4.1. Biosensor preparation.....	178
3.2.4.2. Biosensor results.....	178
4. Summary and Conclusions.....	179

Appendix: QCM operating as a coupled oscillator for non-uniform mass.....	183
VI. SUMMARY AND CONCLUSIONS.....	251
Summary.....	251
Conclusions.....	255
Future work.....	256
VII. BIBLIOGRAPHY.....	258

## LIST OF TABLES

4.1.	Summary of selection procedures used to affinity select phage probes for <i>S. typhimurium</i> .....	102
4.2.	Summary of biopanning results of f8/8 phage library against <i>S. typhimurium</i> using different selection procedures.....	103
4.3.	Peptide structures of selected phage clones as determined by genomic DNA sequencing.....	104
5.1.	Quantity of filamentous phage physically adsorbed to resonators as a function of time.....	187
5.2.	Platform configuration evaluation.....	188
5.3.	Overall biosensor performance.....	189
5.4.	Analogous parameters between a mechanical spring-mass system and LRC series circuit.....	190
5.5.	Optimal surface pressure corresponding to maximal compressibility modulus of biopolymers at 20 °C.....	191
5.6.	Cumulative deposition of biopolymers onto quartz resonators as a function of transfer ratio (TR) at 20 °C.....	192

## LIST OF FIGURES

3.1.	Scanning electron micrograph of the biosensor surface following exposure to <i>S. typhimurium</i> (arrow). The bacteria were attached to somatic O antibodies deposited by Langmuir-Blodgett method to the gold electrode surface of an unpolished resonator. Filaments holding bacteria at the surface are visible opposite arrow. Magnification, $\times 5000$ ; bar = 5 $\mu\text{m}$ .....	52
3.2.	Dark-field microscopy images of bacteria at the surface of the acoustic wave sensor. The images represent time-lapse frames (100 ms intervals) from continuous real-time video recordings. (A) Rigid attachment of <i>S. typhimurium</i> in PBS to the sensor surface by somatic O antibody. The attached bacteria did not exhibit movement. Bar = 4 $\mu\text{m}$ . (B) Flexible attachment of bacteria to the sensor surface by the flagellar H-type antibody allowed oscillation and rotation of cells at the crystal surface. Sequential photographs (1–9) depict clockwise rotation of bacterium attached to the antibody by its flagellum. Arrows indicate relative direction during rotation.....	53
3.3.	Validation of measuring mass of bound monolayers by acoustic wave sensor. The experimental thickness of multilayer is a linear function of the number of stearic acid monolayers transferred to the sensor surface. The labels “wet multilayer” and “dry multilayer” indicate sensors that were immersed (in buffered solution) and dry, respectively. Straight lines represent linear least squares fit to the data points (Wet: $R = 0.921$ , $p < 0.02$ ; Dry: $R = 0.998$ , $p < 0.0001$ ). Bars are SD.....	54
3.4.	Specificity of <i>Salmonella</i> sensor. Curve (1) is the sigmoidal fit ( $X^2 = 5.9 \times 10^{-5}$ ) to mean values of steady-state sensor voltages as a function of <i>S. typhimurium</i> concentrations ranging from $10^2$ to $10^{10}$ cells/ml. Line (2) is the linear least squares fit ( $R = -0.76$ , slope = $-9.0 \times 10^{-5}$ V/decade) to the dose response of the sensor exposed	

	to <i>S. typhimurium</i> suspensions incubated with <i>Salmonella</i> antibodies prior to the exposure. $1.2 \times 10^9$ cells were incubated with <i>Salmonella</i> antibodies ( $\approx 200 \mu\text{g}$ ) in 1 ml of PBS for 3 h 40 min. Experimental data points were obtained by averaging approximately 200 data points of each steady-state level response curve. Bars are SD.....	55
3.5.	Selectivity of <i>Salmonella</i> sensor. Line (1) is the linear least squares fit ( $R = 0.97$ ) to mean values of steady-state output sensor voltages as a function of <i>S. typhimurium</i> concentrations from $1.8 \times 10^6$ to $10^9$ cells/ml in the presence of $5.6 \times 10^6$ cells/ml of <i>E. coli</i> O157:H7. Line (2) is the linear least squares fit ( $R = -0.71$ ) to dose responses of the sensor exposed to <i>E. coli</i> O157:H7. The voltage output was scaled up by a factor of five. Bars are SD.....	56
3.6.	Dose responses for rigid and flexible positioning of bacteria on biosensor. Graph (A) shows <i>Salmonella</i> and <i>E. coli</i> dose responses to sensor prepared with somatic O <i>Salmonella</i> antibodies. Graph (B) shows <i>Salmonella</i> and <i>E. coli</i> dose responses to sensor fabricated with flagellar H-type <i>E. coli</i> antibodies. Curves are sigmoid fit to experimental data; straight lines are the linear least square fit. Bars are SD.....	57
3.7.	Experimental dose responses of sensor fabricated with somatic O <i>Salmonella</i> antibodies and environmentally aged for six days at $4^\circ\text{C}$ . Curve is a sigmoidal fit to experimental data points, obtained by averaging approximately 200 data points of each steady-state level response curve. Bars are SD.....	58
3.8.	The experimental regression coefficient as a function of sensitivity for environmentally aged <i>Salmonella</i> sensors prepared with somatic O antibodies. The linear portions of dose response signals were fitted by linear regression. Curve is the sigmoidal fit to experimental data points at indicated temperatures.....	59
3.9.	Different positioning of bacteria at the surface of biosensor. (A) The rigid attachment of bacteria by somatic O antibodies. The bacterium moves in unison with the sensor. The electrophoretic force ( $F_e$ ) applied to the electric charges of bacterium ("−") is aligned with the cell body. The piezoelectric force ( $F_p$ ) causes the particle displacement at the surface of TSM sensor. (B) The flexible attachment of bacteria by flagellar H-type antibodies. The bacteria have a high degree of freedom and the displacement of the resonator may be not in phase with the displacement of the bacteria. (C) In aged sensors, a biofilm may cover certain antibody	

(Ab) binding sites and guards against polyvalent attachment of bacteria. As a result, the bound bacteria have a higher degree of freedom than the bacteria with the firm attachment.....	60
3.10. Simplified electrical model of biosensor. (A) Equivalent circuit of TSM resonator (Martin et al., 1991): a capacitance $C_0$ in parallel with resistance $R$ , inductance $L$ , and functional capacitance $C$ . (B) Dose response dependency described by Eq. (13). (C) Plot of the regression coefficient as a function of the sensor's sensitivity.....	61
4.1. Signatone FS 70 high power optical microscope used to confirm phage E2 – <i>S. typhimurium</i> binding on Au coated surfaces.....	105
4.2. <i>S. typhimurium</i> -phage binding specificity as a function of ELISA optical density, for phage chosen during selection procedure "A." (A) Phage capture assay. (B) <i>Salmonella</i> capture assay.....	106
4.3. <i>S. typhimurium</i> -phage binding specificity as a function of ELISA optical density ( <i>Salmonella</i> capture assay), for phage chosen during selection procedure "B" from eluate fraction.....	107
4.4. <i>S. typhimurium</i> -phage binding specificity as a function of ELISA optical density ( <i>Salmonella</i> capture assay) for phage chosen during selection procedure "B" from lysate fraction.....	108
4.5. <i>S. typhimurium</i> -phage binding specificity as a function of ELISA optical density ( <i>Salmonella</i> capture assay) for phage chosen during selection procedure "C" from eluate fraction.....	109
4.6. Selectivity of phage E2 as determined by precipitation assay. Mean yield percentage was averaged from three separate experiments then normalized to the maximal mean yield of 3.4% from <i>S. typhimurium</i> . Values beside bars indicate respective normalized mean yield percentages.....	110
4.7. FACS analysis histogram of fluorescently labeled phage E2 and <i>S. typhimurium</i> , both separately (peaks 1 and 2, respectively) and in complex (3), as a function of fluorescence. Binding of cells with phage falls into a distinct population, exhibiting greater fluorescence than controls ( <i>S. typhimurium</i> and phage alone). The negative threshold (sorting gate) was set at 1 AU on the fluorescence scale.....	111
4.8. Selectivity of phage E2 as determined by FACS. Fluorescence (FITC) percentage is that amount of phage associated cell complexes falling within the positive population for $10^6$	



fluorescent events. The negative threshold-sorting gate was set at 1 arbitrary unit on the fluorescence axis scale. Normalization was applied using the maximal mean fluorescence of 33.3% from <i>S. typhimurium</i> . Values beside bars indicate the respective normalized percentages in arbitrary units.....	112
4.9. Mean values ( $n = 3$ ) of yield plotted as a function of mean phage E2 concentration input with B-spline curve fitted to experimental data points. Bars are SD.....	113
4.10. Concentration-dependent phage E2- <i>S. typhimurium</i> binding isotherm as determined by precipitation-titration assay. Straight line is the linear least squares fit to average number of cells with bound phage as a function of the phage concentration ( $n = 3$ , $R = 0.997$ , slope = $0.695 \pm 0.04$ , $p < 0.001$ ). Smooth line is B-spline curve fit to data points. $K_d = 4.77 \times 10^7$ CFU/ml. $K_{d(\text{apparent})} = 3.18 \times 10^9$ CFU/ml. $V_{\text{max}}$ estimated at $3.1 \times 10^7$ CFU/ml. Bars are SD...	114
4.11. Hill plot of binding isotherm. Ratio of bound and free <i>S. typhimurium</i> is shown as a function of phage (E2) concentration. Line represents the linear least squares fit of experimental data points ( $R = 0.967$ , SD = 0.612, $p < 0.001$ ). The binding valency between cell and phage (Hill coefficient, $n = 0.81$ ), and association binding constant ( $K_b = 2.7 \times 10^{-8}$ CFU/ml), were derived from the plot. Explanation of the Hill plot is provided in appendix A.....	115
4.12. Histogram of titrated phage E2- <i>S. typhimurium</i> binding as a function of fluorescence. Phage, binding cells, in concentrations greater than $10^9$ virions/ml ( $10^7$ CFU) fall into distinct populations, exhibiting greater fluorescence than the control ( <i>S. typhimurium</i> alone – peak 1). Peak 2: $2 \times 10^8$ virions/ml. Peak 3: $2 \times 10^9$ virions/ml. Peak 4: $2 \times 10^{10}$ virions/ml. Peak 5: $2 \times 10^{11}$ virions/ml. The negative threshold (sorting gate) was set at 1 AU on the fluorescence scale.....	116
4.13. Fluorescent microscopy image of Alexa labeled phage clone E2 in-complex with <i>S. typhimurium</i> (magnification 1000× prior to digital capture).....	117
4.14. Interaction of <i>S. typhimurium</i> with phage attached to a gold (Au) surface, as observed by Signatone high power optical microscope. Panel A is a negative control demonstrating few cells attaching to a non-related phage (1F20). Panel B shows larger number of cells binding to select phage clone E2 (magnification 1000× prior to digital capture).....	118

- 4.15. Molecular characterization of phage receptor. Phage clone E2 was crosslinked to water-soluble NHS-dextran polymer to prepare an affinity matrix that could be reacted with a prepared lysate of *S. typhimurium*, the surface of which had been previously labeled with non-permeating biotinylation reagent (B). Following phage-receptor specific binding (C) and washing, any captured bacterial surface receptor proteins were eluted from the crosslinked phage-matrix and separated by SDS-PAGE (D), then electroblotted to nitrocellulose, conjugated with streptavidin-horseradish peroxidase, and visualized by radiography (E). ..... 119
- 4.16. SDS PAGE and Western blot analysis of protein eluate. A single 60 – 70 kD band was revealed by radiography. However, N-terminus protein sequencing of the corresponding area from the gel revealed only a protein sequence corresponding to serum albumin, which was present in the acid elution buffer. Lanes: M, protein ladder; 1, protein eluate from E2 phage; 2, protein eluate from wt f8-5 phage (control); 3, protein eluate from E2..... 120
- 4.17. SDS PAGE and Western blot analysis of protein eluate prepared with and without BSA in elution buffer. Lanes: M, protein ladder; 1, protein eluate from E2 phage w/BSA in buffer; 2, protein eluate from wt f8-5 phage (control) w/BSA in elution buffer; 3, protein eluate from E2 wo/BSA in buffer. All bands from the protein eluate on the gel (Lanes 1,2) are attributed to BSA because no bands are noted on the preparations of eluate without BSA (Lane 3) as a component of the elution buffer. Additionally, no band (Lane 3) is notable that corresponds to that band found on the Western blot (Fig 4.16, right). Possibly, the concentration of protein that represents the targeted receptor is too low for the gel stain to pick up, whereas the sensitivity of the Western blot is very high, allowing even extremely small concentrations to be revealed by radiography..... 121
- 4.18. Schematic of the outer membrane of gram-negative bacteria. (OM) outer membrane. (PEP) peptidoglycan. (CM) cytoplasmic membrane. (P) phospholipid. (LP) lipoprotein. (OMP) outer membrane protein. (POR) porin. (A) lipid A. (LPS) lipopolysaccharide (core polysaccharide and O-antigen). (F) fimbriae or flagella or pili..... 122
- 5.1. Four strategies for immobilizing phage to the gold sensing electrode of piezoelectric resonators. (A) Physical adsorption of whole-virion filamentous phage. (B) Molecular self-assembly of biotinylated filamentous phage by biotin-streptavidin multilayering. (C) Langmuir Blodgett (LB) deposition of

filamentous phage major coat proteins (pVIII) prepared as “skinned phage” from spheroids. (D) LB deposition of filamentous phage proteins prepared as skinned phage from spheroids complexed with phosphocholine.....	193
5.2. Sensor probe and associated components. (1) Housing for external oscillatory circuit electrical contacts. (2) Crystal holder cavity with Kalrez® o-ring (black) installed. The gold Pogo® index pins that contact the reverse electrode of the resonator are clearly visible. (3) Teflon® resonator retainer ring. (4) Threaded retainer ring cover. (5) Polished, 5 MHz AT-cut thickness shear mode quartz resonator exhibiting sensing (obverse) electrode. (6) Contact (reverse) electrode of quartz resonator. The “active area” of the resonator is that central portion of the sensing electrode that overlaps the contact electrode ( $\approx 34.19 \text{ mm}^2$ ).....	194
5.3. QCM platform (1) for deposition and biosensor measurements. Maxtek PM-740 plating monitor (shown) or TM-400 thickness monitor was connected to a sensor probe clamped horizontally to a lattice stand then tilted $10^\circ$ transverse to the stand. The sensor probe and stand were positioned atop a marble slab to reduce extraneous environmental vibrations.....	195
5.4. QCM platform configured for deposition studies. The sensor probe and lattice stand of QCM platform 1 (Fig. 5.3) were enclosed within an inflatable glove chamber filled with nitrogen. The probe’s triaxial cable is connected to the frequency counter (outside) through a sealed port on the left side of the bag. Experiments were manipulated through the bag’s extendable arms and gloves.....	196
5.5. Orientation of the quartz resonator in the crystal holder cavity of the sensor probe, with the sensing electrode exposed and the contact electrode connecting to the Pogo® index pins. The sensor retainer ring and cover are not shown.....	197
5.6. QCM operating in conjunction with fluorescent microscope. Fluorescence microscopy was used to visually confirm phage deposition to the resonator in real-time. Shown is the QCM sensor probe attached to lattice stand for visual inspection of the resonator located directly beneath microscope’s objective.....	198
5.7. QCM platform (2) for sensor measurements. Maxtek PM-740 or TM-400 frequency monitor (not shown) was connected to QCM sensor probe converted to a flow chamber. Syringes (1) were used	

to contain <i>S. typhimurium</i> test suspensions. Stopcocks (2) allowed volumetric manipulation and gravimetric flow of test suspensions from syringes to perfusion manifold (3) via individual lines consisting of small diameter polyethylene tubing. Manifold had central outlet leading to inlet of the flow cell (4). The sensor probe's cavity housing was converted to a flow chamber by replacing the Teflon® crystal retainer ring with a Maxtek FC-550 flow cell, secured by the threaded retainer ring cover. Outlet from flow cell was routed to a waste container (5).....	199
5.8. Cross-sectional view of probe housing (QCM platform 1) with <i>S. typhimurium</i> depicted in aqueous solution above the biosensor. The volume of this solution is 1000 µl. The probe housing, in addition to allowing electrical connection to the sensor's electrodes via contact (pogo) pins, provides mechanical integrity of the probe's oscillatory electronics via an o-ring seal.....	200
5.9. Cross-sectional view of flow cell attached to sensor probe housing (QCM platform 2). Flow direction into the cell, over the sensor, and out of the cell is indicated. The volume of the circular flow chamber, excluding inlet and outlet ports, was approximately 100 µl. The resonator's sensing and contact electrodes, and the electrical connections via contact pins of the oscillatory circuit are shown.....	201
5.10. Testing scheme for biosensors using QCM platform 1. (1) Prepared biosensor was installed into sensor probe then (2) interrogated with a graded series of <i>S. typhimurium</i> test solutions. (3) Frequency (or voltage) output of sensor was recorded for data analysis (4).....	202
5.11. Schematic of KSV 2200 Langmuir-Blodgett film balance system. (1) Teflon® trough containing subphase. (2) Compression barrier. (3) Balance head with platinum Wilhelmy surface balance plate. (4) Film collector unit with holder and crystals attached. (5) AFC unit. (6) DFC unit. (7) Data processing unit. (8) External control keyboard for film control mechanics. (9) Water bath. (10) Marble table. (11) Enclosure. (12) Monolayer film depicted on surface of subphase.....	203
5.12. Monolayer deposition to substrate. (A) Resonators oriented in holder. Resonators are placed back-to-back (obverse sides are exposed) so that 4 sensors can be prepared for each run. Holder attachment to the film collector is not shown. (B) Prior to monolayer formation, resonators are lowered to a position below	

the subphase such that the sensing electrode is fully immersed. Thus, the first layer of spheroids is applied as the resonators rise out of the subphase (Y-type deposition).....	204
5.13. Delivery of spheroids, either alone or in conjunction with phosphocholine (PC), to the surface of the subphase to prepare a Langmuir film of “skinned phage.” Holder attachment to the film collector unit is not shown.....	205
5.14. Representative line graph depicting frequency change as a function of phage adherence to the resonator over time. Eighteen-hour incubation period is shown. $f_S$ : Application of phage solution to clean, dry resonator at steady state: 5,012,338 Hz. $f_R$ : Removal of phage solution, washing, and drying of resonator. $f_E$ : Dried resonator at steady state: 5,012,177 Hz. $\Delta f = (f_S) - (f_E) = -161$ Hz.....	206
5.15. Representative line graph of a clean resonator with degassed water only (control) depicting frequency change as a function of time. One-hour incubation period is shown. $f_S$ : Application of phage solution to clean, dry resonator at steady state: 5,000,167 Hz. $f_R$ : Removal of water and drying of resonator. $f_E$ : Dried resonator at steady state: 5,000,167 Hz. $\Delta f = (f_S) - (f_E) = 0$ Hz.....	207
5.16. Conglomerate data from timed deposition studies. Fitted sigmoidal curve indicates a strong relationship ( $R^2 = 0.963$ ) between time and frequency change as a result of phage binding to resonators. Bars are SD.....	208
5.17. Magnified ( $\times 1000$ ) view of a clean resonator (control) operating in real-time, as viewed by fluorescent microscopy. This scope had a short working-distance, high-numerical-aperture 100X high-dry objective allowing non-invasive visualization of phage binding to the resonator’s sensing electrode; cf. Figs. 5.18 and 5.19. The arrow indicates the edge of the sensing electrode.....	209
5.18. Magnified view ( $\times 1000$ ) of same resonator from Fig. 5.17 under operational conditions following the addition of fluorescently labeled filamentous phage E2. The arrows indicate the edge of the sensing electrode. Large bundles of phage floating in suspension are evident.....	210
5.19. Magnified view ( $\times 1000$ ) of same resonator from Fig. 5.18 following phage deposition for 1 h and washing with PBS. The	

field of view encompasses the active area of the sensing electrode. The size differential of phage bundles is easily discernable.....	211
5.20. Representative line graph of a resonator previously adsorbed with filamentous phage for 18 hours then washed ( $f_s$ : 4,999,973 Hz) five times with degassed water and dried ( $f_E$ : 4,999,973 Hz). $\Delta f =$ ( $f_s$ ) – ( $f_E$ ) = 0 Hz, indicating no loss of phage from active area of the sensing electrode.....	212
5.21. Representative line graph of a resonator previously adsorbed with filamentous phage then washed and incubated with degassed water ( $f_s$ : 4,999,077 Hz) for 55 hours ( $f_E$ : 4,999,077 Hz). $\Delta f = (f_s) - (f_E)$ = 0 Hz, indicating no loss of phage from active area of the sensing electrode.....	213
5.22. Viscosity analysis using platform 2. (A) Differential frequency responses of a clean resonator to increasing concentrations of glycerol as a function of time. The resonator failed when a 90% solution of glycerol was assayed. (B) Dose-response relation of mean values ( $n = 450 \pm 4$ ) of steady-state frequency responses as a function of glycerol concentration. Fitted curve (1) is nonlinear sigmoidal fit of Boltzmann equation to experimental data points ( $R^2 = 0.995$ ). Bars are SD. Non-fitted curve (2) is B-spline fit to theory.....	214
5.23. Viscosity analysis using platform 1. (A) Frequency responses of clean QCR to differing concentrations of glycerol as a function of time. The resonator failed when a 90% solution of glycerol was assayed. (B) Dose-response relation of mean values ( $n = 954$ ) of steady-state voltage responses as a function of glycerol concentration. Fitted curve (1) is nonlinear sigmoidal fit of Boltzmann equation to experimental data points ( $R^2 = 0.999$ ). Bars are SD. Non-fitted curve (2) is B-spline fit to theory.....	215
5.24. Viscosity analysis and non-specific binding determination of <i>S.</i> <i>typhimurium</i> using platform 2. (A) Voltage responses of clean resonator to increasing concentrations of <i>S. typhimurium</i> as a function of time. (B) Dose-response relation of mean values ( $n =$ 431) of steady-state output sensor voltages as a function of <i>S.</i> <i>typhimurium</i> concentration. Bars are SD. Line is linear least squares fit to experimental data points ( $R = -0.61$ , slope = $-0.09$ mV, $p < 0.05$ ).....	216
5.25. Viscosity analysis and non-specific binding determination of <i>S.</i> <i>typhimurium</i> using platform 1. (A) Voltage responses of clean	

resonator to differing concentrations of <i>S. typhimurium</i> as a function of time. (B) Dose-response relation of mean values ( $n = 220$ ) of steady-state output sensor voltages as a function of <i>S. typhimurium</i> concentration. Bars are SD. Line is linear fit least squares fit to experimental data points ( $R = 0.08$ , slope = 0.25 mV)	217
5.26. Noise determination of platform 2. (A) Frequency responses of prepared phage biosensor assayed with PBS (all infusions are 1X concentration) as a function of time. (B) Dose response relation of the mean values ( $n = 1552 \pm 2$ ) of steady-state output sensor frequencies as a function of consecutive PBS infusions to the flow cell. Bars are SD = 0.3 – 2.1 Hz. Line is linear least squares fit to experimental data ( $R = 0.25$ , slope = 0.12 Hz).....	218
5.27. Noise determination of platform 1. (A) Frequency responses of prepared phage biosensor assayed with PBS as a function of time. (B) Dose response relation of the mean values ( $n = 1500$ ) of steady-state output sensor frequencies as a function of consecutive PBS solutions. Bars are SD = 2.9 – 10.1 Hz. Line is linear least squares fit to experimental data ( $R = -0.12$ , slope = -0.29 Hz).....	219
5.28. (A) Frequency responses of phage biosensor to differing concentrations of <i>S. typhimurium</i> as a function of time, using platform 2. (B) Dose-response relation of the mean values ( $n = 2800 \pm 2$ ) of steady-state output sensor frequencies as a function of <i>S. typhimurium</i> concentration. Bars are SD = 2.9 – 10.0 Hz. Curve is linear least squares fit to experimental data ( $R = -0.98$ , slope = -10.9 Hz, $p < 0.001$ ).....	220
5.29. Experimental correlation coefficient as a function of sensitivity for 12 filamentous phage (FPI) biosensors prepared by physical adsorption and assayed with <i>S. typhimurium</i> using platform 2. Correlation coefficients, $R$ , were derived from the linear fit to dose-response signals for each tested sensor; sensitivities, $S$ , from the slope of the linear fit. Curve is nonlinear sigmoidal fit of Boltzmann equation to experimental data points ( $R^2 = 0.80$ ).....	221
5.30. Experimental correlation coefficient as a function of sensitivity for 37 filamentous phage (FPI) biosensors prepared by physical adsorption and assayed with <i>S. typhimurium</i> using platform 1. Correlation coefficients, $R$ , were derived from the linear fit to dose-response signals for each tested sensor; sensitivities, $S$ , from the slope of the linear fit. Curve is nonlinear sigmoidal fit of Boltzmann equation to experimental data points ( $R^2 = 0.94$ ). Four of 37 sensors (11%) fit the acceptable performance criteria ( $R \geq$	

0.90 and sensitivity greater than 1 Hz/decade bacteria concentration).....	222
5.31. Experimental correlation coefficient as a function of sensitivity for 59 biosensors (Sab) prepared from <i>Salmonella</i> antibodies (Sab) immobilized by Langmuir Blodgett method. Correlation coefficients, $R$ , were derived from the linear fit to dose-response signals for each tested sensor; sensitivities, $S$ , were derived from the slope of the linear fit. Curve is nonlinear sigmoidal fit of Boltzmann equation to experimental data points ( $R^2 = 0.96$ ). Fifty-three of 59 sensors (90%) fit the acceptable performance criteria ( $R \geq 0.90$ and sensitivity greater than 8 mV/decade bacterial concentration).....	223
5.32. Mechanical models of analyte-resonator interaction as composite and coupled oscillators (cf. Fig. 5.58). (1) Reproduction of coupled oscillator model of Dybwad (1985, Fig. 2.) depicting quartz resonator (QR) as one mass ( $M$ ) spring ( $K$ ) system, and a loosely attached particle ( $p$ ) as a second mass ( $m$ ) spring ( $k$ ) system. Attachment of the loose particle causes QR to oscillate at a new, higher frequency when $k < K$ . When $k = K$ , a composite system is formed that produces expected mass loading effect with corresponding frequency decrease. (2) Corresponding model of Olsen et al. (2003, Fig. 9) that shows bacterial binding positions at the solid/liquid interface of the quartz resonator. When binding is firm between bacteria and receptor (left), the natural frequency of the cell as an independent mass-spring system equals the frequency of the resonator, forming a composite unit that produces expected mass loading effect with corresponding frequency decrease. When binding is loose between analyte and receptor (center and right), a coupled oscillator is formed whose frequency is dictated by the difference in the spring constants between the oscillator and bacteria.....	224
5.33. Fluorescent microscopy image of <i>S. typhimurium</i> attached to the surface of a resonator previously coated with filamentous phage by physical adsorption. Numerous bacteria were visible; some were rigidly attached while others demonstrated flexible movement. The majority of bacteria demonstrated rigidly attached flagella (arrows). The pair of bacteria enclosed within the white circle is displayed in movement in Fig. 5.34. Magnification, $\times 1000$ .....	225
5.34. Fluorescent microscopy images of two <i>S. typhimurium</i> cells attached to the surface of a QCM resonator coated with	



filamentous phage under operational conditions. Images are consecutive still frames (1 s intervals, top left to bottom right) showing two bacterium: one is rigidly attached to the sensor via phage (left) while the other (right) is flexibly attached, allowing oscillation and random directional movement (arrows) of the cell at the resonator surface. Magnification, $\times 1000$ .....	226
5.35. Real-time observation of <i>S. typhimurium</i> attaching to QCM resonator (arrow) previously coated with filamentous phage by physical adsorption. Sequential fluorescent still frames (1 s intervals, top left to bottom right) show a bacterium rigidly attaching out of suspension. No further movement followed attachment. Flagella are evident and firmly “plastered” down to the surface of the sensor. Magnification, $\times 1000$ .....	227
5.36 Scanning electron micrograph demonstrating <i>S. typhimurium</i> binding to phage immobilized to the surface of a sensor by physical adsorption; cf. Fig. 5.37. Magnification, $\times 3000$ ; bar = 5 $\mu\text{m}$ .....	228
5.37 Scanning electron micrograph depicting a sensor prepared with phage by physical adsorption. Acting as a control, the sensor was not exposed to <i>S. typhimurium</i> . The smooth surface is indicative of a polished resonator (cf. Fig. 3.1) and phage resolution was not possible. Magnification, $\times 1000$ ; bar = 10 $\mu\text{m}$ .....	229
5.38. Experimental correlation coefficient as a function of sensitivity for 20 FPB <i>S. typhimurium</i> biosensors prepared from biotinylated filamentous phage adsorbed to streptavidin activated resonators. Correlation coefficients, $R$ , were derived from the linear fit to dose-response signals for each tested sensor; sensitivities, $S$ , were derived from the slope of the linear fit. Curve is nonlinear sigmoidal fit of Boltzmann equation to experimental data points ( $R^2 = 0.98$ ). Eighteen of 20 sensors fall into two groupings shown in ovals (A) and (B), while 2 sensors are indifferent. Overall, 9 of 20 sensors (45%) fit the acceptable performance criteria ( $R \geq 0.90$ and $S \geq 2$ mV/decade bacteria concentration).....	230
5.39. Numerous <i>S. typhimurium</i> exhibiting flagella are clearly visible (arrows) in the foreground. Immobilized phage can be discerned in the background (cf. Figs. 5.17 and 5.19).....	231
5.40. Dose-response relation of the mean values ( $n = 300$ ) of steady-state output sensor frequencies for a FPB fluorescent sensor as a function of <i>S. typhimurium</i> concentration. Curve is nonlinear	

sigmoidal fit of Boltzmann equation to experimental data points ( $R^2=0.98$ ). Bars are SD. $V_{\max} \approx 10^7$ cells/ml.....	232
5.41. Phage morphology induced by chloroform denaturation. Chloroform denaturation at room temperature contracts filamentous phage (A) to an intermediate (I) form (B), I-spheroid form (C) with subsequent DNA extrusion, and finally a spherical particle (spheroid) (D); cf. Figs. 5.43 and 5.44.....	233
5.42. Agarose (0.8%) gel electrophoresis analysis of spheroids as a function of chloroform exposure time and filamentous phage concentration. Lanes: M, <i>BstE</i> II $\lambda$ DNA ladder; 1 – 3: 1 min vortex, 4 – 7: 3 min vortex; 1 and 4: neat phage; 2 and 5: 3 $\times$ dilution of neat phage; 3 and 6: 6 $\times$ dilution of neat phage. 7: solvent-phage interface from prep 1 (lane 1).....	234
5.43. Transmission electron micrograph of chloroform denatured filamentous phage E2. Examples of both I-forms (I) and spheroids (S) are evident following preparation at room temperature. Magnification, $\times 195,300$ ; bar = 100 nm.....	235
5.44. Transmission electron micrograph of chloroform denatured filamentous phage E2. Filamentous phage (F), I-forms (I) and spheroids (S) are evident, as is spheroid DNA extrusion (D) in agreement with the finding of Manning et al., (1981). Magnification, $\times 123,800$ ; bar = 100 nm.....	236
5.45. Agarose (0.8%) gel analysis of spheroid conversion as a function of filamentous phage concentration. All vortex times 1 min. Lanes: M, <i>BstE</i> II $\lambda$ DNA ladder; 2: neat phage E2 (not subjected to chloroform); 3: 3 $\times$ dilution of neat phage; 4: 9 $\times$ dilution of neat phage; 5: 27 $\times$ dilution of neat phage; 6: 81 $\times$ dilution of neat phage; 7: 243 $\times$ dilution of neat phage.....	237
5.46. Transmission electron micrograph of chloroform denatured filamentous phage E2. Phage bundles, as well as spheroids, are apparent in the interface phase between the solvent (chloroform) and aqueous phase that the phage is diluted in. This photo corresponds to Fig. 5.42, lane 7 - bands "A" and "B." No spheroids were noted in the aqueous phase of this sample (Lane 1, Fig. 5.42). Magnification, $\times 30,300$ ; bar = 1 $\mu$ m.....	238
5.47. (A) Schematic of $\Pi$ -A isotherm showing Gaseous (G), Liquid (L), and Solid (S) phases of "skinned phage." Depending upon the	

amphiphile, one or more liquid states ( $L_1$ , $L_2$ ) may exist. (B) Orientation of monolayer in the different phases.....	239
5.48. $\Pi$ -A isotherms of biopolymers as a function of compression at 20 °C. 1: <i>Salmonella</i> polyvalent O antibodies. 2: E2 spheroids. 3: E2 spheroids-PC. 4: Arachidic acid, courtesy Mark Hartell (Olsen, 2000). ....	240
5.49. Elasticity of monolayers as a function of surface pressure at 20 °C. 1: <i>Salmonella</i> polyvalent O antibodies. 2: E2 spheroids. 3: E2 spheroids-PC. 4: Arachidic acid, courtesy Mark Hartell (Olsen, 2000).....	241
5.50. Y-type deposition of a floating monolayer onto a hydrophilic substrate as described by Gaines (1966). Pure monolayers were prepared from either spheroids (right) or spheroids in phosphocholine (left) and are shown on either side of the substrate for illustrative purposes only (cf. Figs. 5.1 and 5.13).....	242
5.51. Cumulative deposition of biopolymers onto quartz resonators as a function of transfer ratio at 20 °C. 1: <i>Salmonella</i> antibodies (Denka Seiken Co., LTD, Tokyo Japan). 2: Spheroids. 3: Spheroids-PC. 4: Arachidic acid, pH corrected to 10.0. Cumulative TR is shown numerically above curves for each respective material.....	243
5.52. Experimental correlation coefficient as a function of sensitivity for 15 <i>Salmonella</i> biosensors prepared with spheroids using LB method. Correlation coefficients, $R$ , were derived from the linear fit to dose-response signals for each tested sensor; sensitivities, $S$ , from the slope of the linear fit. Curve is nonlinear sigmoidal fit of Boltzmann equation to experimental data points ( $R^2 = 0.96$ ). Only 3 of 15 sensors (20%) fit the acceptable performance criteria ( $R \geq 0.90$ and $S \geq 2.5$ mV/decade bacteria concentration).....	244
5.53. Transmission electron micrograph of <i>S. typhimurium</i> interacting with spheroids in aqueous solution. Cells appear to be “cemented” together by spheroids that are visible between adjoining cells. Flagella are also readily apparent. Magnification, $\times 41,300$ ; bar = $1\mu\text{m}$ .....	245
5.54. Transmission electron micrograph of <i>S. typhimurium</i> interacting with spheroids in aqueous solution. Cells appear to be “cemented” together by spheroids that are visibly apparent between adjoining	

cells. I-forms are also readily apparent. Magnification, $\times 93,500$ ; bar = 100 nm.....	246
5.55. Transmission electron micrograph of <i>S. typhimurium</i> interacting with spheroids in aqueous solution. Cells appear to be "cemented" together by spheroids that are visible between adjoining cells. I- forms and flagella are also readily apparent. Magnification, $\times$ 68,800; bar = 1 $\mu$ m. (100 nm = 4.13 cm).....	247
5.56. Experimental correlation coefficient as a function of sensitivity for 24 biosensors prepared with spheroids in PC using LB method. Correlation coefficients, $R$ , were derived from the linear fit to dose-response signals for each tested sensor; sensitivities, $S$ , were derived from the slope of the linear fit. Overall, 15 of 24 sensors (63%) fit the acceptable performance criteria ( $R \geq 0.90$ and $S \geq 2.5$ mV/decade bacteria concentration).....	248
5.57. (A) Amino acid sequence of the pVIII protein of phage clone E2. The peptide insert displayed at the N-terminus is underlined. The hydrophobic region is italicized. Roughly half of the residues are exposed to the solvent, while the other half is buried within the capsid, where C-terminal residues interact with the phage DNA. (B) Hypothetical orientation and interaction of the rod-shaped pVIII protein with phospholipids as a result of phage skinning method. Following rupture of spheroids at the subphase surface in conjunction with phospholipids, the positively charged, basic amino acids of the C-terminus (bolded) may interact with negatively charged phosphate groups, resulting in a well-organized monolayer structure that facilitates the dynamic properties of the protein as a probe following deposition to substrates.....	249
5.58. Externally driven, liquid-damped ( $\Gamma$ , $\gamma$ ), one-dimensional couple harmonic oscillator model with two different masses: bacteria of mass, $m$ , and spring constant, $k$ , attached to resonator of mass, $M$ , and spring constant, $K$ . Points "0" and "a" represent respective stable equilibrium points of resonator and bacteria along a one- dimensional line $\chi$ .....	250

## CHAPTER I

### INTRODUCTION

The consumption of food products tainted with pathogenic agents results in millions of illnesses, hospitalizations, and deaths annually worldwide while extracting a large financial toll ranging in the billions of dollars. Salmonellosis remains a leading etiology of foodborne illness and death, with *Salmonella enterica* serovar Typhimurium (*S. typhimurium*) causing a majority of reported cases. While salmonellosis is largely an inadvertent malady contracted through poor food sanitation practices, confirmation of biological weapons programs aimed at Americans by terrorist states has compelled the United States Government to also categorize *Salmonella* as a food safety threat agent. Food processing, transit, and centralized distribution are highly vulnerable to bioterrorism. Several large, unintentional outbreaks involving *Salmonella* aptly serve to illustrate what a deliberate attack by terrorists might entail, with thousands incurring illness and possibly death.

Next to prevention, a key challenge to food safety will always be our ability to predict how, when, or where an outbreak may occur. According to federal standards, conventional identification of *S. typhimurium* at food processing plants is based on traditional cell culture using differential and selective media. However, these methods

may require several days in order to definitively identify *S. typhimurium* in consumables. During this period, larger processing plants may have unintentionally distributed *Salmonella*-contaminated products to points of sale before the problem is realized, leaving consumers susceptible to exposure. As well, if a food product has been deliberately adulterated after processing, there is no current practice in place to detect the contamination prior to consumption. The United States Department of Agriculture, Food and Drug Administration, Centers for Disease Control and Prevention, and World Health Organization have all acknowledged the need for greater safety and security of our nation's food and water supplies from pathogen contamination, both inadvertent and deliberate, and have renewed the call for commercially deployable, real-time threat agent detectors for consumables to replace traditional methods of food safety analysis that are slower, labor-intensive, costly, and confined to the product's point of origin.

A review of next-generation, miniaturized biosensor assays for food safety reveals that sensors combining reliability, speed and portability, while reducing sample size and assay costs, are being heavily researched. Mass-sensitive acoustic wave transducers such as the quartz crystal microbalance (QCM) that incorporates a selective, high-affinity biorecognition agent appear to be particularly suitable for biological analysis. Any sample coupling between the receptor and its complementary analyte is converted to a signal output that can be amplified and processed to provide specific, sensitive qualitative or quantitative measurement of analyte-receptor interaction, regardless of how the pathogen was introduced. To date, the vast majority of QCM-based biosensors developed for the detection of *Salmonella* utilize antibodies as the high-affinity receptor. Although sensitive and specific, antibodies can possess numerous disadvantages,

including cost of production, availability, fragility, reusability, and the need for laborious immobilization methods to sensor substrates. These qualities make them an insubstantial biological recognition component for use on commercially viable detectors for food safety and security. Therefore, a high-affinity receptor capable of addressing these drawbacks is needed.

The use of phage display to prepare phage-derived probes to overcome the weak points of antibodies has been recently described (Petrenko and Vodyanoy, 2003). The Ff class of filamentous bacteriophage can tolerate the incorporation of foreign DNA through recombinant modification – expressing it as foreign peptides on the surface of the virion for presentation to a complementary target, such as cell receptors on the outer membrane of *Salmonella*. In this way phage-derived probes can act as antibody substitutes, possessing distinct advantages over their natural counterparts including durability, reusability, stability, standardization and low-cost production, while achieving equivalent specificity and sensitivity.

Numerous phage applications have been proposed, including the detection of bacteria (Petrenko and Sorokulova, 2004). However, phage-based QCM affinity detection systems for bacteria have not been described in the literature. Petrenko and Vodyanoy (2003) discussed the potential of phage in conjunction with the QCM for the detection of threat agents. Accordingly, this dissertation describes proof-in-concept development of a biosensor for the rapid, sensitive, specific detection of *S. typhimurium*, based on a novel biorecognition layer of affinity-selected bacteriophage immobilized to a piezoelectric transducer platform as an alternative to antibody-based QCM biosensors.

## *Dissertation organization*

The dissertation is organized as follows: Chapter 1 introduces the background and purpose of the research. Chapter 2 is a comprehensive review of all background knowledge and circumstances pertinent to the subject of the dissertation, followed by research objectives and aims. Chapter 3 describes the preparation and testing of QCM-based antibody biosensors for the detection of *S. typhimurium* both under aqueous conditions and following environmental aging, and provides simplified analysis of the thickness-shear mode acoustic resonator at the solid/liquid interface. Chapter 4 details the derivation of phage clones preferential to *S. typhimurium* for use as probes, and provides quantitative interpretation of phage-cell complex formation. Chapter 5 describes proof-in-concept preparation and testing of QCM-based phage biosensors as rapid, sensitive detectors of *S. typhimurium* under aqueous conditions, and provides quantitative modeling of phage-cell binding as a coupled horizontal harmonic oscillator. Chapter 6 presents an overall summary and conclusions of the research and proposed future work. Chapter 7 chronicles the dissertation references in a cumulative bibliography.



## CHAPTER II

### REVIEW OF LITERATURE

#### *Salmonellosis*

The consumption of food products tainted with pathogenic agents such as bacteria, viruses, parasites, and biological toxins results in over three million deaths annually worldwide (Foodborne Diseases, 1997). Foodborne illness has been noted as our nation's most significant food safety issue (Program summary, program rational, 2001), with cases ranging upwards to 76 million annually, including more than 323,000 hospitalizations and 5,000 associated deaths (Mead et al., 1999). Related costs are estimated at \$6.5 – \$34.9 billion annually (Buzby and Roberts, 1997), reflecting a substantial economic drain on individuals, businesses, health care systems, and entire communities.

While more than 200 diseases are transmitted through food products (Bryan, 1982), salmonellosis remains a leading etiology in the U.S. with a yearly estimate of 1.3 million cases and 15,000 hospitalizations (Mead et al., 1999). *Salmonella* was the leading cause of gastroenteritis in 2003 among all foodborne pathogens under surveillance by the Centers for Disease Control and Prevention (CDC) (Preliminary

foodnet data, 2003). *Salmonella* has been consistently responsible for more foodborne fatalities than any other organism, with greater than 500 deaths occurring annually (Mead et al., 1999). *Salmonella enterica* serovars Typhimurium and Enteritidis are most commonly isolated, with *S. typhimurium* causing the majority (14%) of all laboratory-diagnosed cases of foodborne salmonellosis in 2003 (Preliminary foodnet data, 2003).

*S. typhimurium* is a non-sporeforming, chemoorganotrophic, facultative anaerobe that colonizes the gastrointestinal tract of domestic animals, with poultry, cattle, and pigs being the most highly contaminated. Consequently, *S. typhimurium* can be isolated as a fecal contaminant from a variety of foods including eggs, dairy products, ground beef, vegetables, seafood, and most notably poultry. Salmonellosis is also infrequently associated with the handling of pets, reptiles, and contaminated water.

When isolated from humans, *Salmonella* is almost always pathologically associated. Salmonellosis normally transpires via fecal to oral route. As described by Salyers and Whitt (2002), the disease process occurs between 6 and 24 h post-ingestion of  $\approx 10^5$  organisms<sup>1</sup>. The bacteria resist the acidic conditions of the stomach to pass through and into the small intestine and distal colon, where data suggests the infection of mucosal cells and/or M cells occurs. Here, the bacteria multiply within local macrophages, injecting proteins into neighboring intestinal cells via their Type III secretion systems. Metabolic disruption of the cells ensues with a subsequent release of cytokines that attract polymorphonuclear leukocytes (PMN). PMN in turn release prostaglandins that increase cAMP levels in the intestinal cells. Increased adenylate

---

<sup>1</sup>From Kothary and Babu (2001). However, quantities reported in the literature range from  $10^3$  to  $10^6$  organisms—the difference attributed to factors such as age, gastric acidity, inoculum, and immune system abnormalities.

cyclase inhibits the uptake of  $\text{Na}^+$  while increasing secretion of  $\text{Cl}^-$ , resulting in a profuse diarrhea that is a hallmark of the disease. Other manifestations include nausea, vomiting, fever, and abdominal distress (Salmonellosis, 2004).

Salmonellosis is normally self-limiting, resolving in 4 – 7 days without treatment. However, some individuals such as the elderly, children under 10, and the immunocompromised may require hospitalization for dehydration (Salmonellosis, 2004). In 2002, the CDC reported 44,264 cases of salmonellosis in which age groups 1 – 4 and 40 – 64 had the highest number of reported cases: 7,607 and 7,683, respectively (Summary of Notifiable Diseases – United States, 2002). In these cases, prompt treatment involved rehydration with intravenous electrolytes, and administration of systemic antibiotics such as ampicillin, gentamicin, trimethoprim/sulfamethoxazole, or ciprofloxacin (Salmonellosis, 2004). In susceptible individuals, bacterial invasion of the crypt cells can lead to septic shock, organ disruption, and ultimately death (Tauxe, 1992). A small number of individuals develop Reiter's syndrome, a protracted form of reactive arthritis that requires several months of convalescent treatment (Salmonellosis, 2004). These individuals are debilitated with joint pain, conjunctivitis, urethritis, cervicitis, and rarely carditis (Tauxe, 1992).

Antimicrobial resistance to *Salmonella* is associated with increased antibiotic use to promote the growth of feed animals and poultry (Hamer and Gill, 2002). *S. typhimurium* Definitive Type 104 is the worst emerging pathogenic strain, being resistant to at least five antimicrobial drugs (Threlfall, 2000).

### *Salmonella as a weapon*

Prior to the terrorist attacks of September 2001, any perceived threat to the U.S. public from foodborne salmonellosis was widely considered inadvertent, arising from inadequate sanitation or quality control practices by processing facilities, supply chain food handlers, or even consumers. Biological attack on our food supply was considered low risk. Government efforts have centered on preparedness for and response against biological threats such as *Bacillus anthracis* or chemical agents that could produce mass casualties (Sobel et al., 2002). Subsequent premeditated terrorist attacks against Americans, highlighted by the dissemination of *B. anthracis* spores through the U.S. postal system, served to heighten awareness of our vulnerability to deliberate food and water contamination, forcing us to look not only at food safety, but food security.

Terrorism is not confined to the U.S. military sector. Indeed, those fateful attacks aptly demonstrated that civilians represent easily accessible targets and events deemed even as low-risk, such as using commercial aircraft as weapons, can come to fruition. Since this time, members of the Office of Homeland Defense Food Security, the Food and Drug Administration (FDA) and the United States Department of Agriculture (USDA) have speculated that the question is not if foodborne bioterrorism will occur, but rather when it will occur (Progress report to Secretary Tommy G. Thompson, 2003).

The intentional contamination of food and water historically accounts for the majority of bioterrorism and biocriminal events (Mobley, 1995). Food adulteration would appear to be a particularly effective plan of attack, low-tech compared to other tactics (Lee et al., 2003). The CDC (Khan et al., 2001) confirms that food represents the

most vulnerable medium for terrorists to utilize in a deliberate strike staged against the U.S. population at large. In response, the CDC (Khan et al., 2001) has established a Critical Agents List of pathogenic organisms that bioterrorists or biocriminals might conceivable use against Americans, with *Salmonella* and other foodborne pathogens being designated Category B threat agents. As well, funding for new detection and surveillance methods has been raised to its highest levels, and numerous pieces of legislation have been enacted to strengthen the preparedness of the government in the event of an attack on the food supply system (Program summary, program rational, 2001; Progress report to Secretary Tommy G. Thompson, 2003; Theis, 2002).

*Salmonella* possesses many attractive characteristics as a biological weapon, namely, predilection for causing illness in humans, small infectious dosage, relative ease of production in large amounts, and ease of dissemination – especially through food products. More importantly, *Salmonella*'s delayed incubation period may provide perpetrators with precious time to avoid detection so that even a large, deliberate outbreak could be mistaken for an inadvertent disease epidemic, thus reducing the scrutiny of authorities and the risk of ensuing retribution. That *S. typhimurium* has the distinction of being the first organism utilized in a proven bioterrorism attack in the U.S. should be a forewarning. Seventeen years prior to the attacks of 2001, 751 individuals in Oregon were infected through ten salad bars by members of a religious sect in an effort to sway local political elections (Torok et al., 1997). Forty-five of the victims were hospitalized and nine of ten salad bars were closed. Not only does this demonstrate *Salmonella*'s potential as a weapon, but it also illustrates that the main objective of terrorists is not necessarily mortality. Rather, their priority is coercion to instill fear,

panic, civil disorder, decreased confidence in the government, or to inflict economic losses (Sobel et al., 2002). Lee et al. (2003) state accordingly, "To the average person, biological weapons are mysterious, unfamiliar, indiscriminate, uncontrolled, inequitable and invisible...these characteristics contribute to the 'outrage' factor associated with heightened fear."

Insight regarding our food supply's susceptibility to deliberate *Salmonella* adulteration may be best gleaned through actual epidemics, specifically, the 1985 contamination of pasteurized milk that caused 170,000 infections, and the 1994 contamination of ice cream that caused 224,000 illnesses (Sobel et al., 2002). These two large outbreaks aptly illustrate *Salmonella*'s penchant to cause considerable numbers of illnesses, an inherent safety or security vulnerability in the food system allowing large-scale albeit inadvertent contamination to occur that could be exploited by terrorists (Strongin, 2002), and most importantly an even greater ability to create large epidemics through a centralized supply system.

The nature of our food supply system and associated foodborne illnesses has changed dramatically in the U.S. over the past century. The development of preservation technology has advanced our food distribution system from a state of homegrown, localized dissemination to a centralized, global enterprise (Spake, 2001). Unfortunately, food processing, transit, and centralized distribution now appear to be our greatest points of vulnerability to bioterrorists (Lee et al., 2003). Lee et al. (2003) have noted that 43% of all terrorism attacks have been aimed at food business or industry, and that tampering opportunity directly correlates with shipment distance and handling. The World Health

Organization (WHO) (Terrorist threat to foods, 2002) confirms that, “deliberate contamination of food at one location could have global public health implications.”

Imported foods appear to be a particularly “weak-link in the chain of protection” (Nestle, 2003). They constitute a large part of our supply system: 8 million imports from over 200,000 foreign manufacturers annually (Progress report to Secretary Tommy G. Thompson, 2003), yet only 1% are inspected (Theis, 2002). Additionally, antimicrobial resistant *Salmonella* has been particularly noted in imported foods, especially seafood (Zhao et al., 2003). Zhao et al. (2003) confirm the need for surveillance of both naturally occurring zoonotic bacterial pathogens and those that may be deliberately introduced through imports, in addition to the safety and security considerations required for foods grown in this country. The FDA has acknowledged deficiencies in food import security and the supply chain in general and is investing both manpower and funding to improve the situation (Progress report to Secretary Tommy G. Thompson, 2003). Outgoing Secretary of Health and Human Services Tommy G. Thompson may have summarized the situation best when he stated, “I, for the life of me, cannot understand why the terrorists have not...attacked our food supply because it is so easy to do. We are importing a lot of food from the Middle East, and it would be easy to tamper with that” (Branigin et al., 2004).

#### *Salmonella and poultry processing*

Certainly, while food bioterrorism is a very hot topic at this time in history, inadvertent contamination still represents the greatest public risk. Poultry remains one of

the most popular sources of meat food throughout the world today; it's a cheap source of protein, not subject to any religious restrictions, and relatively versatile as a menu item (Silverside and Jones, 1992). Unfortunately, it's also a major source of foodborne salmonellosis. Worldwide production rates, estimated at approximately 77 million metric tons by the Food and Agriculture Organization of the United Nations (FAO), are currently at an all time high and 40% higher than the previous decade (Poultry meat production, 2004). The United States continues to lead the world in poultry production and export (Poultry and eggs, 2004). The latest estimates available through the USDA (Poultry per capita consumption, 2002) indicate that Americans consume 56.8 lbs of poultry (boneless, trimmed equivalent) per capita annually, which is second in meat food only to beef (64.5 lbs per capita). However, while beef consumption in the United States has consistently decreased (40%) since an all-time high in 1976, poultry consumption has consistently increased (100%) in the same timeframe (Poultry per capita consumption, 2002). Thus, with increased popularity and consumption have come increases in *Salmonella* foodborne illnesses.

Microbiological quality of poultry and the associated monetary and legal ramifications of consumer foodborne illness are a major concern of processing facilities (Yang, 1998). Public awareness and increasing cases of foodborne illness have necessitated closer examination of livestock cleanliness and poultry processing methods (Sofos, 1994). Normally, healthy birds carry extensive amounts of microbes on their skin and feathers. During the growth of the bird, natural defenses keep the microbial population in check. However, when the bird is slaughtered, the carcass becomes extremely vulnerable to a host of microorganisms. Marriot (1995b) estimates that one



square centimeter of unwashed skin holds as many as 155 million microorganisms. Fecal material attached to the hide can contain as many as 220 million microbes per gram whereas one gram of soil may harbor as many as one billion microorganisms (Marriott, 1995b). Bacterial flora from the bird's hide can be directly introduced into the viscera and meat through the practice of bleeding before defeathering (Sofos, 1994). As well, fecal contamination of meat can occur during evisceration if the gut is not completely empty of food – the stomach and intestines are loaded with bacteria, most notably *Salmonella* (Sofos, 1994). To alleviate this problem, farms generally withdraw feeding just prior to slaughter (Sams et al., 2000b). Although *Salmonella* does not grow quickly on carcasses during processing and hardly at all below 7 °C, it can continue to survive and spread between birds if improper evisceration and inadequate thermal regulation (chilling) occur (Silverside and Jones, 1992). Even when proper water chilling is carried out, studies have shown that significant cross contamination occurs. This could be readily decreased by replacing the current water chilling process used mainly in the United States with the air chilling process used almost exclusively in European countries (Fries, 1999). Apparently, a large amount of bacterial cross contamination between healthy and contaminated birds also occurs during the scalding step, when slaughtered birds are grouped in large vats at 50 – 60 °C (Tamblyn et al., 1997) for roughly 45 seconds to aid removal of the outer skin and feathers (Sams et al., 2000a). Even at these temperatures, the vats can foster up to 1 billion viable microorganisms per liter of water (Marriot, 1995b). Undoubtedly, the majority of bacterial cross contamination transpires as a result of poor sanitation practices by handlers during processing (Marriot, 1995a); although bacterial contamination during processing may be unavoidable because some

birds are so heavily infected (Tamblyn et al., 1997). In these cases, water chilling fails to remove significant amounts of *Salmonella* and they become part of the food product. Thus, one infested bird could contaminate 100% of all finished products within that batch (Marriot, 1995b).

The WHO (Terrorist threat to foods, 2002) states that in terms of preparedness, both food safety and food security are inextricably linked and should be jointly managed. Next to prevention, a key challenge to food safety will always be our ability to predict how, when or where an outbreak may occur. Appropriate food sanitation and preparation represent the best defense; cooking at proper temperatures for appropriate durations easily dispatches *Salmonella* (Salmonellosis, 2004). Yet foodborne illness statistics appropriately demonstrate that consumers cannot be relied upon to protect themselves regardless of the means of introduction – especially if contamination occurs in public eating establishments. Because of unavoidable contamination, a biosensor that could be included into processed food packaging or one that could be applied diagnostically to food products just prior to consumption might allow detection of pathogens such as *Salmonella*, and represents a feasible alternative to illness.

#### *Salmonella detection in poultry*

In 1997, the Food Safety Inspection Service's (FSIS) National Advisory Committee on Microbiological Criteria for Foods (HACCP Guidelines, 1997) implemented the Hazard Analysis and Critical Control Point (HACCP) system in an effort to ensure food safety from harvest to consumption. The FSIS arm of the USDA

“...verifies that establishments are meeting the standards [for pathogen reduction as directed by HACCP] by having federal inspection personnel collect randomly selected product samples and send them to FSIS laboratories for *Salmonella* analysis...” (Progress report on *Salmonella* testing, 2002) using established techniques employing selective culture media, biochemical or serological characterization (FSIS, 1996). This represents the only regulated location in the inspection processes where assaying for pathogens is performed (Schumann et al., 1997). Processing companies are also encouraged to conduct their own testing on-site to ensure compliance with HACCP standards and utilize ELISA, PCR (Powell et al., 1994), and conductance methods (Brooks et al., 1992) to some degree in addition to traditional techniques. These methods can be expensive, labor intensive, and untimely. PCR is limited by inhibitors present in some food products and capable of detecting DNA from dead cells.

While traditional methods are appropriate and perform within required HACCP limits, they are also untimely. Definitive results take anywhere from 2 – 4 days (Progress report to Secretary Tommy G. Thompson, 2003). During this period, larger processing plants may have distributed products contaminated with *Salmonella* to points of sale before a problem is realized. Subsequently, consumers may ingest the tainted products before a recall can be initiated. An appropriate example is the case of Hudson Foods, where 25 million pounds of ground beef were recalled due to contamination by *E. coli* O157:H7 (Hamburger recall, 1997). USDA officials stated that much of the beef had already been sold through fast food outlets and well known supermarkets, and probably consumed before the recall was announced (Developments in Hudson Foods *E. Coli* Outbreak, 1997). Ultimately, at least 20 cases of food poisoning were associated with the

contamination. Federal records indicate that in 1999, almost 5 million pounds of meat and meat by-products were recalled yet less than 4.5% were recovered (Recall cases, 1999).

While HACCP represents a worthwhile effort to protect Americans, it's intended to ensure overall compliance to standards – not to detect every contamination event. Worse, in 2001 a federal appellate court ruled against the HACCP testing standard for *Salmonella*, stating that failure of the testing criterion is no longer a reason for closure of food-processing plants in violation (Court rejects bacterial testing on processed meat, 2001). Equally detrimental to consumers is the fact that deliberate contamination of products after testing will not be discovered – HACCP does not address food security. Although some processors have broadened the principles of HACCP (deemed TACCP: Threat Analysis and Critical Control Point) (Theis, 2002) in an attempt to incorporate some components of food security, it still does not represent a long-term, viable solution for identifying individual *Salmonella* contamination events, be it deliberate or unintentional. The FDA (Progress report to Secretary Tommy G. Thompson, 2003) is in agreement with the WHO, stating that while food safety and food security possess different aspects of food protection they are inherently connected. The FDA's latest annual report to Congress (Testing for rapid detection of adulteration of food, 2003) on food safety and security reaffirms the need to develop rapid biodetection systems that will identify infectious agents and their sources in order to prevent epidemics. Simply put, HACCP testing consists of the best methods available that do not fulfill the government's need for simplified, rapid testing to help insure the safety of the public.

Rapid, specific, sensitive detection and enumeration methods for microbial contaminants in food products have long been a subject of research. In a recent market analysis of next generation assays for food safety, innovative miniaturized biosensor assays that combine reliability, speed, and portability while reducing sample size and assay costs, were highly touted over conventional identification techniques (Alocilja and Radke, 2003).

A biosensor can be simply defined as the spatial unity of a physical transducer and a biological recognition system. Hence, it consists of two main components: a receptor that possesses affinity for an analyte of interest, and a transducer to convert the chemical signal of sample-receptor interaction to a functional signal output that can be amplified and processed to provide qualitative or quantitative assessment of analyte-receptor interaction. The first biosensor dates to 1962, when Clark and Lyons (1962) published their essay on a reusable enzymatic electrode. Since then, thousands of published papers have described various engineering approaches used in the development of biosensor assays, which can be mainly categorized into optical, calorimetric, biological-biochemical (D'Souza, 2001), electrochemical (Shah and Wilkins, 2003) and acoustic wave-mass change methods (Bunde et al., 1998). From these, optical methods (e.g. SPR) and acoustic wave-mass change methods appear to suitably combine speed, sensitivity and portability for future development of rapid biodetectors for biological analysis, such as food contamination (Janschhoff et al., 2000; Skládal, 2003).

Acoustic wave-mass change sensor measurements are based on the natural resonant properties of piezoelectric (PZ) crystals prepared as so-called quartz crystal microbalances (QCM) resonators. The QCM has been the subject of intense research since the reporting of the first analytical application of a PZ crystal by King (1964). The transverse shear mode (TSM) QCM consists of a thin, round AT- or BT-cut (i.e. angular orientation in relation to internal crystallography) quartz crystal “wafered” between two metallic electrodes (e.g. gold, silver or palladium) affixed to obverse and reverse sides, and in itself comprises an oscillatory circuit. The quartz substrate can have varying dimensions and resonant frequencies. The piezoelectric properties of the quartz result in deformation of the crystal when an electrical potential is created across the electrodes, which in turn induces a transverse, standing wave of resonance oscillation in the quartz at a fundamental frequency. AT-cut crystals displace the oscillation parallel to the resonator surface and are utilized predominantly due to their temperature stability. Sauerbrey (1959) was the first to describe the principles of the QCM and how it could be utilized as a very sensitive mass measurement tool. Basically, when mass is deposited on the surface of the electrode, there is a corresponding, proportional decrease in the resonant frequency of the crystal if the mass is thin and rigidly attached. While Sauerbrey’s (1959) calculations were originally elucidated for depositions under vacuum conditions, the use of the QCM has been extended to liquid applications – albeit, qualitative interpretation of data must account for other physical forces that can act at the solid/liquid interface including viscous drag, liquid entrainment, and viscoelasticity of any attached mass. The equivalent circuit model proposed by Martin et al. (2000) has notably furthered understanding of the quantitative effects these forces have on the

resonant frequency of the resonator, but total comprehension remains a work in progress. Notwithstanding, the ability to function in liquid environments conducive to bacterial growth and the fact that mass can be detected as a deposition event at the solid/liquid interface are two reasons the QCM has been developed as a rapid detection tool.

Acting as a solitary transducer platform, the QCM is non-specific in its detection of mass. This feature has been exploited in biological analyses for the study of specific molecular interactions such as gold-protein binding (Stadler et al., 2003). On the other hand, when the active area of the electrode is coated with a high affinity receptor/biorecognition component through a reliable deposition process, any sample coupling between the receptor and its complementary analyte is converted to a signal output that can be amplified and processed to provide specific, sensitive qualitative or quantitative measurement of analyte-receptor interaction and is comparable if not better than traditional direct immunoassays (e.g. ELISA) and SPR (Janschoff et al., 2000). The QCM system is relatively inexpensive and simple in operation, requiring only the resonator crystal, external oscillatory circuit, and frequency counter. Numerous commercial systems are available for researching biological applications (O'Sullivan and Guilbault, 1999). Most importantly, frequency changes associated with specific binding are very rapid, being reported within minutes (Pathirana et al., 2000). These features confirm the potential of QCM-based biosensors as an expedient method for detection of pathogens in food products.

The majority of QCM-based biosensors described for the detection of bacteria have utilized antibodies (a.k.a. immunosensors) as the high affinity receptor/biorecognition component. Antibodies can be extremely narrow (monoclonal) or broad (polyclonal) in their specificity and generally have very high affinities (picomolar). In the production of QCM-based immunosensors, they must be immobilized to the substrate via their hydrophobic F<sub>c</sub> (fraction-crystallized) fraction, with the F<sub>ab</sub> (fraction-antibody) fraction being oriented outward to capture the target antigen. Heat-treating the antibodies at high temperature (usually 56 °C for 30 minutes) effects hydrophobic conformational changes to the F<sub>ab</sub> portion, opening it up to increase its ability to bind (Hseih, 2000). Unfortunately, antibodies can also possess numerous disadvantages including cost of production, availability, fragility to degradation from very high temperatures and enzymatic processes, a general lack of standardization and reusability, and the need for laborious immobilization methods to sensor substrates.

Shons et al. (1972) described the first antibody-based QCM sensor for the determination of antibody activity. Since then, antibodies have been coupled to the QCM's electrode surface using numerous immobilization techniques (reviewed in Kaspar et al., 2000; Luong and Guilbault, 1994), including biotin-avidin interaction (Prusak-Sochaczewski and Luong, 1990), glutaraldehyde cross-linking (Prusak-Sochaczewski et al., 1990), physical adsorption, thin silane layers (Prusak-Sochaczewski et al., 1990), antibody thiolation (Park and Kim, 1998); Protein A (König and Grätzel, 1994; König, and Grätzel, 1995; Welsh et al., 1996), Protein G (Minunni et al., 1996),



polyethylenimine-glutaraldehyde (PEG) and dithiobis-succinimidyl propionate coupling (Hermanson et al., 1992; König and Grätzel, 1994; Storri et al., 1998; Yang et al., 1998); enzymatic immobilization (Santos, 1994), alternating monolayers of monoclonal antibody against anti-horse radish peroxidase and dextran sulfate (Brynda et al., 1998), and Langmuir Blodgett (LB) (Pathirana et al., 2000).

The specificity of the sensor is wholly dependent upon the immobilized antibody and most appear to be well suited for the detection of bacteria (Kaspar et al., 2000; Skládal, 2003), particularly food pathogens such as *Bacillus cereus* (Vaughan, et al., 2003), *E. coli* (Pyun et al., 1998, Su and Li, 2004), *Listeria monocytogenes* (Minunni et al., 1996), and most importantly, *Salmonella* (Babacan et al., 2002; Brown, 1998; Dill et al., 1999; Fung et al., 2000; Fung and Wong, 2001; Hartman et al., 1995; Louie et al., 1998; Olsen et al., 2003; Prusak-Sochaczewski and Luong, 1990; Park et al., 2000; Park and Kim, 1998; Pathirana et al., 2000; Seo et al., 1999; Si et al., 1997; Starodub et al., 1994; Yang et al., 1998; Ye et al., 1997; Zhou et al., 1998). However, relatively few of the described sensors have a lower sensitivity threshold capable of detecting an infectious dosage of *Salmonella*, or the capability of the reaching the test performance characteristics for *Salmonella* identification as defined by HACCP (FSIS, 1996). Some of the more notable QCM-based immunosensors for *Salmonella* include: Prusak-Sochaczewski and Luong (1990), who reported the first QCM assay for *Salmonella* with an assay time of 50 – 60 s and lower detection limit of  $10^5$  cells/ml. Unfortunately it required a  $\frac{1}{2}$  – 5 hour incubation period depending on the concentration of the microbial suspension; Yu and Bruno's (1996) immunosensor for the detection of *E. coli* O157:H7 and *S. typhimurium* had a lower detection limit of  $1.0 - 2.0 \times 10^3$  cells/ml and assay time

of less than 1 hour – however, the sensor was not linear; Park and Kim's (1998) thiolated immunosensor possessed an assay time of 30 – 90 minutes, lower detection limit of  $9.9 \times 10^5$  cells/ml and detection range up to  $1.8 \times 10^8$  cells/ml; Ye and colleague's (1997) linear ( $R = 0.942$ ) biosensor assay for *S. typhimurium* had a 25 min response time, lower detection limit of  $5.3 \times 10^5$  CFU/ml, and a range up to  $1.2 \times 10^9$  CFU/ml; and foremost, the rapid and sensitive patent-pending (Vodyanoy et al., 2000) biosensor designed by Pathirana et al. (2000) for *Salmonella*. Somatic O *Salmonella* polyclonal antibodies were immobilized as a bio-recognition layer by LB method. Capable of analytical response times of  $79 \pm 20$  seconds, the sensor required no incubation period, had a linear ( $R > 0.98$ ,  $p < 0.01$ ) dose-response over 5 decades ( $10^2$  to  $10^7$  cells/ml) of bacterial concentration, sensitivity of  $18 \pm 5$  mV/decade of *S. typhimurium* concentration, detection range of  $350 \pm 150$  cells (well below the reported infectious dosage for *Salmonella*-induced gastroenteritis) to  $10^{10}$  cells/ml, and no specificity towards *E. coli* O157:H7 (Pathirana et al, 2000). The LB method is uncomplicated and an excellent tool for building well-engineered monolayers with controllable characteristics, and when applied to PZ crystals produces a QCM that is an extremely accurate detector of mass change (Barrud et al., 1993). The thermodynamic characteristics of LB films are quite sensitive to a wide range of antigen concentrations, with minimum sensitivity limited by the accompanying detection system QCM (Ahluwalia et al., 1991). Although this acoustic wave sensor remains beyond peer, it was subsequently found that the antibody layer degraded quickly (36 h) under conditions of environmental aging (Olsen, 2000) in fluids from raw packaged poultry. This confirms one of the disadvantages of antibodies for sensors,

namely fragility, and their probable unsuitability for extended duration commercial applications in enzymatically-rich, bacteria-laden consumables such as poultry.

In retrospect, the QCM appears to be a viable platform for the sensitive detection of mass deposition under aqueous conditions, which can be indicative of specific interactive binding events when a high affinity receptor such as an antibody is immobilized to its surface. However, antibodies have been shown to possess numerous disadvantages, which may make them an insubstantial biological recognition component for use on a commercially viable detector for food safety and security. Therefore, a high-affinity receptor capable of addressing these drawbacks is needed.

#### *Bacteriophage – a novel biorecognition component*

O'Connell and Guilbault (2001) have stated that "...the future of biosensors is inextricably linked to molecular biology" and discussed the use of phage display to prepare phage as probes to overcome the weak points of antibodies. Bacteriophage (phage) generally demonstrate predilection for some weakness of the bacterial cell, exploiting it in order to transfect its nucleic acid. The Ff class of filamentous phage, such as M13, f1 and fd, possess an outer coat mainly composed of 4000 overlapping 50-residue proteins encoded by gene VIII and are vectors for *E. coli*, infecting via the plasmid-encoded F-pilus of the host. A key, exploitable feature is their tolerance of foreign DNA sequences, incorporated through recombinant modification. Insertion of protein-encoding DNA into gene VIII allows expression of foreign peptides on the surface of the virion, which acts as a scaffold of sorts, for presentation to a

complementary ligand (Smith and Petrenko, 1997). When recombination involves the incorporation of a random stretch of nucleotides as foreign DNA, the displayed peptides are proportionally random in their amino acid sequence (Petrenko and Vodyanoy, 2003). Mixtures of random phage produced from a single recombination event can have as many as one billion different clones ("phage library") that can be refined through affinity-selection techniques to recognize a single complementary target. In this way, they can act as antibody substitutes for binding cell receptors (Petrenko and Smith, 2000) such as those found on the outside of *Salmonella*. A distinct advantage of phage over natural antibodies is their *durability*; they are highly resistant to heat, urea, acids, alkalis and other environmental stresses (Petrenko and Vodyanoy, 2003). Urea resistance can add potential for phage *reusability* in conjunction with sensors through a bacteria-removing/surface regeneration step (Prusak-Sochaczewski and Luong, 1990). Phage exhibits a *long shelf life* and is much *cheaper* to produce in mass than antibodies. Unlike antibodies, phage can be consistently reproduced through phage display technique to achieve quality *standardization*. Recombinant phage are extremely *sensitive* to receptors due to the high concentration of epitopes displayed via major outer coat protein pVIII, which provides a greater chance for local binding events, and because of surface interactions with their immediate surroundings may possess a global "landscape" function that increases overall binding affinity (Petrenko et al., 1996). Consequently, these characteristics have led them to be commended for use in conjunction with biosensors over natural antibodies (Goldman et al., 2000; Mosier-Boss et al., 2003; Petrenko and Sorokulova, 2004; Petrenko and Vodyanoy, 2003).

Numerous phage applications have been described (Smith and Petrenko, 1997) including their use in the detection of bacteria (Mosier-Boss et al., 2003). *Salmonella*-specific phage (SJ2) have been used to successfully detect *Salmonella* using a biosorbent-bioluminescence method, however, the lower limits were less than optimal at  $2 \times 10^6$  cells/ml (Sun et al., 2001). The use of phage in conjunction with the QCM has been rather limited. Hengerer et al. (1999a, 1999b) described the effective use of the QCM as both a method of screening recombinant phage antibody libraries and for the estimation of recombinant phage antibody affinity using a complementary QCM-bound antigen. M13 phage has been successfully detected in solution using antibodies covalently cross-linked to the QCM (Uttenthaler et al., 2001). Dultsev et al. (2001) reversed affinity binding from a QCM bound receptor to detect and quantitate fd phage. Researchers at Auburn University have immobilized peptides derived through fd phage display to quartz resonators by LB methods to detect murine myofibers (Samoylov et al., 2002a, 2002b). Affinity selected filamentous phage, biotinylated for immobilization to QCM bound biotinylated LB monolayers via streptavidin intermediates, have been used to detect beta-galactosidase (Petrenko and Vodyanoy, 2003).

Filamentous phage-based QCM affinity detection systems for bacteria have not been described in the literature; however, Petrenko and Vodyanoy (2003) discussed the potential of phage as probes in conjunction with the QCM for the detection of these threat agents. In addition to previously mentioned advantages over antibodies, the outer coat protein structure of filamentous phage may be highly amenable to simple immobilization through physical adsorption directly to the gold surface of the QCM electrode, thus providing another engineering advantage while maintaining peak biological functionality.

It was therefore hypothesized that affinity-purified phage from a phage library could be immobilized onto QCM resonator platforms to effect a rugged, sensitive, specific, selective alternative to antibody-based QCM biosensors for the detection of *Salmonella*. Proof of concept might allow extension of the biosensing technology to food safety and food security initiatives such as rapid detectors or monitors for *Salmonella* contamination in consumables. Continuous monitoring of products from processing to consumption would allow preemptive disposal of tainted products prior to human consumption and could prevent thousands from incurring foodborne illness or death. If contamination has occurred, traceability is enhanced, possibly leading to further food safety and security enhancements through identification of offenders. This enabling technology could also be applied as a rapid diagnostic method for research, industry, and clinical-based labs, eliminating outdated conventional culturing procedures that are costly and time-consuming. Furthermore, the nature of the methods used to derive phage probes for *Salmonella* holds potential utilization against any bacteria, virus or toxin to which a corresponding phage could be affinity-selected against.

The goal of this research was proof-in-concept development of a biosensor for the rapid detection of *S. typhimurium*, based on a novel bio-recognition layer of affinity-selected filamentous bacteriophage immobilized to a piezoelectric transducer platform. The three primary objectives and specific aims to accomplish this goal were:

- I. Derivation of high-affinity phage probes for immobilization to QCM resonators:
  - Selection of *S. typhimurium*-specific phage clones from an f8/8 landscape library using three multistage landscape phage selection procedures targeting immobilized or aqueous suspended *S. typhimurium*, and peptide characterization through DNA sequencing;
  - Determination of phage clone specificity for *S. typhimurium* through ELISA, titration-precipitation assay, and flow cytometry;
  - Determination of phage clone selectivity for *S. typhimurium* through co-precipitation assay and flow cytometry.
- II. Characterization of the affinity interaction between phage and *S. typhimurium*:
  - Quantitative interpretation of complex formation through binding equations;
  - Qualitative interpretation of complex formation through the use of flow cytometry, agarose gel electrophoresis, and optical, fluorescent and transmission electron microscopy;
  - Determination of the source of affinity interaction between phage and bacterium specific to an outer membrane structure of *S. typhimurium* through molecular studies.
- III. Preparation of phage-based piezoelectric biosensors and their functional determination as rapid biodefectors of *S. typhimurium* under liquid conditions:
  - Immobilization of *S. typhimurium*-selective phage as filaments or phage coat proteins to QCM resonators using physical adsorption, biotin-streptavidin-phage self-assembly, and Langmuir Blodgett method in order to prepare biosensors for the detection of *S. typhimurium*;

- Assaying biosensors using the standard probe technique and novel flow cell configuration of a commercially available QCM system to determine functionality.



## CHAPTER III

### SPECIFIC AND SELECTIVE IMMUNOSENSOR FOR *SALMONELLA* *TYPHIMURIUM* AND ITS DETECTION IN THE ENVIRONMENT

#### **Abstract**

Specific and selective detection of *S. typhimurium* in aqueous samples was demonstrated using biosensors prepared with *Salmonella* polyclonal antibodies immobilized to quartz crystal acoustic wave devices by Langmuir-Blodgett method. Biosensors were selective for *S. typhimurium* even in the presence of large concentrations of *Escherichia coli* (*E. coli*) O157:H7. Specificity to *S. typhimurium* was confirmed by pre-incubating bacteria with free antibody prior to testing, resulting in no relative signal from the biosensor. Dark-field and electron microscopy confirmed different conformations of bacterial attachment at the solid-liquid interface when sensors were prepared with different respective antibodies, either polyvalent *Salmonella* somatic O or *E. coli* flagellar H7. Results indicate that while somatic O antibody exhibits rigid binding of *Salmonella*, flagellar H7 antibody forms a flexible connection with the flagella of *E. coli* allowing a large degree of rotational freedom. Acoustic wave sensor responses correlated with mass changes according to theory when attachment of bacteria was rigid

and strong at the solid-liquid interface. In contrast, when attachment was flexible the sensor signals were inversely proportional to the additional mass of bound bacteria. Interfacial viscoelasticity and acoustic and electromagnetic coupling are thought to determine this difference. Signals of environmentally aged sensors with either predominately rigid or flexible positioning of bacteria were correlated with changes in mass at the liquid-solid interface. Antibody-based immunosensors with O or H type binding could be useful for analytical purposes such as biosensors for food safety and security initiatives where *S. typhimurium* poses risks as a pathogen.

## **1. Introduction**

Sensors prepared from thickness-shear-mode (TSM) acoustic wave platforms have proven to be excellent analytical tools for the study of specific molecular interactions at the solid-liquid interface (Bunde et al., 1998; Cavicacut et al., 1999; Ivnitski et al., 1999; Kaspar et al., 2000; O'Sullivan and Guilbault, 1999). The application of radio frequency alternating voltage results in the propagation of a converse piezoelectric effect, the resonant frequency changes of which can be attributed to the effect of added mass as a result of binding at the sensor's surface. TSM platforms with immobilized biological recognition components have been utilized successfully in real-time biochemical macromolecular adsorption studies (Ghafouri and Thompson, 1999). As immunosensors, acoustic wave devices have been shown to be quite specific in complex biological media containing cells and human serum (Dahint et al., 1999).

Theoretical modeling of the TSM response to mass accumulation has been shown experimentally under various loading conditions, including ideal mass layers (thin layers of Au and SiO<sub>2</sub>), a semi-infinite fluid (glycerol in water), and a viscoelastic layer exemplified by thin layers of oil (Bandey et al., 1999; Martin et al., 1991). In contrast, TSM crystals exposed to relatively large protein and polysaccharide molecules in solution gave responses that did not correlate with mass changes imposed at the solid-liquid interface (Ghafouri and Thompson, 1999). The authors ascribed this phenomenon to viscoelastic and acoustic coupling at the interface. Thus, one would expect especially complicated interfacial properties when the TSM sensor is exposed to larger entities such as viruses and bacteria.

Live organisms in motion may create electromechanical forces at the solid-liquid interface that contribute to the apparent mass of binding bacteria. Nutrition, growth, differentiation, chemical signaling, and mutagenic exposure may also factor in controlling the physical state of binding bacteria. The bacterial cell (e.g. *E. coli*) possesses a mass of approximately 665 fg, making it one million times heavier than a typical (150 kD) antibody molecule (Neidhardt, 1987). Many bacteria carry out or are involved with various movements caused by flagellation, Brownian motion, chemotaxis, swimming behavior, adaptation, and other cell phenomena (Alberts et al., 1994). Binding ability may also depend on the presence of fimbriae or other surface-associated adhesion factors as well as the ability of single cells to associate and form colonies. The interaction of bacteria with the biosensor may therefore become dependent on environmental conditions.

Acoustic wave device theory and relevant biological applications were reviewed (Cavicacute et al., 1999; Ivnitski et al., 1999; Kaspar et al., 2000). Previously, we demonstrated the feasibility of biosensors based on Langmuir-Blodgett antibody monolayers for the rapid and sensitive detection of *S. typhimurium* in liquid samples (Pathirana et al., 2000). In this study the specificity and selectivity of the biosensor under physiological conditions, including environmental aging and the mechanical and electrical implications of bacterial positioning on the biosensor signal at the solid-liquid interface, were investigated.

## **2. Materials and methods**

### *2.1. Cultures*

*S. typhimurium* and *E. coli* O157:H7 cultures from the Auburn University (Department of Biological Sciences, Auburn, AL) culture collection were used in experiments. Cultures were previously confirmed for identity using traditional biochemical, cell morphology, and serologic tests, and maintained on trypticase soy agar (TSA) slants at 37 °C.

### *2.2. Growth of cultures and preparation of test suspensions*

Cultures were streaked for isolation on individual TSA plates. Broth cultures were prepared by inoculating one colony from a plate into trypticase soy broth then

incubating overnight at 37 °C in a shaking water bath incubator. Cell cultures were washed (3×) by centrifugation (3500 rpm, 10 min, room temperature) using sterile phosphate buffered saline (pH 7.0) (PBS) with final resuspension in 2 ml PBS. One ml of resuspended culture was serial diluted with PBS to prepare a series of suspensions, ( $\approx 10^1 - 10^{10}$  cells/ml) for sensor testing. Diluted cells were immediately placed on ice and delivered to another laboratory for testing with the sensor. All suspensions were brought to room temperature (maintained at  $\pm 0.1$  °C) and vortex mixed prior to use. Aseptic procedures were followed throughout all procedures.

### 2.3. Colony forming unit (CFU) determinations

Measurement of bacterial cell counts was performed by an optical enumeration method as described in Olsen (2000) and confirmed by duplicate TSA plate counts using 100  $\mu$ l of each dilution. Average CFU/ml counts were determined from those dilutions yielding 30 - 300 colonies/plate following incubation for 48 h at 37 °C.

### 2.4. Antibodies

Antibodies obtained from Oxoid (Ogdenburg, NY) were utilized as the biological recognition component of sensors. For *S. typhimurium*, a polyvalent somatic O antibody specific for most *Salmonella* serovars was employed. To capture *E. coli* O157:H7, polyvalent H7 (flagellar) antibodies were used. In most cases, the same lot of antibody was used throughout experimentation.

Three different assays were employed to examine the reactivity of antibodies: (1) dot blot ELISA using nitrocellulose or nylon filters with fixed antigen, subjected to chromogenic anti-mouse (for monoclonal antibody) or anti-animal-based antibody conjugated with enzyme assay; (2) commercially available test kits; and (3) slide agglutination.

## *2.5. Acoustic Wave Device (AWD)*

*2.5.1. Substrate.* Round ( $d = 2.54$  cm), AT-cut, 5 MHz nominal oscillating frequency planar piezoelectric quartz resonators (Maxtek, Santa Fe Springs, CA) were used as substrates for sensors. Resonators possessed circular, evaporated gold electrodes on obverse and reverse sides for electrical connection to an external AWD oscillatory circuit. Standard microscope slides ("test slides") were used as substrates for visual observations and cell counting. Resonators and slides were cleaned thoroughly prior to use by overnight immersion in 50% (v/v)  $\text{HNO}_3$  and rinsing under running distilled water for several days to remove all traces of acid. Cleaned resonators were air-dried and stored at room temperature until use.

*2.5.2. Frequency monitor.* Sensor measurements were carried out using Maxtek (Santa Fe Springs, CA) PM-740 or TM-400 plating monitors, both of which possessed a frequency resolution of 0.5 Hz at 5 MHz. The devices were capable of working in both single and dual probe modes. The voltage output from the plating monitor was used to monitor the binding of bacteria to the sensor surface, and is inversely related to the resonance

frequency of the quartz resonator. Voltage output was recorded and analyzed using a standard personal computer equipped with data acquisition card and software.

## *2.6. Monolayer preparation*

*2.6.1. Surface film balance.* Monolayer deposition to substrates was carried out as described by Olsen (2000) using a KSV 2200 Langmuir-Blodgett film balance (KSV-Chemicals, Finland). The fully computerized system possessed a Wilhelmy-type surface balance (range 0-100 mN/m; sensitivity 0.05 mN/m, 4 cm perimeter), a Teflon® trough (45 × 15 cm<sup>2</sup>) mounted on a 200 kg marble table, a variable speed motor-driven Teflon® barrier (0-200 mm/min), and a laminar flow hood. Vibration control was enhanced through interposing rubber shock absorbers and by mounting the laminar flow hood on a separate bench. The subphase used in the experiments was a solution containing 55 mM KCl, 4 mM NaCl, 0.1 mM CaCl<sub>2</sub>, 1 mM MgCl<sub>2</sub> and 2 mM 3-(N-morpholino)-propanesulfonic acid, prepared with deionized double distilled water (pH adjusted to 7.4 with KOH). Subphase temperature was controlled ( $\pm 0.1$  °C) by circulating water through a quartz tube coil on the bottom of the trough. Surface pressure data was collected during slow, steady-state compression of the monolayers.

## *2.6.2. Monolayer formation and deposition*

*2.6.2.1. Phospholipid monolayers.* Phospholipid solutions were spread on the subphase surface as hexane solutions (1 mg/ml) containing 2% EtOH (Ito et al., 1989).

2.6.2.2. *Monolayers with immobilized antibodies.* Antibody monolayers were prepared by slowly pipetting (100  $\mu\text{l}/\text{min}$ ) 150  $\mu\text{l}$  of the respective antiserum down a vertically inclined, wetted glass rod partially immersed into the subphase. Following antiserum delivery to the subphase, the glass rod was removed and the monolayer was allowed to equilibrate for 10 min at  $19 \pm 0.1$  °C. Seven monolayers of either *Salmonella* or *E. coli* O157:H7 antibodies were transferred by Y-type deposition to QCM or glass slide substrates at a vertical rate of 4.5 mm/min and a constant surface pressure of 23 mN/m.

## 2.7. *Bacteria binding measurements*

The AWD was calibrated previously by deposition of well-characterized stearic acid monolayers (data not shown). Bacteria binding measurements were carried out for each prepared sensor as follows. The prepared antibody sensor was secured in the probe's external AWD oscillatory circuit. Following obtainment of a voltage output from the sensor, data recording was commenced and 1 ml of control solution (PBS) was delivered via pipet to the dry sensor surface. After 8 minutes, data collection was stopped and the PBS was carefully removed by pipet. A new recording was initiated and 1ml of test suspension containing the respective target bacteria was added following the same measuring procedure. Test suspensions were assayed on the sensor from least to most concentrated. For examination of bacteria-antibody binding specificity, the sensor was tested with bacteria previously incubated with a solution of free antibody for an optimized contact period.



## 2.8. *Dark-field microscopy*

Optical observation and recording of bacteria binding and bacterial counts were performed with an Olympus microscope fitted with a 100-W mercury lamp illumination source, a polarizer, a Naessens dark-field condenser (COSE, Canada) and a 100× objective (oil, NA 1.4) as described by Olsen (2000). Dark-field high-resolution images (Vodyanoy et al., 1994) were directed to a DEI-470T Optronics CCD Video Camera System (Optronics Engineering, CA). The system provided real-time observation of bacteria in a natural aqueous environment, requiring no freezing, dehydration, staining, shadowing, marking, or other manipulation of samples. The quantity of bound bacteria in the presence of a large concentration of motile cells was used to estimate the surface concentration of specific antibody.

## 2.9. *Scanning electron microscopy*

Scanning electron microscopy (SEM) allowed physical characterization of the biosensor at the microscopic level. Sample preparation followed the protocol of Hoppert and Holzenburg (1998). Previously assayed biosensors were air-dried at room temperature for 24 h in a sealed petri dish by elevating them over a small layer of desiccant using wooden applicator sticks. Dried sensors were mounted onto aluminum stubs with iron-based adhesive, sputter-coated (2 ×) (Pelco Sputter Coater, SC-7) at 0.02 mbar Ar gas pressure with a 60:40 Au/Pd mixture at 30 mA for 1 min, then examined

using a Zeiss DSM 940 SEM (Thornwood, NY) at 10 kV. Digital micrographs (Digital Image Transfer Recognition Program, Zeiss) were processed with Adobe Photoshop 4.0.

#### *2.10. Environmental aging of sensors*

One hundred-forty eight *Salmonella* antibody sensors and 35 test slides were fabricated by transferring seven monolayers prepared from *Salmonella* antiserum to the respective substrate using the LB technique. Prepared sensors and slides were placed into four sets, with each set consisting of 28 sensors and 7 test slides. Each set was immersed in fluids from raw packaged poultry at a temperature of either  $\approx 4$ , 11, 23 or 33 °C (Olsen, 2000). A control group of four sensors and one test slide was tested immediately following preparation. Then, each day for seven days, one set of four sensors and one test slide from each respective temperature was removed from the poultry fluid, rinsed, and assayed as described previously (*cf.* “2.7. Bacteria binding measurements”). As well, 8 prepared sensors were tested to examine interaction of *S. typhimurium* suspended in fluids from raw packaged poultry and in fluids from raw packaged poultry containing no *S. typhimurium*. All dose-response experiments were carried out at room temperature ( $\pm 0.1$  °C).

### 3. Results and discussion

#### 3.1. Rigid versus flexible positioning of bacteria at the sensor surface

When the somatic O antibody against *Salmonella* was employed as a capture agent, rigid whole body attachment of bacteria to the sensor surface was confirmed by electron and dark-field microscopy. Electron micrographs (Fig. 3.1) show that bacterial binding in this case is characterized by parallel alignment of cells with numerous visible filaments firmly attaching cells to the surface. Real-time dark-field recordings of live bacteria bound to the surface confirm this observation (Fig. 3.2A). In contrast, H7 flagellar antibodies allow flexible attachment of cells to the sensor surface. Videotaped sequential frames in Fig. 3.2B depict consecutive clockwise positioning of the rotating bacterium at intervals of about 100 ms. According to the observations of Schuster and Khan (1994), a whole cell attached to the sensor surface by a single flagellum could produce this type of movement as a result of the bacterium rotating around its flagella. Consequently, video recording also showed non-rotational, side-to-side oscillation of cells bound by several flagella to the sensor surface (data not shown). When sensors with somatic O antibodies against *Salmonella* were subjected to environmental aging, dark-field observation of the sensors showed escalating surface buildup of indigenous bacteria as duration and temperature were increased (Olsen, 2000). It is hypothesized that this buildup partially obstructs the antibodies on the sensor surface, decreasing the accessibility of antibodies to *S. typhimurium*. Dark-field microscopy confirmed that rigid, whole body binding of *S. typhimurium* was replaced by loosely attached cells

possessing considerable freedom of movement as the duration of sensor aging and temperature were increased. Thus, positioning of *S. typhimurium* at the sensor surface changed from rigid to flexible as environmental aging occurred.

### 3.2. Validation of mass measurements of monolayers

The deposition of increasing quantities of stearic acid monolayers onto the surface of an acoustic wave resonator resulted in a linear increase of mass (Fig. 3.3). The deposition of a single monolayer of the stearic acid on the crystal adds an additional mass of  $2.5 \times 10^{-7} \text{ g/cm}^2$  (for a 38 mN/m transfer surface pressure). This agrees well with the theoretical estimate based on the molecular area of the stearic monolayer in the condensed state. At this state, the area per molecule is  $\sim 20 \text{ \AA}^2$  (for a single alkyl chain) (Davies and Rideal, 1963). The quantity of stearic acid molecules in a monolayer of  $1 \text{ cm}^2$  is equal  $1 \times 10^{16} / 20 = 5 \times 10^{14}$ . The mass of one stearic acid molecule equals  $284 \text{ g/mol} / 6.023 \times 10^{23} \text{ molecules/mol} = 4.72 \times 10^{-22} \text{ g}$ . The mass of the single monolayer then is  $1 \times 5 \times 10^{14} \times 4.72 \times 10^{-22} \text{ g} = 2.4 \times 10^{-7} \text{ g}$ . This compares well with our experimental value of  $2.5 \times 10^{-7} \text{ g}$ .

### 3.3. Specificity and selectivity of bacterial binding

Response curves obtained by exposing the sensor to test suspensions containing different concentrations of the bacteria are characterized by fast reaction, the attainment of a steady-state, and very low non-specific binding (Pathirana et al., 2000). In Fig. 3.4,

curve 1, the mean values of the steady-state output sensor voltages are plotted as a function of bacteria concentration from  $10^2$  to  $10^{10}$  cells/ml. The dose response is linear over five decades of bacterial concentration ( $R > 0.98$ ,  $p < 0.001$ ). Sensor sensitivity, measured as a slope of the linear portion of the dose response, is  $18 \pm 5$  mV per decade of *S. typhimurium* concentration, based on experiments from 112 sensors. Each of these sensors possesses an individual sensitivity and dose-response characteristic of its preparation. The interaction of *S. typhimurium* with the antibody is specific because the sensor does not respond to the bacteria preincubated with the antibody (Fig. 3.4, line 2). The estimated Hill coefficient,  $n$ , was found to be equal to  $0.45 \pm 0.02$  (Pathirana, et al., 2000), indicating that two binding sites were required to anchor one bacterial cell to the sensor surface. Fig. 3.5 shows the selectivity of the sensor. Line 1 represents the dose response of the *Salmonella* biosensor to *S. typhimurium* in the presence of  $5.6 \times 10^8$  cells of *E. coli*. Line 2 shows the dose response of the same sensor to *E. coli* within the same range of concentration when *S. typhimurium* is not present. For any given concentration the sensor response for *S. typhimurium* is greater than that for *E. coli*. A marked response difference for *S. typhimurium* over *E. coli* was observed even when the number of *E. coli* exceeded the number of *S. typhimurium* by a factor of 1000. Non-specific interactions of the sensor with *E. coli* were small and compared well with those found using an antibody-immobilized QCM sensor (Park et al., 2000; Si et al., 2001; Su et al., 2001; Wong et al., 2002).

### 3.4. Effects of rigid and flexible positioning of bacteria on the apparent mass measured by AWD

The bacterial microenvironment and location of the antigen on the surface of a bacterium determines the value and sign of the analytical signal generated by the AWD. When molecules of antigen were located on the surface of the bacterial envelope, providing firm and tight attachment to the sensor surface, the sensor output voltage was found to be directly proportional to the logarithm concentration of free bacteria in the liquid adjacent to the sensor surface (Fig. 3.6A, upper line). The lower line of Fig. 3.6A indicates that bacteria not possessing antigen matching the sensor antibody do not bind to the sensor surface. In contrast, when the antibody was against the antigen located in the bacterial flagellum, the attachment allowed a great degree of freedom (rotation and oscillation) so that the output signal of the sensor was inversely proportional to the logarithm of free bacteria in solution (Fig. 3.6B, lower line). Again, bacteria having no matching antigen did not bind to the sensor surface (Fig. 3.6B, upper line). The decrease in voltage output of the sensor corresponds to an increase in the resonance frequency of the sensor and hence an “apparent decrease” in effective mass of bacteria attached to the surface. When sensors with somatic O antibodies against *Salmonella* were subjected to environmental aging, the type of attachment of bound bacteria was found to depend on the time of exposure. The flexible positioning of bacteria on the sensor surface replaced the rigid binding as time increased. With rigid positioning of bacteria, dose response plots were identical to those shown in Fig. 3.6A (upper line). When flexible positioning of bacteria became dominant and mobility of bound cells increased, the dose response

signal became similar to that of flagella-bound cells shown in Fig. 3.6B (lower line). As an example, Fig. 3.7 demonstrates decreased voltage responses from a somatic antibody *Salmonella* sensor aged for six days at 4 °C as the *S. typhimurium* concentration increased. When bacteria were bound with mixed positioning, the dose response signal depended on the relative contribution of cells with predominantly rigid or predominantly flexible attachment (Fig. 3.8). Control experiments with fresh (not environmentally aged) *Salmonella* sensors measuring *S. typhimurium* in poultry fluids, and poultry fluids containing no *S. typhimurium*, demonstrated low non-specific adsorption (Olsen, 2000).

If the sensitivity of the biosensor is defined as the slope of the linear portion of the dose response (signal  $\Delta V$  in mV/decade of *S. typhimurium* concentration) then the sensitivity of the sensors is expected to be a positive or negative value for predominantly rigid or flexible positioning, respectively. The experimental dose response data for environmentally challenged sensors was fitted by a linear regression analysis to a line  $\Delta V = A + S \times \log (C)$ ; the slope of the line (sensitivity),  $S$ , and regression coefficient,  $R$ , were calculated for each sensor. We found that the  $R$  ranged from approximately + 0.98 (direct linear correlation), through zero (no linear correlation) to – 0.98 (inverse linear correlation) for positive, zero, and negative sensitivities, respectively (*cf.* Appendix). Fig. 3.8 shows the experimental regression coefficient as the function of sensitivity of *Salmonella* sensors. The majority of the aged sensor sensitivity values for measurements carried out between 4 °C and 33 °C fell between – 30 and + 30 mV/decade. These results clearly indicate that the acoustic wave sensor has acceptable analytical value for detecting bacteria only if positioning of bacteria on the sensor surface is either predominantly rigid or predominantly flexible. In mixed cases, the sensitivity and regression coefficient for

dose response signals are not favorable for the effective detection of bacteria. The practical resolution for this phenomenon would be to ensure adequate bacterial binding by using antibodies (or another biorecognition component) with high affinity and multiple binding valences. If antibodies are used, then they should be specific for either somatic or flagella proteins and they must not to be used simultaneously on the same acoustic wave sensor.

Observed changes of apparent mass as a function of bacterial concentration are hypothesized to be due both to viscoelastic changes of the LB film-bacteria near surface fluid media and the mass change associated with binding of the bacteria. The most peculiar results show that under certain controlled conditions there is a manifestation of a negative apparent mass; i.e., with increasing bacterial concentration there can be a dose dependent decrease of the apparent mass. The exact mechanism producing the negative apparent mass is not known. However, this effect may be due to different physical, chemical, and biological mechanisms. These include electrochemical interaction between cells and the diffusion layer of ions on the sensor/liquid interface, high frequency electrophoretic driving force, the viscoelasticity of bacterial cells, and physiological effects including electromechanical forces created by the live, moving organisms.

There are two very different positions where bacterial antigens may bind with antibodies immobilized on sensor surfaces: O somatic antigens, derived from the outer membrane of bacteria, and H antigens, derived from flagella proteins. Fig. 3.9 shows these different binding sites and at least three different ways in which the bacterial cells may bind to the sensor surface. Viscoelastic properties of the bacterial layer attached to



the surface are anticipated to be different depending on the mechanism of binding: somatic or flagellar. As well, the viscous shear and viscous drag forces of the attached bacteria are very different. Clearly, bacteria rigid and flexibly attached (Fig. 3.9A and B) take different roles in the oscillation of the whole system. When binding is rigid, bacteria oscillate in unison with the sensor and therefore contribute to the effective oscillating mass of the system. This is shown by the increase of the apparent mass when bacterial binding concentration is increased. Conversely, in the case of flexible attachment, the oscillation of the bacteria may be not in phase with the oscillation of the sensor, resulting in a decrease in the apparent mass even when concentration of binding bacteria is increased. Additionally, the electrically charged bacterium on the surface of an acoustic wave sensor is not only engaged in the mechanical oscillations of the crystal but also directly interacts with the electric field driving the sensor crystal. This field drives the piezoelectric quartz crystal and at the same time creates an electrophoretic force applied to the electrically charged bacteria. The piezoelectric and electrophoretic forces can be of different values and directions, depending on positioning of bacteria by O antigen (firm positioning, Fig. 3.9A) or H antigen (flexible attachment, Fig. 3.9B) and their combination may contribute to the change of the apparent mass of the bacteria as measured by the acoustic wave device. Obstruction of antibodies by the buildup of indigenous bacteria may cause decreased accessibility to bacterial targets and weak binding (Fig. 3.9C).

#### 4. Conclusions

The results of this work demonstrate the high specificity and selectivity of biosensors for rapid detection of bacteria in liquid samples based on LB antibody monolayers deposited to piezoelectric crystals. A marked selectivity for *S. typhimurium* over *E. coli* was observed even when the number of *E. coli* exceeded the number of *S. typhimurium* by a factor of 1000. Results also indicate the importance of positioning of bacteria on the sensor surface. When attachment of bacteria was rigid and strong the responses obtained for the interaction of the bacteria with somatic O antibodies on the surfaces of acoustic wave sensors correlated directly with changes in mass imposed at the solid-liquid interface. In contrast, when attachment was flexible – as observed for bacteria attached by flagella to flagellar H antibodies – the sensor signals were inversely proportional to additional mass, and are probably determined by interfacial viscoelasticity and acoustic and electromagnetic coupling. The responses of environmentally aged sensors with the predominantly rigid or flexible positioning of bacteria were correlated with changes in mass at the solid-liquid interface. Sensor response and binding efficiency, as confirmed by dark-field microscopy, decreased as the duration of sensor environmental aging and temperature increased.

This study, and the previous results of Olsen (2000), indicate that antibody-based acoustic wave sensors have acceptable analytical value for detecting bacteria and could function well as diagnostic sensors or possibly as short-term monitors packaged into food products such as poultry. However, proper positioning of bacteria at the sensor's surface is crucial for consistent results. If antibodies are used, then they should be

specific for either somatic or flagellar proteins and they must not to be used simultaneously on the same acoustic wave sensor. Even so, some sensors exhibit mixed behavior with little linear correlation after only 36 hours of environmental aging. This may be due to surface buildup of indigenous bacteria in poultry fluids, resulting in obstruction of antibodies and decreased accessibility to bacterial targets, or possibly degradation of the antibodies due to bacterial enzymatic excretion products and temperature induced changes. Unfortunately, antibodies possess other numerous disadvantages that may make them an insubstantial biological recognition component for use on a long-term commercially viable detector for food safety and security, such as cost of production, standardization, availability, and reusability. A possible resolution to ensure adequate bacterial binding and sensor consistency may be another biorecognition component with equally high affinity and multiple binding valences, yet capable of addressing the drawbacks of antibodies. In Chapter IV, the use of phage display techniques to derive bacteria-specific bacteriophage as probes to overcome the weak points of antibodies is described.

## Appendix

### *Simplified analysis of the thickness-shear mode acoustic resonator*

The acoustic wave resonator (Fig.10A) admittance can be expressed by the equation:

$$Y(\omega) = j\omega C_o + 1/Z_m, \quad (1)$$

where  $\omega$  is the angular frequency

$$\omega = 2\pi f, \quad (2)$$

$C_o$  is the static capacitance of the quartz sensor (parasitic capacitance is neglected), and  $Z_m$  is the motional impedance for the unloaded resonator (Martin, et al., 1991).

$$Z_m = R + j\omega L + 1/j\omega C, \quad (3)$$

where  $R$ ,  $L$ , and  $C$  are the resistance, the inductance and capacitance of the motional arm in parallel with the capacitance  $C_o$ . The series resonant frequency  $f$  can be determined as

$$f = \frac{1}{2\pi} (LC)^{1/2}. \quad (4)$$

When the resonator is loaded with solutions the resonant frequency changes due to small changes of parameters  $L$  and  $C$ . The differential of resonant frequency,  $df$ , can be calculated as:

$$df = (\partial f / \partial L) dL + (\partial f / \partial C) dC, \quad (5)$$

where partial derivatives  $\partial f / \partial L$  and  $\partial f / \partial C$  can be calculated from Eq. (4):

$$\partial f / \partial L = -(f/2)/L \quad (6)$$

$$\partial f / \partial C = -(f/2)/C. \quad (7)$$

Substituting partial derivatives with Eqs. (6) and (7), and replacing the differentials  $df$ ,  $dL$ , and  $dC$  with small changes of the values, we have:

$$\Delta f / f = -1/2 \times (\Delta L / L + \Delta C / C). \quad (8)$$

Eq. (8) fully agrees with Eq. (27) of Martin et al. (1991) if we consider that  $\Delta C / C = 0$ . If binding bacteria increases the effective mass of the resonator then the serial inductance ( $L$ ) representing a mass in the equivalent-circuit model, should increase with the increase of bacteria concentration. On the other hand, the binding of the bacteria increases the effective thickness of the resonator and, consequently, decreases the equivalent capacitance ( $C$ ) of the circuit. The firmly attached dense layer of bacteria creates a small increase of the thickness and the increase in thickness is proportional to

the increase in mass. However, bacteria attached by flagella can be separated from the surface as far away as 5 - 7  $\mu\text{m}$ . In this case, the increase of the effective thickness of the bound layer is not proportional to the mass of bacteria because they occupy only a fraction of the layer. The electrically charged layer of bacteria spatially separated from the sensor surface can create a charge distribution, which is equivalent to the serial capacitor connected to the equivalent capacitor of the crystal. We can speculate, further, that relative changes of the inductance and capacitance are linear functions of the bacterial concentration ( $C$ ):

$$\Delta L/L = \alpha \log(C) \quad (9)$$

$$\Delta C/C = -\beta \log(C), \quad (10)$$

where coefficients  $\alpha$  and  $\beta$  are independent of bacteria concentration.

From Eqs. (8) – (10) we have:

$$\Delta f/f = -1/2 \times \alpha(1-\beta/\alpha) \log(C). \quad (11)$$

The output voltage ( $V$ ) of the Maxtek PM-740 plating monitor (acoustic wave device) is inversely related to frequency  $f$ . So, we can replace  $\Delta f/f$  with  $-\Delta V/V$  in Eq. (11):

$$\Delta V/V = 1/2 \times \alpha(1-\beta/\alpha) \log(C). \quad (12)$$

Eq. (12) indicates that if the relative increase of the effective thickness is small compared to increase of the effective mass ( $\alpha > \beta$ ) then the relative change of the voltage ( $\Delta V/V$ ) is directly proportional to the logarithm of bacteria concentration (Fig. 10B, line  $\alpha > \beta$ ). If the opposite is true, and  $\alpha < \beta$ , then  $\Delta V/V$  is inversely related to the concentration of bacteria (Fig. 10 B, line  $\alpha < \beta$ ). If  $\alpha = \beta$  then  $\Delta V/V$  does not depend on the bacteria concentration (Fig. 10B, line  $\alpha = \beta$ ):

$$\Delta V/V \sim 1/2 \times \alpha \log(C), \text{ if } \alpha > \beta; \quad (13)$$

$$\Delta V/V \approx 0, \alpha \approx \beta; \quad (14)$$

$$\Delta V/V \sim -1/2 \times \beta \log(C), \text{ if } \alpha < \beta. \quad (15)$$

When experimental dose response data are fitted by a linear regression analysis to a line  $\Delta V/V = A + B \log(C)$ , the slope of the line (sensitivity),  $B$ , and the regression coefficient,  $R$ , are calculated for each sensor. When  $\alpha > \beta$ , a good positive correlation with a large slope (sensitivity) is also expected to be confirmed by a high regression coefficient ( $R \approx 1$ ). If  $\alpha < \beta$ , the regression coefficient at a large negative slope tends to approach a large negative value ( $R \approx -1$ ). At conditions when  $\alpha \approx \beta$ ,  $R \approx 0$ . Thus, the regression coefficient can be a function of the slope and can vary from  $-1$  to  $+1$ , for different sensors with an inverse and direct concentration dependence, respectively (Fig. 10C).

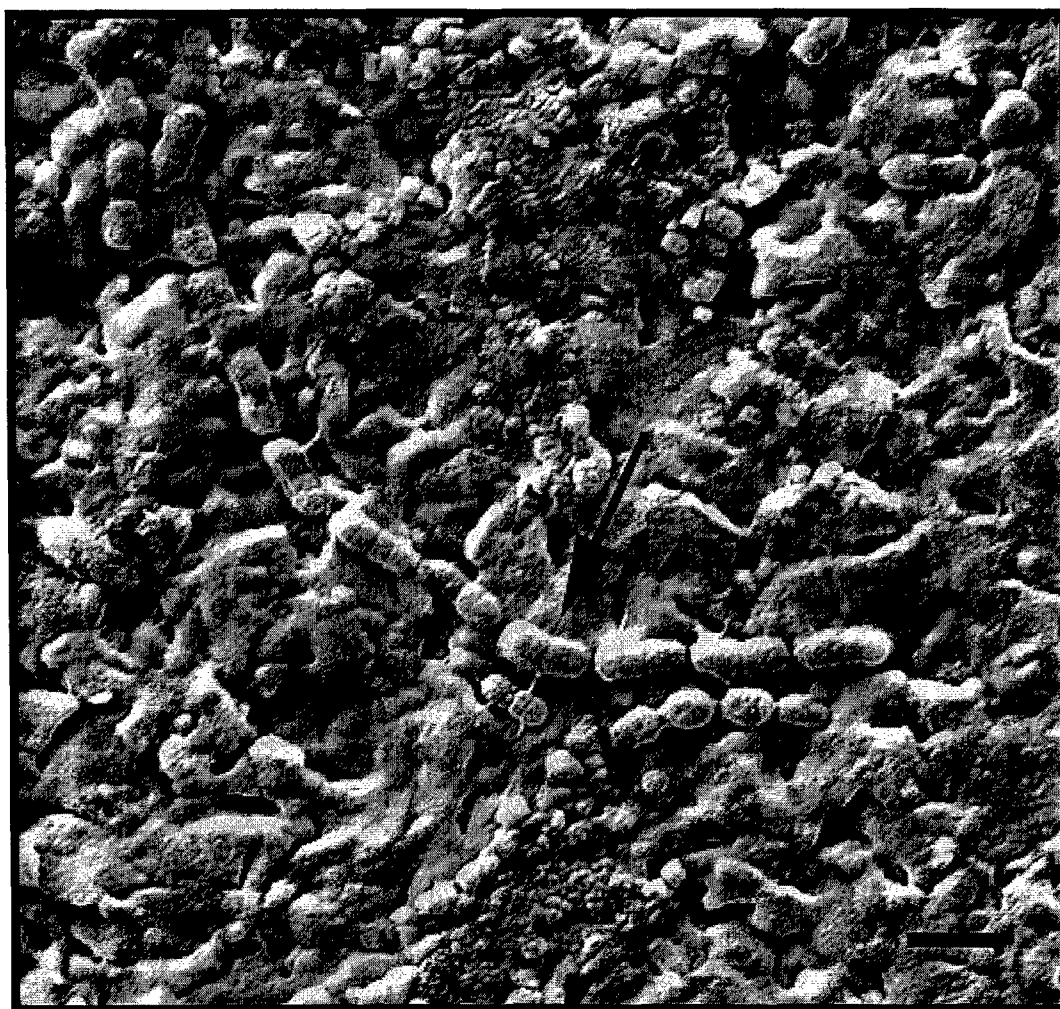


Fig. 3.1. Scanning electron micrograph of the biosensor surface following exposure to *S. typhimurium* (arrow). The bacteria were attached to somatic O antibodies deposited by Langmuir-Blodgett method to the gold electrode surface of an unpolished resonator. Filaments holding bacteria at the surface are visible opposite arrow. Magnification,  $\times 5000$ ; bar = 5  $\mu\text{m}$ .



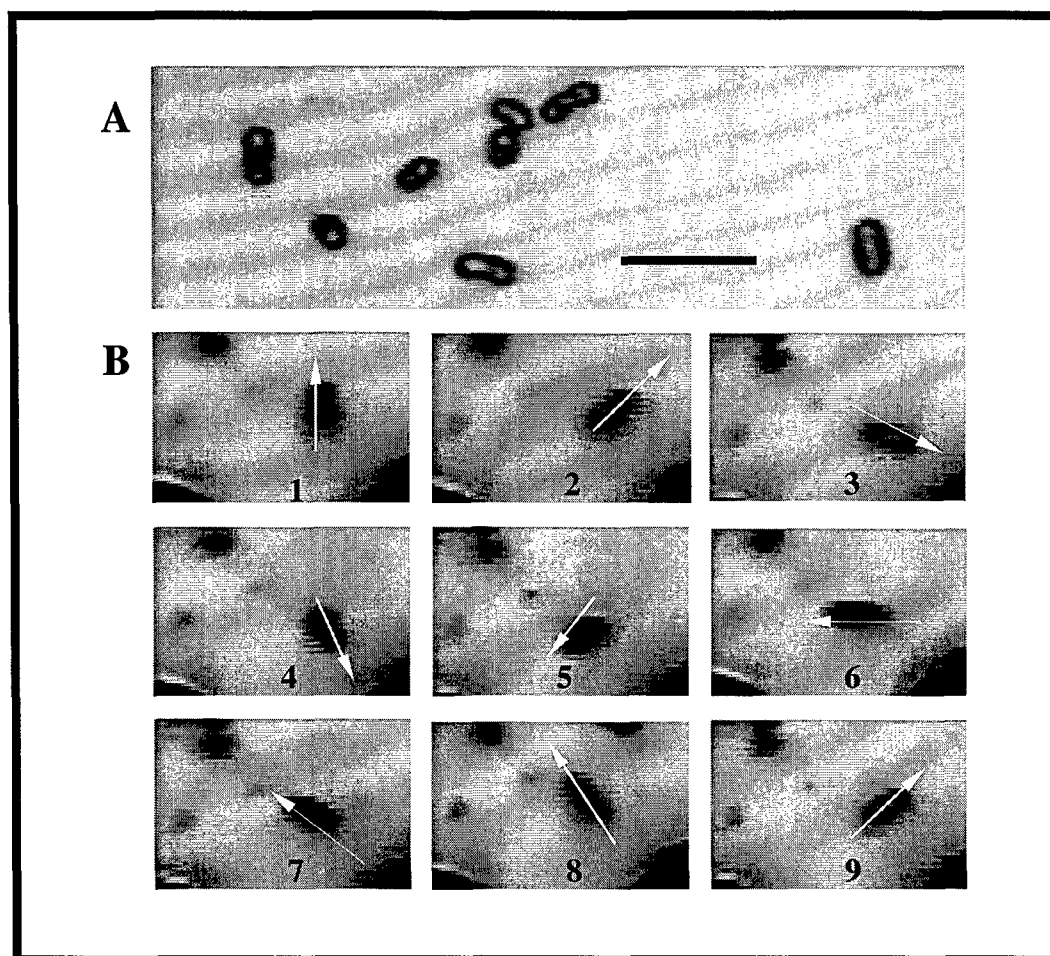


Fig. 3.2. Dark-field microscopy images of bacteria at the surface of the acoustic wave sensor. The images represent time-lapse frames (100 ms intervals) from continuous real-time video recordings. (A) Rigid attachment of *S. typhimurium* in PBS to the sensor surface by somatic O antibody. The attached bacteria did not exhibit movement. Bar = 4 μm. (B) Flexible attachment of bacteria to the sensor surface by the flagellar H-type antibody allowed oscillation and rotation of cells at the crystal surface. Sequential photographs (1–9) depict clockwise rotation of bacterium attached to the antibody by its flagellum. Arrows indicate relative direction during rotation.

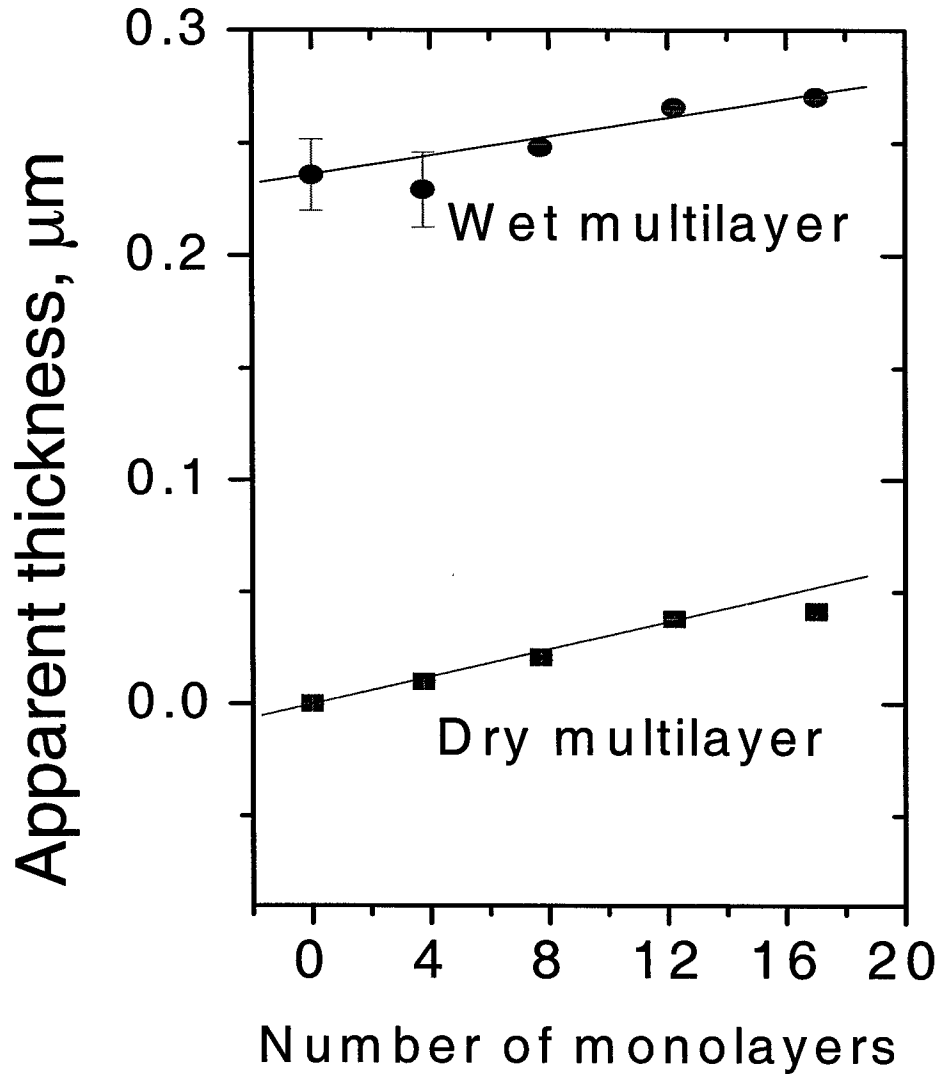


Fig. 3.3. Validation of measuring mass of bound monolayers by acoustic wave sensor.

The experimental thickness of multilayer is a linear function of the number of stearic acid monolayers transferred to the sensor surface. The labels “wet multilayer” and “dry multilayer” indicate sensors that were immersed (in buffered solution) and dry, respectively. Straight lines represent linear least squares fit to the data points (Wet:  $R = 0.921$ ,  $p < 0.02$ ; Dry:  $R = 0.998$ ,  $p < 0.0001$ ). Bars are SD.

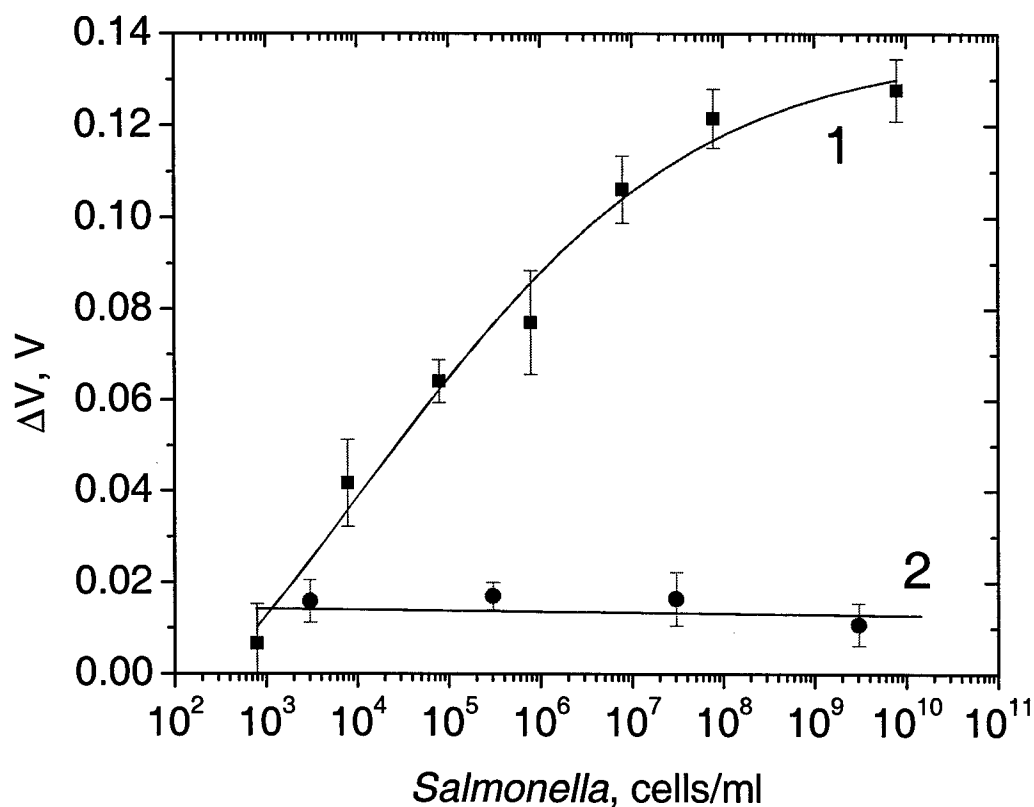


Fig. 3.4. Specificity of *Salmonella* sensor. Curve (1) is the sigmoidal fit ( $X^2 = 5.9 \times 10^{-5}$ ) to mean values of steady-state sensor voltages as a function of *S. typhimurium* concentrations ranging from  $10^2$  to  $10^{10}$  cells/ml. Line (2) is a linear least squares fit ( $R = -0.76$ , slope =  $-9.0 \times 10^{-5}$  V/decade) to the dose response of the sensor exposed to *S. typhimurium* suspensions incubated with *Salmonella* antibodies prior to the exposure.  $1.2 \times 10^9$  cells were incubated with *Salmonella* antibodies ( $\approx 200 \mu\text{g}$ ) in 1 ml of PBS for 3 h 40 min. Experimental data points were obtained by averaging approximately 200 data points of each steady-state level response curve. Bars are SD.

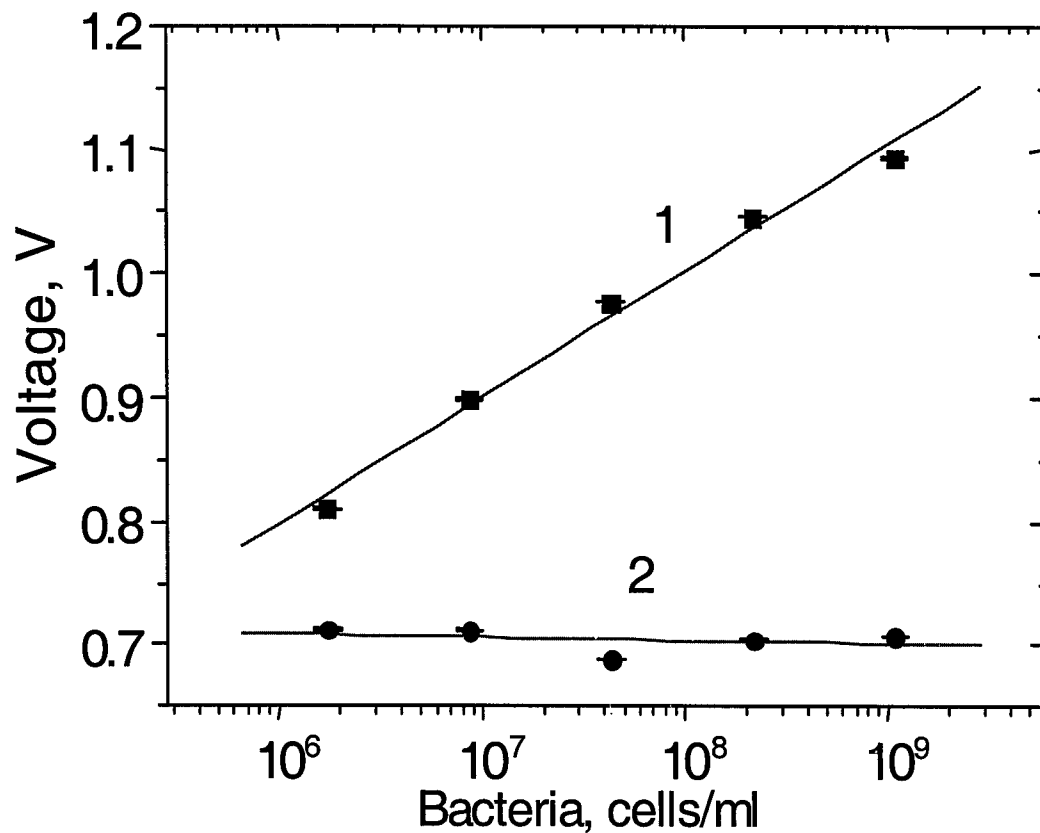


Fig. 3.5. Selectivity of *Salmonella* sensor. Line (1) is the linear least squares fit ( $R = 0.97$ ) to mean values of steady-state output sensor voltages as a function of *S.*

*typhimurium* concentrations from  $1.8 \times 10^6$  to  $10^9$  cells/ml in the presence of  $5.6 \times 10^6$  cells/ml of *E. coli* O157:H7. Line (2) is a linear least squares fit ( $R = -0.71$ ) to dose responses of the sensor exposed to *E. coli* O157:H7. The voltage output was scaled up by a factor of five. Bars are SD.

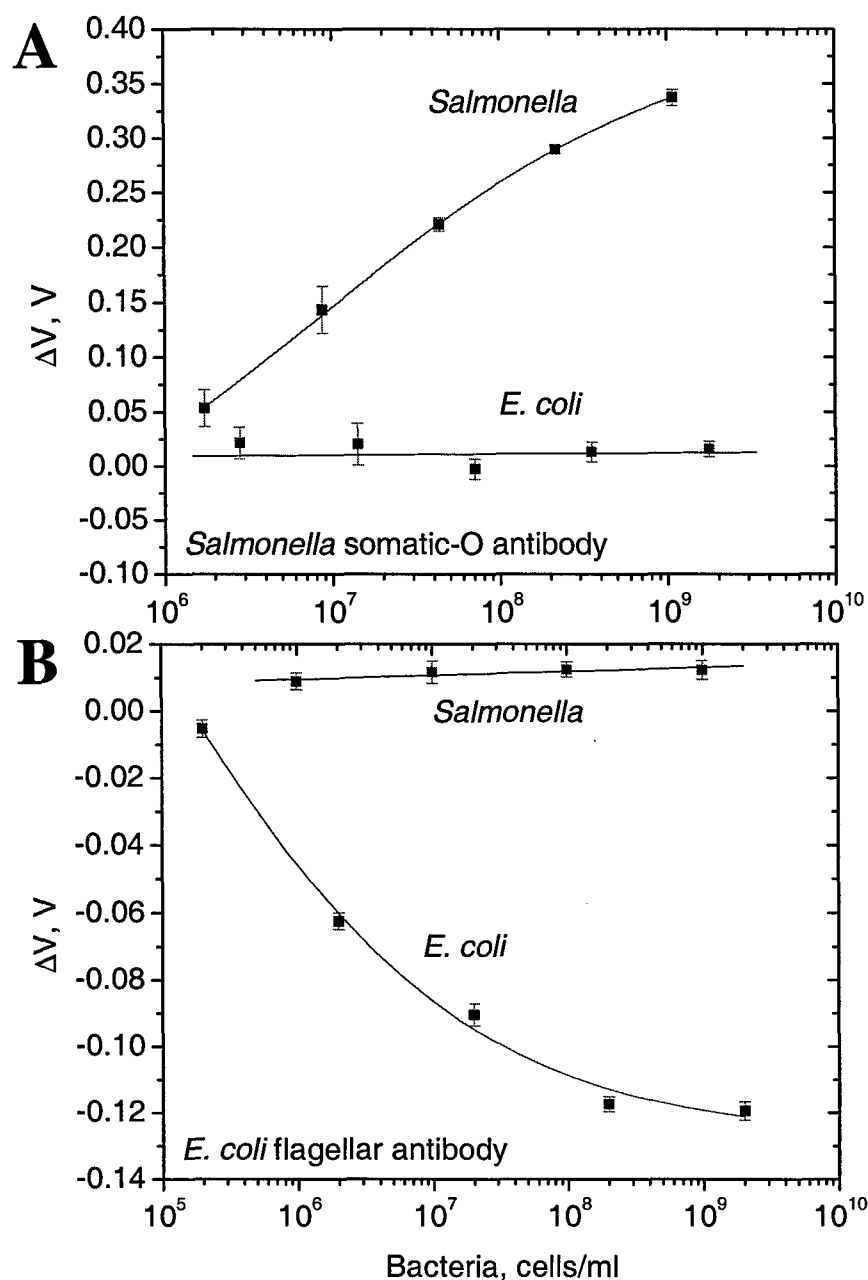


Fig. 3.6. Dose responses for rigid and flexible positioning of bacteria on biosensor.

Graph (A) shows *Salmonella* and *E. coli* dose responses to sensor prepared with somatic O *Salmonella* antibodies. Graph (B) shows *Salmonella* and *E. coli* dose responses to sensor fabricated with flagellar H-type *E. coli* antibodies. Curves are sigmoid fit to experimental data; straight lines are the linear least square fit. Bars are SD.

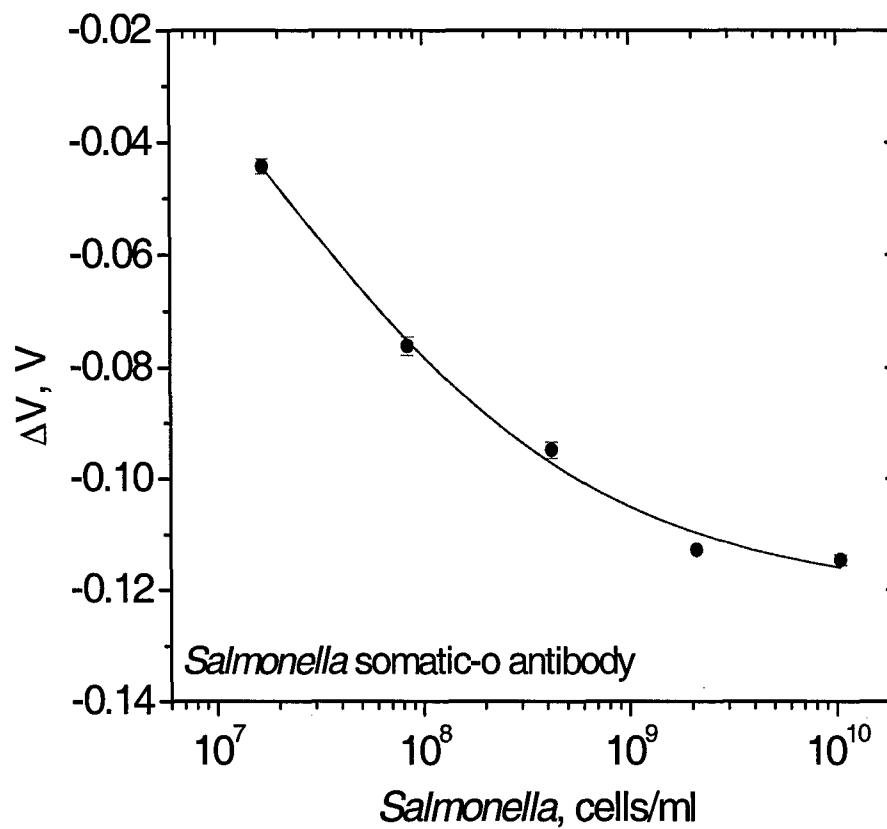


Fig. 3.7. Experimental dose responses of sensor fabricated with somatic O *Salmonella* antibodies and environmentally aged for six days at 4 °C. Curve is a sigmoidal fit to experimental data points, obtained by averaging approximately 200 data points of each steady-state level response curve. Bars are SD.

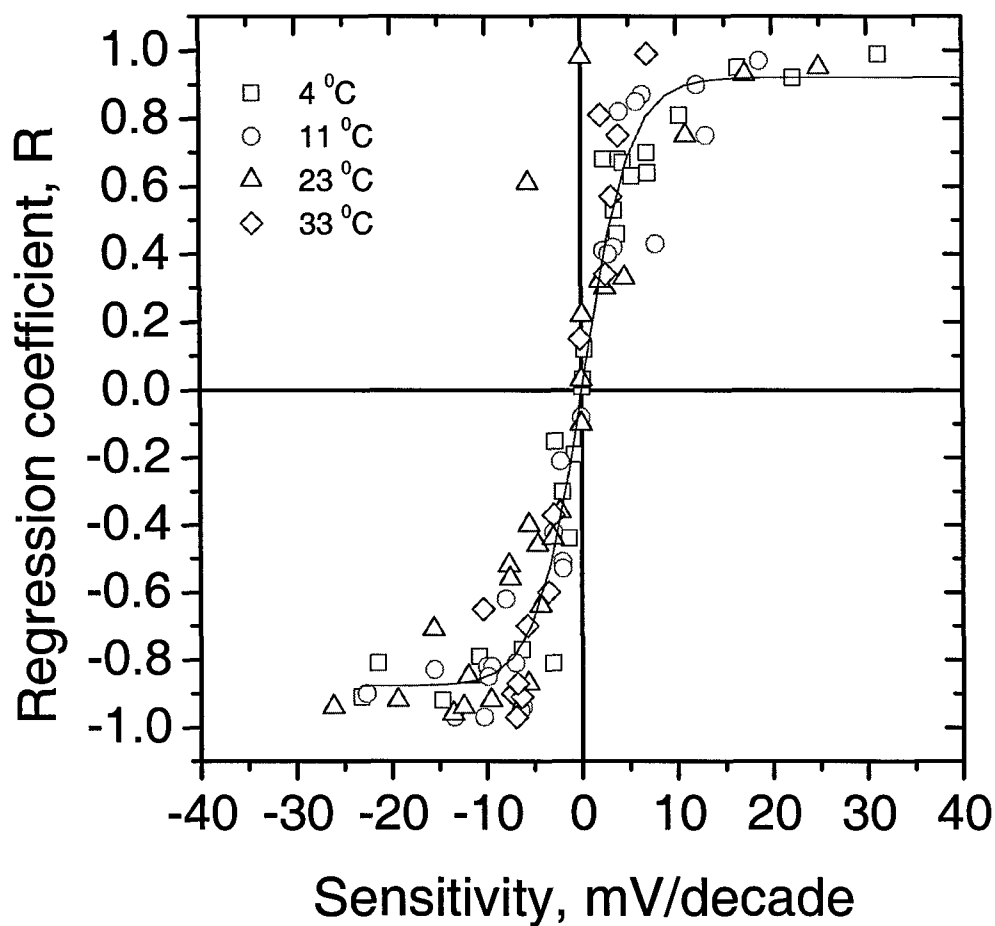


Fig. 3.8. The experimental regression coefficient as a function of sensitivity for environmentally aged *Salmonella* sensors prepared with somatic O antibodies. The linear portions of dose response signals were fitted by linear regression. Curve is the sigmoidal fit to experimental data points at indicated temperatures.

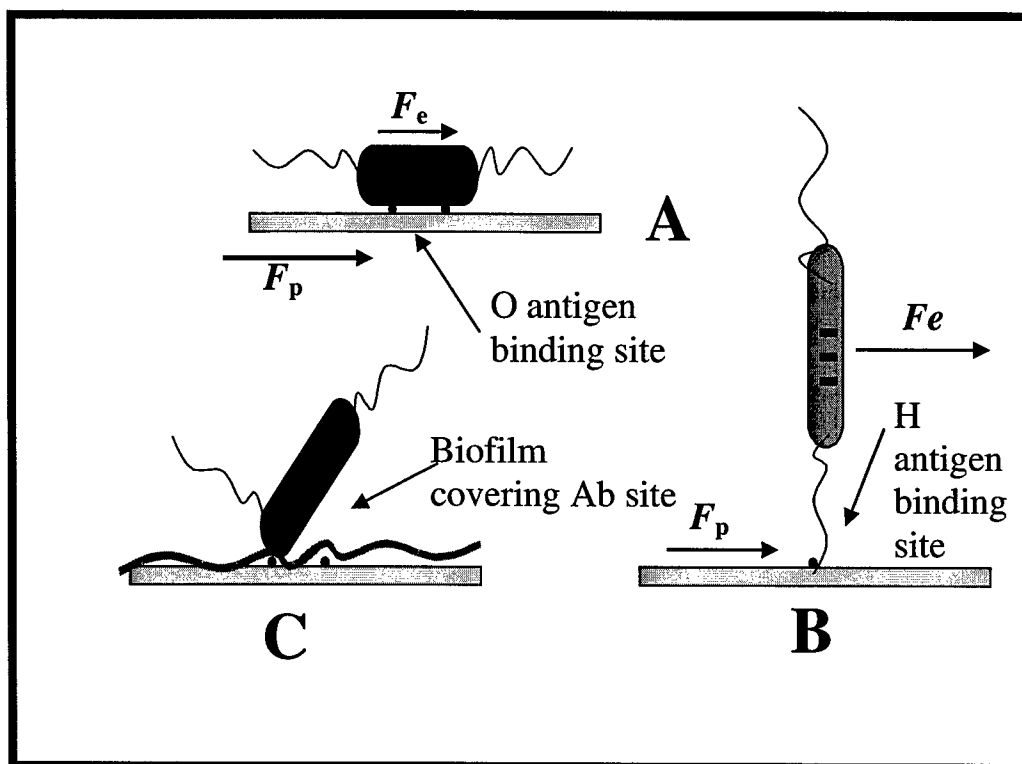


Fig. 3.9. Different positioning of bacteria at the surface of biosensor. (A) The rigid attachment of bacteria by somatic O antibodies. The bacterium moves in unison with the sensor. The electrophoretic force ( $F_e$ ) applied to the electric charges of bacterium (“-”) is aligned with the cell body. The piezoelectric force ( $F_p$ ) causes the particle displacement at the surface of TSM sensor. (B) The flexible attachment of bacteria by flagellar H-type antibodies. The bacteria have a high degree of freedom and the displacement of the resonator may be not in phase with the displacement of the bacteria. (C) In aged sensors, a biofilm may cover certain antibody (Ab) binding sites and guards against polyvalent attachment of bacteria. As a result, the bound bacteria have a higher degree of freedom than the bacteria with the firm attachment.



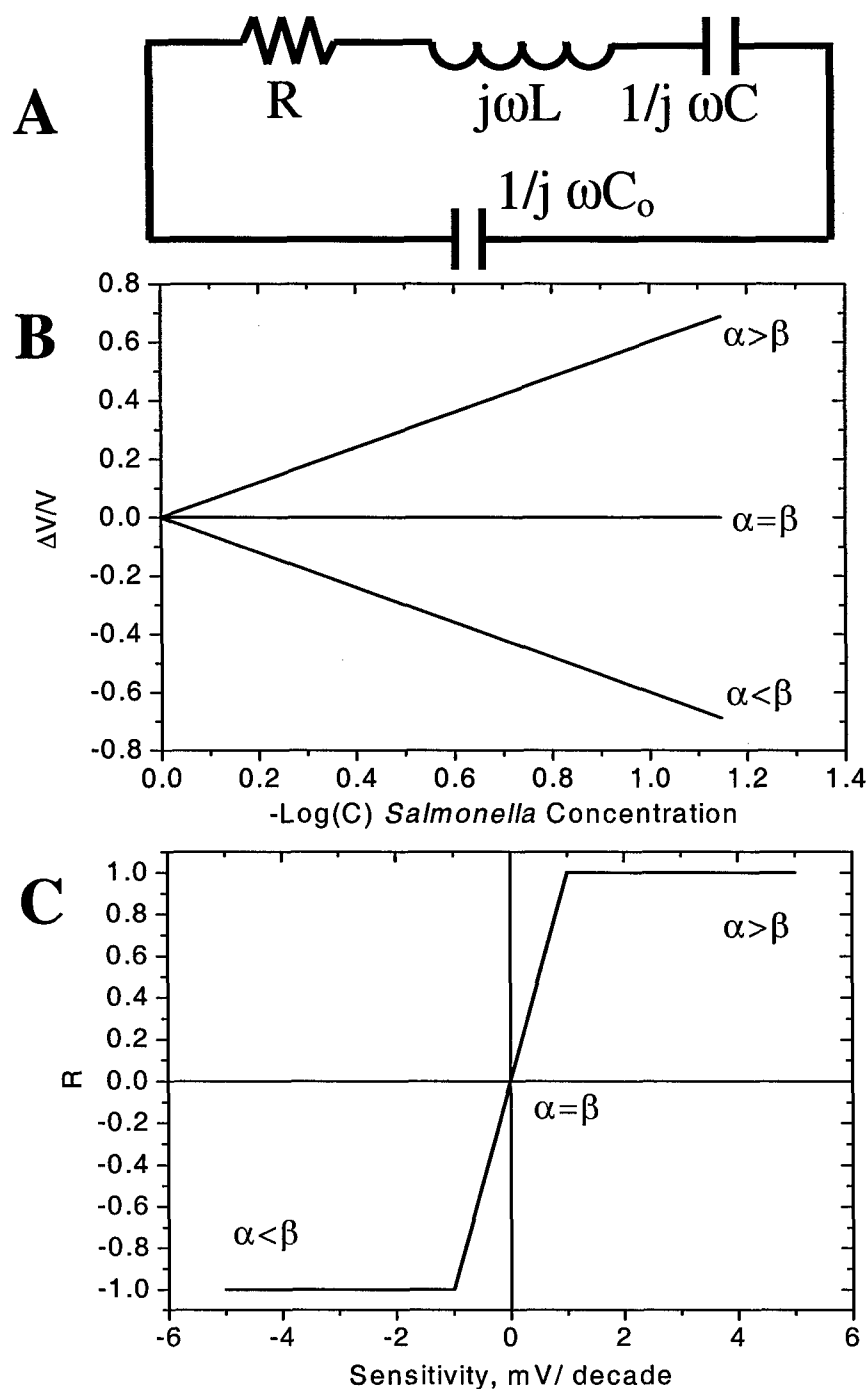


Fig. 3.10. Simplified electrical model of biosensor. (A) Equivalent circuit of TSM resonator (Martin et al., 1991): a capacitance  $C_0$  in parallel with resistance  $R$ , inductance  $L$ , and functional capacitance  $C$ . (B) Dose response dependency described by Eq. (13). (C) Plot of the regression coefficient as a function of the sensor's sensitivity.

## CHAPTER IV

### LANDSCAPE PHAGE PROBES FOR *SALMONELLA TYPHIMURIUM*

#### Abstract

Bacteriophage-based probes that preferentially bind *Salmonella enterica* serovar Typhimurium (*S. typhimurium* ATCC 13311) were selected from a landscape library. Specificity of probes for *S. typhimurium* was determined by modified enzyme-linked immunosorbent assays, and precipitation assay. Selectivity in comparison to other Enterobacteriaceae and dose-dependent binding of select phage to *S. typhimurium* was analyzed by co-precipitation and titration assays, respectively. Fluorescence-activated cell sorting, and fluorescence, optical, and electron microscopy were used to visually characterize binding of select probes to *S. typhimurium*. Results indicate that phage landscape libraries can be used to select highly specific and selective probes for *S. typhimurium*, which may be suitable for use in continuous food and environmental monitoring devices, diagnostic assays, and biosorbents.

## 1. Introduction

Bacterial identification has long been a central tenet of bacteriology, dating back nearly 300 years to Anton Von Leeuwenhoek, who first attempted visualization of bacteria using naturally occurring coloring agents such as beet juice (Wainwright and Lederberg, 1992). Later, Robert Koch developed a heat-mediated staining process using methylene blue for the identification of tubercle bacillus, while Hans Christian Gram elaborated a staining procedure for the differentiation of bacteria based on cell wall components (Donnelly, 1962) that is still widely used today. Since then, numerous methods – including most recently molecular based probes – have been developed for bacteria detection, the majority of which attempt to incorporate speed and simplicity (Dziadkowiec et al, 1995; Madonna et al., 2001; Mansfield and Forsythe, 2000; Meckes and MacDonald, 2003). Simplified, rapid identification is especially important for pathogenic foodborne bacteria such as *S. typhimurium*, which ranks as a leading etiology of foodborne gastroenteritis in the United States (Mead et al., 1999).

Traditional identification of *S. typhimurium* is based on cell culture using differential and selective media (Dusch and Altwegg, 1995). Batteries of carbohydrate utilization and biochemical tests are also available. However, these techniques may take as many as 4 – 5 days to confirm identity. Advanced methods available for *S. typhimurium* detection include polymerase chain reaction (PCR) (Peng and Shelef, 2001; Sanath Kumar et al., 2003; Tseng et al., 1997), DNA hybridization (Meckes and MacDonald, 2003; Miyamoto et al., 1998; Nastasi et al., 1999), and enzyme linked immunosorbent assay (ELISA) (Tapchaisri et al., 1999). While these methods permit

faster identification of microbes in comparison to culture methods, their application to real-time detection and monitoring in food and environmental samples remain in developmental stages due to significant methodological hurdles. As demonstrated in Chapter III (“Specific and selective immunosensor for *Salmonella typhimurium* and its detection in the environment”) and the previous work of the author (Olsen, 2000) and others, biosensors based on bioselective materials such as antibodies have also permitted isolation and detection of microbes. However, the use of antibodies is not without difficulties - high production costs and loss of functionality due to unfavorable environmental conditions such as high temperatures or the presence of organic buildup and solvents have limited their application. Thus, there is a need for resilient, cost-effective capture agents that can be used in conjunction with biosorbents and biosensors, allowing them to operate under diverse environmental conditions for the immediate detection of targeted organisms like threat agents such as *S. typhimurium*.

Bacteriophage (“phage”) represent a likely source of resilient, cost-effective capture agents for bacteria. They are intrinsically specific to host bacteria and survive under severe environmental conditions (Bennet et al., 1997; He and Pan, 1992). There have been numerous attempts to use phage for specific probing of *Salmonella*. In the early 80’s, Hirsh and Martin (1983a, 1983b) utilized phage F01 for the detection of *Salmonella* in milk by HPLC. F01 was also utilized by Bennett et al. (1997) as a biosorbent probe for *S. enteritidis* separation, concentration and detection in food. Recombinant phage containing a luciferase-encoding gene was also recently used for the detection of *Salmonella* (Kuhn et al., 2002). While these studies represent good first

prospects for demonstrating the feasibility of phage as a substitute antibody probe, the lytic character of the phage would appear to limit their application.

Recent studies of landscape phage – filamentous viruses of *Escherichia coli* – have demonstrated it's suitable as a durable, specific diagnostic probe and biosorbent for various analytes (Petrenko et al., 1996). Probes using Ff class phage fd can be affinity-selected from phage display libraries constructed by recombinant technique (Smith and Petrenko, 1997). The outer coat of the phage is dominated by multiple copies of major protein pVIII, which form a tube encasing the viral DNA and comprises 87% of the phage mass (Bonnycastle et al., 2001). The landscape phage library is created by splicing degenerate, synthetic oligonucleotides in-frame into the pVIII protein-encoding gene VIII so that corresponding expressed foreign peptides are fused to the major outer coat protein and thereby displayed as diverse “organic landscapes” on the surface of the virions (Petrenko et al., 2002; Petrenko et al., 1996; Smith and Petrenko, 1997). Thus, a library represents a huge population of designer phage clones possessing billions of different surface structures and biophysical properties.

Landscape phage have served as substitutes for antibodies against various soluble and cell-displayed antigens and receptors (Legendre and Fastrez, 2002; Petrenko and Smith, 2000; Petrenko et al., 2002; Romanov et al., 2001; Samoylova et al., 2003), including bacterial spores and cells (Brigati et al., 2004; Petrenko and Sorokulova, 2004), and have been used in conjunction with ELISA and thickness shear mode acoustic wave biosensors to detect bacterial and mammalian antigens (Petrenko and Smith, 2000; Petrenko and Vodyanoy, 2003). Phage-derived probes inherit the extreme resilience of wild-type phage and allow fabrication of bioselective materials by self-assembly of

phage or its composites on metal, mineral, or plastic surfaces. In this chapter, affinity selection techniques are utilized for the isolation of *S. typhimurium*-complementary phage clones from a landscape phage library. The results validate the concept of landscape phage as antibody substitute probes for the detection of biological threat agents.

## **2. Materials and methods**

### *2.1. Organisms*

*2.1.1. Bacterial cultures.* *Salmonella typhimurium* ATCC 13311 was obtained from the American Type Culture Collection (Rockville, MD). *Escherichia coli* ATCC 25922, *Proteus mirabilis* ATCC 25933, *Enterobacter aerogenes* ATCC 13048, *Citrobacter freundii* ATCC 8090, *Shigella flexneri* ATCC 12022, *Klebsiella pneumoniae* ATCC 13882, *Yersinia enterocolitica* ATCC 9610, *Serratia marcescens* ATCC 13880, and *Pseudomonas aeruginosa* ATCC 27853 were acquired from the Auburn University (Department of Biological Sciences, Auburn, AL) culture collection. Isolates were previously confirmed for identity by standard biochemical and serological assays, cell morphology, and pulsed-field gel electrophoresis. All strains were grown in NZY broth, pH 7.5 (1% [w/v] NZ amine A, 0.5% [w/v] yeast extract, 0.5% [w/v] NaCl) or on NZY agar plates (1.1% [w/v] Bacto-agar, 50% [v/v] NZY broth) at 37 °C. Stock organisms were maintained in NZY broth containing 20% (v/v) glycerol at – 20 °C. Aseptic technique was followed throughout all procedures and henceforth.

*2.1.2. Bacterial suspensions.* Bacterial suspensions for selectivity testing were prepared for each respective organism as follows. A starter culture was prepared by inoculating one isolate from a respective plate into 3 ml NZY broth, followed by incubation for 3 h in an orbital shaker-incubator (New Brunswick Scientific, Edison, NJ) (37 °C,  $\approx$  200 rpm). One ml of the culture was inoculated into 25 ml NZY broth and incubated overnight (approximately 18 h) in an orbital shaker-incubator (37 °C,  $\approx$  200 rpm). The overnight culture was washed by centrifugation (Allegra 21R, Beckman Coulter, Fullerton, CA) (5500 rpm, 15 min, 10 °C) in phosphate buffered saline, pH 7.0 (0.15 M NaCl, 5 mM NaH<sub>2</sub>PO<sub>4</sub>) (PBS) with final resuspension in 2 ml PBS. For each culture suspension, an aliquot (ranging from 125  $\mu$ l to 600  $\mu$ l depending upon the growth of the inoculum) was added to 4 ml 0.5% (v/v) Tween20 in TBS, pH 7.5 (50 mM Tris-HCl, 0.15 M NaCl) to prepare a suspension of OD<sub>620</sub> 0.8. Sterile NZY broth in a clean 13  $\times$  100 mm glass tube was used to blank the spectrophotometer prior to measurement of culture optical density.

*2.1.3. Starved cells.* *E. coli* K91BlueKan (lacZ $\Delta$ M15 kanamycin-resistant F+) cells prepared as “starved cells” were used for propagation of phage clones. Starved cells were prepared at a high concentration ( $\approx$  10<sup>10</sup> cells/ml) in early logarithmic phase to be nutritionally deficient, thereby promoting transfection by the experimental phage through improved adsorption of phage to the F pilus. For each organism used in selectivity testing, starved cells were prepared in duplicate following the procedure of Yu and Smith, 1996. One colony of *E. coli* K91BlueKan cells from a NZY + kanamycin (100  $\mu$ g/ml) isolation plate was inoculated into 3 ml sterile NZY broth + kanamycin (100  $\mu$ g/ml) then incubated overnight (approximately 18 h) in an orbital shaker-incubator (37

°C,  $\approx$  200 rpm). Three hundred microliters of overnight culture was inoculated into a 250 ml 12 mm side-arm culture flask (with aluminum culture cap) containing 20 ml sterile NZY broth and incubated approximately 2.25 h in an orbital shaker-incubator (37 °C,  $\approx$  200 rpm) to  $OD_{600} \approx 0.45$ . Sterile NZY broth in a clean 13  $\times$  100 mm glass tube was used to blank the spectrophotometer prior to measurement of culture optical density. Cells were incubated at low rotational speed (37 °C,  $\approx$  50 rpm) an additional five minutes to allow regeneration of any sheared F pili then transferred into a polypropylene screw cap Oak Ridge centrifuge tube (Nalgene, Rochester, NY). Cells were pelleted by centrifugation (Model RC5C, SA-600 rotor, Beckman Coulter) (2200 rpm, 10 min, 4 °C), and resuspended gently in 2 ml 80 mM NaCl (pH 7.0). Following resuspension, an additional 18 ml 80 mM NaCl (pH 7.0) was added. The suspension was transferred into a 125 ml Erlenmeyer culture flask with aluminum culture cap and incubated in an orbital shaker-incubator (37 °C,  $\approx$  50 rpm) for 45 min. Suspension was transferred to new Oak Ridge centrifuge tube. Cells were pelleted (2200 rpm, 10 min, 4 °C) and supernatant decanted. Cells were resuspended gently with 1 ml cold (4 °C) NAP buffer, pH 7.0 (80mM NaCl, 50mM  $NH_4H_2PO_4$ , pH adjusted with  $NH_4OH$ ). Starved cells were maintained at 4 °C for use up to 24 h.

## *2.2. Phage growth, purification, and titering*

A landscape f8/8 phage library, containing about two billion different clones, was used as previously prepared (Petrenko et al., 1996). The library was constructed by



replacing amino acids E2, G3 and D4 on every copy of the pVIII coat protein of vector f8-1 (fd-tet derivative) with eight random amino acids.

General procedures used for recombinant phage production and analysis, including media and buffers, are detailed in Bonnycastle et al. (2001). Phage were purified by double PEG precipitation as previously described (Smith and Scott, 1993; Yu and Smith, 1996). The total number of viral particles present in phage preparations was determined spectrophotometrically, where:

$$\text{Virions/ml} = (A_{269} \times 6 \times 10^{16}) / \text{number of nucleotides in phage genome.} \quad (1)$$

The concentration of the recombinant phage in solution (physical titer) (9,198 nucleotides) was calculated from (1), where

$$A_{269} = 6.5 \times 10^{12} \text{ vir/ml.} \quad (2)$$

### *2.3. Selection of Salmonella-binding phage clones*

Salmonella binding phage clones were derived from the landscape library using three selection schemes. In selection procedures “A” and “B,” *S. typhimurium* was adsorbed to a solid substrate. Selection procedure “B” supplemented “A” by first depleting the library against plastic and BSA while using a higher concentration of Tween20/TBS for washing. In selection procedure “C,” phage were first reacted with *S. typhimurium* in solution to form complexes then separated from complexes by a

centrifugal precipitation method. DNA from phage clones isolated by selection procedures was amplified by PCR and sequenced to determine the amino acid structure of the displayed peptides.

*2.3.1. Selection procedure* *A. S. typhimurium* was propagated in 20 ml NZY medium overnight on shaker-incubator (37 °C,  $\approx$  200 rpm), precipitated by centrifugation (5500 rpm for 15 min), then washed (2 $\times$ ) with PBS and finally resuspended in 4 ml PBS. One milliliter of suspension was added to the bottom of a 35 mm polystyrene Petri dish to allow *S. typhimurium*-substrate binding, facilitated by drying overnight at 37 °C. The dish was blocked by adding 0.1% BSA in TBS (1 h, room temperature), then washed 3 $\times$  with 1 ml 0.1% (v/v) Tween20 in TBS (Tween20/TBS). The f8/8 phage library ( $10^{11}$  virions in 400  $\mu$ l TBS, 0.1% BSA) was added to the dish for 1 h at room temperature (RT) to allow phage-*S. typhimurium* binding, then washed (6 $\times$ ) with 1 ml 0.1% Tween20/TBS to remove any non-binding phage. Those phage clones bound to *S. typhimurium* were eluted with 400  $\mu$ l of elution buffer (0.1 N HCl, 1 mg/ml BSA [pH 2.2, adjusted with glycine]) for 10 min at room temperature. Eluate was transferred to a microcentrifuge tube and neutralized with 75  $\mu$ l 1M Tris (pH 9.1). The dish was then washed with 0.5 ml TBS, decanted, and combined with eluate. Eluate was concentrated by centrifugation (Centricon 100 kD unit, Fisher Scientific, Pittsburgh, PA) according to manufacturer's instructions to a final volume  $\approx$  100  $\mu$ l. Any remaining cell-associated phage in the dish were recovered by treating with 250  $\mu$ l DOC lysis buffer (2% sodium deoxycholate, 10mM Tris, 2mM EDTA [pH 8.0]) for 30 min at room temperature.

Eluate and lysate fractions were then propagated separately in *E. coli* K91BK and purified for use in four proceeding rounds of selection by following the same procedures as the first round. Following the fifth round of selection, individual phage clones were propagated in *E. coli* K91BK for use in specificity, selectivity and titration experiments.

**2.3.2. Selection procedure B.** The primary f8/8 phage library ( $10^{11}$  virions in 400  $\mu$ l of 0.1% BSA, 0.5% Tween20/TBS) was added to the bottom of an empty 35 mm plastic Petri dish for 1 h at room temperature. Following incubation, the phage suspension was transferred to another 35 mm plastic Petri dish blocked with 0.1% BSA in TBS (previously incubated overnight at 4 °C) for 1 h at room temperature. Non-binding phage were recovered and transferred to a third 35 mm plastic Petri dish previously coated with *S. typhimurium* and blocked with 0.1% BSA in TBS for 1 h at room temperature, as previously outlined (*cf.* “2.3.1. Selection procedure A”). Three proceedings rounds of selection were performed as previously outlined (*cf.* “2.3.1. Selection procedure A”) with the exception that washes was performed with 0.5% Tween20/TBS. Following the fourth round of selection, individual phage clones were propagated *E. coli* K91BK for use in specificity, selectivity and titration experiments.

**2.3.3. Selection procedure C.** To avoid selection of aggregating and self-precipitating phage clones, the library ( $2 \times 10^{11}$  CFU/ml) was first heated at 70 °C for 10 min. Tween20/TBS was then added to a 0.5% final concentration. The suspension was centrifuged (13000 rpm, 15 min, RT) then 400  $\mu$ l of *Salmonella* ( $10^8$  cells/ml) was added. Following incubation of *S. typhimurium* and phage for 1 h at room temperature,

complexes of bacteria-bound phage were pelleted (3500 rpm, 10 min, 4 °C) then washed (10×) by centrifugation (3500 rpm, 10 min, 4 °C) using 1 ml 0.5% TBS/Tween20. Following final wash, any remaining cell-bound phage were eluted by adding 400 µl elution buffer (10 min, RT). Cells were pelleted (3500 rpm, 10 min, 4 °C) and supernatant (eluate) was recovered and neutralized with 75 µl 1M Tris (pH 9.1). Cells were treated with 250 µl DOC buffer. Phage from both fractions (eluate and lysate) were propagated separately in *E. coli* K91BK and used as input for two proceeding rounds of selection, carried out as previously described (cf. "2.3.1. Selection procedure A"). Following the third round of selection, individual phage clones were propagated *E. coli* K91BK for use in specificity, selectivity and titration experiments.

#### *2.4. Confirming specificity of Salmonella-binding phage clones*

*2.4.1. Phage capture ELISA.* The wells of an ELISA microtiter plate were filled (100 µl/well) with suspensions of *S. typhimurium* (OD<sub>620</sub> 1.0) prepared in PBS, and then incubated overnight at 37 °C. The plate was washed (5×) (Elx405 plate washer, BIO-TEK® Instruments, Inc., Winooski, VT) using 0.5% Tween20/TBS then blocked with 0.1% BSA (in TBS) for 1 h at room temperature, washed again, and reacted with  $5 \times 10^{10}$  phage clones (in 50 µl of binding buffer: 1% BSA, 0.5% Tween20/TBS) for 1h at room temperature. The plate was washed then reacted with 45 µl Biotin-IgG (Smith et al., 1998) for 1h at room temperature, washed, reacted with 40 µl AP-SA (2.5 µl/ml) for 1.5 h at room temperature then plate-washed again. Reaction was developed with NPP

substrate (Yu and Smith, 1996) and read (EL 808 microplate reader, BIO-TEK® Instruments). The slope of color development was measured as a change in optical density per 1,000 min (mOD/min). Wild-type vector f8-5 served as a negative control for evaluation of nonspecific background binding.

**2.4.2. *Salmonella* capture ELISA.** The wells of an ELISA microtiter plate were filled with 55 µl of derived phage clones ( $2.7 \times 10^{10}$  virions/ml) prepared in TBS, then incubated overnight at 4 °C. The plate was washed (5×) using 0.5% Tween20/TBS then blocked with 1% BSA (in TBS) for 1 h at room temperature, washed again, and reacted with  $\approx 5 \times 10^7$  *S. typhimurium* (OD<sub>620</sub> 0.8) diluted 1:20 with 0.05% Tween20/TBS) for 2 h at room temperature. The plate was washed then reacted 1 h at room temperature with 45µl *Salmonella* O Poly-1 antiserum (Becton Dickinson, Franklin Lakes, NJ) diluted 1:500 in 0.5% Tween20/TBS. The plate was washed then reacted with 40 µl AP-conjugated goat anti-rabbit antibodies (Jackson ImmunoResearch Laboratories, West Grove, PA) diluted 1:5000 in 0.5% Tween20/TBS for 1 h at room temperature. The plate was washed, and the reaction developed with NPP substrate (Yu and Smith, 1996). The slope of color development was measured as a change in optical density per 1,000 min (mOD/min). Wild-type (WT) vector f8-5 served as a negative control for evaluation of nonspecific background binding.

## *2.5. Co-precipitation assay to determine phage E2 selectivity*

To determine the selectivity of respective phage clone E2, a co-precipitation assay was elaborated and performed in triplicate ( $n = 3$ ) as follows. Following preparation of individual bacterial suspensions (*cf.* “2.1.2. Bacterial suspensions”), 400  $\mu$ l of each respective culture suspension was combined with 100  $\mu$ l of aggregate-free E2 in separate tubes. Negative controls were prepared for cultures by substituting 100  $\mu$ l sterile 0.5% Tween20/TBS for aggregate-free E2 with 400  $\mu$ l aliquots of each bacterial suspension. As well, a negative control containing only 100  $\mu$ l aggregate-free E2 and 100  $\mu$ l sterile TBS was prepared. All tubes were incubated on 360° rotator (Barnstead International, Dubuque, IA) 1 h at room temperature to allow phage-cell binding. Cells were washed (5 $\times$ ) by centrifugation (3500 rpm, 10 min, RT) using 1 ml 0.5% Tween20/TBS. Following final wash, cells in each tube were resuspended in 50  $\mu$ l cell DOC lysis buffer and incubated 30 min at room temperature. Four hundred fifty microliters TBS was added to neutralize lysis buffer then tubes were vortexed and centrifuged briefly at 3500 rpm. Ten microliters of prepared starved cells were added to each tube. Tubes were incubated for 15 min at room temperature for transfection to proceed. One hundred eighty microliters NZY broth + tetracycline (0.2  $\mu$ g/ml) was added to all tubes. Tubes were incubated 40 min at 37 °C to develop tetracycline resistance. Aliquots from each respective tube were diluted 1:10 to 1:100 with NZY broth + tetracycline (0.2  $\mu$ g/ml), then (spread) plated to separate, pre-warmed NZY + tetracycline (20  $\mu$ g/ml) + kanamycin

(100 µg/ml) plates and incubated overnight at 37 °C. Colonies were counted on respective dilution plates and averaged for the three separate experiments.

## 2.6. Dose-dependent binding of E2 to *S. typhimurium*

Logarithmic dilutions of E2 in PBS, ranging from  $10^1$  to  $10^{13}$  virions/ml, were prepared from stock phage then titrated against stable suspensions of *S. typhimurium* ( $\approx 10^8$  cells/ml; cf. “2.1.2. Bacterial suspensions”) using precipitation assay (cf. “2.5. Co-precipitation assay to determine phage E2 selectivity”). Experiments were performed in triplicate ( $n = 3$ ) and plate counts averaged.

## 2.7. Calculations

The concentration of infective phage particles (biological titer) in solution was determined by infecting the starved *E. coli* K91BlueKan cells with the phage, followed by growth of the infected cells for 16 h on NZY plates containing 20 µg/ml tetracycline. Recombinant phage confer tetracycline resistance to infected cells, allowing them to form colonies. The biological titer of the recombinant phage (expressed in CFU) was typically 20-fold lower than the physical titer (virions/ml), and calculated as the INPUT for experiments:

$$\text{CFU} \times 100 \times \text{culture plate dilution factor.} \quad (3)$$

The quantity of bound phage in co-precipitation and titration assays (OUTPUT) was calculated as:

$$\text{average CFU (n = 3)} \times 100 \times \text{dilution factor} \times \text{volume (0.5 ml)}. \quad (4)$$

Yield percentage for organisms was calculated from Eqs. (3) and (4) as

$$\text{OUTPUT/INPUT} \times 100. \quad (5)$$

## 2.8. Flow cytometry studies

Phage E2 clones ( $1.2 \times 10^{14}$  virions) were fluorescently labeled using an Alexa Fluor 488 Protein Labeling Kit (Molecular Probes, Eugene, OR) as described by the manufacturer's package insert. Labeled virions were precipitated from the reaction mixture by double-PEG precipitation, vortex mixed then incubated overnight at 4 °C. Precipitated phage were pelleted by centrifugation (12000 rpm, 15 min, 4 °C), decanted, and resuspended in 1 ml PBS, then vortexed and precipitated by double-PEG precipitation. Phage pellet was dissolved in PBS and stored at 4 °C until use. Phage concentration and degree of labeling determined spectrophotometrically at  $A_{269, 494}$  (dye absorption maxima) indicated that the phage was labeled with a density of 300 fluorescent dye molecules per phage (Petrenko and Sorokulova, 2004).



Fluorescence-Activated Cell Sorting (FACS) was used to quantitate the degree of phage-*S. typhimurium* binding as a function of phage concentration. Fluorescently labeled stock phage E2 diluted to concentrations ranging from  $2 \times 10^8$  –  $2 \times 10^{11}$  CFU/ml were added to suspensions of *S. typhimurium* prepared in 0.5% Tween20/TBS ( $10^9$  cells/ml) then rotated 1 h at room temperature. Samples were washed (2×) by centrifugation (3500 rpm, 10 min, RT) using 0.5% Tween20/TBS. Following the final wash, phage-bacteria complexes were resuspended in 1 ml PBS and analyzed on a Beckman Coulter Elite XL (Fullerton, CA) four-color flow cytometer equipped with an Ar-ion laser tuned to 488 nm. Forward scatter and fluorescence of cells and phage, alone and complexed together, were measured. Fluorescence emission was measured at 518 nm. Prior to analysis, calibration of the cell-sorting module was performed with Flow-Check™ Fluorospheres (6605359, Beckman Coulter). FACS sorting was performed by examining  $10^5$  total fluorescent events from preparations. Data files transferred from the unit to a data processor were analyzed using Expo 32 software (Beckman Coulter). Hard copies of histograms were scanned to file then digitally processed with Adobe® Photoshop® 5.0LE (Adobe Systems, San Jose, CA).

FACS was also used to confirm selectivity of phage clone E2 for *S. typhimurium*, as determined by the co-precipitation assay. The study was limited to *S. typhimurium*, *C. freundii*, *P. mirabilis*, *Y. enterocolitica*, *S. marcescens*, *E. aerogenes*, and *P. aeruginosa*. Fluorescently labeled E2 were diluted to  $10^9$  CFU/ml then incubated with prepared cells as previously described (*cf.* “2.1.2. Bacterial suspensions”) for 1 h at room temperature. Complexes were precipitated by centrifugation (3500 rpm, 10 min, RT), then washed (5×) by centrifugation using 0.5% Tween20/TBS, resuspended in 1 ml PBS, and analyzed.

Hard copies of histograms were scanned to file then digitally processed with Adobe® Photoshop® 5.0LE.

### *2.9. Peptide insert sequence analysis*

PCR was performed using a Perkin Elmer GeneAmp 2400 system (Norwalk, CT) on 1 µl intact phage suspension per 25 µl reaction. PCR reactions consisted of 0.3 µl forward primer f8s-20 (5'-CAAAGCCTCCGTAGCCGT TG -3'), 0.3 µl reverse primer f8as-20 (5'-CATTCCACAGACAGCCCTCA -3'), 2.5 µl of 10X Mg free buffer (Promega, Madison, WI), 2 µl MgCl<sub>2</sub> (25 mM) (Promega), 0.04 µl *Taq* polymerase (Promega), and 2 µl dNTPs (2.5 mM), prepared to a final volume of 25 µl with filter-purified water. Amplification consisted of initial denaturation at 94 °C for 2 min, then 35 cycles of 94 °C for 10 s, 46 °C for 20 s, and 72 °C for 45 s, followed by a final incubation of 4 min at 72 °C. Three microliter PCR products containing bromophenol blue dye (BPB) were resolved on a 0.8% (w/v) agarose gel (DNA high-melting agarose prepared with 0.05M NaH<sub>2</sub>PO<sub>4</sub> and 1mM MgCl<sub>2</sub> [pH 7.5]) using a Bio-Rad Mini-sub® cell GT system (Hercules, Ca). λ<sub>BSI</sub> II DNA (New England Biolabs, Beverly, MA) heated at 70 °C for 10 min was used as a size standard. Gels were run at room temperature in 0.05 M NaH<sub>2</sub>PO<sub>4</sub> with 1 mM MgCl<sub>2</sub> [pH 7.5] for 45 – 60 min at 50 V. Compounds used to prepare buffer and gels were analytical grade or higher. Following electrophoresis, DNA was stained with SYBR® Green I nucleic acid gel stain (10000X concentration in DMSO, Cambrex Bio Science, Rockland, MD) and visualized at 521 nm using a

KODAK 290 Electrophoresis Documentation and Analysis system (Eastman Kodak, Rochester, NY), equipped with a DR40 Kodak camera, DR40 amber camera filter (Clare Chemical Research, Denver, CO) and dark reader transilluminator (Clare Chemical Research). Images (exposure = 8 s) were captured and processed electronically using Kodak 1D software (Ver. 3.5.3, Eastman Kodak).

Relevant bands were excised, purified, and sequenced using an ABI 3100 Genetic Analyzer (Foster City, CA) by personnel at the Department of Biological Sciences, Auburn University, AL.

#### *2.10. Salmonella interaction with phage adsorbed to Au*

Visual confirmation and quantitation of phage-*Salmonella* binding was also confirmed by optical microscopy. Gold (Au) magnetic strips were coated with phage E2 ( $5 \times 10^{11}$  virions/ml in PBS) by rotating them for 1 h at room temperature. Strips were gently washed (5 $\times$ ) with PBS to remove unbound phage then incubated in a suspension of *S. typhimurium* (diluted in PBS to OD<sub>620</sub> 1.0) on rotator for 3 h at room temperature. Subsequently, the strips were washed (5 $\times$ ) with filter-purified water and analyzed microscopically with a Signatone FS 70 (Mitutoyo Corp. Kanagawa, Japan) high power optical microscope (Fig. 4.1) mounted to a Checkmate 100 probe station and equipped with the following: TC 8600 temperature chuck connected to a Trio Tech International TC 100 Temperature Controller (Van Nuys, CA), Checkmate J200 joystick, Dolan Jenner MI-156R Fiber-Lite® fiber optic illuminator (Lawrence MA), digital color CCD camera,

and M Plan Apo SL 100 objective (100×, NA 0.55). Digital photos were transferred to a data processor (Dell GX 260 Optiplex, Austin, TX) for storage and analysis using Adobe® Photoshop® 5.0LE.

### *2.11. Fluorescence microscopy*

Visual confirmation and quantitation of phage-*S. typhimurium* binding was also performed by fluorescence microscopy. Fluorescently labeled phage diluted to concentrations ranging from  $2 \times 10^8$  –  $2 \times 10^{11}$  CFU/ml were added to suspensions of *S. typhimurium* prepared in 0.5% Tween20/TBS ( $10^9$  cells/ml) and rotated 1 h at room temperature. Samples were washed (2×) by centrifugation (3500 rpm, 10 min, RT) using 0.5% Tween20/TBS. Following final wash, the pellet was resuspended in PBS and examined by Nikon (Tokyo, Japan) ECLIPSE E800 fluorescent microscope equipped with 100W Hg lamp, 4× (NA 0.13), 40X (Plan Fluor DIC M, NA 0.75), 60× (Plan Apo, NA 1.40) and 100× objectives (Plan Apo, NA 1.40). Digital microscopic photos (500-550 nm) were acquired via a SPOT RT Slider CCD video camera (1520 × 1080 pixel optical resolution) (Diagnostic Instruments, Inc., Sterling Heights, MI) with the following exposure settings: red – 1.3 s, green – 2.02 s. Images were transferred to a data processing unit (Dell Corp., Round Rock, TX) for image storage and processing using SPOT Advanced software (Ver. 3.5.9 for Windows 2000; build 6 August 2003, Diagnostic Instruments) and Adobe® Photoshop® 5.0LE.

## 2.12. Molecular characterization of phage receptor

2.12.1. *Affinity matrix.* Phage was crosslinked by vortex-mixing 1 ml stock phage (clone E2 or WT f8-5 in PBS) with 10  $\mu$ l *N*-hydroxysuccinimide (NHS)-dextran (82 mg/ml stock in dimethylsulfoxide; CarboMer, Inc., Westborough, MA) and 150  $\mu$ l polyethylene glycol (PEG) (50% w/v in water) as described by Smith et al., 1998. The mixture was rotated at room temperature for 18 h. Eight milliliters of 1 M Tris (pH 9.1) and 890  $\mu$ l 5 M NaCl were added, followed by an additional rotation at room temperature for 2 h. Following incubation, the suspension was transferred to an Oak Ridge tube (Nalgene) and centrifuged to pellet (Model RC5C, SA-600 rotor, Beckman Coulter) (10000 rpm, 15 min, 4 °C). The supernatant was removed from the pellet then re-centrifuged (10000 rpm, 15 sec, 4 °C) to concentrate any remaining PEG, and reaspirated. The pellet was washed (5 $\times$ ) by centrifugation with 10 ml TBS (10000 rpm, 15 min, 4 °C) then resuspended in 1 ml TBS and transferred to a microfuge tube and stored at 4 °C until use. All chemicals and compounds were analytical grade or higher.

2.12.2. *S. typhimurium* biotinylation. Sulfo-NHS-LC-LC-Biotin (Sulfosuccinimidyl-6'-(biotinamido)-6-hexanamidohexanoate; Pierce, Rockford, IL) prepared to 1 mg/ml concentration with 2 mM NaOAc [pH 6.0]) was added to 5 ml prepared bacterial suspension in PBS to prepare a final biotin concentration of 100  $\mu$ M. The suspension was rotated 2 h at room temperature to biotinylate the bacterial outer membrane. Following incubation, cells were washed (3 $\times$ ) by centrifugation (5500 rpm, 10 min, 10 °C) in 10 ml PBS, leaving a dry pellet.

*2.12.3. Cell lysate preparation.* The pellet of biotinylated cells was resuspended in 10 ml DOC lysis buffer (2% sodium deoxycholate, 10 mM Tris, 2 mM EDTA [pH 8.0]), vortexed and rotated 1 h at room temperature. Following incubation, the suspension was centrifuged (14000 rpm, 10 min, RT) to prepare a cell-free lysate.

*2.12.4. Isolation of phage-targeted bacterial outer membrane receptors.* Five hundred microliters of affinity matrix (either clone E2 or WT f8-5) was added to 10 ml lysate and rotated overnight ( $\approx$  16 h) at room temperature to effect phage-bacteria receptor binding. Phage-receptor complexes were pelleted (14000 rpm, 15 min, RT) then washed (2 $\times$ ) by centrifugation (14000 rpm, 15 min, RT) with 1 ml DOC lysis buffer, leaving a dry pellet. The pellet was resuspended in 200  $\mu$ l acid elution buffer (0.1 N HCl, 1 mg/ml BSA, [pH 2.2 adjusted with glycine]), vortexed, and centrifuged (10000 rpm, 10 min, RT) to pellet phage. Eluate was retained and neutralized by addition of 37.5  $\mu$ l 1 M Tris-HCl (pH 9.0). Eluate was maintained at 4 °C until analysis.

*2.12.5. Eluate analysis.* In order to confirm the isolation of an outer membrane structure complementary to E2, the cell lysate was subjected to sodium dodecyl sulfate polyacrylamide gel electrophoresis (SDS PAGE), Western blot analysis, and protein sequencing.

*2.12.5.1. SDS PAGE.* Five microliter samples of eluate were resolved in pre-cast 4 – 20% gradient gels (Pierce) using a Mini-PROTEAN® 3 electrophoresis system (Bio-Rad Laboratories, Hercules, CA) with running buffer (Laemmli: 0.025 M Tris, 0.192 M

Glycine and 0.1% SDS; or Tris-HEPES-SDS) for 1.5 h at 100 V. Samples were prepared with 8  $\mu$ l 5X reducing sample loading buffer (Pierce) and 27  $\mu$ l running buffer then heated 3 min at 95 °C. Chemiluminescent BlueRanger® peroxidase-labeled protein marker (Pierce) was used as a size standard. Gels were stained in 0.25% Brilliant Blue R (Sigma-Aldrich, Milwaukee, WI), containing 40% (v/v) MeOH and 7% (v/v) acetic acid for 2 h with rocking (Reliable Scientific, Hernando, MS) (30 rpm). Gels were destained in 40% (v/v) MeOH and 10% (v/v) acetic acid with rocking. Proteins were visualized at 521 nm using a KODAK 290 Electrophoresis Documentation and Analysis system (Eastman Kodak), equipped with a DR40 Kodak camera, DR40 amber camera filter (Clare Chemical Research, Denver, CO) and dark reader transilluminator (Clare Chemical Research). Images (exposure = 8 s) were captured and processed electronically using Kodak 1D software (Ver. 3.5.3, Eastman Kodak), Kodak EasyShare software (Ver. 2.1.0.55, Eastman Kodak) and Adobe® Photoshop® 5.0LE.

*2.12.5.2. Western blot.* Proteins from prepared gels were electroblotted to nitrocellulose using the Mini-PROTEAN® 3 electrophoresis system (Bio-Rad Laboratories) with Tris-Glycine buffer (25 mM Tris, 192 mM glycine, 10% [v/v] MeOH, [pH 8.3 adjusted with HCl]) for 1 h at 300 mA. Nitrocellulose was washed (2 $\times$ ) in 0.05% Tween20/TBS while rocking for 20 min at room temperature. After decanting, 50 ml of 1:5000 streptavidin-HRP conjugate solution prepared with 0.05% Tween20/TBS was added for 90 min at room temperature while rocking. The membrane was washed (6 $\times$ ) with 0.05% Tween20/TBS for 5 min then developed using a Supersignal® East Pico

Chemiluminescent Substrate Kit (Pierce). Blot was exposed (15 s) by radiography using CLXposure cassette and paper (Kodak).

*2.12.5.3. Protein sequencing.* Protein samples for N-terminal sequencing were prepared from SDS PAGE as previously described with the following exceptions. A 0.1 mM final concentration of sodium thioglycolate was incorporated into the running buffer as a scavenger to prevent N-terminal blockage during electrophoresis. Proteins were electroblotted to a polyvinylidene fluoride (Immobilon-P, Millipore, Bedford, MA) membrane using Tris-glycine buffer (25 mM Tris, 192 mM glycine, 10% (v/v) MeOH, [pH 8.3 adjusted with HCl]) for 90 min at 300 mA. The membrane was rinsed in DDH<sub>2</sub>O for 4 min, stained with 0.05% (w/v) Brilliant Blue R (1% acetic acid, 50% MeOH) for 5 min, then de-stained with 50% (v/v) MeOH 15 min. Membrane was rinsed in DDH<sub>2</sub>O for 10 min and relevant bands were excised, air-dried, and shipped to Baylor College of Medicine, TX, for analysis.

### **3. Results**

#### *3.1. Selection of phage clones binding to S. typhimurium*

An f8/8 landscape library as described by Petrenko et al. (1996) was utilized as the source of phage probes for *S. typhimurium*. These recombinant fd-tet phage clones possess random octapeptides fused to all 4000 copies of major coat protein pVIII. The three multistage landscape phage selection procedures outlined in Table 1 were followed



for the selection of *S. typhimurium* probes. Using selection procedure “A,” a portion of the prepared library ( $2 \times 10^9$  CFU or  $10^{11}$  virions) was selected by reacting against immobilized *S. typhimurium*, followed by washing, then eluting cell-associated binders through mild acid treatment. The cells were then treated with DOC buffer to recovery any residual binders (Ivanenkov et al., 1999a, 1999b). Both fractions (eluate and lysate) were amplified separately in *E. coli* K91BK in the presence of kanamycin to ensure destruction of any residual *S. typhimurium* ( $\text{kan}_r$ ). These sub-libraries, now enriched for *S. typhimurium* binders, were used in subsequent rounds of selection to further increase the pool’s specificity. In contrast to selection procedure “A,” selection procedure “B” introduced an increased stringency by depleting the library against both plastic and BSA in order to exclude the selection of unrelated clones. Additionally, a higher concentration of Tween20 was used for washing.

Taking into account that *S. typhimurium* can display different receptors under differing environmental conditions (Gawande and Bhagwat, 2002), a third selection procedure “C” was employed to recover phage that may interact optimally with *S. typhimurium* in suspension as opposed to cells immobilized onto a solid surface. Self-aggregating, precipitating phage clones were depleted from the library by heat treatment/high-speed centrifugation then reacted with *S. typhimurium* under aqueous conditions to form complexes. As in previous selection procedures, following washing of cells, any cell-associated phage were isolated by acid elution and lysis of cells then amplified separately in *E. coli* K91BK and used for subsequent rounds of selection. Using this procedure, the yield of *S. typhimurium*-associated phage determined as a ratio of output to input increased for each subsequent round, indicating successful selection of

specific phage clones as displayed in Table 2. Following the last round of affinity selection [5<sup>th</sup> (A), 4<sup>th</sup> (B) or 3<sup>rd</sup> (C)], individual phage clones were amplified by PCR and DNA sequenced.

The selected phage clones can be grouped into at least five homologous families (Table 3). Peptides from acid fractions isolated in procedures "A" and "B" demonstrated prominent similarities, forming family I with a leading motif VT/SP, followed by dominant P, frequent T/S, frequent T/S/Q and frequent H. Dominant phage clone VSSNQAPP (for simplicity, phage clones will be designated by the peptide sequences they bear as determined by DNA sequencing of gene VIII insert) is strikingly similar to one phage clone from selection "A"; VSPQSAPP may belong to family I or may form a discrete family. Another dominant phage, DRSPSSPT from selection "C," belongs to family III, which includes phage from the eluate fraction of procedure "A." Phage VSPPSNPS and VTPPSQHA from the lysate fraction of procedure "A," and phage VTPPQQGS from the lysate fraction of procedure "B," belong to family I and probably originated from corresponding eluate fractions that can contaminate the lysate fractions.

Analysis of phage sequences demonstrates the influence that depletion and increased stringency of washing have on the composition of phage found in the eluate and lysate fractions of procedures "A" and "B." Furthermore, changing the mode of separation for phage-bacterial complexes, i.e., procedure "C," dramatically affects the composition of the phage isolated from the eluate fraction and does not allow isolation of any phage from the lysate fraction. This may imply that substrate-immobilized bacteria, vice bacteria in suspension, display different receptors or that multivalent binding of

phage to bacteria in suspension occurs less readily in contrast to bacteria adsorbed to a plastic matrix.

### 3.2. Specificity of phage binding to *S. typhimurium*

Specificity of binding is defined as the ability of select landscape phage, possessing specific peptide sequences, to interact with select bacteria possessing complementary surface-bound receptors. To determine specificity, the relative binding ability of select phage clones was compared to that of the wild-type vector (f8-5) and non-related recombinant phage from the f8/8 landscape library using a modified ELISA procedure and precipitation assay.

Using the “phage-capture” ELISA assay, *S. typhimurium* cells were adsorbed to microtiter plate wells then interacted with selected phage clones. Following incubation to effect cell-phage specific binding, non-binding phage were washed away to reveal specific binders that were subsequently conjugated with biotinylated anti-phage antibodies. As shown in Fig. 4.2, the select clones bind to *S. typhimurium* to a much greater degree in comparison to wild-type phage. The “*Salmonella*-capture” modified-ELISA was a direct reversal of the “phage-capture” modified-ELISA in that select phage clones were adsorbed to the wells of a microtiter plate, reacted with *S. typhimurium* then washed. Specific bacteria-phage binding was detected with biotinylated anti-*Salmonella* antibodies, followed by reaction with alkaline phosphatase conjugated to streptavidin (AP-SA) and *p*-nitrophenylphosphate (NPP). As shown in Figs. 4.2 – 4.5, many of the isolated phage clones demonstrate a higher degree of binding to *S. typhimurium* in

comparison to the control wild-type phage. However, some clones were bound strongly to *S. typhimurium* in both assays, while other clones gave inconsistent results between the two assays. This is not completely unexpected since the immobilization of the phage, and thus its conformation, is different between the two assays and may be a result of mono- or multivalent interactions with the bacteria as demonstrated previously in binding experiments with phage selected against  $\beta$ -galactosidase (Petrenko and Vodyanoy, 2003).

Clones demonstrating ELISA signals higher than the control wild-type phage were further characterized by precipitation assay to confirm their specificity for *S. typhimurium*. This assay, previously described for the analyses of phage binding to zoospores and bacterial spores (Bishop-Hurley et al., 2002; Knurr et al., 2003), was optimized in this study to avoid aggregation and self-precipitation of phage. As previously reported in Petrenko and Sorokulova (2004), yields of *S. typhimurium*-bound phage were 12,000 — 22,000 times higher than those of the control wild-type phage, indicating very high specificity of the selection procedure. Phage VTPPTQHQ (designated hereafter as phage clone E2) demonstrated the highest specificity of binding (22,000-fold higher recovery than wild-type phage).

### *3.3. Selective binding of phage E2 to S. typhimurium*

Co-precipitation assay was utilized to confirm the discriminatory power of phage clone E2 for *S. typhimurium* in comparison to the nine other genera of gram-negative bacteria, predominately Enterobacteriaceae selected for their phylogenic relatedness to *S. typhimurium*. Following incubation of each organism with an equal amount of E2,

unbound phage were washed from the cells, which in turn were lysed to recover any membrane bound phage. Phage was then titered using *E. coli* K91BK host cells for characterization of phage binding to the challenge bacteria. Precipitation assay demonstrated 10 – 1,000 times greater binding of phage E2 (mean yield percentage normalized) to *S. typhimurium* in comparison to the challenge bacteria (Fig. 4.6). Negative controls worked correctly, demonstrating no transfection of *E. coli* K91BK.

FACS confirmed selectivity of phage-targeted binding for *S. typhimurium*, *C. freundii*, *P. mirabilis*, *Y. enterocolitica*, *S. marcescens*, *E. aerogenes*, and *P. aeruginosa*. Preliminary control analyses (Fig. 4.7) of  $10^6$  E2 particles (peak 1) or *S. typhimurium* cells (peak 2) alone demonstrated only 0.4% fluorescence within the positive population (negative sorting gate set at 1 arbitrary unit [AU] on the fluorescence scale) in comparison to  $10^6$  E2 phage–*S. typhimurium* complexes (peak 3), which demonstrated 83% greater fluorescence (33.3% absolute fluorescence within positive population). E2 phage–*S. typhimurium* complexes also demonstrated greater absolute fluorescence than other E2 phage–bacterial complexes with other panel bacteria (Fig. 4.8).

### 3.4. Dose-dependent binding of phage E2 to *S. typhimurium*

Phage clone E2 was studied in more detail by precipitation-titration assay in order to estimate affinity and equilibrium binding to *S. typhimurium*. Dose-dependent binding of phage to cells in solution was observed in phage concentrations ranging from  $10^1$  to  $10^{12}$  CFU/ml. The highest recovery of bound phage (15%), measured as a ratio of output to input phage, was obtained when roughly equal amounts of phage and bacteria were

involved in the complex formation ( $10^6 - 10^8$  CFU/ml phage versus  $\approx 10^8$  CFU/ml *S. typhimurium*) (Fig. 4.9). Fig. 4.10 demonstrates that saturation ( $V_{\max}$ ) occurs at  $3.1 \times 10^7$  CFU, corresponding to  $\approx 2 \times 10^8$  phage particles, matching the number of bacterial cells involved in the complex formation. This is in good agreement with the equilibrium constant ( $K_d$ ) calculated (appendix A) from the Hill plot (Fig. 4.11), which is  $4.77 \times 10^7$  CFU/ml, corresponding to 1.6 pM phage, or 6.3 nM of the phage-borne peptide. This extraordinary high affinity phage binding may be an avidity effect contributed by the multivalent interaction of phage carrying 4,000 binding peptides, with multiply distributed bacterial surface receptors. The Hill coefficient ( $n = 0.81$ ) estimated from Hill plot (Fig. 4.11) indicates that on average one phage particle interacts with one bacterial cell, roughly corresponding to the phage recovery data. This contrasts slightly with associated FACS (Fig. 4.12) and TEM data previously reported in Petrenko and Sorokulova (2004) which indicated multivalent interaction of E2 with *S. typhimurium*, as confirmed by fluorescent microscopy (Fig. 4.13) and high powered optical microscopy (Fig. 4.14). The latter allowed real-time observation of specific binding between phage immobilized to Au plated surfaces and *S. typhimurium* cells under aqueous conditions. Therefore, affinity and equilibrium data describing phage-cell interaction should be considered with prejudice – the possibility that bacterial cells are not equally competent to phage binding cannot be excluded.

### 3.5. Molecular characterization of phage receptor

Identification of the phage-targeted outer membrane protein or structure of *S. typhimurium* was attempted using the methods of Smith et al. (1998) for affinity purification of T4 antibodies, with modifications. Colleagues have successfully utilized this method to isolate glioma cell membrane proteins (Samoylova et al., 2004) and to identify phage-binding receptors on LnCAP cancer cells (Romanov et al., 2001). Phage clone E2 was crosslinked to water-soluble NHS-dextran polymer through amine-reactive NHS side-chains in the presence of PEG to prepare an affinity matrix (Fig. 4.15–A). This matrix was reacted with a prepared lysate of *S. typhimurium*, the surface of which had been previously labeled with non-permeating biotinylation reagent (Fig. 4.15–B), to promote phage-receptor specific binding (Fig. 4.15–C). Following washing to remove any non-specific proteins, any captured *S. typhimurium* surface receptor proteins were eluted from the crosslinked phage-matrix and separated by SDS-PAGE (Fig. 4.15–D). These biotinylated proteins were electroblotted to nitrocellulose, conjugated with streptavidin-horseradish peroxidase, and visualized by radiography (Fig. 4.15–E). Western blot (Fig. 4.16) revealed a single 65 – 70 kD band. However, N-terminus protein sequencing of the corresponding area from the gel revealed only a protein sequence corresponding to serum albumin (PNTLCDEFKA – 100% consensus as determined through National Center for Biotechnology Information). This was not unexpected since BSA is a necessary component of the elution buffer. In fact, all bands from the protein eluate on the gel are attributable to BSA (Fig. 4.17–Lanes 2, 3) because no bands are noted on preparations of eluate without BSA as a component of the elution

buffer (Fig. 4.17–Lane 4). As well, no band in the gel is notable (Fig. 4.17–Lane 4) that corresponds to the band found on the Western blot in this preparation. Thus, identifying the receptor by protein sequencing was not possible. It is probable that the concentration of protein that represents the targeted receptor is too low for the gel stain to pick up, whereas the sensitivity of the Western blot is very high, allowing even extremely small concentrations to be revealed by radiography.

#### **4. Discussion**

Screening for biological threat agents in food and environmental samples, such as *Salmonella*, necessitates the isolation and/or development of highly specific and selective probes capable of pathogen separation, purification and detection (Mansfield and Forsythe, 2000; Petrenko and Sorokulova, 2004). Although antibodies serve well in this capacity, they possess distinct drawbacks that restrict their application including cost and vulnerability to unfavorable environmental conditions. The isolation of phage-based probes from diverse peptide or antibody libraries of filamentous phage fd (Petrenko and Smith, 2000; Petrenko et al., 1996) using phage display (Petrenko and Vodyanoy, 2003), and their prospective use for the specific, selective detection of various bacterial, viral and toxic agents (Petrenko and Sorokulova, 2004) has demonstrated the maturing of this technology and its promise as an economical alternative to antibodies for preemptive monitoring of food and environmental samples, in addition to diagnostic assays. As well, wild-type parental phage fd is an extremely stable nucleoprotein capable of withstanding high temperatures, denaturing agents, organic solvents, mild acids, and alkaline solutions



(Petrenko and Sorokulova, 2004). Consequently, recombinant phage-derived probes, composed of foreign peptides fused to all 4000 copies of major coat protein pVIII, inherit the substantial resilience of the wild-type phage (Brigati and Petrenko, 2005). As an inexpensive alternative to antibodies, phage possess the potential for fabrication of biosorbent layers via self-assembly on numerous substrates including metals, minerals and plastics.

This research outlined three multistage landscape phage selection procedures targeting immobilized or suspended *Salmonella*, resulting in the discovery of five families of bacteria-binding peptides possessing proline commonality, a prominent quality of some anti-bacterial peptides (Cudie et al., 2002). Specificity of select phage clones for *S. typhimurium* was demonstrated using two variations of ELISA (phage capture and *Salmonella* capture) and confirmed by precipitation assay in reference to wild-type phage f8-5. Specificity of representative clone E2 to *S. typhimurium* was confirmed by fluorescence, optical and electron microscopy. The selectivity of E2 to *S. typhimurium* was comparatively analyzed by precipitation assay and flow cytometry using a select panel of bacteria, primarily Enterobacteriaceae, revealing high selectivity of the phage to the targeted bacterium. Some cross-reactivity was noted, especially with *Y. enterocolitica* and *C. freundii*, and may be attributed to the use of non-biased selection conditions, i.e., allowing phage from a diverse landscape library to interact randomly with any one of numerous exposed surface receptors of *S. typhimurium*, including those that may be common for the panel strains.

A unique attribute of the outer membrane (OM) may explain the overwhelming discriminatory power of E2 for *S. typhimurium*. E2 specificity, derived through affinity

selection, results from the constrained interaction of the 8-mer peptide incorporated into major outer coat protein VIII via phage display, with a complementary portion of the *S. typhimurium* bacterial outer membrane surface. Molecular characterization revealed a narrow band that may be indicative of a single low molecular weight protein receptor. The outer membrane (Fig. 4.18) is unique to gram negative bacteria and can be oversimplified as a relatively permeable lipid bilayer that separates extracellular elements from the gelatinous cellular periplasm, acting as a coarse sieve to retain larger molecules such as periplasmic enzymes, while preventing uptake of foreign proteins such as enzymes and antibiotics. The innermost layer of the outer membrane – not exposed to phage – is primarily phospholipid bound to underlying peptidoglycan via lipoprotein anchors, whereas the outermost layer – a variable montage exposed to phage – consists of protein (60%) and lipopolysaccharide (LPS) (40%) that confers a negative charge to the cell, repels hydrophobic molecules, and acts as an endotoxin (Brandenburg et al., 2003). Several proteinaceous structures involved in adhesion, motility and conjugation may also be present. Any of these constituents – LPS, outer membrane proteins, or proteinaceous structures – could therefore be responsible for phage specificity and selectivity. However, definitive identification was not possible by protein sequencing. It should also be noted that proteins and LPS from the outer membrane or surface of bacteria are difficult to isolate alone and thus this band may actually represent several non-specific proteins complexed with the specific target of the phage.

LPS is highly variable between genera, species and even strains, differing in a number and structure of repeating oligosaccharide units, known as O-antigens or O-chains, which are linked to lipid A via a genera-specific core polysaccharide. These

differences account for serotype specificity. To date, well over 40 major serogroups in *Salmonella* species, over 170 serotypes in *E. coli*, greater than 40 in *Shigella* spp., *Citrobacter* spp., and *Proteus* spp., and greater than 10 in *Klebsiella* spp have been identified (Weintraub, 2003). The structures of the O-antigen in *S. typhimurium*, a 22-mer, the core polysaccharide, and associated linkages have been thoroughly elucidated (Olsthoom et al., 2000). Conversely, lipid A is essentially conserved among gram-negative bacteria and composed of 6-7 saturated fatty acids linked to the dimer *N*-acetylglucosamine via ester-amine linkages. Lipid A mediates the physiological activities of the endotoxin in conjunction with the O-antigen when released from the bacteria in a host. Hence, the variable nature of the O-antigen resulting from differences in monomer sequence, linkage and composition (Samuel and Reeves, 2003) may be responsible for the specificity of E2 for *S. typhimurium*.

Interestingly, results (Fig. 4.6) demonstrate that while phage E2 is selective for *S. typhimurium*, *C. freundii* and *Y. enterocolitica* do appear to cross-react to a small degree. Immobilized LPS has been shown to serve as a receptor for some natural strain-specific phage (Romanowska et al., 1976) and may serve as a target for landscape phage. If it is true, then some of the noted cross-reactivity of *S. typhimurium*-targeting phage with *C. freundii* and *Y. enterocolitica* may be attributed to identical or near identical monosaccharide and disaccharide O-antigen components, which have been noted between *Salmonella* and *Citrobacter* species (Knirel et al., 2002).

Interlaced among LPS is a plethora of highly specialized, variable major and minor proteins that may be also plausible targets for landscape phage. They serve common functions among the gram-negatives including selective and nonselective

translocation and structural integrity, e.g. murine-lipoprotein and OmpA (Benz and Bauer, 1988), but may vary in peptide sequence greatly. Major proteins of the gram-negative bacteria in general include beta-barrel outer membrane porins such as OmpF, OmpC, OmpD, PhoE, Oms1, OmpN, NmpC, and OprP, which allow nonspecific, hydrophilic, low molecular weight substances to diffuse across the membrane by size exclusion, and porin receptors that bind specific extracellular target substances via molecular recognition such as LamB (maltodextrines, mono- and disaccharides), Tsx (nucleotides), ScrY (saccharose), OprB (phosphate), OprO (*P. aeruginosa* - pyrophosphate). Minor proteins include iron transporters such as FhuB, and those that function in vitamin uptake.

Phage clone E2, prior to affinity selection from the phage landscape library, was propagated in *E. coli* K12 (Petrenko et al., 1996) resulting in the elimination of clones specific for *E. coli*-surface receptors. Therefore, it is reasonable to hypothesize that the targeted receptor of selected phage on the surface of *S. typhimurium* differs from *E. coli* receptors. A comparison of OmpC, OmpF and NmpC porins between the two strains has shown that although the encoding genes map and function correspondingly, only half of the proteins are similar or identical (Lee and Schnaitman, 1980). For example, N-acetyl phenylalanine  $\beta$ -naphthyl esterase (ApeE) has been demonstrated in *S. typhimurium* but not *E. coli* (Carinto et al., 1998) whereas OmpA, – a phage receptor of *E. coli* (Osborn and Wu, 1980), has not been demonstrated in *S. typhimurium*.

Finally, there exist several outer membrane associated proteinaceous structures such as fimbriae, and in some genera, pili and flagella, which are antigenic and highly variable between genera. Fimbriae, in particular, are hair-like appendages composed of

protein subunits called fimbrins, which extend outward from the bacterial surface and may function as an adhesion factor for specific receptors on target cells. They are prevalent on *S. typhimurium* as well as other enteric bacteria and multiple types can be expressed by a single isolate. Nowotarska and Mulczyk (1977) demonstrated a distinct serological relationship between *Salmonella* and *Citrobacter* Type I fimbriae through cross agglutination and adsorption assays, which also may explain the cross reactivity noted between these two genera during precipitation assay if fimbriae are the source of phage affinity for *S. typhimurium*. Any fimbrial relationship between *S. typhimurium* and *Y. enterocolitica* is unknown.

Thus, while many outer membrane-associated structures are common to gram-negative bacteria, and in particular the enteric bacteria, the potential structural dissimilarities in components between genera lend it to explain the selective nature of E2 for *S. typhimurium*. While it's evident these phage clones are somewhat cross-reactive to other bacteria, phage clone E2 does nevertheless demonstrate a basic discriminatory power for *S. typhimurium* that could be further modified for greater affinity through biased phage display selection schemes (Petrenko and Sorokulova, 2004) including the elimination of cross-reacting clones from the landscape library by depletion against competing strains. The depleted library would then serve as a reservoir of probes that could be harnessed for unique *S. typhimurium* markers. Furthermore, probe affinity could be increased through directed molecular evolution, including repetitive phage mutagenesis and selection of the bacterial-binders under increasingly stringent conditions (Petrenko and Sorokulova, 2004). Thus, the performance of the selected phage-derived probes could be gradually enhanced, resulting in a new generation of robust, inexpensive,

efficient alternatives to antibodies for separation, concentration, and detection systems employed in food and environmental monitoring.

Select landscape phage clones revealed in this work hold potential application as biosorbents or diagnostic probes for monitoring *Salmonella* in conjunction with platforms traditionally based on antibodies or peptides, including the separation and purification of bacteria prior to PCR identification, immunoassays, flow cytometry, and biosensors. In Chapter V, the use of E2 as a substitute antibody for the preparation of acoustic wave biosensors for *S. typhimurium* is detailed.

## Appendix

### *Binding equations*

Characterization of phage-cell interaction through known binding equations allows for quantitative interpretation of complex formation; however, applicability is not inconsequential and special considerations are required.

The identity of the phage-complementary surface receptor(s) on *S. typhimurium* was not determined in this research. Thus, the equilibrium interaction of individual phage outer coat peptides with surface receptor(s) cannot be calculated. However, if we accept that one or more binding sites on the phage can be involved with one or more identical complementary cell surface receptors then the reaction between individual phage particles (*P*) and cells (*S*) may be schematically represented as:



where *n* is the number of phage particles bound via complementary surface receptor(s) to a single *S. typhimurium* cell; *P* is variable, dependent upon titration concentration, whereas *S* is constant ( $\approx 10^8$  cells/ml). The association binding constant ( $K_b$ ) for this reaction can be defined by the law of mass action (Connors, 1987) with the following assumptions: surface receptors are equally accessible to phage, receptors are either free or bound to phage, binding does not alter either the receptor or phage, and binding is reversible:

$$K_b = [SP_n]/([S][P]^n). \quad (2)$$

If the number of cells with phage bound to non-specific cell receptors is considered negligible, then the total number of phage available for binding ( $C_s$ ) is composed of free phage in solution and those involved with complementary binding interactions:

$$C_s = [S] + [SP_n]. \quad (3)$$

Combining equations (2) and (3) yields that fraction of cells with complementary binding phage:

$$Y = [SP_n]/C_s = K_b [P]^n / (1 + K_b [P]^n). \quad (4)$$

The ratio of phage bound with cells to free cells can therefore be defined as

$$Y/(1 - Y) = K_b[P]^n. \quad (5)$$

Taking the logarithm of both sides yields

$$\log(Y/(1 - Y)) = \log K_b + n \log[P] \quad (6)$$



A Hill plot of  $\log(Y/(1 - Y))$  versus  $\log[P]$  allows an estimate of the Hill coefficient ( $n$ ) from the slope, and association binding constant ( $K_b$ ) from the ordinate intercept. The dissociation constant can be calculated from  $K_b$  as

$$K_d = 1/ K_b. \quad (7)$$

The  $K_d$  apparent is calculated by taking the Hill coefficient into account:

$$K_d \text{ (apparent)} = [K_d]^{1/n}. \quad (8)$$

Table 4.1

Summary of selection procedures used to affinity select phage probes for *S. typhimurium*.

<b>Selection Procedure</b>	<b>Separation method</b>	<b>Blocking, BSA (%)</b>	<b>Library depletion</b>	<b>Wash, Tween20 (%)</b>	<b>Rounds of selection</b>
A	Immobilization	0.1	NO	0.1	5
B	Immobilization	0.1	Plastic, BSA-coated plastic	0.5	4
C	Precipitation	0	Centrifugation	0.5	3

Table 4.2

Summary of biopanning results of f8/8 phage library against *S. typhimurium* using different selection procedures.

Procedure Fraction	Round of selection Yield (%)				
	1	2	3	4	5
<b>Selection A</b>					
Eluate	$1.1 \times 10^{-2}$	$2.4 \times 10^{-3}$	$1.1 \times 10^{-2}$	$3.8 \times 10^{-2}$	$1.6 \times 10^{-1}$
Lysate	$9.1 \times 10^{-3}$	$8.8 \times 10^{-3}$	$8.6 \times 10^{-3}$	$2.3 \times 10^{-2}$	$4.7 \times 10^{-2}$
<b>Selection B</b>					
Eluate	$8.6 \times 10^{-3}$	$1.0 \times 10^{-2}$	$1.5 \times 10^{-1}$	$1.3 \times 10^{-1}$	
Lysate	$6.3 \times 10^{-3}$	$2.2 \times 10^{-5}$	$3.1 \times 10^{-5}$	$1.3 \times 10^{-4}$	
<b>Selection C</b>					
Eluate	$2.4 \times 10^{-4}$	$3.1 \times 10^{-3}$	$3.0 \times 10^{-2}$		
Lysate	0	0	0		

Table 4.3

Peptide structures of selected phage clones as determined by genomic DNA sequencing.

Selection procedure	Phage borne peptide(s) <sup>a</sup>			
	Family	Eluate fraction	Family	Lysate fraction
A	I	<b>VTPPTQH</b> <sup>4</sup>	III	<b>ERPPNPSS</b> <sup>8</sup>
	I	<b>VTPPSQHA</b> <sup>10</sup>	III	<b>ERSSQANM</b>
	I	<b>VSPPPQHS</b>	III	<b>ERTTSAHT</b>
	I	<b>VSPQSAPP</b>	III	<b>DRTSNQAT</b>
			III	<b>DLTSNQAT</b>
			I	<b>VSPPSNPS</b> <sup>2</sup>
			I	<b>VTPPSQHA</b>
B	I	<b>VTPPQSSS</b>	IV	<b>DPRSPASL</b> <sup>2</sup>
	I	<b>VTPPTSPO</b>	IV	<b>DPRPAQHT</b>
	I	<b>VTPSSPHS</b>	IV	<b>DPHLAGGL</b>
	I	<b>VTPQGSH</b>	IV	<b>DPKSPLHT</b>
	I	<b>VSTQSTHP</b>	IV	<b>DPKSPQQT</b>
	II	<b>VPPPSPOS</b> <sup>2</sup>	IV	<b>DPKGPHSM</b>
	II	<b>VPPPSPHS</b> <sup>3</sup>	IV	<b>EPHRAASV</b>
	II	<b>VPPPSASS</b>	IV	<b>EPRLAHGA</b>
	II	<b>VPPPSQSQ</b> <sup>2</sup>	IV	<b>DNKMTSOS</b>
	II	<b>VPPPSNPS</b>	V	<b>DPSKRTQP</b>
	II	<b>VPPPGQHQ</b>	V	<b>EPNKHSSQ</b>
	II	<b>VPPSSSSP</b>	III	<b>DRPSPNTV</b>
		<b>VPQQNKAAQ</b>	I	<b>VTPPQQGS</b>
		<b>TPGQDKAQ</b>		
C	I	<b>VSSNQAPP</b> <sup>18</sup>		
	III	<b>DRSPSSPT</b> <sup>4</sup>		
		<b>VPIPYNGE</b>		

<sup>a</sup>Superscript values indicate total number of isolated clones possessing this sequence.

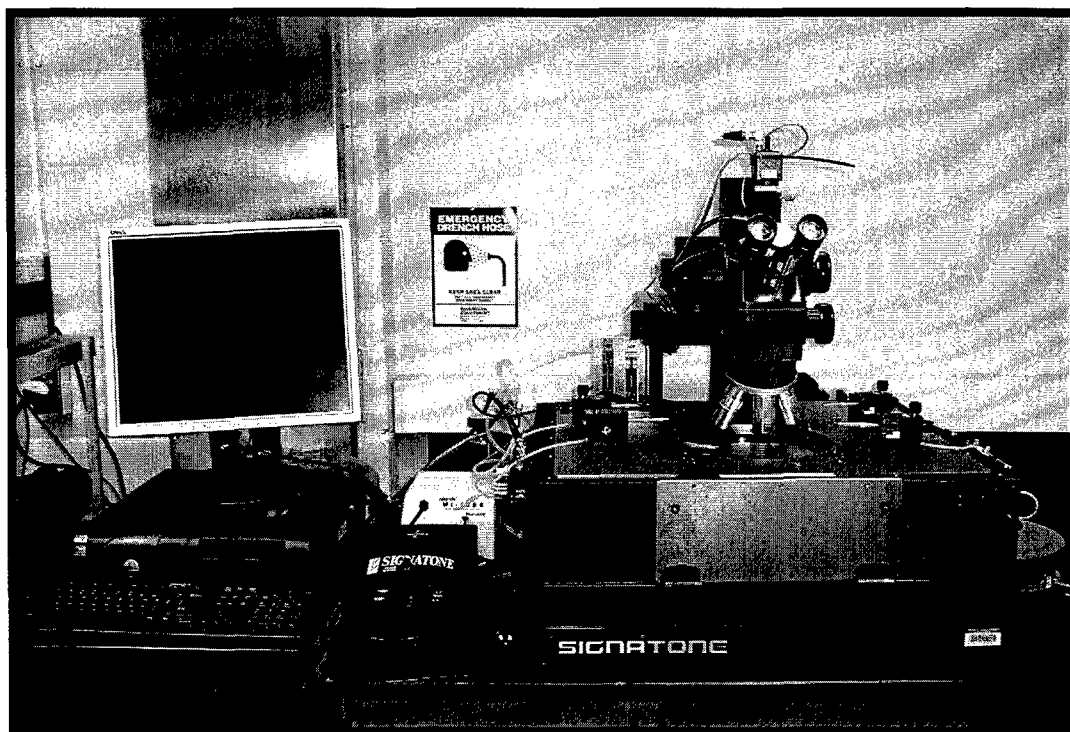


Fig. 4.1. Signatone FS 70 high power optical microscope used to confirm phage E2 – *S. typhimurium* binding on Au coated surfaces.

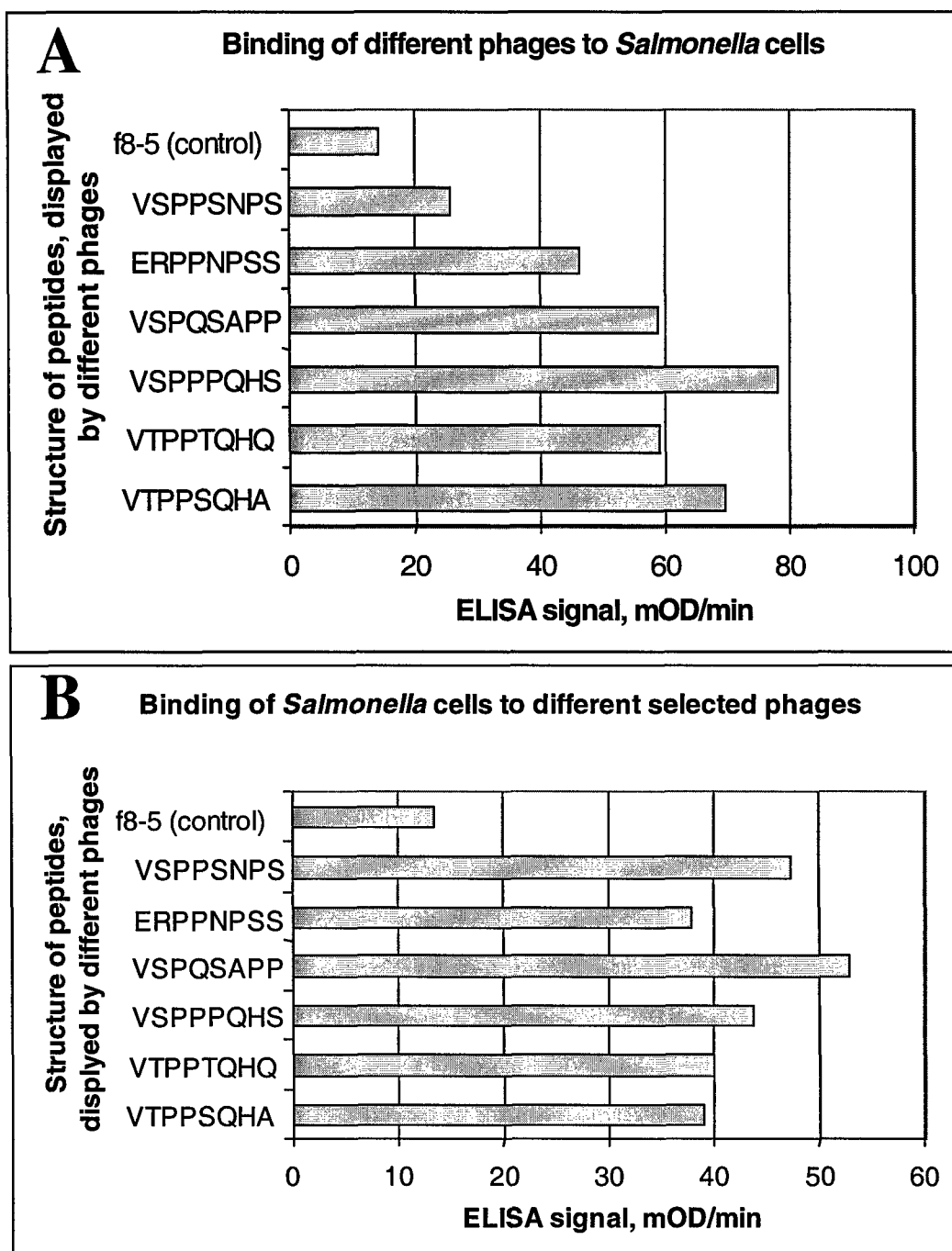


Fig. 4.2. *S. typhimurium*-phage binding specificity as a function of ELISA optical density, for phage chosen during selection procedure "A." (A) Phage capture assay. (B) *Salmonella* capture assay.

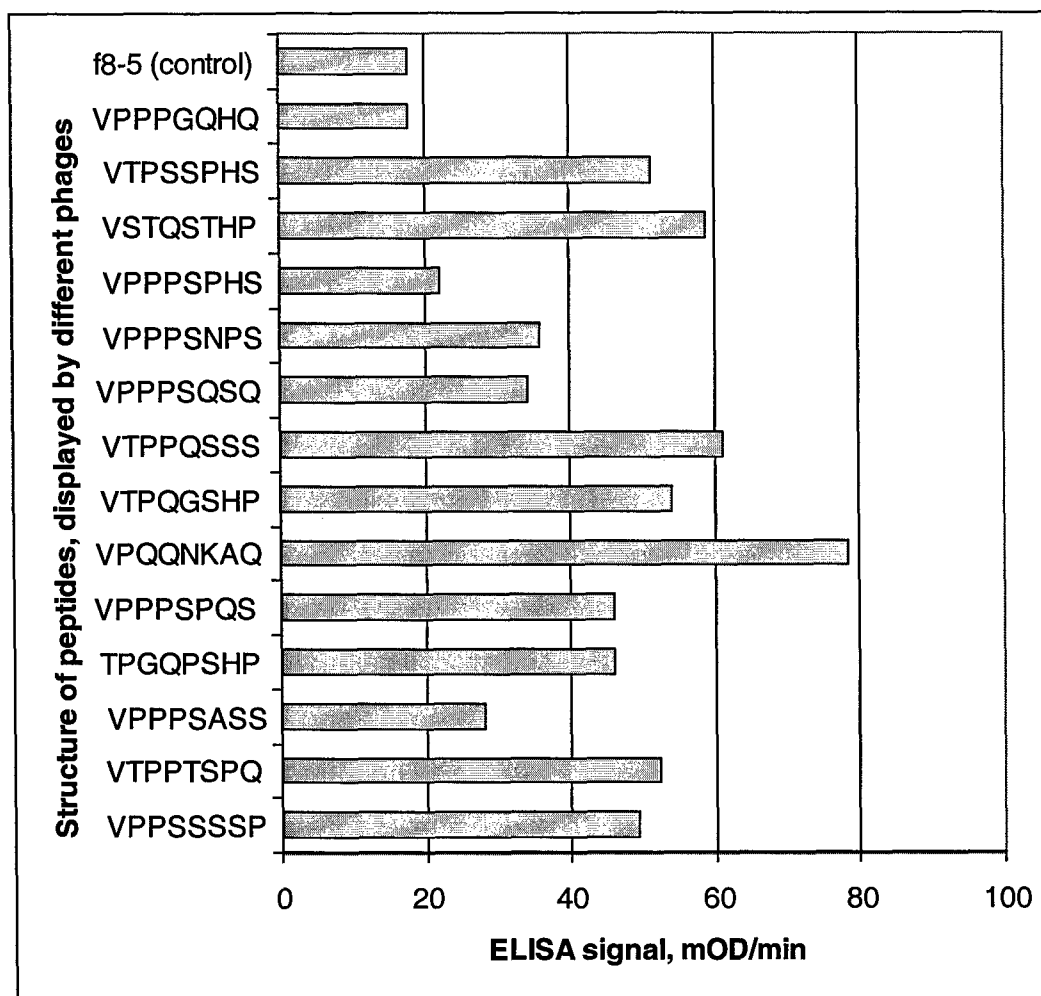


Fig. 4.3. *S. typhimurium*-phage binding specificity as a function of ELISA optical density (*Salmonella* capture assay), for phage chosen during selection procedure "B" from eluate fraction.

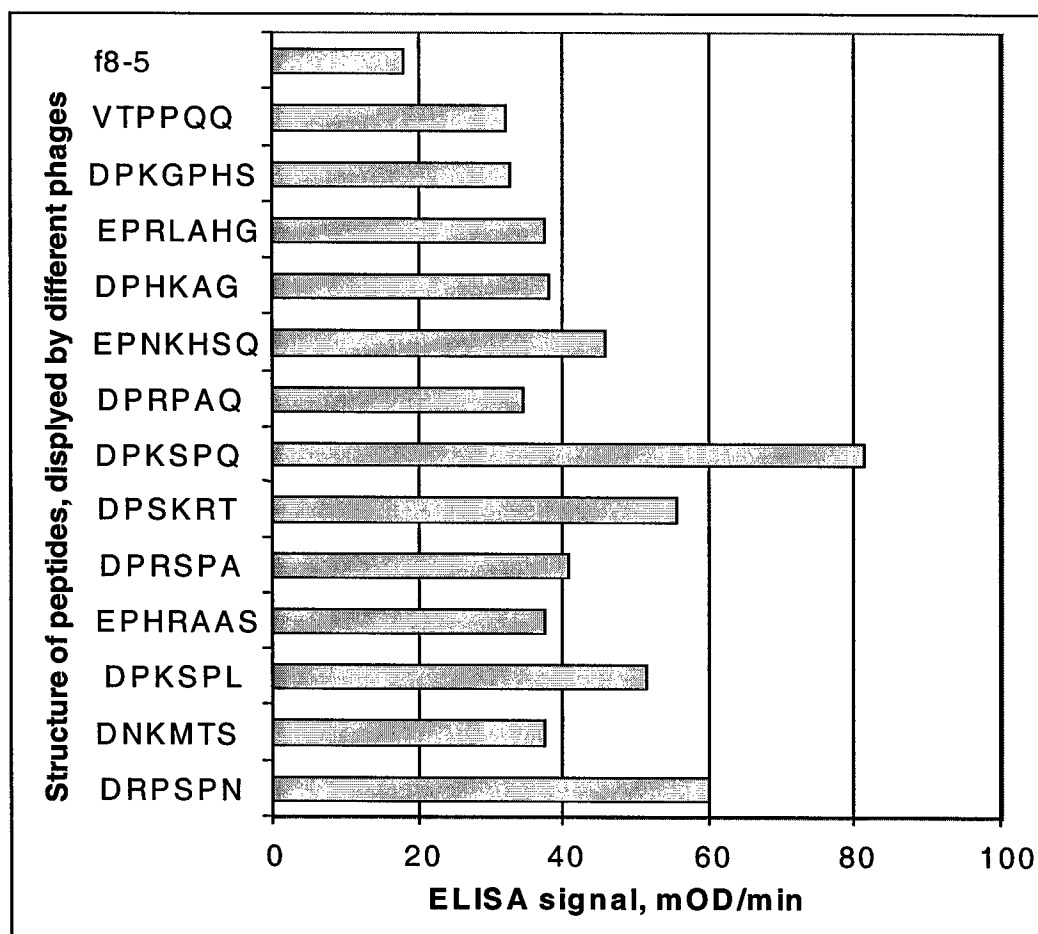


Fig. 4.4. *S. typhimurium*-phage binding specificity as a function of ELISA optical density (*Salmonella* capture assay) for phage chosen during selection procedure “B” from lysate fraction.



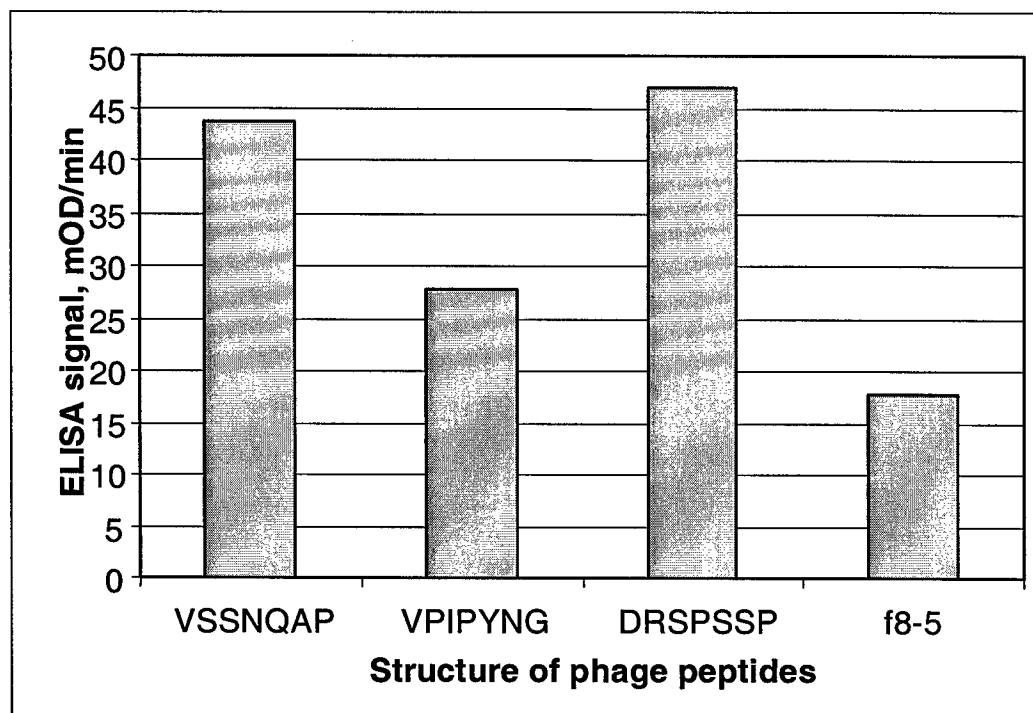


Fig. 4.5. *S. typhimurium*-phage binding specificity as a function of ELISA optical density (*Salmonella* capture assay) for phage chosen during selection procedure "C" from eluate fraction.

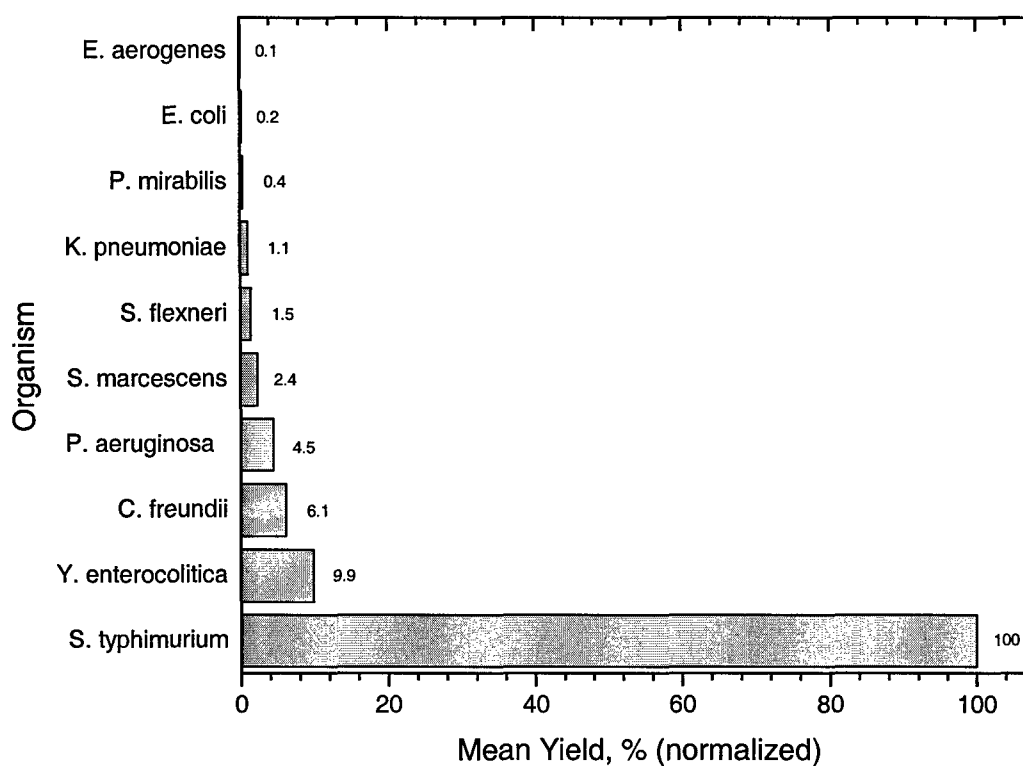


Fig. 4.6. Selectivity of phage E2 as determined by precipitation assay. Mean yield percentage was averaged from three separate experiments then normalized to the maximal mean yield of 3.4% from *S. typhimurium*. Values beside bars indicate respective normalized mean yield percentages.

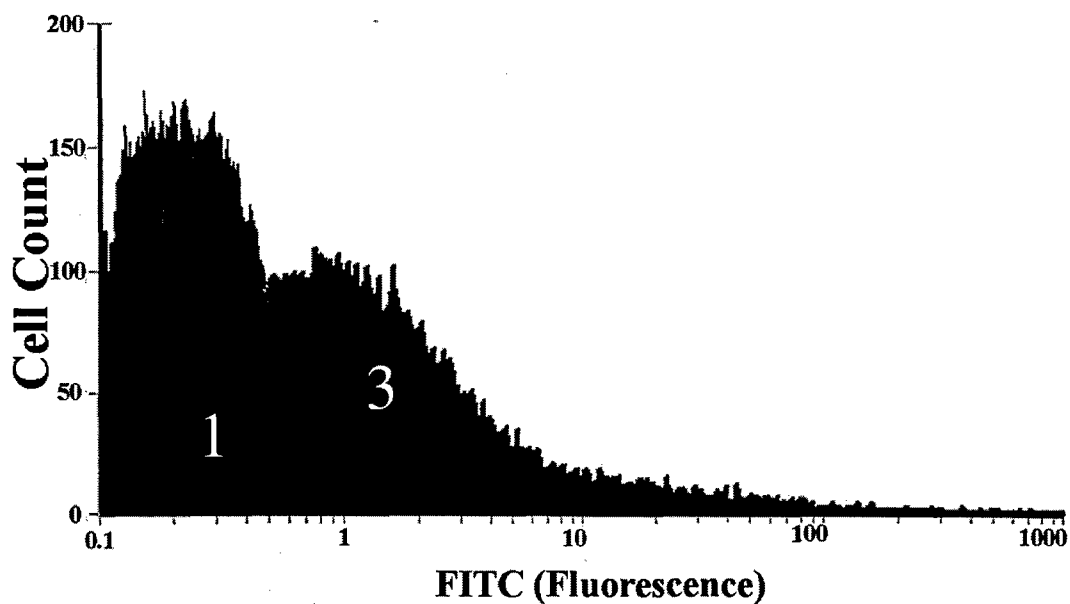


Fig. 4.7. FACS analysis histogram of fluorescently labeled phage E2 and *S. typhimurium*, both separately (peaks 1 and 2, respectively) and in complex (3), as a function of fluorescence. Binding of cells with phage falls into a distinct population, exhibiting greater fluorescence than controls (*S. typhimurium* and phage alone). The negative threshold (sorting gate) was set at 1 AU on the fluorescence scale.

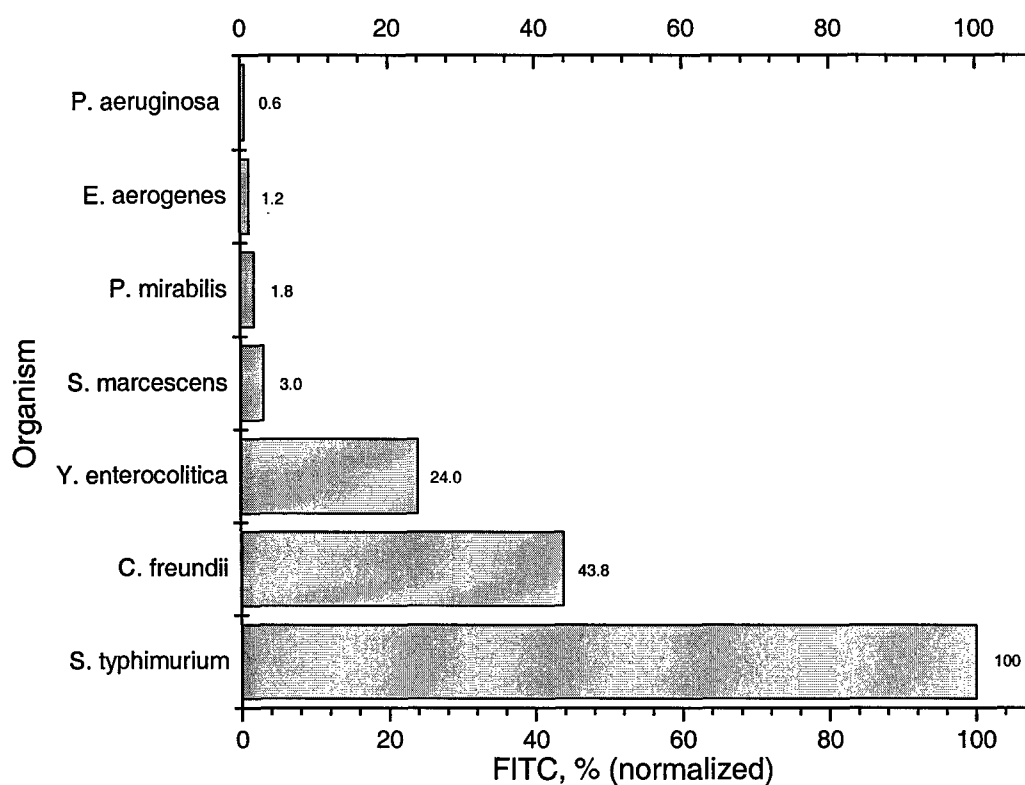


Fig. 4.8. Selectivity of phage E2 as determined by FACS. Fluorescence (FITC) percentage is that amount of phage associated cell complexes falling within the positive population for  $10^6$  fluorescent events. The negative threshold-sorting gate was set at 1 arbitrary unit on the fluorescence axis scale. Normalization was applied using the maximal mean fluorescence of 33.3% from *S. typhimurium*. Values beside bars indicate the respective normalized percentages in arbitrary units.

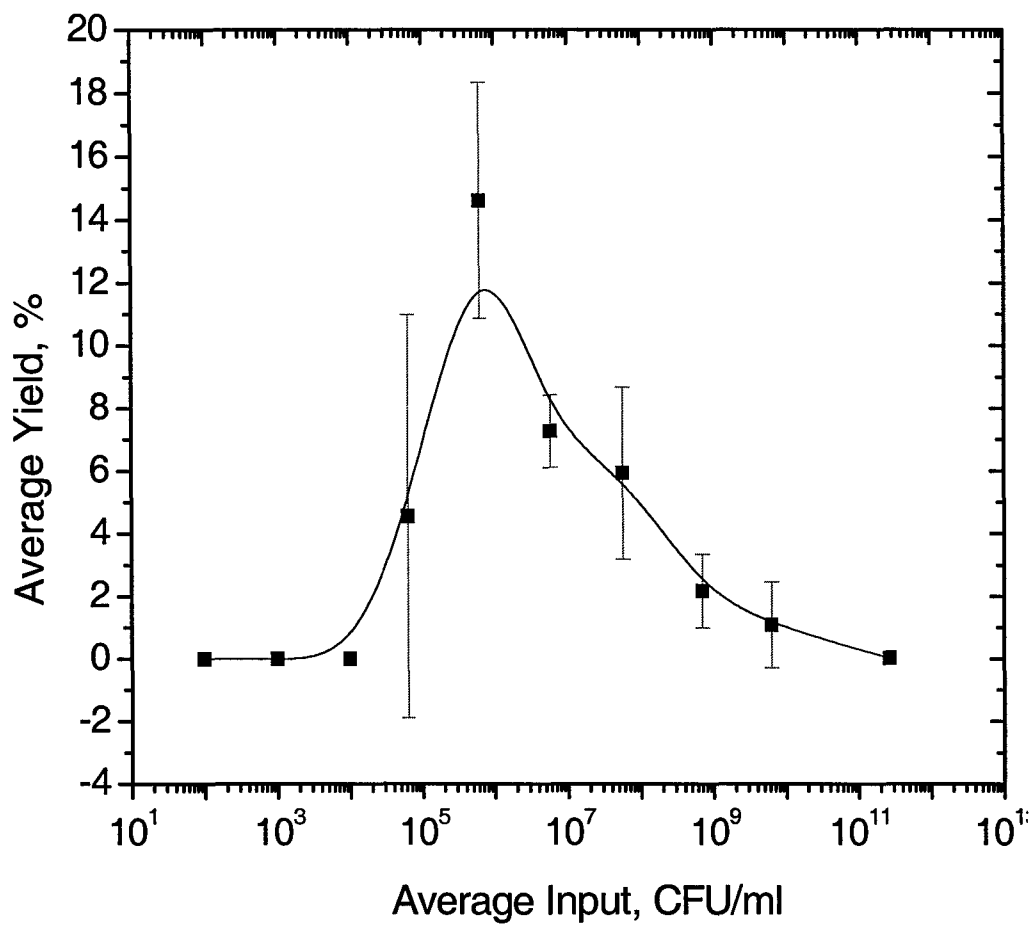


Fig. 4.9. Mean values ( $n = 3$ ) of yield plotted as a function of mean phage E2 concentration input with B-spline curve fitted to experimental data points. Bars are SD.

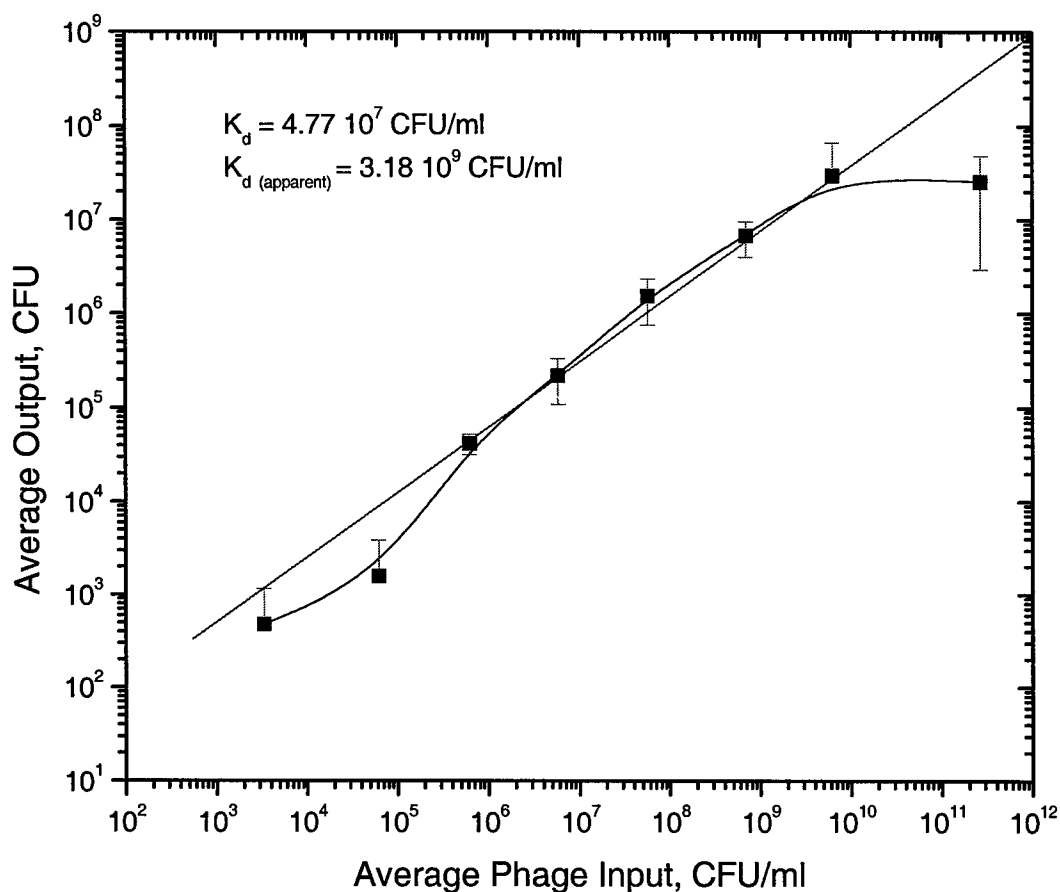


Fig. 4.10. Concentration-dependent phage E2-*S. typhimurium* binding isotherm as determined by precipitation-titration assay. Straight line is the linear least squares fit to average number of cells with bound phage as a function of the phage concentration ( $n = 3$ ,  $R = 0.997$ , slope =  $0.695 \pm 0.04$ ,  $p < 0.001$ ). Smooth line is B-spline curve fit to data points.  $K_d = 4.77 \times 10^7 \text{ CFU/ml}$ .  $K_{d(\text{apparent})} = 3.18 \times 10^9 \text{ CFU/ml}$ .  $V_{\text{max}}$  estimated at  $3.1 \times 10^7 \text{ CFU/ml}$ . Bars are SD.

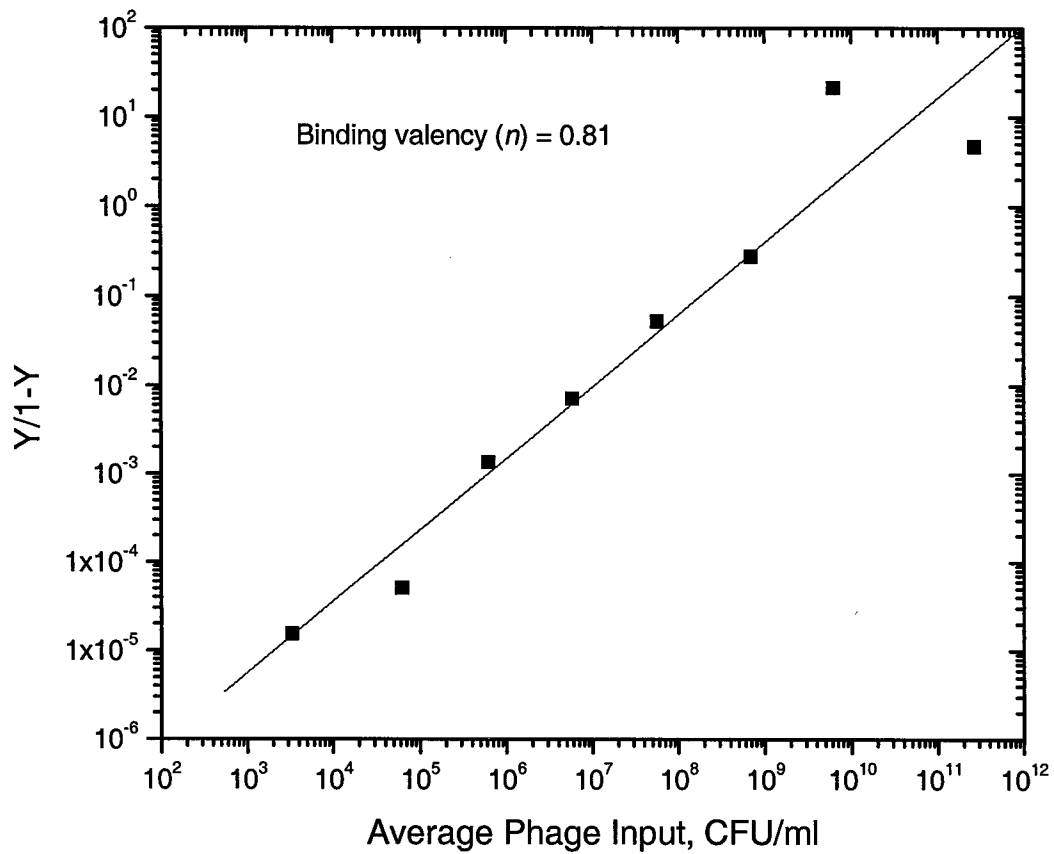


Fig. 4.11. Hill plot of binding isotherm. Ratio of bound and free *S. typhimurium* is shown as a function of phage (E2) concentration. Line represents the linear least squares fit of experimental data points ( $R = 0.967$ ,  $SD = 0.612$ ,  $p < 0.001$ ). The binding valency between cell and phage (Hill coefficient,  $n = 0.81$ ), and association binding constant ( $K_b = 2.7 \times 10^{-8}$  CFU/ml), were derived from the plot. Explanation of the Hill plot is provided in appendix A.

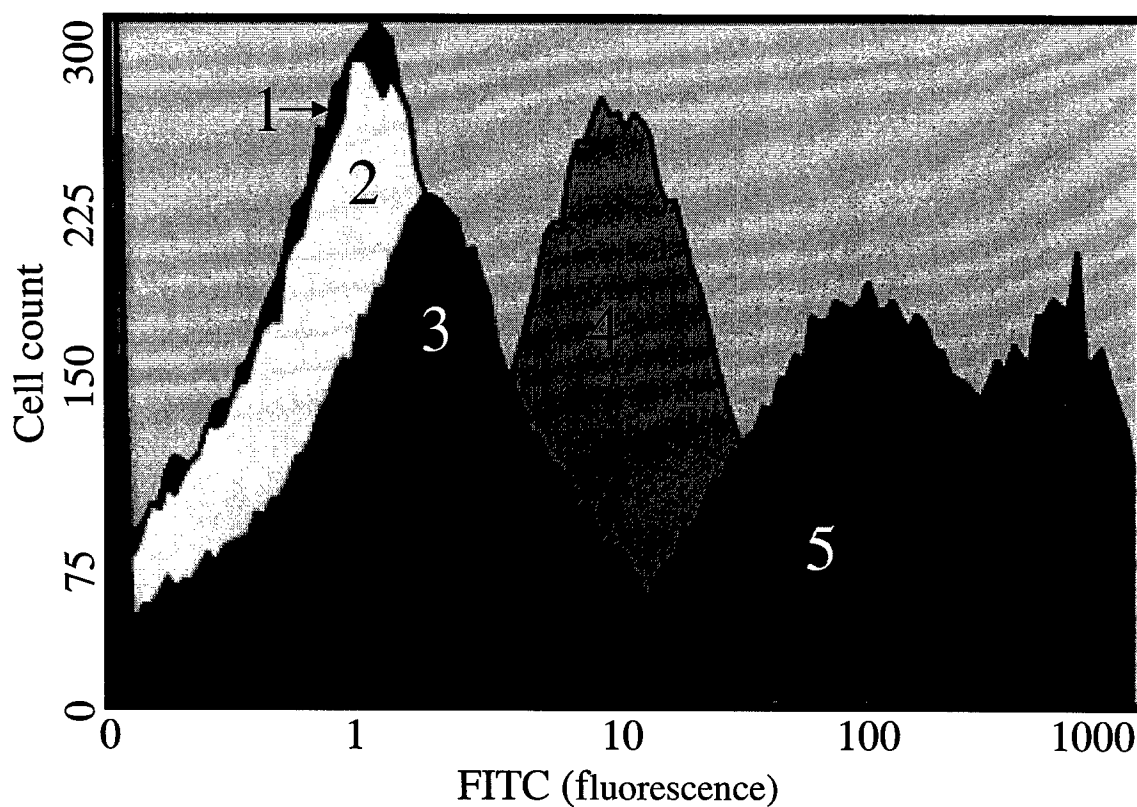


Fig. 4.12. Histogram of titrated phage E2-*S. typhimurium* binding as a function of fluorescence. Phage, binding cells, in concentrations greater than  $10^9$  virions/ml ( $10^7$  CFU) fall into distinct populations, exhibiting greater fluorescence than the control (*S. typhimurium* alone – peak 1). Peak 2:  $2 \times 10^8$  virions/ml. Peak 3:  $2 \times 10^9$  virions/ml. Peak 4:  $2 \times 10^{10}$  virions/ml. Peak 5:  $2 \times 10^{11}$  virions/ml. The negative threshold (sorting gate) was set at 1 AU on the fluorescence scale.





Fig. 4.13. Fluorescent microscopy image of Alexa labeled phage clone E2 in-complex with *S. typhimurium* (magnification 1000 $\times$  prior to digital capture).

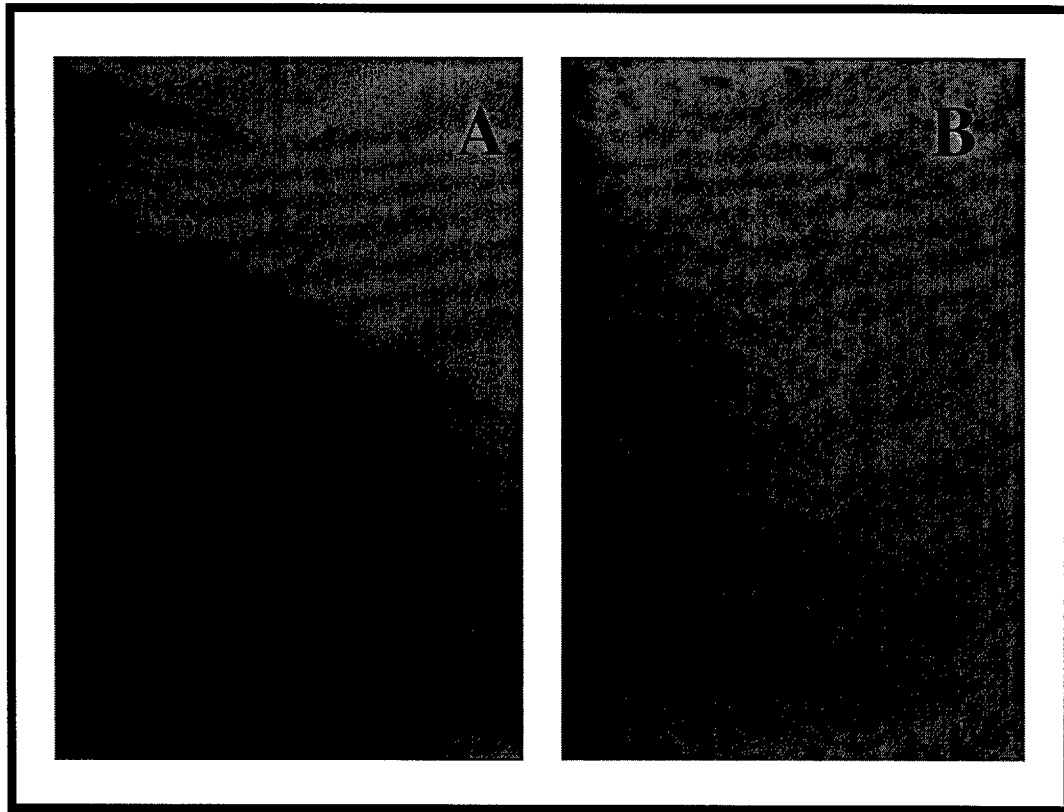


Fig. 4.14. Interaction of *S. typhimurium* with phage attached to a gold (Au) surface, as observed by Signatone high power optical microscope. Panel A is a negative control demonstrating few cells attaching to a non-related phage (1F20). Panel B shows larger number of cells binding to select phage clone E2 (magnification 1000 $\times$  prior to digital capture).

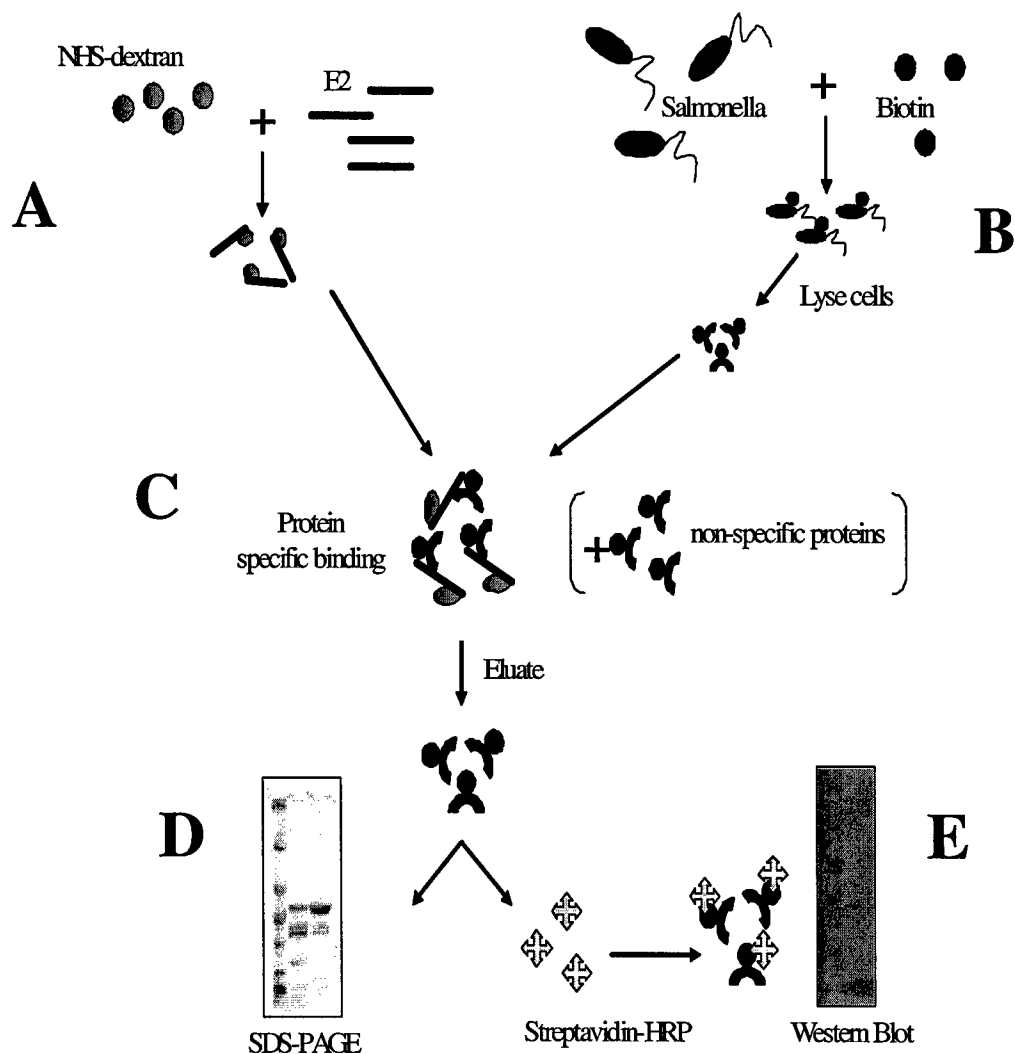


Fig. 4.15. Molecular characterization of phage receptor. Phage clone E2 was crosslinked to water-soluble NHS-dextran polymer to prepare an affinity matrix that could be reacted with a prepared lysate of *S. typhimurium*, the surface of which had been previously labeled with non-permeating biotinylation reagent (B). Following phage-receptor specific binding (C) and washing, any captured bacterial surface receptor proteins were eluted from the crosslinked phage-matrix and separated by SDS-PAGE (D), then electroblotted to nitrocellulose, conjugated with streptavidin-horseradish peroxidase, and visualized by radiography (E).

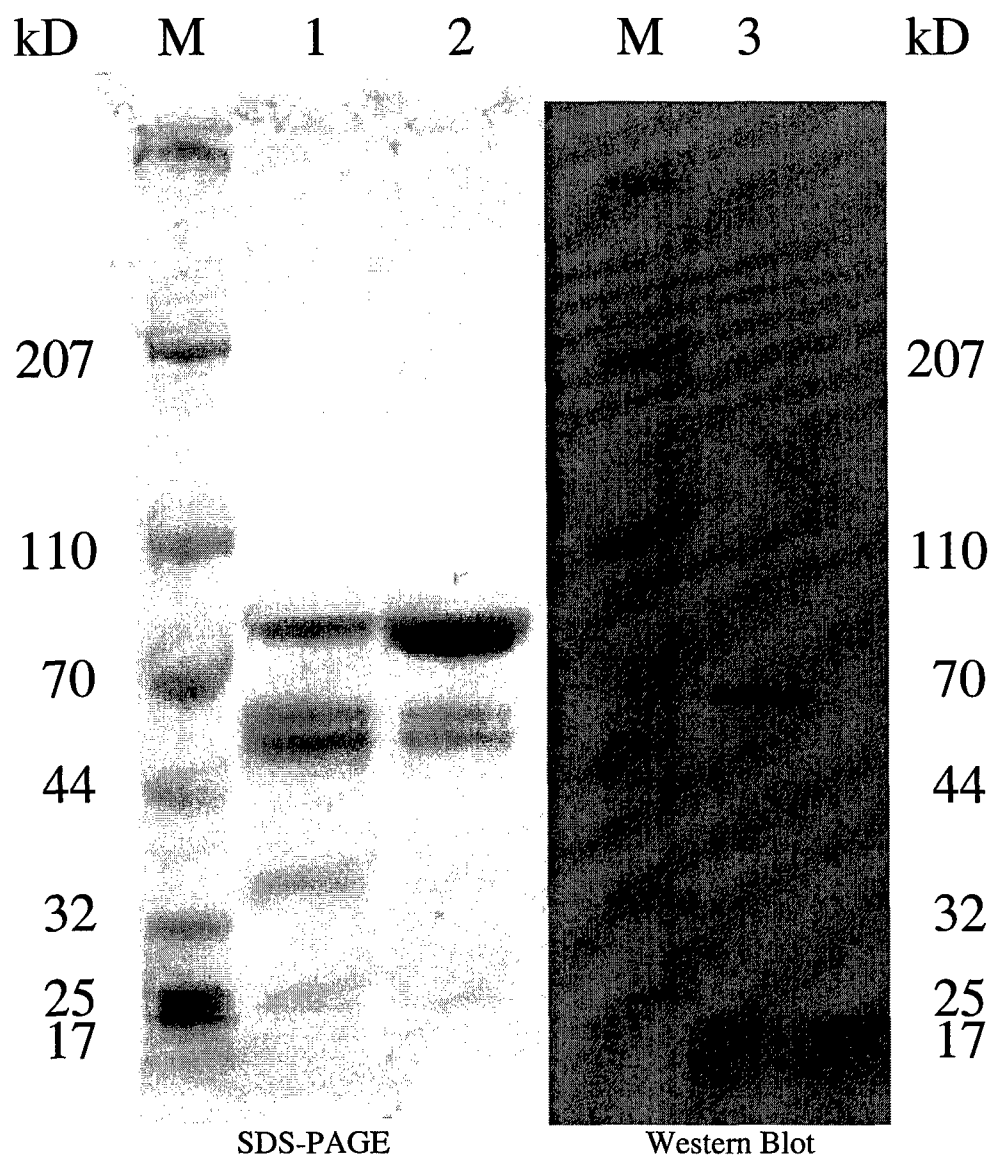


Fig. 4.16. SDS PAGE and Western blot analysis of protein eluate. A single 60 – 70 kD band was revealed by radiography. However, N-terminus protein sequencing of the corresponding area from the gel revealed only a protein sequence corresponding to serum albumin, which was present in the acid elution buffer. Lanes: M, protein ladder; 1, protein eluate from E2 phage; 2, protein eluate from wt f8-5 phage (control); 3, protein eluate from E2.

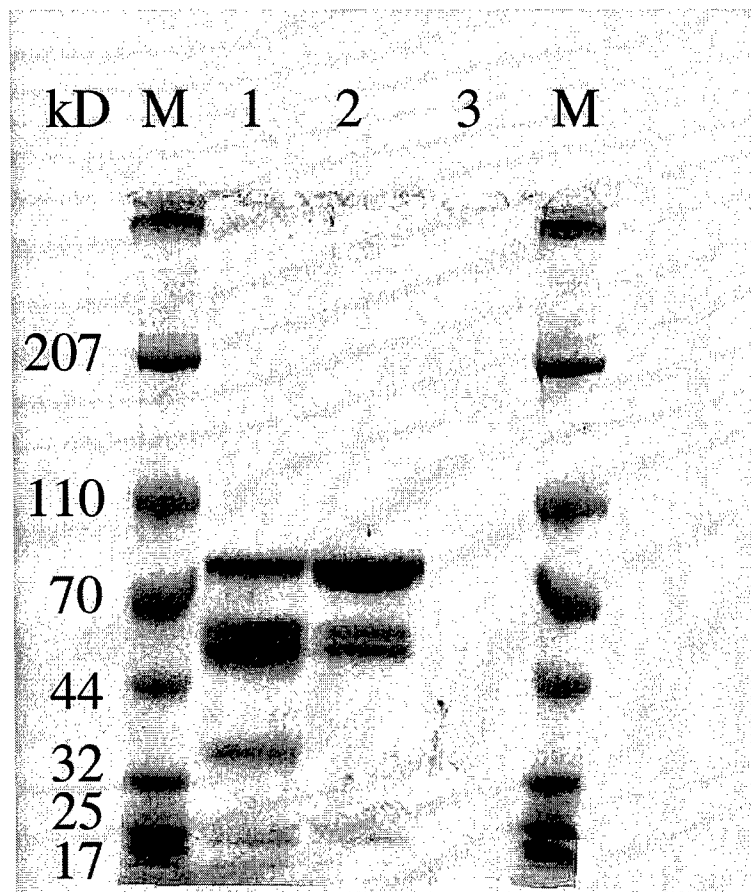


Fig. 4.17. SDS PAGE and Western blot analysis of protein eluate prepared with and without BSA in elution buffer. Lanes: M, protein ladder; 1, protein eluate from E2 phage w/BSA in buffer; 2, protein eluate from wt f8-5 phage (control) w/BSA in elution buffer; 3, protein eluate from E2 wo/BSA in buffer. All bands from the protein eluate on the gel (Lanes 1,2) are attributed to BSA because no bands are noted on the preparations of eluate without BSA (Lane 3) as a component of the elution buffer. Additionally, no band (Lane 3) is notable that corresponds to that band found on the Western blot (Fig 4.16, right). Possibly, the concentration of protein that represents the targeted receptor is too low for the gel stain to pick up, whereas the sensitivity of the Western blot is very high, allowing even extremely small concentrations to be revealed by radiography.

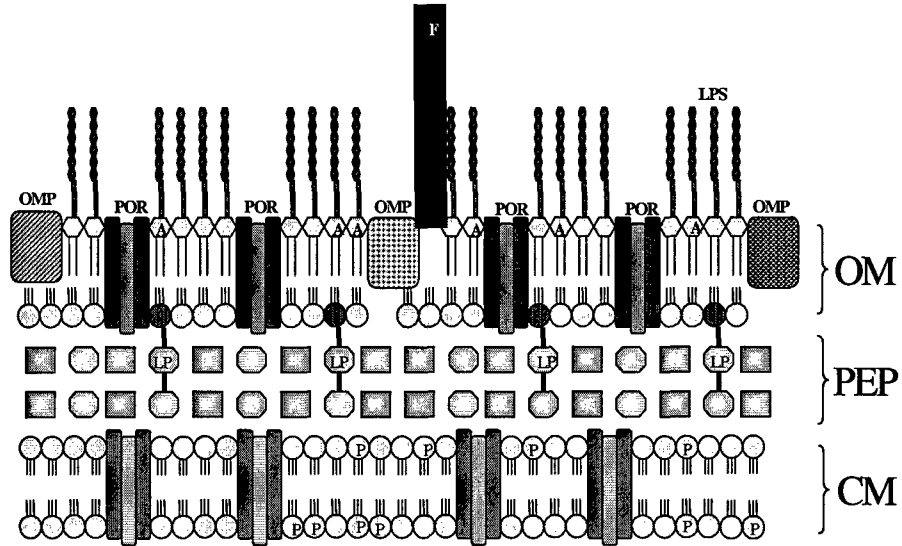


Fig. 4.18. Schematic of the outer membrane of gram-negative bacteria. (OM) outer membrane. (PEP) peptidoglycan. (CM) cytoplasmic membrane. (P) phospholipid. (LP) lipoprotein. (OMP) outer membrane protein. (POR) porin. (A) lipid A. (LPS) lipopolysaccharide (core polysaccharide and O-antigen). (F) fimbriae or flagella or pili.

## CHAPTER V

### PHAGE-COUPLED PIEZOELECTRIC BIODETECTOR FOR *SALMONELLA*

#### *TYPHIMURIUM*

##### **Abstract**

Biosensors were prepared for the rapid and sensitive detection of *S. typhimurium* in solution, based on a novel bio-recognition layer of affinity-selected bacteriophage immobilized to a piezoelectric transducer. Three immobilization methods (physical adsorption, biotin-streptavidin-phage self-assembly, and Langmuir-Blodgett) using two morphological phage forms (filamentous and phage coat proteins) were evaluated as proof-in-concept. Quantitative physical adsorption studies indicated time dependent immobilization of filamentous phage to resonators, with 92% of applied phage adsorbing within 2 hours. Approximately  $10^{10}$  -  $10^{11}$  virions/ml incubated for 1 h at room temperature were sufficient to effect working biosensors by physical adsorption. Phage adsorption was confirmed by fluorescent microscopy. Specific bacterial binding resulted in resonance frequency changes of prepared sensors, which were evaluated using linear regression analysis. Best sensor results were obtained when  $10^{10}$  -  $10^{11}$  filamentous

phage particles converted to phage coat proteins by chloroform denaturation were immobilized by Langmuir-Blodgett technique. Sensors possessed an average response time of  $< 180$  s, had a lower detection threshold of  $10^2$  cells/ml and were linear over a range of  $10^1$ – $10^7$  cells/ml with a sensitivity of approximately 2 Hz/mV per order of magnitude of *S. typhimurium* concentration. Phage-bacterial binding was confirmed by fluorescence, transmission, and scanning electron microscopy. Overall, results demonstrate proof-in-concept development of biosensors using phage-derived probes as bioreceptors for the rapid, specific, sensitive detection of *S. typhimurium*. With further refining, it could be an effective analytical method for detecting and monitoring quantitative changes of bacterial agents under any conditions that warrant recognition of such agents, including food products and possibly biological warfare applications.

## 1. Introduction

As a leading etiology of inadvertent foodborne illness in the United States, *Salmonella*'s recognized potential as a biological weapon has recently evoked critical threat agent status by the Centers for Disease Control and Prevention. Although few actual accounts of deliberate food contamination have been documented in the United States, the latest advent of global biocrimes and terrorism suggests that this trend will not continue, highlighting the importance of rapidly identifying biological agents as one part of a comprehensive, strategic plan to secure the public's food supply. There exists an urgent need for deployable, real-time threat agent detectors to replace traditional methods of food safety analysis that are slower, labor-intensive, and cost-inefficient.



Contemporary pathogen detection by culture takes as long as 96 hours regardless of the contamination origin – deliberate or unintentional.

Current rapid biodetection initiatives described in the literature include platforms such as piezoelectric transducers or so-called quartz crystal microbalances (QCM). Traditionally, the QCM has served as a mass-sensitive monitor for commercial applications such as thin-film deposition under vacuum, and electroless and electroplating processes (Krause, 1993). However, the functionality of the QCM under liquid conditions has been well characterized and their use in the development of extremely sensitive biosensors has grown enormously in the past decade. In itself, the QCM is non-specifically sensitive to mass deposition. However, when receptor-specific biorecognition agents are firmly immobilized to the QCM's sensing electrode in a thin layer it can be an extremely precise and sensitive detector of biological analytes. Generally speaking, there is a linear relationship between deposited mass and frequency response as described by Sauerbrey (1959).

QCM biosensor schemes routinely incorporate antibodies as a high affinity biorecognition unit (e.g. cf. "Chapter III – Specific and selective immunosensor for the detection of *Salmonella typhimurium* and its detection in the environment"). Although sensitive and specific, antibodies can possess numerous disadvantages including degradation under less than favorable environments, cost, and lack of standardization. Conversely, filamentous phage engineered as an antibody substitute through phage display and affinity selection techniques possesses distinct advantages over its counterpart in terms of durability, affinity, cost, sensitivity and ruggedness, and may therefore provide a more suitable biorecognition layer for biosensors.

As demonstrated in Chapter IV (*cf.* “Landscape phage probes for *Salmonella typhimurium*”), affinity-selected landscape phage probes for *S. typhimurium* possess the specificity, selectivity and affinity of monoclonal antibodies and can be used in solution as a biodetection scheme or biosorbent. However, the accompanying co-precipitation assay was time-consuming and labor intensive. Therefore, the combination of phage derived probes with QCM transducers should prove to be an effective strategy for preparing a rapid, yet specific and selective alternative. Phage-based QCM affinity detection systems for bacteria have not been described in the literature. However, Petrenko and Vodyanoy (2003) have demonstrated the potential of phage in conjunction with the QCM for the detection of model threat agents in solution.

The goal of this research was proof-in-concept development of a novel biosensor for the rapid, specific, sensitive detection of *S. typhimurium* in solution, based on a bio-recognition layer of affinity-selected filamentous bacteriophage immobilized to a QCM transducer platform. For these purposes, fd phage clone E2 – affinity-selected for *S. typhimurium* as described in Chapter IV – was used as the biorecognition agent.

## **2. Materials and methods**

### *2.1. Microorganisms*

#### *2.1.1. Bacteria*

*S. typhimurium* (ATCC 13311) was obtained from the American Type Culture Collection (Rockville, MD). Bacteria were cultured in NZY broth, pH 7.5 (1% [w/v] NZ

amine A, 0.5% [w/v] yeast extract, 0.5% [w/v] NaCl) or on NZY agar plates (1.1% [w/v] Bacto-agar, 50% [v/v] NZY broth) at 37 °C. Stock organisms were maintained in NZY broth containing 20% (v/v) glycerol at – 20 °C. All procedures involving bacteria, with the exception of biosensor testing, were performed in a biological safety cabinet using aseptic technique.

The functional performance of biosensors was evaluated bacterial suspensions prepared as follows. A single isolate from a *S. typhimurium* NZY culture plate was inoculated into 3 ml NZY broth then incubated 3 h in an orbital shaker-incubator (New Brunswick Scientific, Edison, NJ) (37 °C,  $\approx$  200 rpm) to prepare  $\approx 10^6$  cell/ml starter culture. One ml of starter culture was inoculated into 25 ml NZY broth and incubated overnight (approximately 14 – 18 h) in the orbital shaker-incubator (37 °C,  $\approx$  200 rpm). The overnight culture was washed (3  $\times$ ) by centrifugation (Allegra 21R, Beckman Coulter, Fullerton, CA) (5500 rpm, 15 min, 10 °C) in 20 ml phosphate buffered saline (0.15 M NaCl, 5 mM NaH<sub>2</sub>PO<sub>4</sub>, pH 7.0) (PBS) with final resuspension in 2 ml PBS. An aliquot (ranging from 125  $\mu$ l to 600  $\mu$ l depending upon growth) of the culture was inoculated into 4 ml 0.5% (v/v) Tween20 in TBS (50 mM Tris-HCl, 0.15 M NaCl, [pH 7.5]) (0.5% Tween20/TBS) to prepare a final suspension of OD<sub>620</sub> 0.8. The suspension was serial diluted seven times over with PBS to prepare a series of logarithmic dilutions ranging from approximately  $10^1$  to  $10^7$  cells/ml. Bacterial cell counts were confirmed through standard plate count of the three most dilute cell suspensions giving 30-300 colonies. Plate counts were performed in triplicate, averaged, and multiplied by the dilution factor to derive CFU count per milliliter. All test solutions were prepared the

day of biosensor testing and maintained on ice or at 4 °C until use, then brought to room temperature and vortex mixed prior to delivery to sensors.

### 2.1.2. Bacteriophage

Filamentous phage specific for *S. typhimurium* (clone E2; stock  $6.7 \times 10^{13}$  virions/ml) was derived previously from a landscape f8/8 phage library through affinity selection procedures as described in Chapter IV (*cf.* “Landscape phage probes for *Salmonella typhimurium*”). All procedures involving phage were performed in a biological safety cabinet using aseptic technique.

### 2.2. QCM-based phage biosensor preparation

Biosensors for the detection of *S. typhimurium* were based on phage that had been affinity-selected phage for *S. typhimurium* then immobilized to piezoelectric quartz resonators by three different methods: (1) physical adsorption, (2) biotin-streptavidin-phage self-assembly, and (3) Langmuir Blodgett (Fig. 5.1). The first two methods utilized filamentous (natural morphological form) phage, while the third required the generation of spherical phage forms by chloroform denaturation to prepare phage coat proteins for monolayers. These spherical forms, termed “spheroids,” were used for the preparation of Langmuir films (L-film) as either pure protein monolayers or in reconstitution with phospholipids.

### *2.2.1. Biosensors prepared by physical adsorption*

#### *2.2.1.1. Filamentous phage deposition study*

*2.2.1.1.1. Substrate.* AT-cut plano-plano quartz liquid-plating resonators possessing a 5 MHz nominal ( $N = 1$ ) resonant frequency were obtained from Maxtek, Inc. (Sante Fe Springs, CA) as substrates for phage deposition studies. The resonator acted as a transducer to convert the chemical signal of sample/receptor binding to a change of the sensor's resonant frequency. Resonators (2.54 cm diameter, 333  $\mu\text{m}$  thickness) possessed Au sensing (obverse) and contact (reverse) electrodes evaporated onto Ti adhesion layers (Fig. 5.2). According to the manufacturer, electrodes were polished to an average surface roughness of approximately 50 Å to minimize liquid entrapment within the pores at the crystal surface, thus reducing the creation of apparent mass loadings under liquid measurement (PM-740 Series Operation and Service Manual, 1996). As well, resonators were pre-tested to assure conformance to critical accuracy specifications required for reproducibility, and rate and thickness measurements (PM-740 Series Operation and Service Manual, 1996).

Resonators were cleaned prior to use in accordance with manufacturer's instructions as follows (RQCM Operation and Service Manual, 2003). Resonators were immersed for 5 min in 1:1:5 solution of hydrogen peroxide (30%), ammonia (25%), and ultra-purified, filter-sterilized water (Millipore Direct-Q double-distilled water subsequently vacuum filtered with a 0.22  $\mu\text{m}$  Millipore Stericup filter unit, Millipore

Corp., Bedford, MA) (“water”) heated to  $75 \pm 5$  °C, then rinsed copiously by immersion in water for several days with periodic changes. Resonators were then dried under desiccated nitrogen gas and subjected to Ar plasma cleaning (Harrick Scientific Corporation, Ossining, NY) for approximately 30 – 45 min. Cleaned resonators were stored in individual plastic petri dishes at room temperature prior to phage application. Resonators were reused in subsequent experiments only if the quality of the electrodes was found to be acceptable after cleaning.

*2.2.1.1.2. Measurement apparatus.* A Maxtek QCM “apparatus” was utilized for quantitative measurement of phage adsorption to resonators. The apparatus consisted of a 50 cm Teflon® sensor probe connected via a 3 m RG58 tri-axial sensor cable to either a TM-400 thickness monitor or PM-740 plating monitor through a rear converter port. Monitors possessed a frequency resolution of 0.03 Hz and mass resolution of 0.375 ng/cm<sup>2</sup> at 5 MHz (PM-740 Series Operation and Service Manual, 1996). Monitors were calibrated prior to use (Vodyanoy, 2005). The sensor probe was clamped horizontally to a portable lattice stand (Sigma-Aldrich, Milwaukee, WI) then tilted  $\approx 10^\circ$  transverse to the stand in order to smooth frequency readings (Fig. 5.3). The stand was positioned atop a marble block (Cole-Palmer, Vernon Hill, IL) of dimensions 330 mm  $\times$  508 mm  $\times$  51 mm to reduce extraneous vibrations from the surrounding environment. The frequency monitor was interfaced to a data-processing unit (Dell Optiplex, Dell Corp., Round Rock, TX) via RS-232C cable, where transducer responses were recorded using a Microscale software program developed locally. The sensor probe, attached to the stand, and all

necessary components of the experiment were contained within an Atmosbag™ isolation chamber (Sigma-Aldrich) (Fig. 5.4) inflated with inert nitrogen gas to prevent possible contamination of the resonator by particulate matter (e.g. dust) during deposition experiments. Procedures within the chamber were carried out through the Atmosbag's built-in dual gloves. All experiments were conducted at room temperature.

*2.2.1.1.3. Procedure.* The crystal holder cavity of the sensor probe and its associated components, i.e., Kalrez® o-ring, Teflon® crystal retainer ring, and retainer ring cover (Fig. 5.2), were thoroughly cleaned using 100% EtOH, then air-dried. The o-ring was positioned into its groove within the crystal holder cavity. The o-ring served to seal the cavity beneath the installed resonator, protecting the electrical contacts of the reverse electrode and allowing measurements in liquids. A clean resonator equilibrated to room temperature was installed obverse side up atop the o-ring using clean forceps, such that the contact electrode of the resonator was seated against the Pogo® pins in the cavity and the wraparound electrode was 90° in relation to the index pin of the housing (Fig. 5.5). The resonator was held in place with the crystal retainer ring then secured with the retainer ring cover, screwed onto the sensor probe housing and tightened approximately 1/8 turn beyond finger tight. The resonator was plated (rate and thickness were reset to zero) and data collection was started on the data processing unit at a rate of one frequency reading per second. After obtaining a steady-state baseline frequency from the clean, dry resonator, 1 ml of phage (stock E2 diluted to  $6.7 \times 10^{10}$  virions/ml) was gently pipetted to the surface of the resonator. Degassed water, prepared by boiling for 15 min under

vacuum, was used for all stock phage dilutions. Following a timed deposition period, ranging from 20 min to 24 h in duration as examined in 14 separate experiments, the phage solution was gently removed from the resonator by pipet at an edge away from the sensing electrode. The resonator was then washed (3×) with degassed water to remove any non-bound phage, and allowed to dry thoroughly. Data collection was stopped when the resonator appeared dry and had consequently re-obtained a steady-state frequency.

*2.2.1.1.4. Data analysis.* All frequency response data was analyzed off-line using Microcal™ Origin® software (Ver. 6.0, Microcal Software, Inc., Northampton, MA) as follows. ASCII files for each resonator, consisting of frequency responses recorded over the timed phage deposition period, were imported into individual spreadsheets. A line graph depicting frequency change as a function of time was prepared, and the frequency difference between beginning (prior to deposition) and ending (following deposition) steady-state levels was calculated.

*2.2.1.1.5. Visual confirmation of phage deposition.* Real-time observation of phage adsorption to resonators was performed by fluorescence microscopy. The deposition procedure was the same as previously described (*cf.* “2.2.1.1.3. Deposition procedure”), except that fluorescently labeled phage clone E2 (stock  $3.0 \times 10^{11}$  virions/ml in PBS) was utilized as previously prepared (*cf.* “Chapter IV – Landscape phages probes for *Salmonella typhimurium*”). As well, the inflatable glove chamber (*cf.* “2.2.1.1.2. Deposition measurement apparatus”) was not used due to size limitations. The



equipment arrangement (Fig. 5.6) consisted of an operational QCM apparatus with installed resonator viewed under a Nikon (Tokyo, Japan) ECLIPSE E800 fluorescent microscope equipped with 100W Hg lamp, and 4× (NA 0.13), 40× (Plan Fluor DIC M, NA 0.75), 60× (Plan Apo, NA 1.40) and 100× objectives (Plan Apo, NA 1.40). Digital images (500 – 550 nm) were captured using a SPOT RT Slider CCD video camera (1520 × 1080 pixel optical resolution) (Diagnostic Instruments, Inc., Sterling Heights, MI) with exposure settings: red – 1.3 s, green – 2.02 s. Images were transferred to a data processing unit (Dell Optiplex, Dell Corp., Round Rock, TX) for storage and processing using SPOT Advanced software (Ver. 3.5.9 for Windows 2000; build 6 August 2003, Diagnostic Instruments) and Adobe® Photoshop® (Ver. 5.0LE, Adobe Systems, San Jose, CA).

Sequential photos of phage adsorption to resonators were taken in 20 s increments for up to 2 h. Following phage adsorption for a specified duration, the resonator was removed from the sensor probe using clean forceps, rinsed of excess phage by immersion in degassed water (3×), and examined under fluorescent oil immersion (× 1000). Phage particles were considered to be any individual fluorescent particles or bundles of particles distinguishable from each other in the field of view. A negative control, consisting of a new, clean resonator treated with Alexa 488 fluorescent dye, was incorporated into the study for comparison.

#### 2.2.1.2. Biosensor preparation and testing

2.2.1.2.1. *Substrate.* Pre-cleaned resonators previously described (cf. “2.2.1.1.1. Substrate”) were used as substrates for biosensor preparation methods, including physical adsorption, biotin-streptavidin-phage self-assembly, and Langmuir Blodgett.

2.2.1.2.2. *Preparation.* Stock phage clone E2 was diluted to  $6.7 \times 10^{10}$  virions/ml with PBS. One ml of diluted phage was added by pipet to the obverse side of a resonator, still in its individual plastic petri dish, ensuring that the sensing electrode was immersed. The solution was incubated on the resonator for 1 h at 4 °C. Following this period, the phage solution was gently removed from the resonator by pipet at an edge away from the sensing electrode. Resonators were washed (3×) by immersion in 25 ml PBS with gentle rocking (Reliable Scientific, Hernando, MS) then blocked with bovine serum albumin (BSA) (1 µg/ml for 1 h at 4 °C). The resonator was again washed (3×) by immersion in 25 ml PBS with gentle rocking then left with  $\approx 100$  µl of PBS on the electrode to keep the phage hydrated. The prepared biosensor was stored in the petri dish at 4 °C until testing, generally within 1-4 h after preparation. Sixty biosensors were prepared.

2.2.1.2.3. *Measurement apparatus.* Two QCM configurations were utilized to measure biosensor response to *S. typhimurium* test suspensions.

Platform 1 was the QCM arrangement previously described (cf. “2.2.1.1.2. Deposition measurement apparatus”), with the exceptions that the sensor was not

enclosed within the inflatable chamber, and voltage output from the frequency monitor was collected for analysis of some sensors, instead of frequency output. The voltage output of Maxtek monitors is corresponding but inversely related to frequency output (Pathirana et al., 2000). The voltage output of the monitor was obtained via RS-232 interface of a voltmeter hard wired from its COM and V/ $\Omega$  terminals to the thickness ground and thickness return output pins of the monitor's digital to analog converter.

Platform 2 (Fig. 5.7) was a novel flow cell arrangement based on the configuration of platform 1, except that a Maxtek FC-550 flow cell was attached to the sensor probe cavity in place of the crystal retainer ring, allowing full enclosure of the sensor (Fig. 5.8 vice Fig. 5.9). Thus, delivery of test suspensions to the biosensor was changed from one of manual pipetting to gravity flow by employing a series of plastic 30 ml syringes (Becton Dickinson, Franklin Lakes, NJ) outfitted with stopcocks that were connected to the flow cell via a central perfusion manifold (MP-8, Warner Instruments Inc., Hamden, CT). Connections between the syringes, manifold, and flow cell were made with 1/16" ID polyethylene tubing. This system allowed steady, pulseless delivery of test solutions to the sensor surface with minimal pressure. Prior to use in biosensor testing, the flow cell was evaluated with PBS, bacterial test suspensions, and a graded series of glycerol solutions ranging from 0% (water) to 100% (stock glycerol). The cavity volume of the flow chamber was approximately 100  $\mu$ l.

2.2.1.2.4. *Assay procedure.* Biosensors were tested with either platform configuration 1 or 2 as follows.

Platform 1. The crystal holder cavity of the sensor probe and its associated components were cleaned and assembled as previously described (*cf.* “2.2.1.1.3. Deposition procedure”). A prepared biosensor equilibrated to room temperature was installed into the cavity as previously described for a clean resonator (*cf.* “2.2.1.1.3. Deposition procedure”) (Fig. 5.10–1). The biosensor was plated and data collection was started on the data processing unit at a rate of one to ten frequency or voltage readings per second. After obtaining a steady-state baseline frequency or voltage reading, 1 ml of PBS was pipetted to the top of the sensor and the crystal holder cavity was covered with a 1” diameter plastic petri dish lid to prevent air currents from causing disturbance of the liquid (Fig. 5.10–2). After seven minutes, data collection was stopped (Fig. 5.10–3) and the PBS was gently suctioned off the sensor at an edge away from the sensing electrode (Fig. 5.10–4). Prepared logarithmic series of *S. typhimurium* test suspensions was then assayed from least concentrated ( $10^1$  cells/ml) to most concentrated ( $10^7$  cells/ml) in the same manner as the PBS (Fig. 5.10–2, 3, 4). Data collection (ASCII) files were prepared for each corresponding test solution. Following testing and removal of the last test solution, the sensor was removed and placed into 100% EtOH to degrade the phage and bacteria until further sensor cleaning could be performed. This procedure was repeated for subsequent sensors tested the same day.

Platform 2. The testing procedure for platform 2 was the same as that outlined for platform 1, with the exception of test suspension delivery to the biosensor. Instead of

pipetting solutions to the surface of the biosensor, vertically positioned syringes were utilized as vessels for containing and delivering *S. typhimurium* test suspensions to a flow cell enclosing the biosensor; an additional syringe was filled with PBS only. The polyethylene tubing connecting the syringe stopcocks to the manifold and the central line leading from manifold to flow cell were priming from most concentrated to least concentrated. PBS was always the last primed solution, allowing any *S. typhimurium* left in the central line to be purged before testing commenced. The crystal holder cavity of the sensor probe and its associated components were cleaned and assembled as previously described (*cf.* "2.2.1.1.3. Deposition procedure"). A prepared biosensor equilibrated to room temperature was installed into the cavity as previously described for platform 1, except that the flow cell was added in place of the crystal retainer ring (Fig. 5.9). The retainer ring cover was screwed onto the sensor probe housing and tightened approximately 1/8 turn beyond finger tight. The central line leading from the manifold was then connected to the inlet of the flow cell. A waste line leading to an Erlenmeyer flask was attached to the outlet of the flow cell. The biosensor was plated and data collection was started on the data processing unit at a rate of one to ten frequency or voltage readings per second. The remainder of the testing procedure was the same as described for platform 1. All measurements were taken with the analyte in static state.

*2.2.1.2.5. Biosensor data analysis.* All frequency or voltage response files (ASCII) were maintained in the database of the computer or copied to compact disk and analyzed off-line using Microcal™ Origin software program (Ver. 6.0, Microcal Software) and Microsoft® Excel (Ver. 2000, Microsoft Corp, Seattle, WA). The multiple ASCII files

for each sensor, comprising individual test suspension frequency or voltage responses over time, were imported into a single spreadsheet by utilizing a column format for each test suspension concentration. A conglomerate line graph of frequency or voltage changes as a function of assay time was plotted for all suspensions tested on that sensor. Visual inspection of this graph allowed determination of steady-state responses of the sensor. Generally, this steady-state was achieved within several minutes following administration of test suspensions to the biosensor. However, in order to maintain data congruency between all sensors, the steady-state was considered to be the last two minutes of each seven-minute test suspension incubation. From these last two minutes, an average steady-state frequency response for each test suspension applied to a sensor was determined statistically (generally 120 – 1200 data points depending upon the number of frequency/voltage readings captured per second), then plotted to derive a graph of the mean steady-state responses of the sensor as a function of the bacterial test suspension concentration. Linear regression was applied to the data points to determine correlation coefficient, slope, and significance. For the purposes of this study, biosensor results were considered statistically different when the *p*-value was less than 0.05 (95% confidence interval).

Data analysis for biosensors prepared by biotin–streptavidin multilayers (*cf.* 2.2.2) and Langmuir–Blodgett method (*cf.* 2.2.3) was performed in the same manner.

*2.2.1.2.6. Fluorescence microscopy.* Real-time observation of phage-bacteria binding at the sensor surface was also confirmed by fluorescence microscopy in conjunction with an

operational QCM platform. The equipment arrangement was the same as previously described for phage deposition studies (cf. "2.2.1.1.5. Visual confirmation of phage deposition").

Fluorescently labeled phage clone E2 was used as prepared (cf. "Chapter IV – Landscape phages probes for *Salmonella typhimurium*") in place of non-fluorescently labeled phage to fabricate four biosensors as previously described (cf. "2.2.1.2.2. Fabrication procedure"). *S. typhimurium* cells were fluorescently labeled (Alexa Fluor 488 Protein Labeling Kit, Molecular Probes, Eugene, OR) by adding 1 of  $10^7$  cell/ml suspension (cf. "2.1.1. Bacteria") to one vial of reactive dye then incubating 1 h at 4 °C. Cells were washed (3×) with 20 ml PBS by centrifugation (3500 rpm, 10 min, 4 °C) prior to measurement of fluorescence. The suspension was serial diluted six times over with PBS to prepare a series of logarithmic dilutions ranging from approximately  $10^1$  to  $10^6$  cells/ml. Bacterial cell counts were confirmed through standard plate count of the three most dilute cell suspensions. Plate counts were performed in triplicate, averaged, and multiplied by the dilution factor to derive CFU count per milliliter. All test solutions were prepared the day of biosensor testing and maintained on ice or at 4 °C until use then vortex mixed prior to delivery to sensors.

The four biosensors were assayed with the fluorescently labeled *S. typhimurium* test suspensions as previously described for platform 1 (cf. "2.2.1.2.4. Assay procedure"), then examined by fluorescence microscopy under oil immersion (× 1000). A new, clean resonator treated with Alexa 488 fluorescent dye was incorporated into the study as a negative control.

#### 2.2.1.2.7. Scanning electron microscopy

Phage-bacteria binding was also confirmed by scanning electron microscopy (SEM). The protocol for SEM preparation and analysis of sensors was based on that previously described in Chapter III (cf. "Specific and selective immunosensor for *Salmonella typhimurium* and its detection in the environment"). Previously assayed biosensors were air-dried at room temperature for 24 h in a sealed petri dish by elevating them over a small layer of desiccant using wooden applicator sticks. As well, a resonator with only phage immobilized was prepared in the same manner as a control. The dried sensors were mounted onto aluminum stubs with carbon adhesive tape then sputter-coated at 0.02 mbar Ar gas pressure with a 60:40 Au/Pd mixture at 30 mA for 1.5 min. Sensors were examined using a Zeiss DSM 940 SEM (Thornwood, NY) at 10 kV. Digital micrographs captured using a Digital Image Transfer Recognition Program (Zeiss) were processed with Adobe Photoshop 5.0LE.

#### 2.2.2. Biosensors prepared by biotin-streptavidin-phage self assembly

**2.2.2.1. Preparation.** One ml of biotinylated BSA (Lyophilized Sulfo-NHS-LC-LC-Biotin, Pierce, Rockford, IL prepared to 100  $\mu$ M final concentration with PBS) was added by pipet to the obverse side of a resonator still in its individual plastic petri dish, ensuring that the sensing electrode was immersed. The resonator was incubated with the solution for 1h at 4 °C then washed (3 $\times$ ) by immersion in 25 ml PBS (in the plastic petri dish) with gentle rocking to enhance removal of excess BSA. After the last decant, 1 ml



of streptavidin (Pierce) diluted with PBS to 1  $\mu\text{g/ml}$  final concentration was added by pipet to the now functionalized biotin-BSA-gold surface of the resonator and incubated  $\approx$  24 h at 4  $^{\circ}\text{C}$ . The resonator was washed (5 $\times$ ) again with PBS. After the last decant, 1 ml of biotinylated stock phage clone E2 ( $3.0 \times 10^{11}$  virions/ml; 478 biotin residues per phage particle), prepared previously (Sorokulova et al., 2005), was added by pipet to the resonator and incubated for 1 h at 4  $^{\circ}\text{C}$ . The resonator was washed (5 $\times$ ) with PBS and left with  $\approx$  100  $\mu\text{l}$  of PBS on the electrode to keep the phage hydrated. The prepared biosensor was stored in the petri dish at 4  $^{\circ}\text{C}$  until testing, generally within 1 — 4 h after preparation. Twenty-five biosensors were prepared.

*2.2.2.2. Assay procedure.* Prepared biosensors were tested using platform 1 configuration as previously described (cf. “2.2.1.2.4. Assay procedure”).

### *2.2.3. Biosensors prepared by Langmuir–Blodgett method*

*2.2.3.1. Spheroid preparation.* The phage denaturation method of Manning et al. (1981), with modifications, was used to convert filamentous phage E2 to spheroid forms for surface pressure–area ( $\Pi$ –A) isotherms and biosensor preparation. Stock phage clone E2 in PBS ( $6.7 \times 10^{13}$  virions/ml) was diluted to  $2.68 \times 10^{12}$  virions/ml with Tris EDTA (TE) buffer (0.01 M Tris, 0.001 M EDTA, [pH7.5]). Four hundred microliters of diluted phage was combined with an equal volume of spectrophotometric-grade chloroform (99.8% A.C.S., Sigma–Aldrich). All reactants were at room temperature. Spheroid

formation was induced by gently vortexing 5 – 6 times (5 s intervals) over a one-minute duration. The top phase (aqueous) containing the spheroids was retained for phage coat monolayer preparation. Spheroids were prepared <1 h prior to isotherm measurement and maintained at 4 °C until use. Polypropylene products used in spheroid preparation were considered chloroform-safe for short duration usage (Eppendorf technical service, 2004; USA Scientific technical service, 2004). All applicable materials were autoclave sterilized prior to use. Glass Pasteur pipets (Fisher Scientific, Pittsburgh, PA) were used for the transfer of stock chloroform to polypropylene containers. Procedures were performed in a biological safety cabinet and aseptic technique was followed throughout.

*2.2.3.2. Spheroids in phospholipid base.* Prepared spheroids were also combined with 1,2-diphytanoyl-sn-glycero-3-phosphocholine (PC) (Avanti Polar Lipids, Inc., Alabaster, AL) to prepare lipid-based spheroid mixtures for  $\Pi$ -A isotherms and biosensor preparation. Six hundred microliters of spheroids in aqueous solution, as prepared by chloroform denaturation, were combined with an equal volume of PC previously reconstituted in hexane (1 mg/ml concentration) (Yilma, 2004). The mixture was vortexed vigorously for 2 min to derive a homogenous emulsion. Following standing formation of an interface, the top phase containing the spheroid forms and PC was carefully removed and retained for monolayer preparation. Spheroids in PC were prepared <1 h prior to isotherm measurement and/or biosensor preparation and maintained at 4 °C until use.

*2.2.3.3. Spheroid electrophoresis.* Ten microliter aliquots of spheroids and 4  $\mu$ l aliquots of stock phage clone E2, both containing 20% (v/v) bromophenol blue dye, were resolved in 0.8% (w/v) agarose gels (DNA high-melting agarose prepared with 0.05 M  $\text{NaH}_2\text{PO}_4$  and 1mM  $\text{MgCl}_2$ , pH 7.5; Fisher Scientific, Fair Lawn, NJ) using a Mini-sub® cell GT system (Bio-Rad Laboratories, Hercules, Ca) with 0.05 M  $\text{NaH}_2\text{PO}_4$  buffer containing 1mM  $\text{MgCl}_2$ , (pH 7.5).  $\lambda_{\text{BstEII}}$  DNA heated at 70 °C for 10 min was used as a size standard. Agarose gel electrophoresis (AGE) was performed for 1.5 h at 50 V.

Compounds used to prepare buffer and gels were analytical grade or higher. Gels were rinsed in double-deionized water and rocked (r/r) in 0.2 N NaOH for 1 h; r/r in 1 M Tris-HCl (pH 7.5) for 15 min; and r/r in 40 ml 0.05 M  $\text{NaH}_2\text{PO}_4$  buffer with 1mM  $\text{MgCl}_2$ , (pH 7.5) containing 7  $\mu$ l nucleic acid gel stain (SYBR® Green I, 10000X concentration in DMSO, Cambrex Bio Science, Rockland, MD) for 1 h. Following final rinse, filamentous phage and spheroid DNA were visualized at 521 nm using a KODAK 290 Electrophoresis Documentation and Analysis system (Eastman Kodak Company, Rochester, NY), equipped with a DR40 Kodak camera, DR40 amber camera filter (Clare Chemical Research, Denver, CO) and dark reader transilluminator (Clare Chemical Research). Images (exposure = 8 s) were captured and processed electronically using Kodak 1D software (Ver. 3.5.3, Eastman Kodak Company).

*2.2.3.3.1. Timed chloroform exposure studies.* AGE was utilized to determine the optimal conversion time of filamentous phage to spheroids by chloroform denaturation. Stock phage clone E2 in PBS was diluted to separate concentrations of  $2.2 \times 10^{13}$

virions/ml and  $1.1 \times 10^{13}$  virions/ml then induced to spheroids as previously described (cf. "2.2.3.1. Spheroid preparation") using either a 1 min or 3 min exposure duration. Spheroids were prepared <1 h prior to AGE and maintained at 4 °C until use.

*2.2.3.3.2. Phage-chloroform concentration studies.* AGE was also used to study the degree to which filamentous phage contract into spheroids when titrated against stable amounts of chloroform. Stock phage E2 in PBS was diluted to five separate logarithmic concentrations ranging from  $2.2 \times 10^{13}$  to  $2.76 \times 10^{11}$  virions/ml then induced to spheroids as previously described (cf. "2.2.3.1. Spheroid preparation"). Spheroids were prepared <1 h prior to electrophoresis and maintained at 4 °C until use.

*2.2.3.4. Visualization of spheroids.* Transmission Electron Microscopy (TEM) allowed visual characterization of spheroids both as independent entities and in complex with *S. typhimurium*. Spheroids independent of *S. typhimurium* were prepared as previously described (cf. "2.2.3.1. Spheroid preparation") then diluted 1:100 in DDH<sub>2</sub>O. Spheroids in complex with *S. typhimurium* were prepared by incubating 1 ml of prepared spheroids with (1 ml)  $10^8$  cells *S. typhimurium* (cf. "2.1.2. Bacteria") for 10 min while rotating, then diluting 1:100 in DDH<sub>2</sub>O. Ten microliter aliquots of the spheroids, alone or in complex with *S. typhimurium*, were incubated with formvar/carbon-coated grids (EMS, Hatfield, PA) for 45 s – 1 min; excess fluid was removed by absorption to filter paper. Grids preps were washed and negatively stained with either filter-purified (0.22 µm) 2% (w/v) uranyl acetate (pH ≈ 4.5) or 2% (w/v) phosphotungstic acid (pH 7.0) for 3 – 5 min, then

examined under a Philips EM 301 TEM (Netherlands) at 60 kV. Hand-developed micrographs were digitally scanned and processed with Adobe® Photoshop® (Ver. 5.0LE, Adobe Systems).

*2.2.3.5. Salmonella antibodies.* Rabbit polyvalent O (mixture of O2/O4/O7/O8/O9/O9,46/O3,10/O1,3,19) *Salmonella* antiserum (Denka Seiken Co., Tokyo, Japan) was procured from Oxoid (Ogdenburg, NY). Reactivity of the antiserum against *S. typhimurium* (ATCC 13311) was confirmed through standard slide agglutination test. PBS was utilized as a negative control. Antibodies had been “heat-treated at 56 °C for 30 min, absorbed to remove cross-agglutinins, and sterilized by antibacterial filtration” according to the manufacturer (*Salmonella* Immune Sera “SEIKEN” Package Insert, 1996). The antibody concentration was not available through the distributor or manufacturer. Antiserum was warmed to room temperature prior to use, otherwise stored at 4 °C.

*2.2.3.6. Apparatus for  $\Pi$ -A isotherm and biosensor preparation.* A microprocessor-controlled KSV 2200 Langmuir film balance (Fig. 5.11) (KSV Chemicals, Helsinki, Finland) (thoroughly described in Olsen, 2000) was used to prepare  $\Pi$ -A isotherms of spheroid and *Salmonella* antibody monolayers, and subsequently deposit them to substrates for biosensor preparation. Surface monolayers were prepared on a pH balanced subphase consisting of 55 mM KCl, 4 mM NaCl, 0.1 mM CaCl<sub>2</sub>, 1 mM MgCl<sub>2</sub>, and 2 mM MOPS, (pH 7.40 ± 0.01) in ultra-purified (resistance ≥ 18 MΩ/cm) water

(Milli-Q Water Purification System, Millipore Corp.). Compounds (Sigma-Aldrich) used to prepare stock solutions were analytical grade or higher. All stock solutions and subphase were prepared with clean glassware and pipets then filter-purified (Millipore Stericup 0.22  $\mu\text{m}$ , Millipore Corp.) to ensure utmost purity. Subphase was stored in inert I-Chem<sup>TM</sup> amber glass jugs (Nalgene, Rochester, NY) tightly capped to prevent evaporation and used within one week of preparation, otherwise discarded.

*2.2.3.7. Isotherm procedure.* The procedure described by Olsen (2000) for *Salmonella* antibodies, with modifications, was used to prepare spheroid surface monolayers for  $\Pi$ -A isotherms. Spheroids in solution, prepared alone or in combination with PC as previously described, were brought to room temperature if applicable, vortexed to a homogenous mixture, then pipetted to the subphase surface ( $\approx 10 \mu\text{l}$  drops) via a cleaned, wetted glass rod until a surface pressure of 0.5 – 0.9 mN/m was obtained. The amount of spheroid solution pipetted to the surface was variable, generally between 100 – 200  $\mu\text{l}$ ; pure spheroids required greater volumes and those in combination with PC required less. A constant temperature circulator maintained the subphase at  $20 \pm 0.1 \text{ }^{\circ}\text{C}$ . Following 10 – 20 min for equilibration and evaporation of hexane (spheroids in PC only), the surface layer was compressed at 10 mm/min. The data processing unit of the film balance instrument automatically performed acquisition and recording of deposition data to include elapsed time, surface pressure, and barrier position. *Salmonella* antibody surface layers for isotherm measurement were prepared as previously described (Olsen, 2000).

2.2.3.8. *Isotherm data analysis.* ASCII data files from the data processing unit of the film balance instrument were copied to floppy disk and analyzed off-line using Microsoft® Excel (Ver. 2000, Microsoft) and Microcal™ Origin® (Ver. 6.0, Microcal Software) as follows. The ASCII file data for each isotherm, including compression barrier position (mm), surface pressure (mN/m), and trough area (mm<sup>2</sup>) was imported into an individual spreadsheet. The area (%) of the trough, and compressibility modulus,  $K$ , (mN/m) for the elasticity plot, were derived from this data. The isotherm was plotted as a line graph depicting surface pressure,  $\Pi$ , as a function of trough area,  $A$ . Elasticity was plotted as a line graph depicting compression modulus,  $K$ , as a function of the surface pressure,  $\Pi$ .

2.2.3.9. *Phage coat biosensor preparation.* Immobilization of phage coat proteins onto resonators, either as pure protein monolayers or in combination with PC, followed the procedure described by Olsen (2000) for *Salmonella* antibodies with the following modifications.

Using forceps, four clean resonators were secured back to back (obverse exposed) in an aluminum holder specially designed to accommodate resonators for dipping through the film. The holder was attached to the film collector unit and the resonators were lowered into position below the subphase such that the gold electrodes on the obverse side of the resonators were just below the air-liquid interface (Fig. 5.12). Spheroids in solution, prepared alone or in combination with PC, were brought to room temperature (if applicable), vortexed to a homogenous mixture and pipetted to the subphase surface ( $\approx 10$   $\mu$ l drops) via a cleaned, wetted glass rod (Fig. 5.13) until a surface pressure of 8 – 10

mN/m was obtained. As stated previously, the amount of spheroid solution pipetted to the surface to achieve the necessary initial pressure was variable; generally the volume was between 600 – 2000  $\mu$ l. A constant temperature circulator maintained the subphase at  $19 \pm 0.1$  °C. Following 10 – 20 min for equilibration and evaporation of hexane (spheroids in hexane only), the surface layer was compressed at a rate of 30 mm/min until a surface pressure of 36 mN/m (spheroids only) or 38 mN/m (spheroids in PC) was reached. These optimal surface pressures were derived from isotherm/elasticity analysis. The compression rate was manually changed to 230 mm/min once the correct surface pressure was reached then monolayer deposition was commenced by raising the resonators out of and into the surface film at a rate of 4.5 mm/min, with 90 s intervals between directions. Using this method, approximately 7 – 13 monolayers were deposited onto resonators; variability in the number of monolayers depended upon the efficiency of spheroid transfer from the subphase to the resonators as determined by transfer ratio (TR). The data processing unit automatically performed acquisition and recording of deposition data to include elapsed time, surface pressure, barrier position, and TR. Following deposition, prepared biosensors were removed from the holder using clean forceps and placed into individual Petri dishes atop o-rings. Sensors were stored at 4 °C until testing, normally within 1 - 4 h of preparation. Fifty-two biosensors were fabricated in total.

*2.2.3.10. Biosensor assay procedure.* Prepared biosensors were tested using platform 1 configuration as previously described (cf. “2.2.1.2.4. Assay procedure”).



### 3. Results and discussion

#### 3.1. Filamentous phage deposition to resonators

An initial phage deposition study based on the “dip and dry” gravimetric procedure of Prusak-Sochaczewski and Luong (1990) was conducted to determine the feasibility of physically adsorbing filamentous phage to resonators and if successful, the optimal conditions of time and concentration necessary for the preparation of biosensors capable of detecting *S. typhimurium* under liquid conditions. Dip and dry refers to measurement of the change in the resonant frequency,  $\Delta f$ , of a dry resonator prior to and after deposition of mass. According to theory (Sauerbrey, 1959), a mass (attributed here as phage),  $m$ , deposited to the active area of the sensing electrode results in a decrease of the resonator's oscillation frequency, the total quantity of which can be solved for using Sauerbrey's (1959) equation as follows, assuming that the mass creates a rigid, uniform film that does not slip and has the same acousto-elastic properties as quartz:

$$\Delta f = -Cf(\Delta m) \quad (1)$$

where,  $\Delta f$  is the observed change in frequency (Hz) of the resonator under oscillation at its fundamental frequency due to mass loading,  $Cf$  = sensitivity factor of the resonator in Hz/ng/cm<sup>2</sup>, and  $\Delta m$  = change in mass per unit area in g/cm<sup>2</sup>. The sensitivity factor ( $Cf$ ) of Maxtek's 5 MHz AT-cut resonator is 0.0566 Hz/ng/cm<sup>2</sup> at 20 °C, and takes into

account the harmonic number at which the resonator is driven, resonant frequency (Hz) of the fundamental mode of the resonator, and the density and effective piezoelectrically stiffened shear modulus of the quartz substrate (RQCM Operation and Service Manual, 2003).

Using this approach, the resonator acts as a gravimetric sensor, much like a very sensitive nanobalance. A representative line graph demonstrating phage adsorption as a function of time is shown in Fig. 5.14. The graph depicts the steady-state oscillation of a dry, clean resonator at resonance prior to the application of 1 ml of diluted stock phage E2 in suspension ( $6.7 \times 10^{10}$  virions/ml) ( $f_S$ ), followed by an 18 h incubation period at room temperature, removal ( $f_R$ ) of the phage suspension and washing with degassed water, and finally drying, with a subsequent return to steady-state resonance ( $f_E$ ). The resulting frequency change,  $\Delta f$ , measured as a decrease,  $f_S - f_E$ , was  $-161$  Hz, indicating that phage adsorbed to the resonator. This is contrasted by a control (Fig. 5.15) consisting of a clean resonator interrogated with degassed water only, which resulted in no frequency change ( $f_S - f_E = 0$  Hz).

Resonance frequency changes due to phage adsorption were determined for periods up to 24 h (1440 min) (Table 5.1). When the quantity of adhered phage is graphed as a function of time (Fig. 5.16) and a sigmoidal curve is fitted to the experimental data points, a strong relationship is evident ( $R^2 = 0.963$ ). Extrapolation of the curve at the 120 min time point yields  $\Delta f$  of approximately  $-150$  Hz. This represents a 92% total frequency change in relation to the maximum frequency change observed at

24 h ( $-163$  Hz), indicating that the majority of phage appears to adsorb within the first few hours after deposition was commenced.

The quantity of phage, in virions, can be calculated from the total adsorbed biomass,  $\Delta m$ , if the mass of a single recombinant fd-tet phage is estimated at  $2.66 \times 10^7$  daltons, based on 4000 pVIII outer coat proteins each containing 55 amino acids with a total molecular weight  $2.35 \times 10^7$  (Kouzmitcheva, 2005), and DNA with a molecular weight of  $3.04 \times 10^6$  (Petrenko, 2004). As shown in Table 5.1, the total number of phage particles deposited to the active area of the sensing electrode ranged from  $1.8 \times 10^{10} - 6.5 \times 10^{10}$  virions as a function of the substrate's exposure time (20 min – 24 h, respectively) to phage in suspension.

Phage adsorption to the sensing electrode of the resonator was confirmed in real-time by fluorescence microscopy for a period of two consecutive hours. Figs. 5.17 – 5.19 show the resonator prior to, during, and after the application of phage, respectively. Visual observations indicate that phage deposition may be affected by several factors in addition to the attractive force between the phage and gold (electrode of the resonator), including sedimentation, refractory movements of the phage in suspension due to resonator perturbations, and the tendency of phage to aggregate in solution, resulting in decreased quantity and quality of deposition when large bundles deposit outside that portion of the sensing electrode where piezoelectricity, and thus frequency changes associated with the resonator, is active. This was confirmed by large standard deviations in 20, 40, and 60 min deposition experiments (Fig. 5.16)

Consideration of quantitative deposition data in conjunction with visual observations suggests that lateral phage aggregates or “bundles,” rather than individual particles, might be the prevalent orientation of deposition to the electrode if one considers the size of individual phage particles and the available area for deposition to the active region of the sensing electrode. If the dimensions of a single recombinant fd-tet virion are estimated at 10 nm (diameter)  $\times$  1300 nm (length) (Petrenko, 2004), then the approximate electrode surface area that would be occupied by a single, laterally adsorbed phage particle would be 13000 nm<sup>2</sup> or  $1.3 \times 10^{-14}$  m<sup>2</sup>. It should be noted that “occupied” refers only to that area of the sensing electrode that would be unavailable for another phage particle to bind to. It does not represent the total surface area of the phage, nor is it the actual area of interaction between the phage and the sensing electrode, since phage is a long cylindrical polymer and its cross-sectional curvature would realize a dramatically decreased footprint where physical adsorption between the gold electrode and phage coat proteins might occur. The active area of the obverse sensing electrode is dictated by the reverse contact electrode, and is specifically that portion of the lower electrode that overlaps with the upper electrode, representing only the central 34.19 mm<sup>2</sup> or  $34 \times 10^{-6}$  m<sup>2</sup> of the upper sensing electrode (Fig. 5.2). Given these dimensions, the estimated total number of adsorbed phage particles that could occupy the active electrode area, if laterally aligned one layer thick, is  $34 \times 10^{-6} \text{ m}^2 / 1.3 \times 10^{-14} \text{ m}^2 = 2.6 \times 10^9$  virions. Experimental data (Table 5.1) shows that the amount of phage deposited within only 20 min exceeds this quantity five-fold. This would seem to indicate that either 5 or more unidirectional aligned layers of individual particles, or more likely large bundles of phage

particles that bind to each other as aggregates in solution, are deposited. An alternative explanation is that phage is adsorbed on-end, i.e., the particle attaches by its tip hydrophobically through charge differences or via cysteine residues in minor coat proteins. Cysteine-Au linkage represents a strong covalent bond through disulfide bridges. Overman et al., (2004) have demonstrated salt- and concentration-dependent associative properties of phage aggregates, resulting in different physical alignments (unilateral or non unidirectional) based on molar concentration of salt and virion concentration in solution. Thus, further experimentation with salt-virion proportions and concentrations may reveal different physical adsorption properties.

Deposition of phage to the sensing electrode was characterized by strong, non-reversible binding under aqueous conditions, as washing with numerous changes of water (Fig. 5.20) or extended immersion in water under operational conditions for durations up to 55 h (Fig. 5.21) resulted in no measurable loss of adsorbed phage from the surface of the resonator. While the exact nature and strength of the attractive force between phage and resonator was not determined, possible explanations attributed by the literature for protein physisorption to gold include hydrophobic bonding, weak H<sup>+</sup> bonding, and Van der Waals forces.

### *3.2. Evaluation of biosensors*

Prepared biosensors were interrogated with *S. typhimurium* test suspensions. Two different QCM platform configurations were used (*cf.* “2.2.1.2.3. Measurement apparatus”), one of which was under assessment in the initial portion of biosensor

evaluation. Due to differences in the configurations, QCM output (dose response) was collected in the form of frequency or voltage readings. The linear part of the experimental dose response data of sensors was fitted by regression analysis to a line:

$$\Delta f \text{ (or) } \Delta V = A + S \times \log (C) \quad (2)$$

where, the slope of the line,  $S$ , representing sensitivity, and the correlation coefficient,  $R$ , were calculated for each sensor. Conglomerate graphs of individual sensor data, depicting  $R$  as a function of  $S$ , were prepared for each different biosensor preparation methodology (i.e. physical adsorption, biotin-streptavidin-phage self-assembly, and LB) in order to make a qualitative/quantitative assessment of biosensor functioning. It is reiterated to the reader that frequency and voltage output from the QCM are inversely related and as such,  $R$  and  $S$  are inversely related for the respective outputs although in the interest of maintaining congruence between data sets for the purpose of comparison, conglomerate frequency sensor data was plotted comparatively to voltage data.

### *3.2.1. Biosensors prepared by physical adsorption*

Based on phage deposition studies with concurrent visual observations, a period of 1 h was selected for the fabrication of 60 filamentous phage biosensors by physical adsorption ("FPI").

*3.2.1.1. Platform evaluation.* Prior to biosensor testing, platform configuration 2 was evaluated for signal stability, noise, and biohazard reduction in comparison to platform

configuration 1. Platform 1 (Fig. 5.3) was basically an “open system,” allowing direct test suspension delivery (by pipette) to the biosensor, and represents the traditional QCM configuration used in our facility’s previous biosensor studies (Bailey et al., 2002; Naylor 2002; Olsen, 2000; Olsen et al., 2003; Pathirana et al., 2000; Petrenko and Vodyanoy, 2003; Samoylov et al., 2002a, 2002b). Conversely, platform 2 (Fig. 5.7) was a “closed system,” merging a unique flow cell assemblage (Fig. 5.9) with the probe cavity housing of platform 1 (Fig. 5.8). This converted the open system to a flow chamber enclosing the biosensor. Test suspension delivery into and out of the chamber was accomplished through a complementary gravity flow system (Fig. 5.7).

*Rationale.* Practical experience using QCM platform 1 has demonstrated that the stability of the oscillator’s resonant frequency under aqueous conditions can be affected (increased or decreased) by numerous factors, including damping (motional resistance) due to increased density and viscosity of the liquid contacting the resonator, and pressure due to liquid volume that the sensor is immersed in. For example, when the sensor probe is positioned horizontally (as in platform 1) and a small layer of liquid (approximately 4 - 5 mm thick from the addition of 1 ml of aqueous-based solution) is added atop an installed resonator, the signal instability – deviation of frequency or voltage amplitude in the steady-state – can be high, as much as 20 – 30 Hz or mV even over a short duration. The manufacturer has stated that instability of rate/thickness readings, when a small layer of a liquid is present on the resonator, stems from the generation of reflective, incident waves off the air/liquid interface, causing a creative/destructive effect on frequency resolution (Boykin, 2003). While this instability does not generally affect interpretation of the biosensor’s ability to discriminate binding (through resonance change as a function

of analyte concentration) provides observed changes are greater than the background noise of the system (as interpreted from the standard deviations of observed steady-state frequency changes over time), it can interfere with interpretation of the biosensor's binding sensitivity. In cases where frequency changes due to binding are small in relation to changes in test analyte concentration, this background may be high enough to mask true binding, leaving interpretation of the sensor's functioning indeterminable. Incidentally, practical experience has shown that one way to combat this instability is slightly tilting the probe ( $\approx 10^\circ$ ) so that the air/liquid interface is not parallel to the solid/liquid interface. Damping as a result of viscosity increases conversely enhances frequency stability and noise reduction in a horizontally positioned resonator, as noted in conjunction with high concentrations of glycerol (RQCM Operation and Service Manual, 2003). Signal stability was also observed when the probe was operated under totally immersed conditions, e.g. probe was vertically positioned into an enclosed container holding 1L of aqueous solution, as much as 100 fold (data not shown). This increased stability probably stems from decreased incident wave generation as a result of greater distance/angle between the resonator and the air/liquid interface, and/or increased pressure on the resonator due to increased volume of the liquid, causing motional resistance (Boykin, 2003). Not surprisingly, vertical immersion is the usual configuration of the QCM apparatus in commercial applications such as electroless and electrolytic baths, for which the plating system was designed (Boykin, 2003; Krause, 1993). Although this increased stability is noteworthy, biosensor evaluation using 1 L of a liquid bacterial culture is obviously not practical.



A detailed investigation of the damping phenomenon was beyond the scope of experimentation, however, the physical nature of these observations inferred that the use of a pressurized flow chamber in conjunction with the platform 1 should increase frequency stability while reducing noise, thus improving quantitative interpretation of biosensor functioning. Numerous published accounts detailing the use of flow chambers in the evaluation of QCM antibody-based sensors support this theory, although the use of a flow cell in conjunction with this particular QCM apparatus has not been described previously in the literature. Another potential advantage of a flow cell/chamber was decreased sample volume requirement, reducing the biohazardous conditions associated with pathogenic bacteria.

*Testing.* Resonator resistance and signal stability for both platforms was initially evaluated using a graded series of glycerol solutions. Using platform 2, a clean resonator responds to increasing liquid viscosity with low-amplitude steady-state frequency responses (Fig. 5.22–A), and excellent dose-response agreement ( $R^2 = 0.995$ ) (Fig. 5.22–B) in accordance with theory (Kanazawa and Gordon, 1985). These results are very comparable to platform 1, also characterized by low-amplitude steady-state frequency responses (Fig. 5.23–A) and outstanding dose-response agreement ( $R^2 = 0.999$ ) (Fig. 5.23–B) in accordance with theory (Kanazawa and Gordon, 1985). Resonator failure occurred for both platforms at > 88% viscosity due to increased resistance (> 5k $\Omega$ ) at the solid/liquid interface, in concurrence with manufacturer's observations (RQCM Operation and Service Manual, 2003). Viscosity considerations due to increasing

bacterial concentration are inconsequential as confirmed by dose-response curves (Fig. 5.24-B:  $R = -0.61$ , slope =  $-0.09$  mV; and Fig. 5.25-B:  $R = 0.08$ , slope =  $0.25$  mV). Analysis of the system's background noise was investigated to ascertain the low threshold of sensitivity and encompassed all constituents that could potentially participate with the exception of the test analyte (*S. typhimurium*). Fig. 5.26-A displays the frequency responses of a prepared FPI biosensor assayed with PBS as a function of time using platform 2. Pressure changes due to analyte infusion via opening and closing individual stopcocks of the gravity flow system are evident at the beginning of each individual frequency response. Signal stability for individual frequency responses was very good, ranging from  $\pm 0.3 - 2.1$  Hz (as interpreted from the standard deviations of mean values of observed steady-state frequency changes over time, but applied in positive or negative direction depending upon the sign of  $R$  for the sensor). Fig. 5.26-B shows the mean values of steady-state frequency readings plotted as a function of unvarying PBS concentrations administered consecutively. Dose-response correlation was expectedly indifferent ( $R = 0.25$ ) since the sensor should not respond when challenged with a non-specific analyte. The background noise of the system, as determined by the slope of the linear regression, was excellent at  $0.12$  Hz. In comparison, Fig. 5.27-A displays frequency responses of a FPI biosensor assayed with PBS as a function of time, using platform 1. While steady-state frequency readings of the sensor are very stable in respect to time of analysis, their amplitude was visibly higher in comparison to platform 2 (Fig. 5.26-A). Thus, signal stability was decreased ( $\pm 2.9 - 10.1$  Hz) for the same sensor using the open system. When the mean values of the steady

state frequency readings were plotted as a function of analyte concentration (Fig. 5.27–B) and a linear line fit, correlation between dose and response was again expectedly indifferent ( $R = -0.11$ ), however, the noise level was higher ( $-0.29$  Hz), albeit still inconsequential.

Use of the flow cell use also decreased sample size requirements by 90%, from 1000  $\mu$ l to 100  $\mu$ l. This translates to an overall decrease in potential bacterial contamination of the test area, equipment, and personnel.

Finally, while not a problem specific to either platform, one point of concern warranting further investigation was the potential for *S. typhimurium* to physically adsorb or attach to the resonator's gold electrode non-specifically, thereby inducing false-positive frequency changes. Although the gold surface of all sensing electrodes was blocked with BSA following physical adsorption of filamentous phage, obviously if BSA or phage did not bind to a region for some reason it may leave an opening for non-specific binding of bacteria through outer membrane proteins and/or structures. The sensors prepared by other methods did not require further blocking. Fig. 5.24–A shows frequency responses of a clean, unblocked resonator assayed with increasing concentrations *S. typhimurium* as a function of time using platform 2. When the mean values of steady-state frequency readings were plotted as a function of bacterial concentration (Fig. 5.24–B) and a linear line fit, does-response correlation was indifferent ( $R = -0.61$ , slope =  $-0.09$  mV), indicating little or no bacterial binding to the resonator non-specifically. Comparatively, Fig. 5.25–A displays frequency responses of a clean, unblocked resonator assayed with *S. typhimurium* as a function of time using platform 1.

When the mean values of steady-state frequency readings were plotted as a function of bacterial concentration (Fig. 5.25–B) and a linear line fit, dose-response was again expectedly indifferent ( $R = 0.08$ , slope = 0.25 mV) indicating little or no bacterial binding to the resonator non-specifically.

*Conclusions.* Novel platform 2 was found to be comparable to the traditional configuration of platform 1 in terms of dose responsiveness, and even better in terms of signal stability and noise reduction (Table 5.2). Biohazard conditions using platform 2 were decidedly improved by reducing the extent of bacteria handling and volume. Non-specific binding of *S. typhimurium* was not significant for either configuration nor was viscosity increases due to increasing cellular constituents of bacterial test suspensions. Based on these results, it was decided that both platforms would be used equally to evaluate all prepared FPI biosensors.

*3.2.1.2. Biosensor results.* Frequency changes of assayed biosensors are a result of bacterial binding, and a function of the logarithmic concentration of free bacteria in the test suspensions (Pathirana, et al., 2000). These changes are hypothetically due not only to mass changes associated with binding bacteria, but also viscoelastic changes resulting from bioreceptor-bacteria interaction at the solid/liquid interface (Pathirana, et al., 2000). Fig. 5.28–A depicts frequency response curves of a FPI biosensor interrogated with increasing concentrations of *S. typhimurium* using platform 2. For each concentration, the sensor quickly comes to steady-state equilibrium within several hundred seconds following specific phage-bacteria binding. When the mean values of steady-state frequency readings are plotted as a function of bacterial concentration (Fig. 5.28–B), and

a linear line fit, a high dose-response relationship was evident ( $R = -0.98$ ,  $p < 0.001$ ) with the biosensor being linear over six decades of bacterial concentration. The sensitivity of the biosensor ( $-10.9$  Hz) was vastly greater than the established background ( $< \pm 1$  Hz). The lower limit of detection based on the dose response curve was estimated at 100 cells/ml, well below the infectious dosage reported for *Salmonella*-induced gastroenteritis.

Unfortunately, while this particular sensor was quite comparable to previously prepared *Salmonella* QCM antibody biosensors (Sab) (Olsen, 2000; Pathirana et al., 2000), it was also the exception. When the correlation coefficients derived from the experimental dose response data for 12 FPI sensors assayed using platform 2 were plotted as a function of the sensitivity (Fig. 5.29), a negative apparent mass, i.e. increasing bacterial concentrations resulting in dose-dependent decreases in apparent mass, was observed for the majority of the sensors (75%). Although these observations are not necessarily inconsistent with previous observations using the QCM (Olsen et al., 2003), whether this deviation is an accurate picture of biosensor performance using this platform (2) was not determinable; unexpected functional problems arising with the flow cell during biosensor testing resulted in its discontinuance and removal of associated FPI biosensor data from consideration. Specifically, the flow chamber is by design circular to accommodate matching resonators. Unfortunately, the chamber design suffers in that any solution injected appears to be redirected around its inside walls (to the outlet) in a non-laminar flow whenever air becomes introduced. As such, an air bubble becoming trapped directly over the center (active) area of the sensing electrode would exclude solution from passing over it evenly, resulting in spurious frequency shifts. Once trapped, any air

became impossible to evacuate even when pressure exceeding the recommended PSI was exerted. Although none of the 12 sensors included in the preceding data analysis appeared to exhibit this problem (others prepared and tested with this platform did), due to the flow cell's irregularities, the data for platform 2 was removed from consideration from the total bulk of FPI sensors tested. All further testing involving FPI biosensors was carried out with platform 1.

Fig. 5.30 depicts the experimental correlation coefficient,  $R$ , of 37 FPI sensors assayed with platform 1, as a function of their sensitivity,  $S$ . The correlation coefficient ranges from 0.99 (direct linear correlation) through 0 (no linear correlation) to  $-0.99$  (inverse linear correlation) for positive, zero, and negative sensitivities, respectively. A sigmoidal curve fit to the experimental data points indicates a high strength of association ( $R^2 = 0.94$ ). However, performance comparison of these sensors against 59 Sab sensors assayed with platform 1 (considered here as the "gold standard"), finds the FPI biosensors functionally deficient on the whole. Fig. 5.31 depicts the experimental correlation coefficient,  $R$ , of assayed Sab sensors as a function of their sensitivity,  $S$ . The mean  $R$  of the 59 Sab sensors tested against *S. typhimurium* solutions using platform 1 was 0.90 with mean  $S$  of 28.8 mV, while the 37 FPI biosensors had a mean correlation coefficient of  $-0.12$  and mean sensitivity of  $-3.1$  Hz. Fifty-three of 59 (90%) Sab sensors met or exceeded their predefined acceptable criteria ( $R \geq 0.90$ ,  $S \geq 8$  mV/decade as determined in Olsen, (2000) with excellent strength of association ( $R^2 = 0.96$ ), while only 4 of 37 (11%) FPI sensors met or exceeded their predefined acceptable criteria ( $R \geq 0.90$ , sensitivity  $\geq 1$  Hz) (Table 5.3). Whereas only 2 of 59 Sab sensors gave an indifferent result, the majority (22) of FPI sensors appeared indifferent (no linear

correlation) with only a few (4) being acceptable (direct linear correlation), and a large number (11) exhibiting a negative apparent mass (inverse linear correlation) as seen previously in FPI sensor results for platform 2 (Fig. 5.29).

Although lacking in desired performance, the results of the 37 FPI (Fig. 5.30) sensors are very consistent with previous observations for environmentally-aged Sab biosensors (*cf.* “Chapter III, Specific and selective immunosensor for *Salmonella* and its detection in the environment” – Fig. 3.8), where it was hypothesized that the bacterial microenvironment and the location of the receptor on the surface of the bacterium determines the sign and value of the analytical response of the sensor. When attachment between antigen and antibody was firm, the sensor’s output was directly proportional to the logarithmic concentration of free bacteria in suspension and the sensor’s behavior could be described as that predicted by mass theory (*cf.* “Chapter III, Appendix – Simplified analysis of the thickness-shear mode acoustic resonator”). Conversely, loose binding between antigen and antibody at the solid/liquid interface resulted in inversely proportional sensor signals. This premise was confirmed in the same study through the application of tight (outer membrane antigen) and loose (flagella) receptor-specific antibodies to *E. coli* and *S. typhimurium* (*cf.* “Chapter III, Specific and selective immunosensor for *Salmonella* and its detection in the environment” – Fig. 3.6). In the intervening time period since this model was initially proposed, numerous authors have reported the same contradictions to mass loading theory, including Fawcett et al. (1998, 2004) using phage lambda and M13 DNA tethered to QCM resonators; Hayden et al. (2003) and Dickert et al. (2003a) in response to loose binding of bacterial cells in yeast imprinted layers; Dickert et al. (2003b) due to loose binding of *E. coli* using a bacteria

imprinted polymer layer; Dickert et al. (2004), due to loose binding of non-specific compounds to Tobacco Mosaic Virus imprinted polymers; Marxer et al. (2003) who attributed frequency increases to alterations in cytosolic viscosity of adsorbed epithelial cells; Thompson et al. (1986) due to immunochemical interactions at the liquid/solid interface; and Pereira de Jesus et al. (2002) during the determination of Boron.

Collectively, these papers confirm our previous hypothesis regarding frequency increases with non-uniform colloidal mass loading. Accordingly, we have updated our previous hypothesis to propose loose phage-*S. typhimurium* binding as a coupled oscillator system exhibiting non-uniform colloidal mass loading (Appendix), since the parameters of a LRC series equivalent circuit model of the QCM are perfectly analogous to a damped harmonic oscillator system (Table 5.4). Our results confirm that for weak or loose attachment resonator frequency should increase with increasing non-uniform colloidal mass loading. In contrast with Sauerbrey's (1959) observations for a thin, firmly attached film, this expanded hypothesis and seeming contradiction of normal mass loading theory is consistent with the observations of Dybwad (1985), who first described mass-dependent frequency increases in conjunction with particulates, such as small (10 – 50  $\mu\text{m}$  diameter) Au spheres, under normal atmospheric conditions while loosely attached to a horizontally positioned QCM resonator. Dybwad's (1985) proposed equivalent mechanical model of a loosely bound particle as a coupled mass-spring system corresponds exactly with Fig. 9 of our previous model (Olsen et al., 2003; or cf. "Chapter III, Specific and selective immunosensor for *Salmonella* and its detection in the environment" – Fig. 3.9) depicting bacterial positioning at the sensor surface as the determinant factor of the sensor's analytical response (Fig. 5.32). Dybwad's (1985)



results were confirmed by Vig and Ballato (1998), who stated, "Significant deviation from the Sauerbrey equation will...occur when the mass is not rigidly coupled to the QCM surface," in regard to the distribution of non-uniform colloidal masses such as biological materials (cells). Accordingly, Berg et al. (2002) used a single asperity contact to show that frequency shifts associated with a quartz resonator operating in shear mode increased linearly with increasing contact radius; Borovsky et al. (2001) used a nanoindenter probe in conjunction with a QCM to elicit positive frequency shifts characteristic of the contact stiffness; and Sorial and Lec (2004) experienced size-dependent frequency increases with polystyrene spheres under aqueous conditions.

If we accept this premise for the behavior of the FPI biosensors, then there exist at least two possibilities to explain the loose binding, given that these 37 sensors were not environmentally aged and the majority (90%) of commensurate Sab sensors react as predicted by theory. First, while the physical adsorption of filamentous phage to the resonator appeared to be non-reversible in water during deposition studies (Figs. 5.20 and 5.21), the actual quality of binding under aqueous conditions was suspect when visually observed in real-time (by fluorescent microscopy during deposition studies); it was not unusual to see numerous flexible particles or bundles firmly anchored to the surface of the resonator at one end while the opposite end wavered loosely in suspension. The other possible explanation is the converse, that is, the entire phage particle is firmly attached to the surface of the sensor, but attachment of the bacterium is flexible due to the nature of the targeted surface receptor, which could be a poorly bound membrane protein or possibly a flexible appendage such as a flagellum or pili (Fig. 5.32-2). Visual observation by fluorescent microscopy has confirmed both loose and tight attachment of

bacteria to the surface of resonator coated with filamentous phage (Figs. 5.33 and 5.34). Real-time attachment of *S. typhimurium* to the biosensor surface was also noted by fluorescent microscopy under operational conditions (Fig. 5.35) and scanning electron microscopy (Fig. 5.36) in comparison to a control, which showed no *S. typhimurium* binding (Fig. 5.37)

Accepting this basis then, it is very probable that every sensor “works” in a physical sense, just to different analytical degree. Specific, tight binding between the QCM, phage and bacteria results in mass increases corresponding to theory, whereas specific, yet loose binding anywhere between the three results in apparent mass decreases corresponding to non-theory behavior. Obviously, a combination of the two results in indifferent behavior. As stated previously in Chapter III, it is clear that sensors possess acceptable analytical value for detecting *S. typhimurium* only if positioning of bacteria on the sensor surface is either predominantly rigid or predominantly flexible. Those that are indifferent are not favorable for the effective detection of bacteria. In summary, sensors prepared from filamentous phage are functional; however, a better method of phage immobilization is needed to elicit only frequency responses indicative of mass loading theory.

### *3.2.2. Biosensors prepared by biotin-streptavidin-phage self-assembled layers*

The quantitative results and visual observations of FPI sensors indicated that the quality of phage immobilization was suspect. Weak immobilization may result from less than optimal bonding through physical adsorption. It was therefore decided to enhance

binding of filamentous phage to resonators through covalent bonding. A multilayer, molecular assembly approach (Fig. 5.1-B) based on Dultsev et al. (2000) was fashioned to provide firm phage-resonator interaction, yet preserve simplicity and speed of preparation as well as sensor functionality and sensitivity. Resonators were functionalized first by chemisorbing biotinylated BSA to their gold sensing electrodes. BSA possesses extremely high affinity for gold and as such is considered irreversible, whereas the presence of numerous biotin residues per molecule allows immobilization without adversely affecting surface orientation. BSA also blocks non-specific binding of *S. typhimurium* to gold. Then, streptavidin was conjugated to the immobilized biotin-BSA as an intermediate for biotinylated phage. Streptavidin is a slightly anionic protein produced by *Streptomyces avidinii* and possesses a tertiary structure composed of four identical 159 amino acid residue chains. It binds biotin stoichiometrically (1:4) with great affinity ( $K_d = 0.6 \times 10^{-15}$  M) (Green, 1990) and can act as a building block for multilayering processes due to its dihedral symmetry that allows dual biotin molecules to bind opposite faces. Finally, biotinylated filamentous phage clone E2 was conjugated to the streptavidin intermediate layer to form a “sandwich” biosensor (FPB) of sorts.

Fig. 5.38 depicts the experimental correlation coefficient of 20 FPB sensors as a function of their sensitivity. A sigmoidal fit to experimental data points indicates a very high strength of association ( $R^2 = 0.98$ ). The majority of the sensors (18 of 20) tend to group into two clusters at opposite ends of the curve, possessing either direct linear correlation or indirect linear correlation. Two of the sensors are indifferent. Those sensors (12) within oval “A” possess a mean  $R = 0.93$  and mean sensitivity of 6.38 mV, while the 8 sensors falling within oval “B” have a mean  $R = -0.93$  and mean sensitivity

of  $-5.78$  mV. Nine of the total 20 sensors (45%) possess goodness of fit and sensitivity greater than the FPB acceptance criteria ( $R \geq 0.90$ ,  $S \geq 2$  mV as determined from sensor background testing – Table 5.3). This is comparable to the results of Sykora (2003) who reported 46% acceptability of phage-based QCM sensors for the detection of a model threat agent, streptavidin.

Fluorescence microscopy confirmed binding of biotinylated filamentous phage to streptavidin during preparation of biosensors, and binding of *S. typhimurium* to the sensor surface during testing (Fig. 5.39). Fig. 5.40 depicts the mean steady-state dose-responses for an assayed FPB biosensor under fluorescent microscopy observation using platform 1. A sigmoidal fit indicates a high dose-response relationship ( $R^2 = 0.98$ ) with saturation at higher concentrations ( $\approx 10^7$  cells/ml). The sensitivity of the biosensor (5 mV/decade) was greater than the established background (2 mV). The lower limit of detection, based on the dose response curve, was estimated at 100 cells/ml.

Interpretation of comparative biosensor performance, using each method's respective acceptance criteria, concludes that biosensors prepared using biotin-streptavidin interaction (FPB) are 33% more effective at sensitively detecting *S. typhimurium* in solution compared to those prepared by physical adsorption (FPI) (Table 5.3). If the quantity of mean averaged sensors only fitting the criteria is considered (Fig. 5.38 – oval A), then efficiency increases to 60%. However, while this molecular self-assembly method appears to be more effective and viable for the preparation of functional biosensors, the manifestation of a negative tail (Fig. 5.38 – oval B), akin to those prepared by physical adsorption, still indicates a less than desirable process.

Accepting that a negative apparent mass occurs due to elastic (vice firm) binding between phage and resonator, or phage and analyte, or both, at the solid/liquid interface, and that the preparation of FPB sensors resulted in firmly immobilized phage, then the negative apparent mass behavior exhibited by the 8 FPB sensors (Fig 5.38 – oval B) must be attributed to poor binding between phage and analyte (*S. typhimurium*), specifically as a result of interaction between the phage's outer coat peptides and its complementary receptor on *S. typhimurium*. Speculating, numerous scenarios can be envisioned. First, while the affinity of this phage for *S. typhimurium* (cf. "Chapter IV, Landscape probes for detection of *Salmonella typhimurium*") has been shown to be comparable to antibodies, the identity and thus quality of the targeted receptor is unknown. Certainly, a flexible receptor (flagella, pili, fimbriae) on the surface of a bacterium or one that is low in quantity or accessibility would be a poor prospect, resulting in elastic binding even with the most firmly immobilized phage. The effect could be compounded if phage affinity for *S. typhimurium*, which is very high in solution, decreases as a result of conformational changes induced to the phage particle during the immobilization process (e.g. flat and rigid on the sensor versus flexible in solution), resulting in less binding contacts or binding opportunity between phage outer coat peptides and receptor. As well, the curvature of the cell may create a smaller focal point of contact with a flatly immobilized phage, resulting in diminished opportunity to bind receptors.

An immobilization process lacking deposition control may further compound these effects. While the procedural aspects of testing were common among prepared FPB sensors, the physical facets of phage immobilization were not equivalent since the conditions of deposition at the liquid/solid interface were not controlled. During

deposition studies, fluorescence microscopy revealed that filamentous phage in solution will deposit randomly in relation to the electrode. Thus, it is very probable that phage deposition is still not uniform using this molecular self-assembly process. Subsequently, weak, flexible, and/or limited interactions of immobilized phage with *S. typhimurium*, compounded by a reduced number of binding contacts due to poor spatial deposition quality could result in a negative apparent mass even with increasing concentrations of analyte. Whereas the same weak, flexible, and/or limited interactions of phage with *S. typhimurium* aided by an increased number of phage contacts as a result of highly uniform spatial deposition to the resonator could result in binding according to mass theory. Those sensors that are indifferent are probably more or less a deviation to some degree of either situation.

In summary, as noted previously for FPI sensors, the FPB sensors appeared to be functional, even more so than FPI sensors according to mass theory. However, a more suitable method of phage immobilization was needed to confirm speculations and prepare sensors that would only elicit responses indicative of mass loading theory.

### *3.2.3. Biosensors prepared with phage coat proteins*

Based on a perceived need for better control of the deposition process and the established results of 59 Sab sensors (Fig. 5.31), the Langmuir-Blodgett (LB) method was chosen to further study the suitability of phage as a biorecognition unit of QCM biosensors for *S. typhimurium*. LB is controllable deposition technique capable of producing spatially organized monolayers for quartz resonators (Bailey et al., 2002;

Naylor 2002; Olsen, 2000; Olsen et al., 2003; Pathirana et al., 2000; Petrenko and Vodyanoy, 2003; Samoylov et al., 2002a, 2002b). However, while filamentous phage was easily adsorbed to resonators as a linear particle in previously prepared sensors, this morphological property was not conducive to monolayer formation using LB. Therefore, vesicle-like spherical forms of filamentous phage for phage coat protein monolayers were first prepared by chloroform denaturation using the modified method of Manning et al. (1981). Although phage does not contain a lipid component, chloroform can act on the hydrophobic interactions between the major coat protein subunits, causing it to contract from a filament into a “spheroid” (Fig. 5.41), mimicking the natural infective process of Ff phages (Manning et al., 1981). As reported by Sykora (2003), although the transformation from filamentous form to spheroid alters the native phage structural design, affinity of binding is not affected. When added to a subphase solution at the air/liquid interface, the spheroids rupture much like vesicles to prepare a monolayer of phage coat proteins or “skinned phage” (Figs. 5.1-C and 5.13).

*3.2.3.1. Spheroid preparation.* The spheroid procedure was optimized for phage E2 prior to preparation of LB monolayers for isotherms and biosensors. Filamentous phage conversion to spheroids by chloroform denaturation was confirmed by whole-virion AGE (Fig. 5.42). Interestingly, densitometry revealed that the highest yield of spheroids occurred when there was a concurrent decrease in both the exposure duration and concentration of phage (lane 3) in relation to chloroform. A one-minute exposure appears to be sufficient for phage conversion, in good agreement with the procedure of Manning et al. (1981) and previous observations by Petrenko and Smith (2000) and

Petrenko et al. (1996). Spheroids were easily prepared at room temperature; however, in contrast to the findings of Manning et al. (1981), I-forms were also readily apparent (Fig. 5.43). Spheroid conversion and DNA extrusion was also confirmed by TEM (Fig. 5.44). To further investigate yield as a function of phage concentration, a logarithmic dilution series of stock phage was prepared and subjected to equal volumes of chloroform as before, then again analyzed by whole-virion AGE (Fig. 5.45). Densitometry of bands indicates that a 27 – 81 fold dilution of phage subjected to chloroform denaturation results in the highest yields of spheroids. Speculating, increased yields of spheroids with decreasing concentrations of phage may be attributed to phage-solvent interaction opportunity. Phage aggregation in solution possibly decreases with increased aqueous dilution, resulting in greater numbers of free particles in solution. Perhaps these individual phage particles have a greater opportunity to interact freely with the solvent, resulting in correspondingly increased yields of spheroids in the aqueous phase.

It is interesting to note that spheroids are produced but not found in great numbers in the aqueous phase of highly concentrated phage preparations (Fig 5.42, lanes 1 and 4); rather, they are located at the phase interface (Fig. 5.42, Lane 7, band B and corresponding Fig. 5.46) interlocked with large fibrils of filamentous phage that do not convert. Correspondingly, a second band, "A," is also noted in Figs. 5.42 and 5.45. This band corresponds exactly with the forward migratory face of filamentous phage not subjected to chloroform denaturation (Fig. 5.45 – lane 1), but rather electrophoresed then denatured with NaOH. Fig. 5.45 confirms filamentous phage aggregation in solution, as a large, prevalent band that barely migrates out of the well. However, smaller aggregates and individual particles migrate equivalent to band "A." This band must therefore be free



filamentous phage not converted by chloroform denaturation, but which appears only after NaOH degradation. It should be noted that the size marker cannot be used to identify the filamentous phage DNA, which is 6.4 kb; because the DNA is still attached to the spheroid it migrates either further (band B) or less (band A) based on the morphology of the attached particles. Thus, perfectly round spheroids will migrate further than linear I-forms.

Based on these results, a phage dilution of 1:27 (corresponding to  $2.48 \times 10^{12}$  virions/ml) vortexed with an equal volume of chloroform for 60 s was used to prepare spheroids for isotherm analysis and biosensors.

*3.2.3.2. Isotherm analysis.* The ideal surface pressure at which to form an organized, optimally compressed monolayer of skinned phage for transfer to a substrate is determined by its surface pressure – area ( $\Pi$ -A) isotherm and elasticity. Analysis of the isotherm reveals the different phases of the monolayer as determined by the physical and chemical properties of the molecules (Fig. 5.47A), as well as the subphase temperature and composition. Typically, discontinuities in the curve indicate the orientation of the molecules in different phases (Fig. 5.47B), which exist in a weakly interactive, two-dimensional gaseous state when uncompressed (G), but undergo phase transition to liquid ( $L_1$ ,  $L_2$ ) and solid state (S) densities upon compression. These phases are distinct for different molecules. If the monolayer is compressed beyond the solid state, it will undergo collapse to a three-dimensional structure. LB deposition is traditionally carried out in the solid phase, where  $\Pi$  is sufficiently high to ensure adequate cohesion to the substrate, allowing the build up of multiple spatially organized monolayers.

Isotherms of monolayers prepared from spheroids were measured by gradually compressing a prepared surface film at constant rate and temperature into a defined area (LB trough) while monitoring changes in surface pressure. The  $\Pi$  is a two-dimensional analogue of repulsive pressure exerted by phage coat proteins, as described by the equation:

$$\Pi = \gamma - \gamma_0 \quad (3)$$

where,  $\gamma$  is the surface tension in the absence of a surface film, and  $\gamma_0$  is the surface tension of the subphase in the presence of a surface film. Eq. (3) is plotted as a function of the subphase surface area available to each particle. As shown in Fig. 5.48, the isotherm for skinned phage, in comparison to a standard, arachidic acid, was characterized by a very long gaseous phase, requiring over 60% compression before a liquid-expanded ( $L_1$ ) state is reached at 10 mN/m. A liquid-condensed state ( $L_2$ ) was visible between 29 and 35 mN/m and a solid phase was reached at 35 mN/m, after which the compression barrier of the trough reached the end of its stroke. This solid phase  $\Pi$  is very high for a pure protein monolayer and greater than that found for *Salmonella* antibodies in conjunction with phospholipids (Fig 5.48), although less than arachidic acid (Fig 5.48) and those found for amphotericin B spheroid prepared monolayers (Sykora, 2003).

$\Pi$ -A isotherm data was further utilized to determine the compressibility modulus,  $K$ , of the film, which is a quantitative elastic property of the spheroids describing its compactness and stability and is as a function of  $\Pi$ :

$$\text{Elasticity, } K = -A \left( \frac{d\Pi}{dA} \right)_T \quad (4)$$

where,  $A$  = area of the film =  $(450 - 1) \times 150$  [mm<sup>2</sup>];  $\Pi$  = surface pressure, and  $T$  = temperature at compression. Elasticity provides a more lucid characterization of the best  $\Pi$  at which to compress the monolayer for optimal packing and transfer to a substrate, especially for monolayers prepared from spheroid- or antibody-lipid mixtures, where it is becomes necessary to consider the immobilization of protein in the lipid-based film and its two dimensional compressibility. When Eq. (4) is plotted as a function of Eq. (3) (Fig. 5.49), an optimal  $\Pi$  from the curve of maximum  $K$  is derived (Table 5.5). For monolayers prepared from spheroids, this  $\Pi$  was 35.98 mN/m, which corresponds to the highest  $\Pi$  obtained in the solid phase on the isotherm. This was three times higher than *Salmonella* antibodies (Table 5.5).

Based on isotherm and elasticity analysis, a surface pressure of 36 mN/m was used for the transfer of spheroid monolayers to quartz resonators.

**3.2.3.3. Biosensor preparation.** Biosensors (SPH) were prepared by transferring phage coat monolayers onto quartz resonators by Y-type LB deposition (Fig. 5.50 – right). The

quantity and quality of monolayer deposition was measured by the transfer ratio (TR), defined as the ratio between the decrease in monolayer area during a deposition stroke, and the area of the substrate. For a square object of identical length and height, the TR scale ranges from 0 to 1.0, with ideal deposition equaling 1.0; TR >1.0 indicates excess deposition of film layer, i.e. that the layer was wrinkled, while TR <1.0 indicates partial deposition of the layer. Typical cumulative deposition of phage coat monolayers, in comparison to *Salmonella* antibodies and arachidic acid, is shown as a function of the transfer ratio in Fig. 5.51. The standard, arachidic acid, exhibits a cumulative TR of 6.7 for 7 (96%) deposited layers, equating to near-perfect assembly of monolayers (Table 5.6). In comparison, spheroids have much lower transfer efficiency, (31%), indicating that non-ideal monolayers were transferred. This was not surprising since spheroids prepared as pure protein (phage coat) monolayers required 10 times the amount of material to achieve an sufficient initial surface pressure, in comparison to arachidic acid. This indicated that the skinned phage possessed poor buoyancy, probably sinking in the subphase during the initial deposition of spheroids at the time of monolayer preparation. However, in comparison to *Salmonella* antibodies (10% – Table 5.6), monolayers prepared from spheroids more readily deposit to quartz resonators.

*3.2.3.4. Biosensor results.* Fig. 5.52 depicts the experimental correlation coefficient,  $R$ , of 15 assayed spheroid sensors as a function of their sensitivity. A sigmoidal fit to experimental data points indicates a very high strength of association ( $R^2 = 0.96$ ). As seen previously with filamentous phage sensors prepared by physical adsorption, the correlation coefficient,  $R$ , of the 15 sensors ranged from + 0.99 (direct linear correlation)

through 0 (no linear correlation) to  $-0.99$  (inverse linear correlation) for positive, zero, and negative sensitivities, respectively. The majority of results were indifferent (no linear correlation). Only three sensors tested acceptable (20%), possessing goodness of fit and sensitivity greater than the established acceptance criteria ( $R \geq 0.90$ ;  $S \geq 2.5$  mV/decade as determined from sensor background testing – Table 5.3). Several exhibited a negative apparent mass (inverse linear correlation) as seen previously. The mean  $R$  of SPH sensors tested against *S. typhimurium* solutions was 0.10 with a mean  $S$  of 0.86 mV (Table 5.3). When whole spheroids were reacted with *S. typhimurium* in solution and examined by TEM, binding was confirmed (Figs. 5.53 – 5.55). Taken in total, these results again appear to point to a less than desirable preparation process, possibly the result of patchy deposition as confirmed by TR values. While LB is an excellent technique for building organized multilayers, the sensor is only as good as the film's composition and transfer to the substrate.

#### *3.2.4. Biosensors prepared with phage coat proteins in phosphocholine*

Spheroids prepared as previously described were combined with 1,2-diphytanoyl-sn-glycero-3-phosphocholine (PC) in an attempt to recover greater amounts of phage from monolayers. Twenty-four biosensors (SPC) were again prepared by transferring phage coat-PC monolayers onto quartz resonators using Y-type LB film deposition (Fig. 5.50 – left).

*3.2.4.1. Biosensor preparation.* In comparison to pure spheroids,  $\Pi$ -A isotherms of monolayers prepared from spheroids combined with PC (Fig. 5.48) revealed a shorter gaseous phase, probably due to earlier film organization as a result of the incorporated phospholipids. A liquid-expanded ( $L_1$ ) state was reached at 10 mN/m. A liquid-condensed state ( $L_2$ ) was visible between 29 and 40 mN/m and a solid phase was seen between 40 and 46 mN/m, after which the compression barrier of the trough reached the end of its stroke. Elasticity analysis (Fig. 5.49) revealed an optimal  $\Pi$  of 37.81 mN/m at  $K_{\max}$  48.64 mN/m (Table 5.5) indicating high stability (Davies and Rideal, 1963). This was slightly higher than that of spheroids alone and is a reflection of the added phospholipids. Based on the isotherm and elasticity analysis, a surface pressure of 38 mN/m was used for phage coat-PC transfer to quartz resonators. Typical cumulative deposition of phage coat -PC monolayers, in comparison to *Salmonella* antibodies and arachidic acid, is shown as a function of the transfer ratio in Fig. 5.51. In comparison to pure spheroid monolayers (Table 5.6) spheroids combined with PC have a higher transfer efficiency (40%). This is indicative of the incorporated phospholipids, which lend greater buoyancy to the skinned phage, thus allowing more to be transferred to the substrate.

*3.2.4.2. Biosensor results.* Fig. 5.56 depicts the experimental correlation coefficient,  $R$ , of 24 assayed spheroid-PC sensors as a function of their sensitivity. The majority of the sensors (22 of 24) tend to group, possessing direct linear correlation with a mean  $R = 0.90$  and mean sensitivity of 8.1 mV (Table 5.3). Fifteen of these sensors (63%) possess goodness of fit and sensitivity greater than the acceptance criteria of  $R \geq 0.90$  and sensitivity greater than 2.5 mV/decade (as determined from sensor background testing –

Table 5.3). Most importantly, there is a lack of a negative tail, indicating that spheroid monolayer deposition using phospholipids results in spatially superior deposition, allowing firm capture of *S. typhimurium* and binding that follows mass theory for quartz crystal resonators. Speculating, positively charged, basic amino acids at the C-terminus of the protein may allow ionic interaction with negatively charged phosphate groups of phospholipids following rupture and orientation at the subphase surface during the preparation of monolayers for LB deposition (Fig 5.57). Biosensors prepared with spheroids in phospholipids may therefore facilitate the dynamic properties of the protein as a probe for *S. typhimurium*, thus explaining the superior results to those prepared with spheroids alone.

#### **4. Summary and Conclusions**

QCM biosensors for the rapid and sensitive detection of *S. typhimurium* in solution, based on recombinant fd phage probes, were prepared using three immobilization methods (physical adsorption, molecular self-assembly by covalent biotin-streptavidin-phage multilayering, and Langmuir-Blodgett technique) and two morphological phage forms (filamentous and phage coat proteins). Specific bacterial binding resulted in resonance frequency changes of prepared sensors, which were evaluated using linear regression analysis.

Evaluation of a novel QCM flow cell configuration in comparison to the conventional standard revealed equivalence in dose responsiveness, and improvement in terms of signal stability, noise reduction, and biohazard reduction. Non-specific bacterial

binding and viscosity-induced effects due to increasing cellular constituents of bacterial test suspensions were inconsequential to proper resonator functioning. However, inferior engineering design necessitated discontinuance during sensor testing due to reduced laminar flow when air became trapped as a result of the infusion process. While unsuitable for this study, future evaluation using a pulseless, low PSI pump may prove this configuration valuable.

Quantitative deposition studies were conducted to investigate optimal conditions of concentration and duration necessary for the preparation of functional phage biosensors by physical adsorption. Results indicated that  $\approx 10^{10} - 10^{11}$  filamentous virions incubated for 1 hour at room temperature was sufficient to effect working biosensors. Physical adsorption was characterized by strong, non-reversible binding under aqueous conditions, as washing or extended immersion under operational conditions for durations up to 55 h resulted in no measurable loss of phage from the surface of resonators. The quality of phage deposition was confirmed by fluorescent microscopy.

The best operational results were obtained when filamentous phage particles converted to phage coat proteins by chloroform denaturation were immobilized by Langmuir-Blodgett technique. Sixty-three percent of these sensors achieved acceptance criteria outlined ( $R \geq 0.90$ ,  $S \geq 2\text{mV}$ ) and possessed a high average  $R$  (0.90) of sensor groupings with acceptable sensitivity of 8.1 mV. Sensors were capable of rapidly detecting *S. typhimurium* (< 3 min for steady state response) in solutions ranging from  $10^1 - 10^7$  cells/ml, lower than reported values for *Salmonella*-induced gastroenteritis.

The utility of spheroids as bacterial probes for sensors was confirmed. The procedural aspects of filamentous phage induction to spheroids by chloroform



denaturation were optimized to achieve greatest conversion yields possible as a function of preparation time and input concentration. Results from whole-virion AGE indicated that a phage concentration of  $2.48 \times 10^{12}$  virions/ml in aqueous solution vortexed with an equal volume of chloroform for 60 s was optimal. Spheroid binding to *S. typhimurium* was confirmed by TEM. Transitional I-forms produced by chloroform denaturation at room temperature were revealed, countering the observations of previous researchers. Spheroids, prepared as pure protein phage coat monolayers and in combination with phospholipids, were evaluated by isotherm, elasticity, and transfer ratio analysis for deposition to quartz resonators by LB method. Results showed that phage coat proteins combined with phospholipids produced a monolayer having higher elasticity and capable of higher transfer ratios than monolayers of phage coat proteins alone, resulting in spatially superior deposition to quartz resonators and subsequent firm binding of *S. typhimurium* that followed mass theory for quartz crystal resonators.

Normal mass loading theory described by Sauerbrey (1959) was contradicted for the majority of sensor groupings, with the exception of sensors prepared with phage coat protein in phospholipids by LB. This contradiction has been noted in previous QCM studies by the author and other researchers working with non-uniform masses and is ground on less than firm phage-resonator-bacteria immobilization and/or binding, resulting in an elastic motion out of phase with resonance frequency. Consequently, a model complementary to our previous LRC series mechanical model was formulated, comparing it to an externally driven, liquid-damped, one-dimensional couple harmonic oscillator with two different masses. Taken in whole, these results indicate that more research in phage immobilization and/or preparation is needed.

Overall, the results of this research demonstrate proof-in-concept development of biosensors for the rapid, specific, sensitive detection of *S. typhimurium*, based on recombinant phage probes immobilized to quartz crystal microbalance transducers. With further refining, it could be an effective analytical method for detecting and monitoring quantitative changes of bacterial agents under any conditions that warrant recognition of such agents, including food products and possibly biological warfare applications. Furthermore, the nature of the biological recognition layer holds potential utilization for development against any bacteria, virus or toxin to which a corresponding phage could be affinity selected for. Therefore, other potential markets include clinical-based diagnostics, research, and industrial use. However, the reproducibility of the sensor must be increased, possibly through the development of better immobilization schemes, or a rigorous quality control process must be elucidated that will allow exacting selection of only functional sensors from prepared batches. As well, while it is hypothesized that the flexibility of phage, analyte or possibly both at the solid/liquid interface of sensors causes loose binding with subsequent negative apparent mass (inverse linear correlation), it remains unclear which scenario is correct. The identity of the specific bacterial receptor targeted by the phage would provide great insight.

## Appendix

### *QCM operating as a coupled oscillator for non-uniform mass*

The equations of motion describing an externally driven, liquid-damped, one-dimensional couple harmonic oscillator model with two different masses (Fig 5.58) are defined by second order linear differential equations (we assume that the springs obey Hooke's law):

$$\left. \begin{aligned} \sum F_1 &= M \ddot{X} = -KX - \Gamma \dot{X} + \sum_i k(x_i - X - a) + F_0 \sin \omega t \\ \sum F_2 &= m \ddot{x}_i = -\gamma \dot{x}_i - k(x_i - a - X), \text{ where } i = 1, 2, 3 \dots n \end{aligned} \right\} \quad (1)$$

rewritten as nonhomogeneous and homogeneous equations:

$$\left. \begin{aligned} \sum F_1 &= M \ddot{X} + \Gamma \dot{X} + KX - \sum_i k(x_i - a - X) = F_0 \sin \omega t \\ \sum F_2 &= m \ddot{x}_i + \gamma \dot{x}_i + k(x_i - a - X) = 0, \text{ where } i = 1, 2, 3 \dots n. \end{aligned} \right\} \quad (2)$$

The left sides of Eq. (2) are linear functions of  $X$  and  $x_i$ ,

$$\left. \begin{aligned} L_1(X, x_i) &= F_0 \sin \omega t \\ L_2(X, x_i) &= 0. \end{aligned} \right\} \quad (3)$$

Substituting exponent  $e^{i\omega t}$  for  $\sin \omega t$  we arrive at a solution of:

$$\left. \begin{aligned} L_1(Y, y_i) &= F_0 e^{i\alpha x} \\ L_2(Y, y_i) &= 0, \end{aligned} \right\} \quad (4)$$

and we can reduce to the solution of Eq. (3) using

$$\left. \begin{aligned} \text{Im} L_1(Y, y_i) &= L_1(\text{Im} Y, \text{Im} y_i) = \text{Im} F_0 e^{i\alpha x} = F_0 \sin \alpha x \\ \text{Im} L_2(Y, y_i) &= L_2(\text{Im} Y, \text{Im} y_i) = 0. \end{aligned} \right\} \quad (5)$$

Thereby, we can solve for Eq. (3) using:

$$X = \text{Im} Y, x_i = \text{Im} y_i. \quad (6)$$

Hence, we will find the steady solution of:

$$\left. \begin{aligned} M\ddot{X} + \Gamma\dot{X} + KX - \sum_i k(x_i - a - X) &= F_0 e^{i\alpha x} \\ m\ddot{x}_i + \gamma\dot{x}_i + k(x_i - a - X) &= 0, \text{ where } i = 1, 2, 3 \dots n \end{aligned} \right\} \quad (7)$$

that is periodic in time with the frequency of external force:

$$X = X_0 e^{i\alpha x}; x_i - a = x_{i0} e^{i\alpha x}. \quad (8)$$

Substituting Eq. (8) into Eq. (7) we find:

$$\left. \begin{aligned} (-M\omega^2 + i\Gamma\omega + K)X_0 - \sum_i k(x_{i0} - X_0) &= F_0 \\ (-m\omega^2 + i\gamma\omega)x_{i0} + k(x_{i0} - X_0) &= 0. \end{aligned} \right\} \quad (9)$$

To solve Eq. (9) with respect to  $X_0$ , substitute in:

$$\begin{aligned}
 x_{i0} &= \frac{kX_0}{-m\omega^2 + i\gamma\omega + k} = \\
 &\left. \begin{aligned}
 (-M\omega^2 + i\omega\Gamma + K)X_0 - \sum_i k \left( \frac{kX_0}{-m\omega^2 + i\gamma\omega + k} - X_0 \right) &= F_0 \\
 \left[ (-M\omega^2 + i\omega\Gamma + K) - \sum_{i=1}^N \frac{k(m\omega^2 - i\gamma\omega)}{-m\omega^2 + i\gamma\omega + k} \right] X_0 &= F_0.
 \end{aligned} \right\} \quad (10)
 \end{aligned}$$

Using initial resonance frequencies:

$$\Omega_0^2 \equiv K / M ; \omega_0^2 \equiv \frac{k}{m}, \quad (11)$$

Eq. (10) takes the form:

$$\left[ M(\Omega_0^2 - \omega^2) + i\omega\Gamma - \frac{Nk(m\omega^2 - i\gamma\omega)}{m(\omega_0^2 - \omega^2) + i\gamma\omega} \right] X_0 = F_0 \quad (12)$$

$$\text{or, } X_0 = \frac{F_0}{M(\Omega_0^2 - \omega^2) + i\omega\Gamma - \frac{Nk(m\omega^2 - i\gamma\omega)}{m(\omega_0^2 - \omega^2) + i\gamma\omega}}. \quad (13)$$

The sensor's frequency range is near  $\Omega_0$ , whereas  $\omega_0 \ll \Omega_0$ , hence, the denominator,  $D$ , can be estimated as:

$$D \cong M(\Omega_0^2 - \omega^2) + i\omega\Gamma - \frac{Nk(m\Omega_0^2 - i\gamma\Omega_0)}{-m\Omega_0^2 + i\gamma\Omega_0} = M(\Omega_0^2 - \omega^2) + i\omega\Gamma + Nk \quad (14)$$

where,  $(\omega = \Omega_0)$ .

To simplify analysis, we assume that we can neglect the damping of the oscillator; therefore, Eq. (14) can be written as:

$$D \equiv M(\Omega_0^2 - \omega^2) + Nk \quad (\Gamma \rightarrow 0). \quad (15)$$

Resonance occurs when  $D = 0$ , i.e.,

$$\begin{aligned} M(\Omega_0^2 - \omega^2) + Nk &= 0 \\ \omega^2 &= \frac{M\Omega_0^2 + Nk}{M}; \end{aligned} \quad (16)$$

therefore, the resonance frequency,  $\omega$ , increases as the number of attached particles (bacteria),  $N$ , increases. To understand physically, we return to the second part of Eq. (9).

When  $\omega \approx \Omega_0 \gg \omega_b$ :

$$(-m\omega^2 + i\omega\gamma)x_{i0} \equiv kX_0. \quad (17)$$

Eq. (17) shows that, neglecting  $i\omega\gamma$ ,  $x_{i0}$  and  $X_0$  have different signs, i.e., which possess  $180^\circ$  shift in phase. Therefore, attached particle  $m$  increases the restoring force that returns  $M$  to equilibrium position  $O$ , thus increasing frequency.

Table 5.1

Quantity of filamentous phage physically adsorbed to resonators as a function of time.

Incubation (min)	$-\Delta f$ (Hz)	$\Delta m$ (ng) <sup>d</sup>	Phage adsorbed (virions) <sup>e</sup>
20	45 <sup>a</sup>	795	$1.80 \times 10^{10}$
40	60 <sup>b</sup>	1065	$2.41 \times 10^{10}$
60	92 <sup>c</sup>	1625	$3.68 \times 10^{10}$
1080	136	2402	$5.45 \times 10^{10}$
1440	163	2880	$6.50 \times 10^{10}$

<sup>a</sup>Mean average of 5 experiments, SD = 31.1 Hz.<sup>b</sup>Mean average of 3 experiments, SD = 46.5 Hz.<sup>c</sup>Mean average of 4 experiments, SD = 59.2 Hz.<sup>d</sup>Adsorbed phage mass as determined by Sauerbrey equation,  $\Delta f = (0.0566)(\Delta m)$ .<sup>e</sup>Quantity of phage deposited to the active area (34.19 mm<sup>2</sup>) of the upper sensing electrode as calculated from  $\Delta m / m_v$ , where the mass of a single virion ( $m_v$ ) is  $2.66 \times 10^7$  dal/ $6.023 \times 10^{23}$  dal =  $44.1 \times 10^{-9}$  ng.

Table 5.2  
Platform configuration evaluation.

Parameter	Platform 1	Platform 2
Configuration	Open cavity housing	Flow cell
Viscosity dose-response, $R^{2a}$	0.999	0.995
Signal stability <sup>b</sup>	$\pm 2.9 - 10.1$ Hz	$\pm 0.3 - 2.1$
Noise, $R^c$	-0.11	0.25
Noise, $S^d$	-0.29 Hz	0.12 Hz
Non-specific binding, $R^e$	0.08	-0.61
Non-specific binding, $S^f$	0.25 mV	-0.09 mV
Test sample volume	1000 $\mu$ l	100 $\mu$ l

<sup>a</sup>Coefficient of determination from nonlinear sigmoidal fit of Boltzmann equation to mean values of steady-state frequency readings plotted as a function of increasing glycerol concentrations.

<sup>b</sup>Range of standard deviations of the mean values of observed steady-state frequency changes over time, applied in positive or negative direction depending upon the sign of  $R$  for the sensor.

<sup>c</sup>Correlation coefficient of linear regression analysis using mean values of steady-state frequency readings plotted as a function of the analyte concentration.

<sup>d</sup>Sensitivity as derived from the slope of linear regression analysis using mean values of steady-state frequency readings plotted as a function of the analyte concentration.

<sup>e</sup>Correlation coefficient of linear regression analysis using mean values of steady-state frequency readings plotted as a function of increasing *S. typhimurium* concentrations.

<sup>f</sup>Slope of linear regression analysis using mean values of steady-state frequency readings plotted as a function of increasing *S. typhimurium* concentrations.



Table 5.3  
Overall biosensor performance.

Parameter	Biosensor Designation				
	Sab <sup>a</sup>	FPI <sup>b</sup>	FPB <sup>c</sup>	SPH <sup>d</sup>	SPC <sup>e</sup>
Sensors assayed	59	37	20	15	24
Strength of association, $R^f$	0.96	0.94	0.98	0.96	NA
Mean, $R^g$	0.90	-0.12	(A) 0.93; (B) -0.93 <sup>i</sup>	0.10	0.90
Mean, $S^h$	28.8 mV	-3.1 Hz	(A) 6.4 mV; (B) -5.7 mV <sup>j</sup>	0.86 mV	8.1 mV <sup>m</sup>
Acceptance criteria, $R$	≥0.90	≥0.90	≥0.90	≥0.90	≥0.90
Acceptance criteria, $S$	≥8 mV	≥1 Hz	≥2 mV	≥2.5 mV	≥2.5 mV
Sensors meeting acceptance criteria	53 (90%)	4 (11%)	9 (45%)	3 (20%)	6 (25%)

<sup>a</sup>Sensors prepared by LB using antibodies against *Salmonella* O-antigen.

<sup>b</sup>Sensors prepared by physical adsorption of filamentous phage.

<sup>c</sup>Sensors prepared by streptavidin-biotin-filamentous phage self-assembly.

<sup>d</sup>Sensors prepared by LB using spheroids.

<sup>e</sup>Sensors prepared by LB using spheroids with phospholipids.

<sup>f</sup>Coefficient of determination from nonlinear sigmoidal fit of Boltzmann equation to experimental correlation coefficient,  $R$ , of sensors as a function of their sensitivity,  $S$ .

<sup>g</sup>Mean correlation coefficient of all sensors tested, except where otherwise noted.

<sup>h</sup>Mean sensitivity of all sensors tested as derived from slope of linear regression analysis, except where otherwise noted.

<sup>i</sup>Mean correlation coefficient of sensors depicted in Fig. 5.38 ovals A and B, respectively.

<sup>j</sup>Mean sensitivity of sensors depicted in Fig. 5.38 ovals A and B, respectively.

Table 5.4

Analogous parameters between a mechanical spring-mass system and LRC series circuit.

System			
Harmonic Oscillator	Unit	LRC Circuit	Unit
Displacement	x	Charge	q
Velocity	v	Current	i
Force	F	Voltage	V
Mass	m	Inductance	L
Damping constant	b	Resistance	R
Spring constant	k	capacitance <sup>-1</sup>	1/C
Natural frequency	$\omega_0 = (k/m)^{1/2}$	Natural frequency	$\omega_0 = (1/C)^{1/2}$

Table 5.5

Optimal surface pressure corresponding to maximal compressibility modulus of biopolymers at 20 °C.

Biopolymer <sup>e</sup>	$\Pi$ (mN/m)	$K_{\max}$ (mN/m)
<i>Salmonella</i> Ab <sup>b</sup>	11.23	29.88
Spheroids - chloroform	35.98	20.57
Spheroids - PC <sup>c</sup>	37.81	48.64
Arachidic acid <sup>d</sup>	59.93	351.60

<sup>a</sup>Spheroids prepared by chloroform denaturation.

<sup>b</sup>*Salmonella* somatic-O polyvalent antibodies, Denka Seiken Co., LTD., Tokyo, Japan.

<sup>c</sup>Spheroids prepared by chloroform denaturation, in phosphocholine (PC), then deposited to subphase as monolayers of presumably phage coat proteins.

<sup>d</sup>pH corrected to 10.0. Data from Olsen (2000).

<sup>e</sup>Representative isotherms and elasticities are shown in Figs. 5.48 and 5.49.

Table 5.6

Cumulative deposition of biopolymers onto quartz resonators as a function of transfer ratio (TR) at 20 °C.

Biopolymer	Cum. TR <sup>a</sup>	Layers deposited	Efficiency, (%) <sup>b</sup>
<i>Salmonella</i> Ab	0.9	9	10
Spheroids - chloroform	7.2	23	31
Spheroids - PC <sup>c</sup>	4.4	11	40
Arachidic acid	6.7	7	96

<sup>a</sup>Representative cumulative depositions shown in Fig. 5.51.

<sup>b</sup>Represents typical deposition data for a single batch (n = 4) of sensors; some batches had better or worse efficiencies.

<sup>c</sup>Deposition to sensors presumably as phage coat proteins.

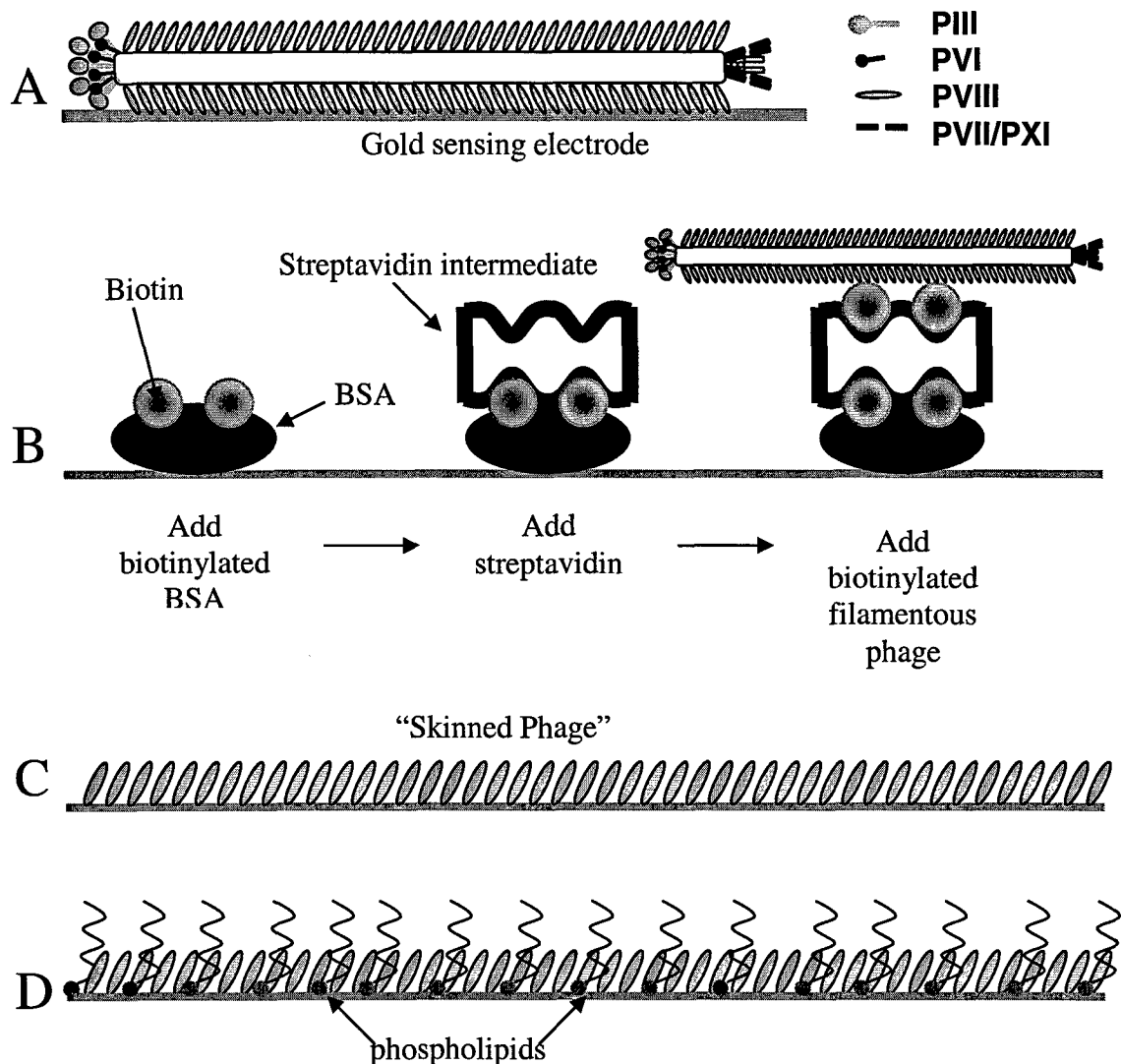


Fig. 5.1. Four strategies for immobilizing phage to the gold sensing electrode of piezoelectric resonators. (A) Physical adsorption of whole-virion filamentous phage. (B) Molecular self-assembly of biotinylated filamentous phage by biotin-streptavidin multilayering. (C) Langmuir Blodgett (LB) deposition of filamentous phage major coat proteins (pVIII) prepared as "skinned phage" from spheroids. (D) LB deposition of filamentous phage proteins prepared as skinned phage from spheroids complexed with phosphocholine.

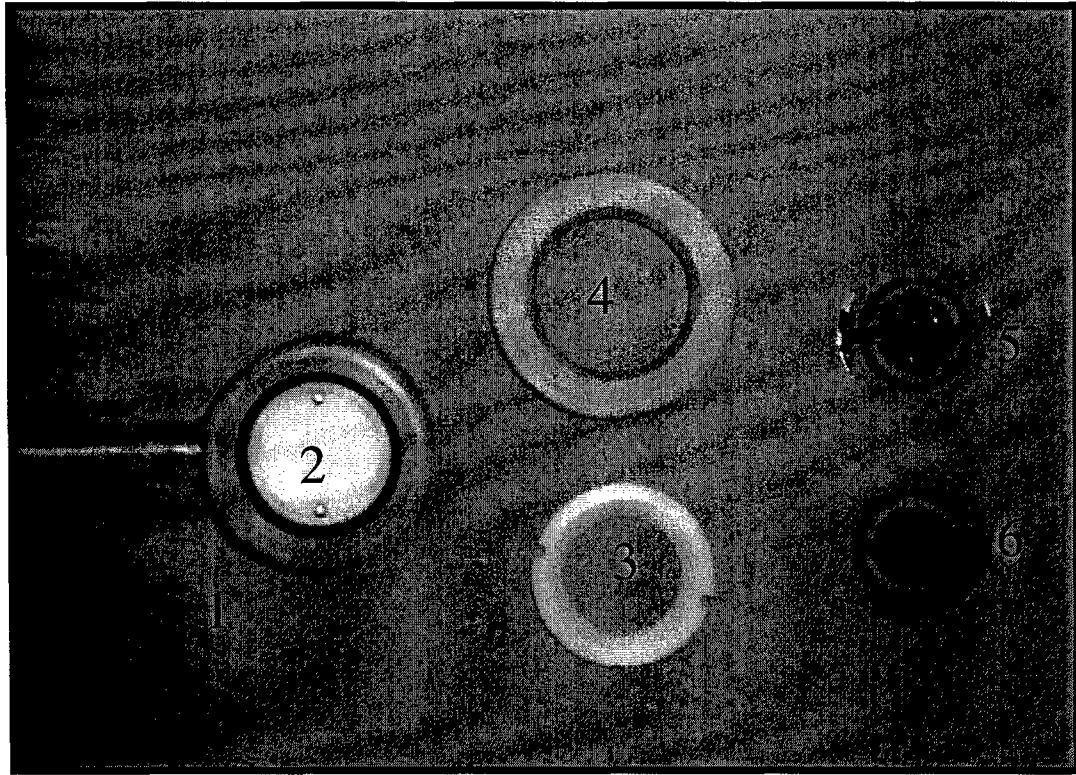


Fig. 5.2. Sensor probe and associated components. (1) Housing for external oscillatory circuit electrical contacts. (2) Crystal holder cavity with Kalrez® o-ring (black) installed. The gold Pogo® index pins that contact the reverse electrode of the resonator are clearly visible. (3) Teflon® resonator retainer ring. (4) Threaded retainer ring cover. (5) Polished, 5 MHz AT-cut thickness shear mode quartz resonator exhibiting sensing (obverse) electrode. (6) Contact (reverse) electrode of quartz resonator. The “active area” of the resonator is that central portion of the sensing electrode that overlaps the contact electrode ( $\approx 34.19 \text{ mm}^2$ ).

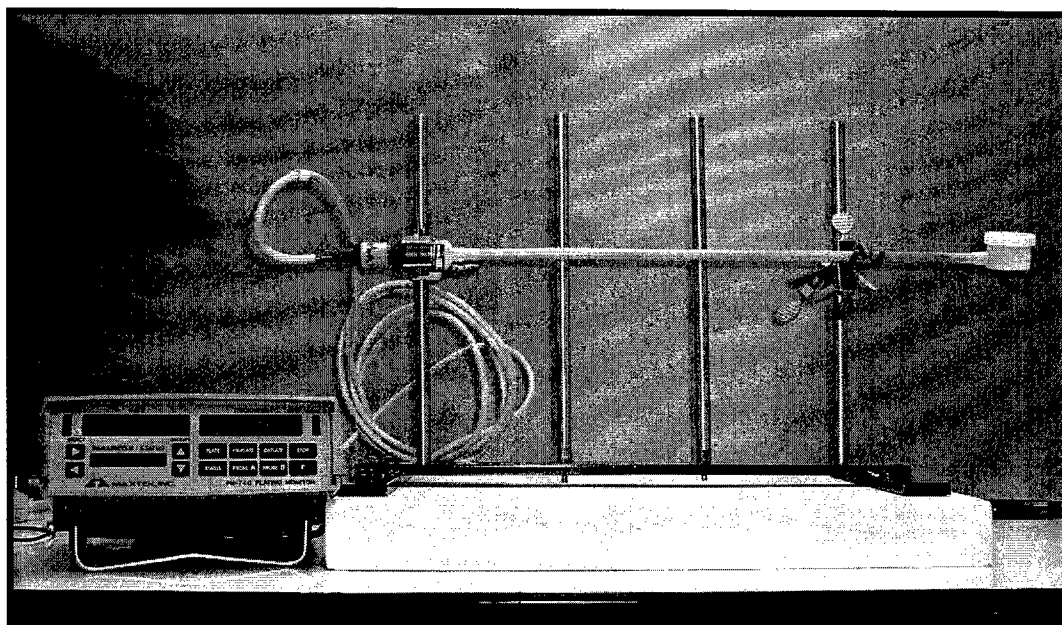


Fig. 5.3. QCM platform (1) for deposition and biosensor measurements. Maxtek PM-740 plating monitor (shown) or TM-400 thickness monitor was connected to a sensor probe clamped horizontally to a lattice stand then tilted  $10^\circ$  transverse to the stand. The sensor probe and stand were positioned atop a marble slab to reduce extraneous environmental vibrations.

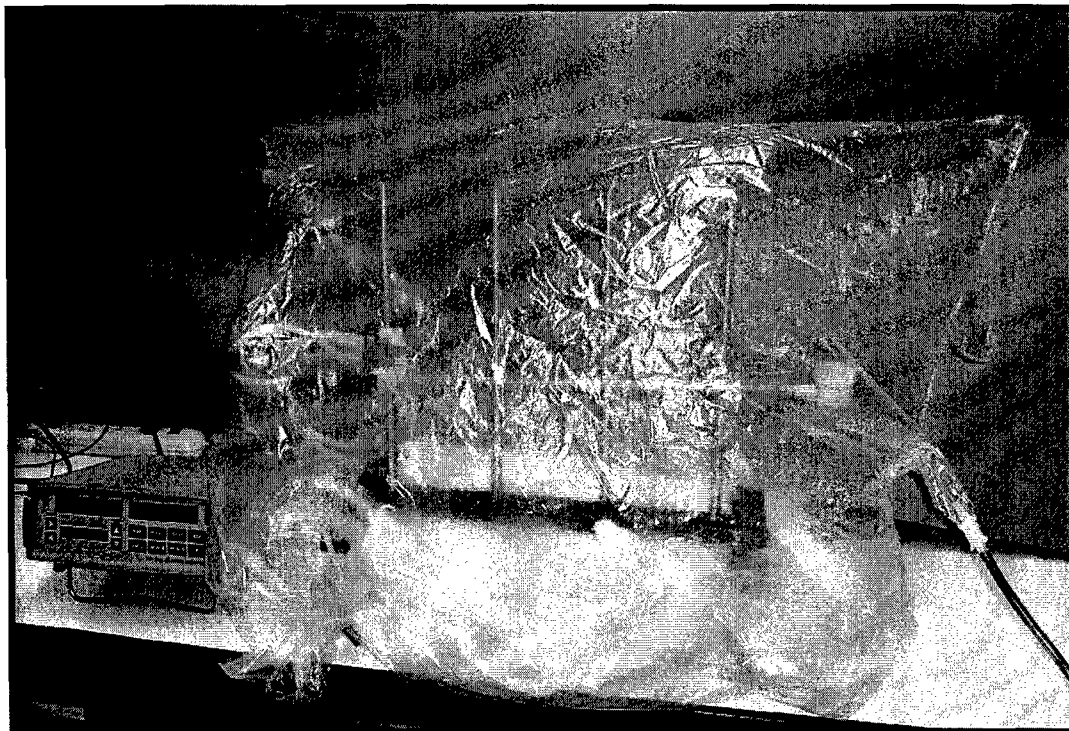


Fig. 5.4. QCM platform configured for deposition studies. The sensor probe and lattice stand of QCM platform 1 (Fig. 5.3) were enclosed within an inflatable glove chamber filled with nitrogen. The probe's triaxial cable is connected to the frequency counter (outside) through a sealed port on the left side of the bag. Experiments were manipulated through the bag's extendable arms and gloves.



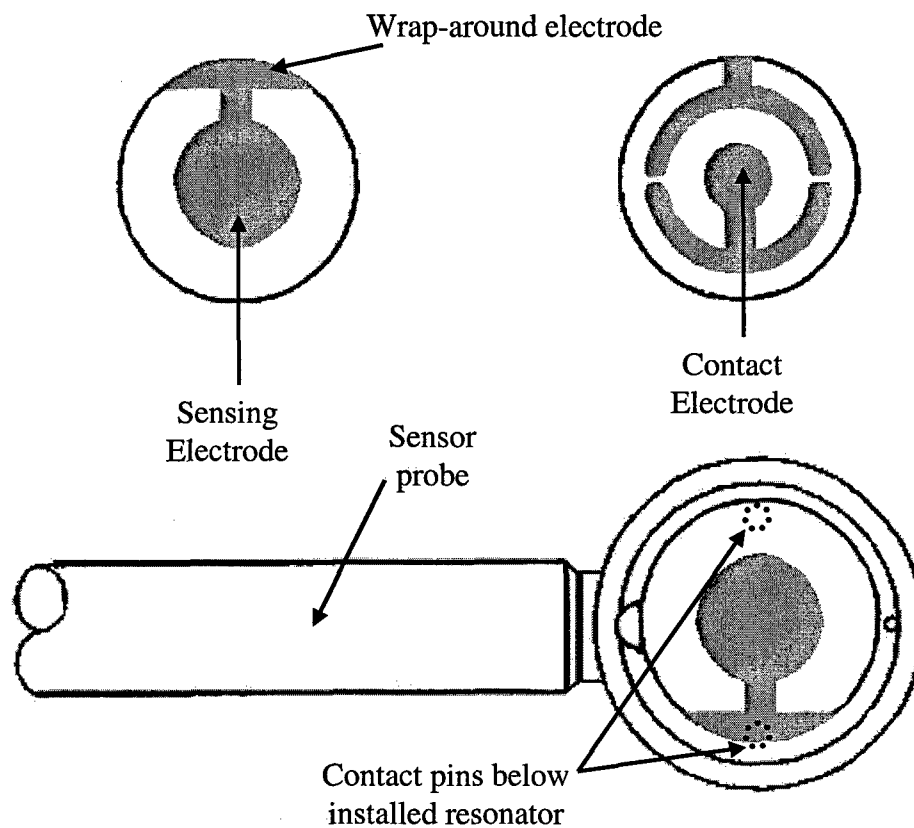


Fig. 5.5. Orientation of the quartz resonator in the crystal holder cavity of the sensor probe, with the sensing electrode exposed and the contact electrode connecting to the Pogo® index pins. The sensor retainer ring and cover are not shown.

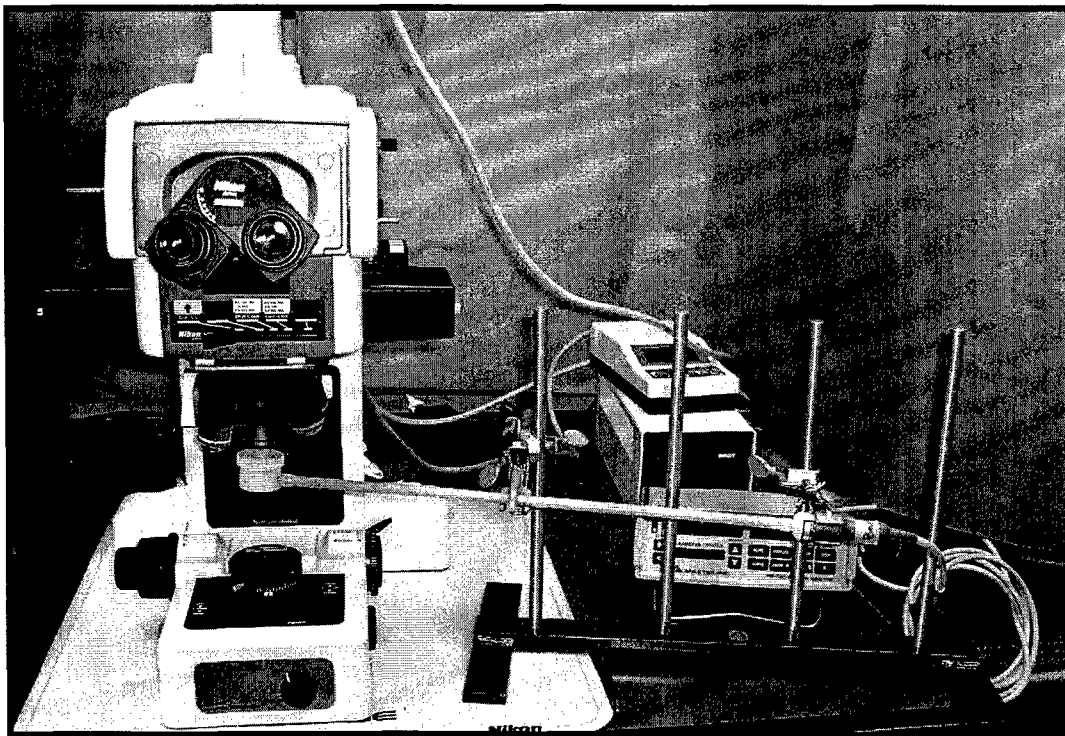


Fig. 5.6. QCM operating in conjunction with fluorescent microscope. Fluorescence microscopy was used to visually confirm phage deposition to the resonator in real-time. Shown is the QCM sensor probe attached to lattice stand for visual inspection of the resonator located directly beneath microscope's objective.

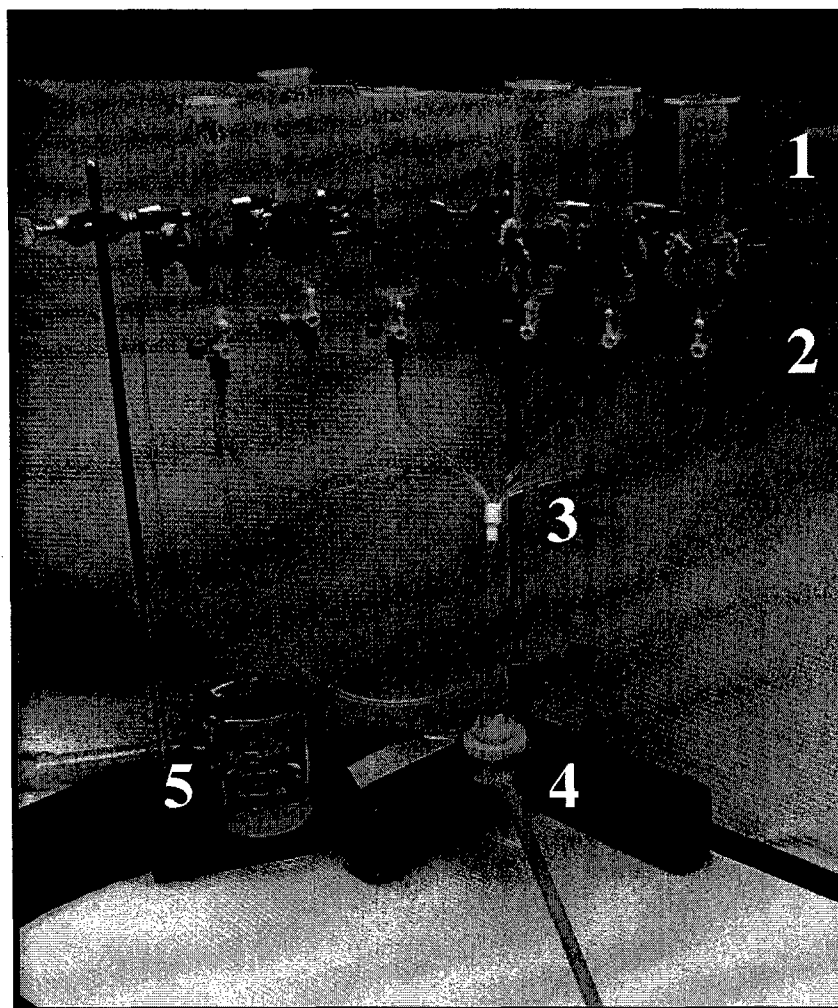


Fig. 5.7. QCM platform (2) for sensor measurements. Maxtek PM-740 or TM-400 frequency monitor (not shown) was connected to QCM sensor probe converted to a flow chamber. Syringes (1) were used to contain *S. typhimurium* test suspensions. Stopcocks (2) allowed volumetric manipulation and gravimetric flow of test suspensions from syringes to perfusion manifold (3) via individual lines consisting of small diameter polyethylene tubing. Manifold had central outlet leading to inlet of the flow cell (4). The sensor probe's cavity housing was converted to a flow chamber by replacing the Teflon® crystal retainer ring with a Maxtek FC-550 flow cell, secured by the threaded retainer ring cover. Outlet from flow cell was routed to a waste container (5).

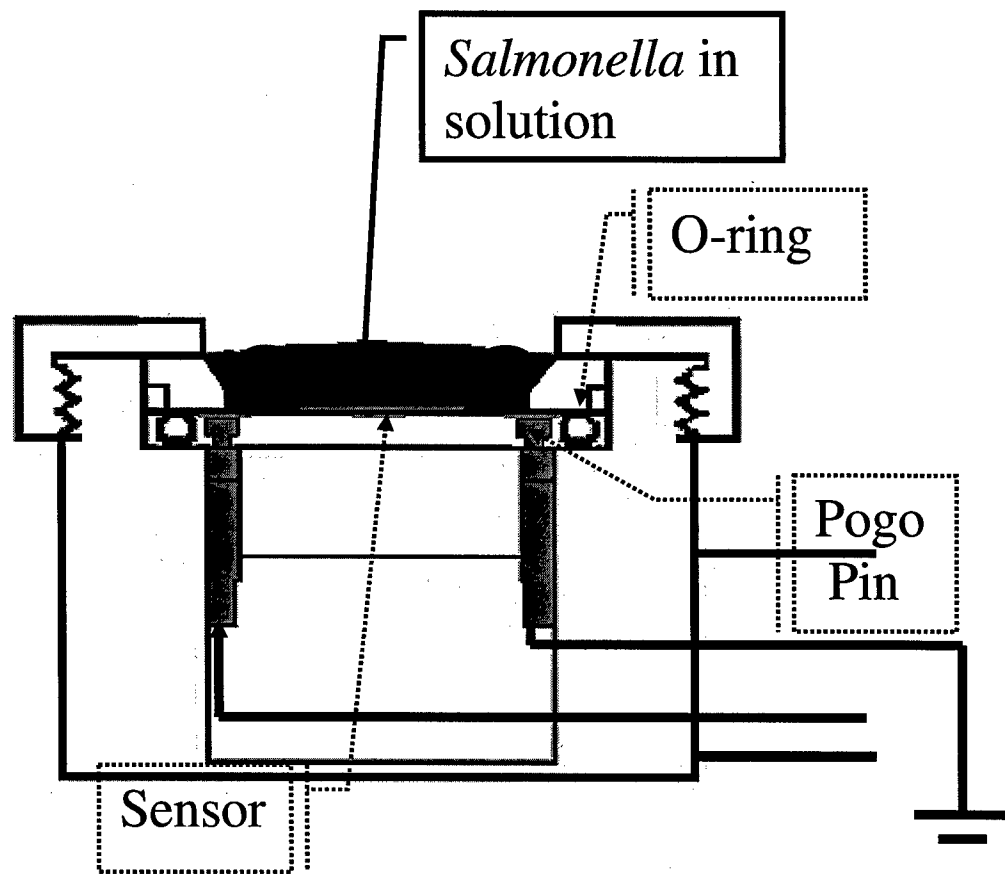


Fig. 5.8. Cross-sectional view of probe housing (QCM platform 1) with *S. typhimurium* depicted in aqueous solution above the biosensor. The volume of this solution is 1000  $\mu\text{l}$ . The probe housing, in addition to allowing electrical connection to the sensor's electrodes via contact (pogo) pins, provides mechanical integrity of the probe's oscillatory electronics via an o-ring seal.

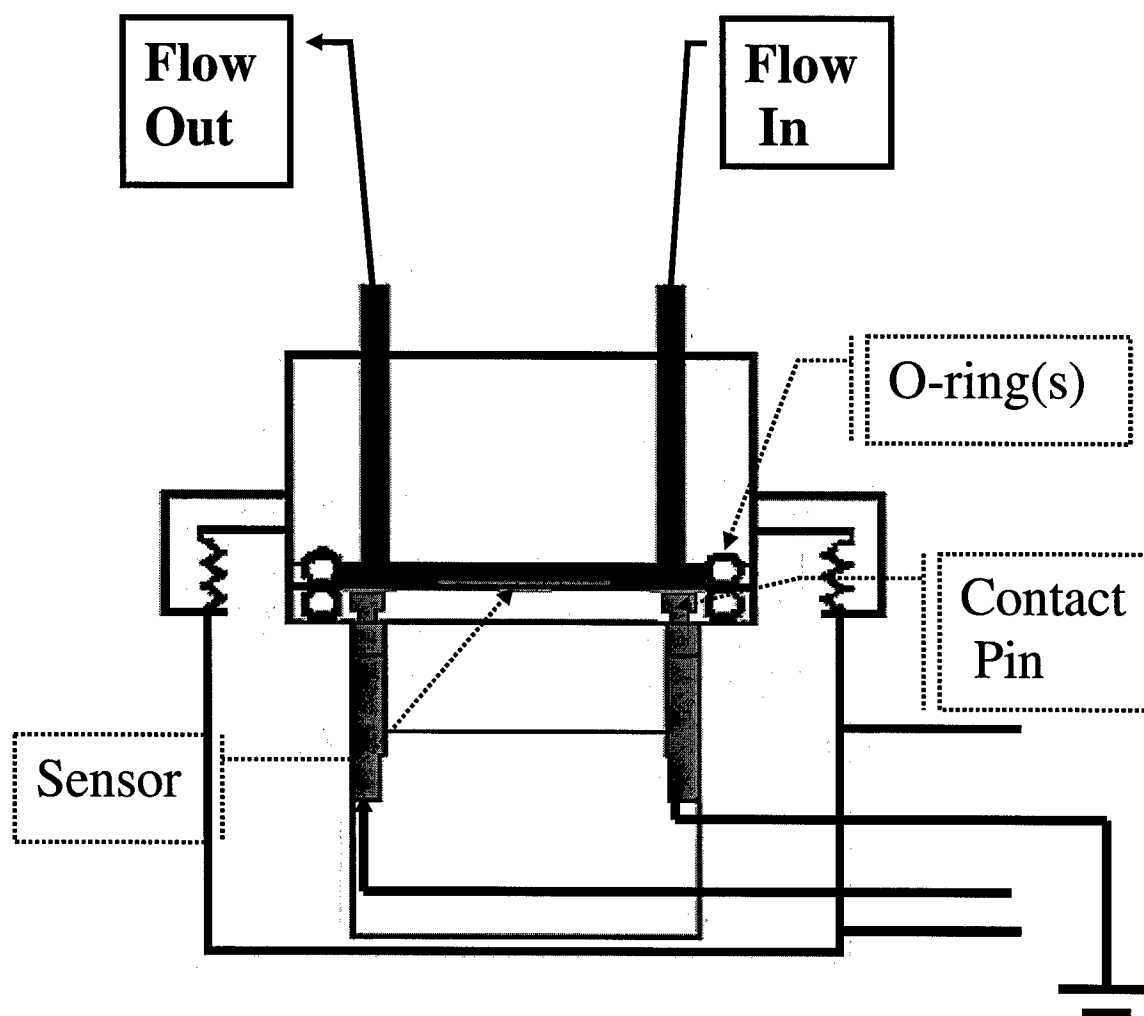


Fig. 5.9. Cross-sectional view of flow cell attached to sensor probe housing (QCM platform 2). Flow direction into the cell, over the sensor, and out of the cell is indicated. The volume of the circular flow chamber, excluding inlet and outlet ports, was approximately 100  $\mu\text{l}$ . The resonator's sensing and contact electrodes, and the electrical connections via contact pins of the oscillatory circuit are shown.

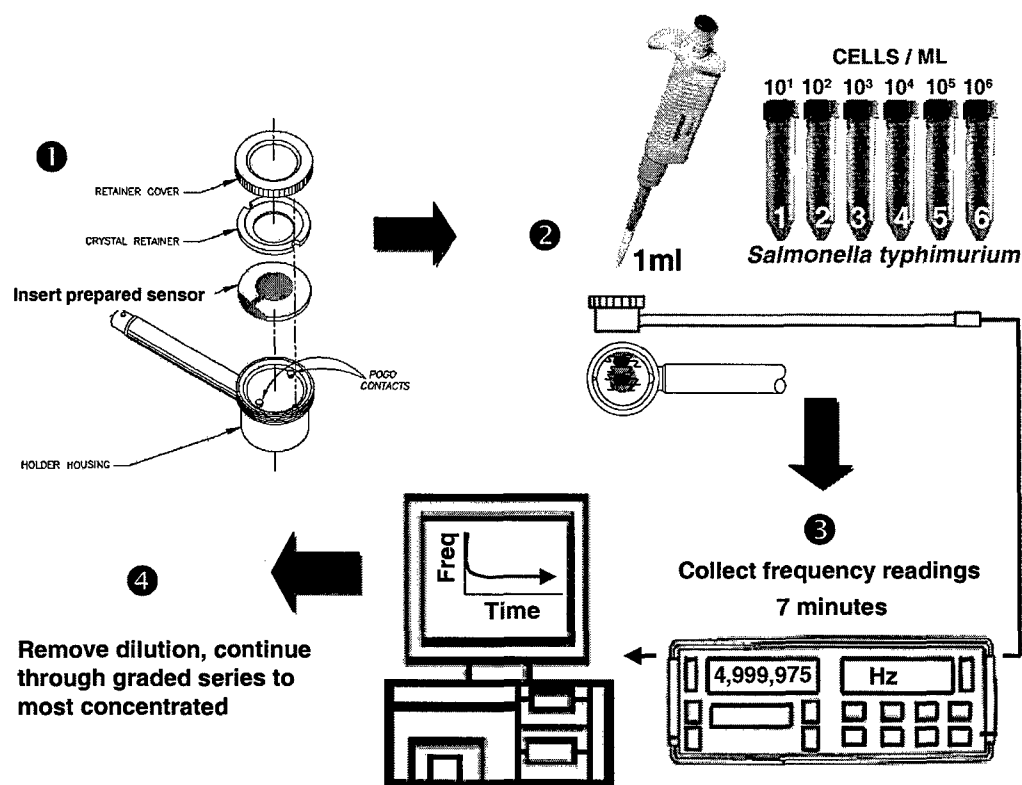


Fig. 5.10. Testing scheme for biosensors using QCM platform 1. (1) Prepared biosensor was installed into sensor probe then (2) interrogated with a graded series of *S. typhimurium* test solutions. (3) Frequency (or voltage) output of sensor was recorded for data analysis (4).

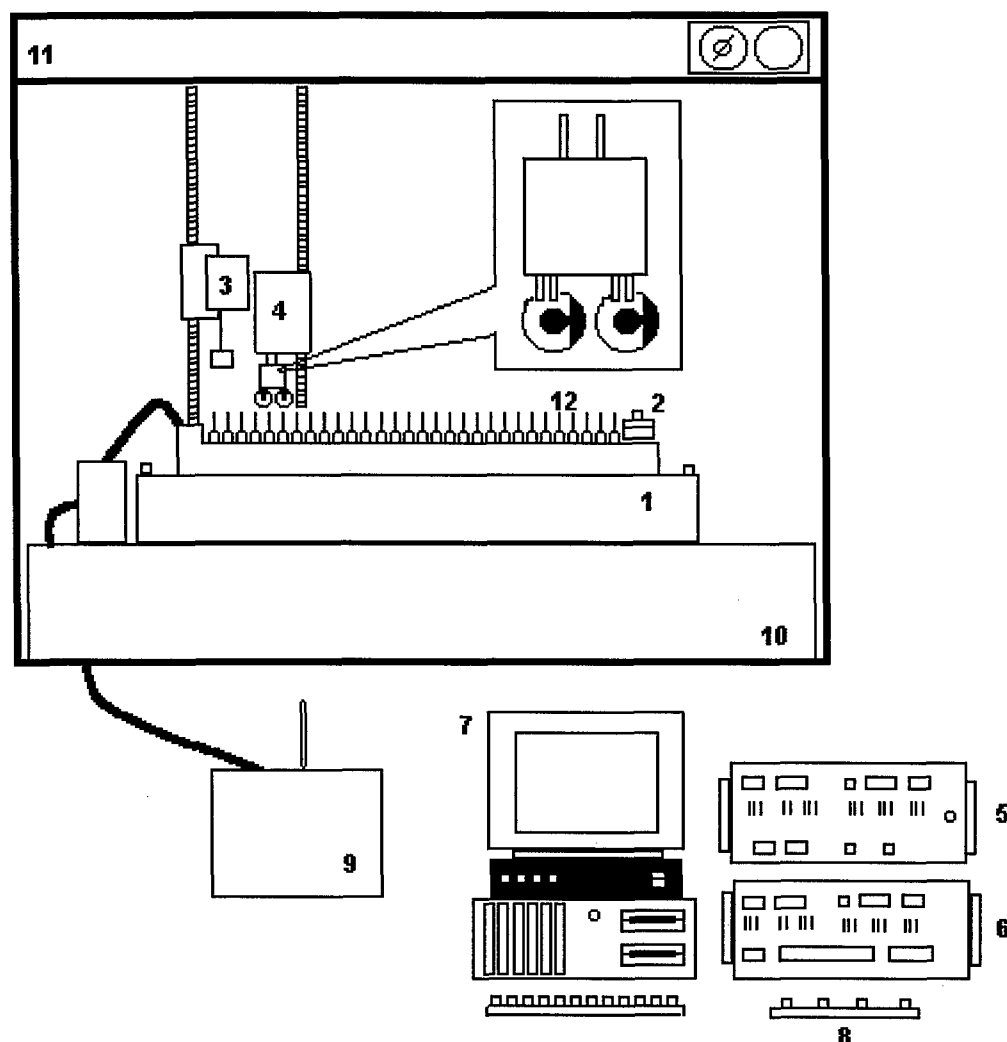


Fig. 5.11. Schematic of KSV 2200 Langmuir-Blodgett film balance system. (1) Teflon® trough containing subphase. (2) Compression barrier. (3) Balance head with platinum Wilhelmy surface balance plate. (4) Film collector unit with holder and crystals attached. (5) AFC unit. (6) DFC unit. (7) Data processing unit. (8) External control keyboard for film control mechanics. (9) Water bath. (10) Marble table. (11) Enclosure. (12) Monolayer film depicted on surface of subphase.

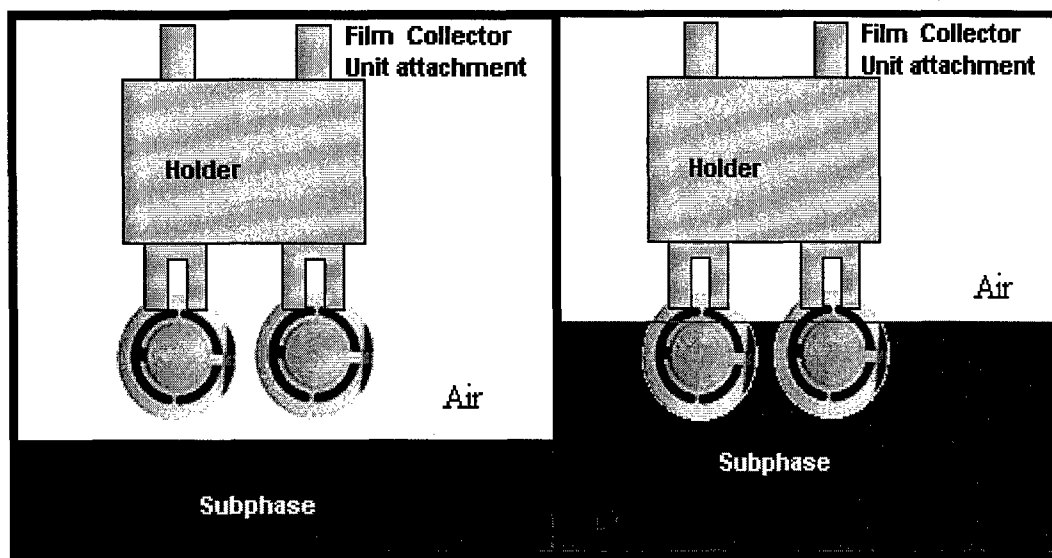


Fig. 5.12. Monolayer deposition to substrate. (A) Resonators oriented in holder.

Resonators are placed back-to-back (obverse sides are exposed) so that 4 sensors can be prepared for each run. Holder attachment to the film collector is not shown. (B) Prior to monolayer formation, resonators are lowered to a position below the subphase such that the sensing electrode is fully immersed. Thus, the first layer of spheroids is applied as the resonators rise out of the subphase (Y-type deposition).



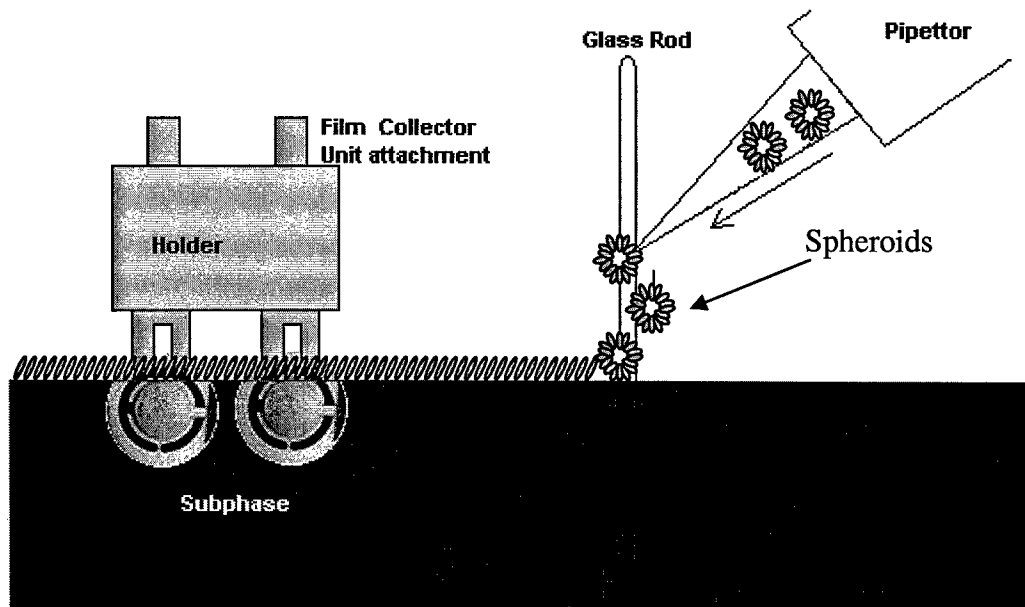


Fig. 5.13. Delivery of spheroids, either alone or in conjunction with phosphocholine (PC), to the surface of the subphase to prepare a Langmuir film of "skinned phage." Holder attachment to the film collector unit is not shown.

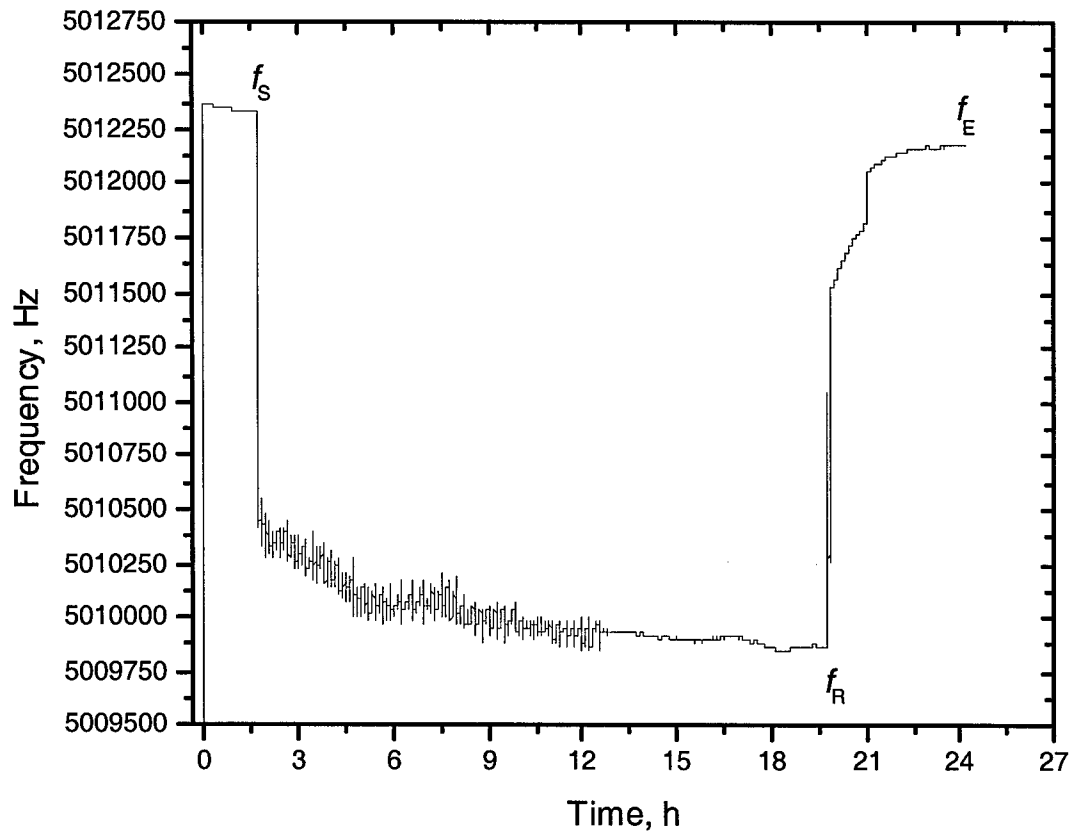


Fig. 5.14. Representative line graph depicting frequency change as a function of phage adherence to the resonator over time. Eighteen-hour incubation period is shown.  $f_S$ : Application of phage solution to clean, dry resonator at steady state: 5,012,338 Hz.  $f_R$ : Removal of phage solution, washing, and drying of resonator.  $f_E$ : Dried resonator at steady state: 5,012,177 Hz.  $\Delta f = (f_S) - (f_E) = -161$  Hz.

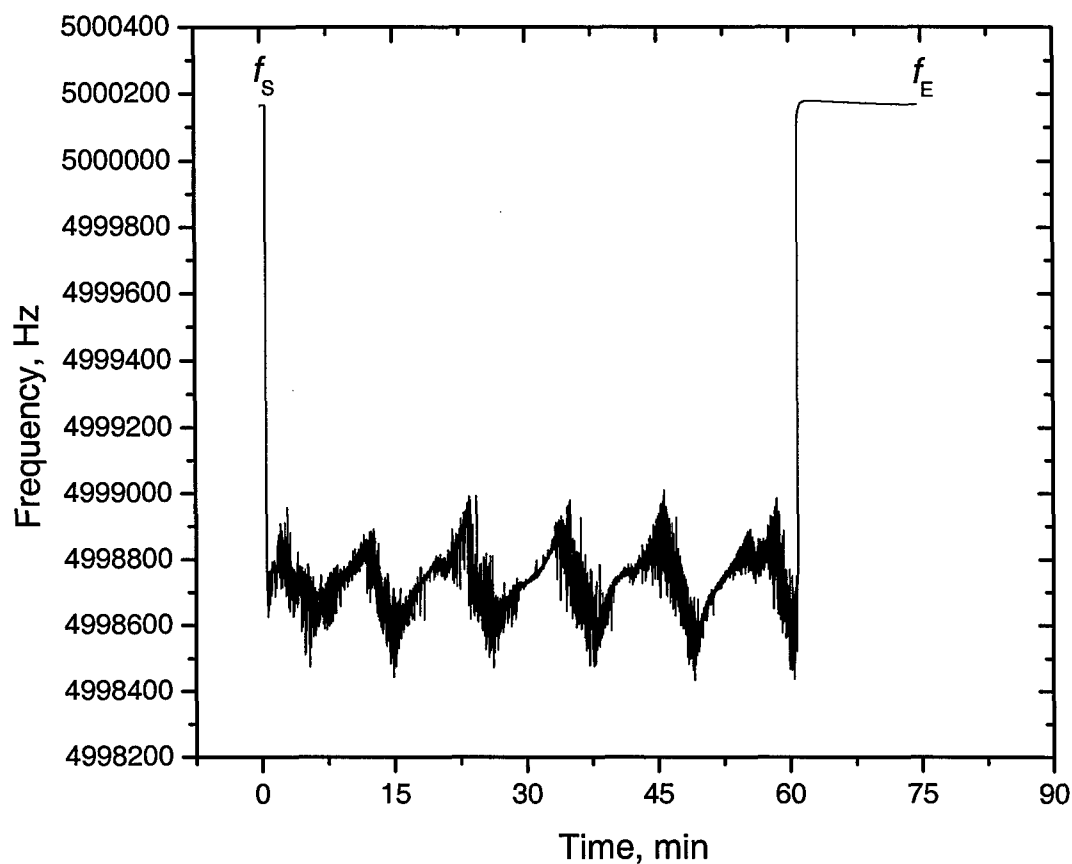


Fig. 5.15. Representative line graph of a clean resonator with degassed water only (control) depicting frequency change as a function of time. One-hour incubation period is shown.  $f_S$ : Application of water to clean, dry resonator at steady state: 5,000,167 Hz.  $f_R$ : Removal of water and drying of resonator.  $f_E$ : Dried resonator at steady state: 5,000,167 Hz.  $\Delta f = (f_S) - (f_E) = 0$  Hz.

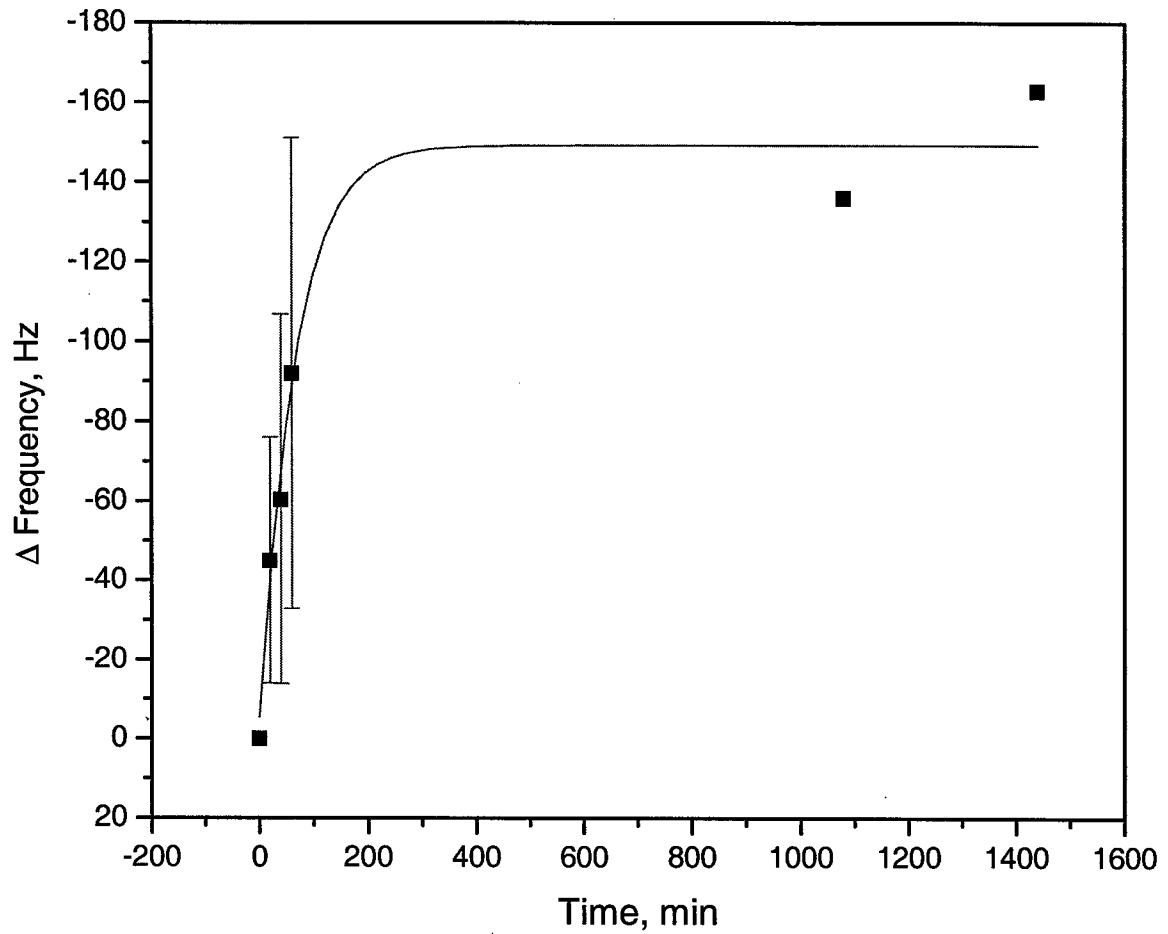


Fig. 5.16. Conglomerate data from timed deposition studies. Fitted sigmoidal curve indicates a strong relationship ( $R^2 = 0.963$ ) between time and frequency change as a result of phage binding to resonators. Bars are SD.

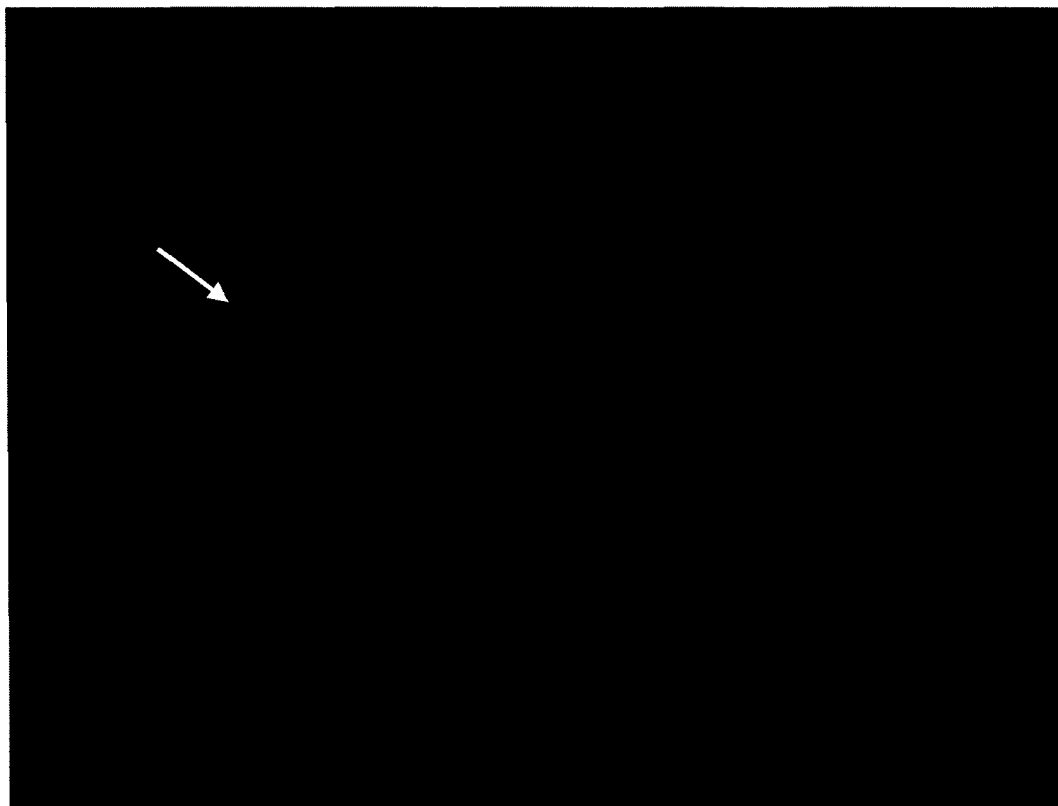


Fig. 5.17. Magnified ( $\times 1000$ ) view of a clean resonator (control) operating in real-time, as viewed by fluorescent microscopy. This scope had a short working-distance, high-numerical-aperture 100X high-dry objective allowing non-invasive visualization of phage binding to the resonator's sensing electrode; *cf.* Figs. 5.18 and 5.19. The arrow indicates the edge of the sensing electrode.



Fig. 5.18. Magnified ( $\times 1000$ ) view of same resonator from Fig. 5.17 under operational conditions following the addition of fluorescently labeled filamentous phage E2. The arrows indicate the edge of the sensing electrode. Large bundles of phage floating in suspension are evident.



Fig. 5.19. Magnified ( $\times 1000$ ) view of same resonator from Fig. 5.18 following phage deposition for 1 h and washing with PBS. The field of view encompasses the active area of the sensing electrode. The size differential of phage bundles is easily discernable.

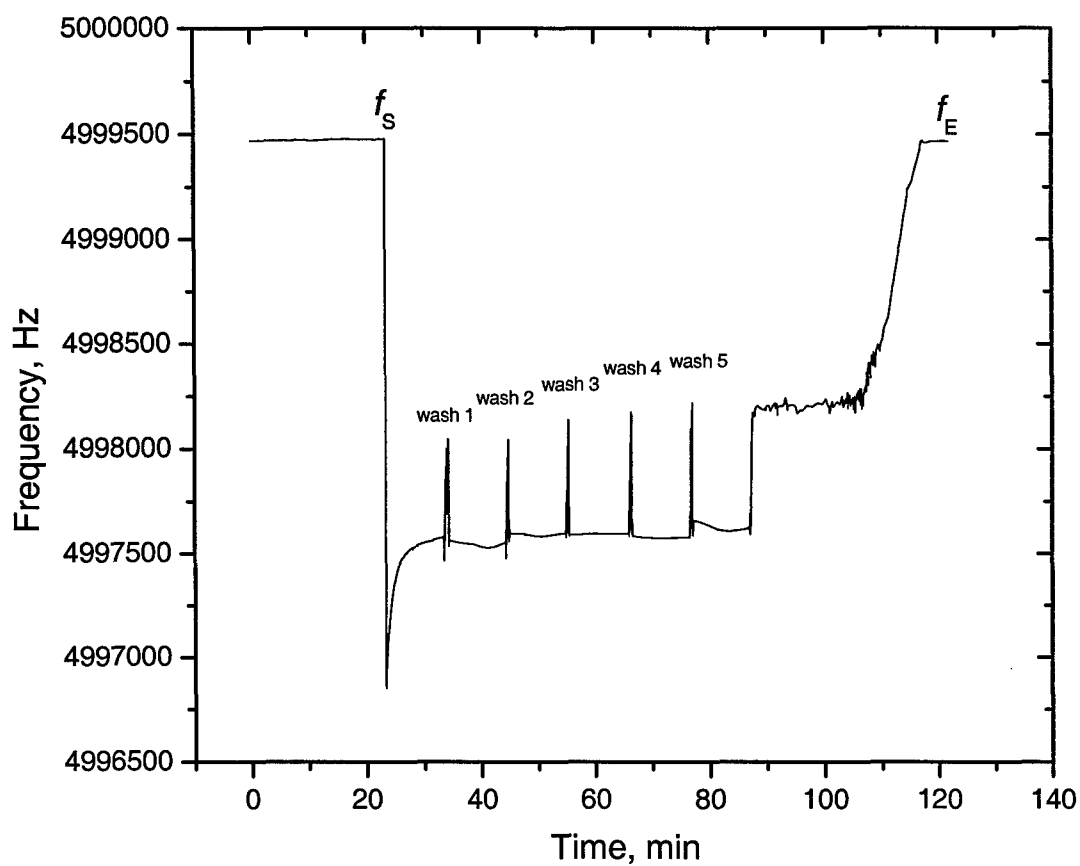


Fig. 5.20. Representative line graph of a resonator previously adsorbed with filamentous phage for 18 hours then washed ( $f_s$ : 4,999,973 Hz) five times with degassed water and dried ( $f_E$ : 4,999,973 Hz).  $\Delta f = (f_s) - (f_E) = 0$  Hz, indicating no loss of phage from active area of the sensing electrode.



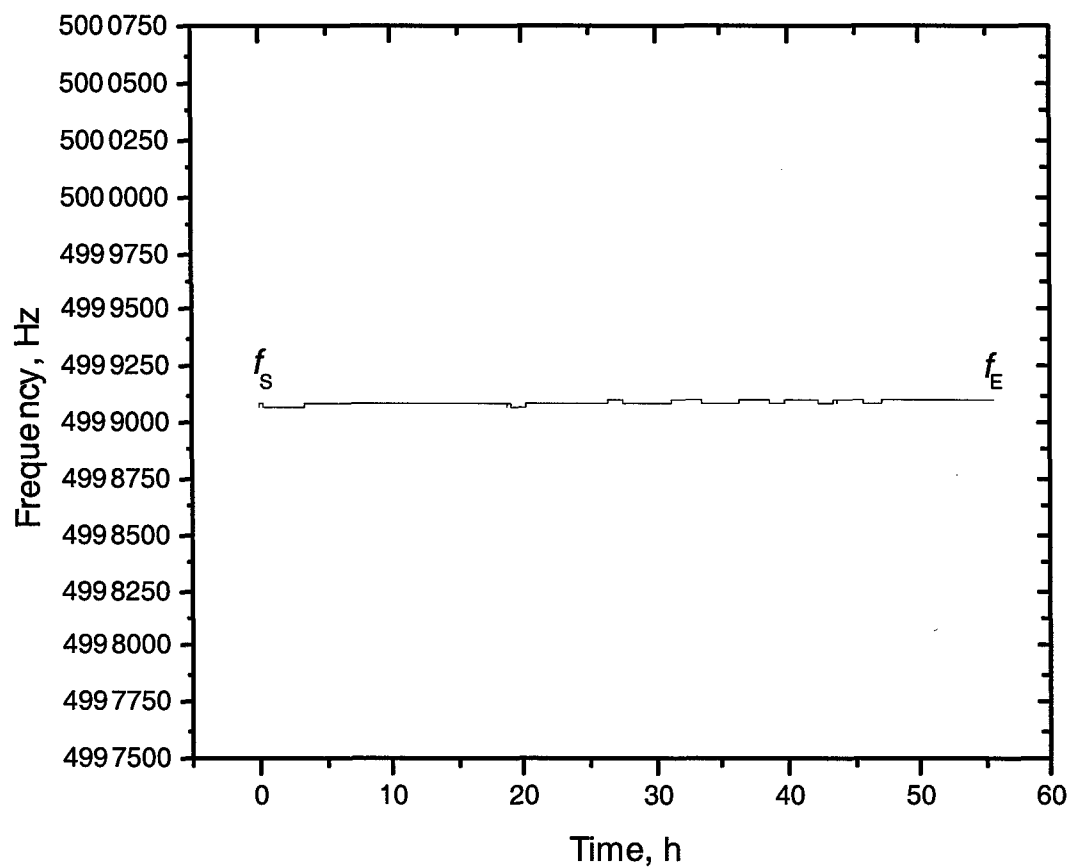


Fig. 5.21. Representative line graph of a resonator previously adsorbed with filamentous phage then washed and incubated with degassed water ( $f_S$ : 4,999,077 Hz) for 55 hours ( $f_E$ : 4,999,077 Hz).  $\Delta f = (f_S) - (f_E) = 0$  Hz, indicating no loss of phage from active area of the sensing electrode.

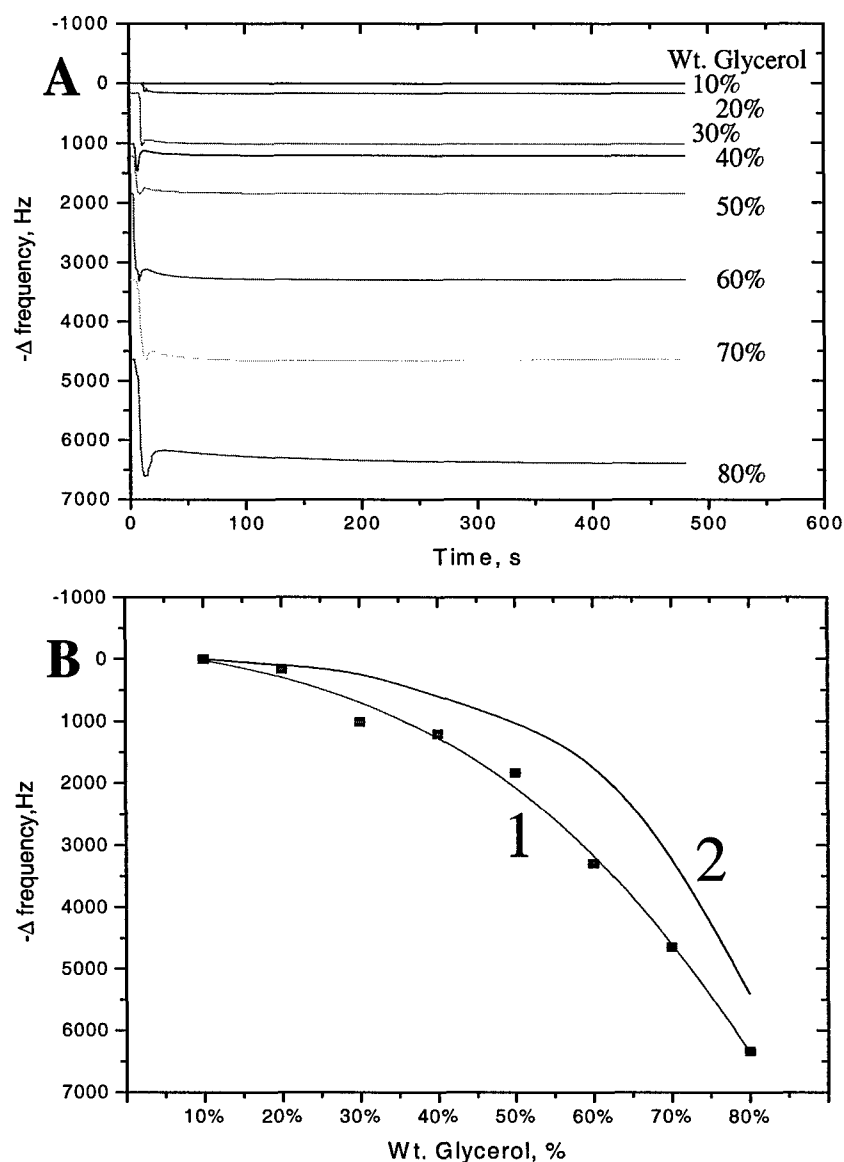


Fig. 5.22. Viscosity analysis using platform 2. (A) Differential frequency responses of a clean resonator to increasing concentrations of glycerol as a function of time. The resonator failed when a 90% solution of glycerol was assayed. (B) Dose-response relation of mean values ( $n = 450 \pm 4$ ) of steady-state frequency responses as a function of glycerol concentration. Fitted curve (1) is nonlinear sigmoidal fit of Boltzmann equation to experimental data points ( $R^2 = 0.995$ ). Bars are SD. Non-fitted curve (2) is B-spline fit to theory.

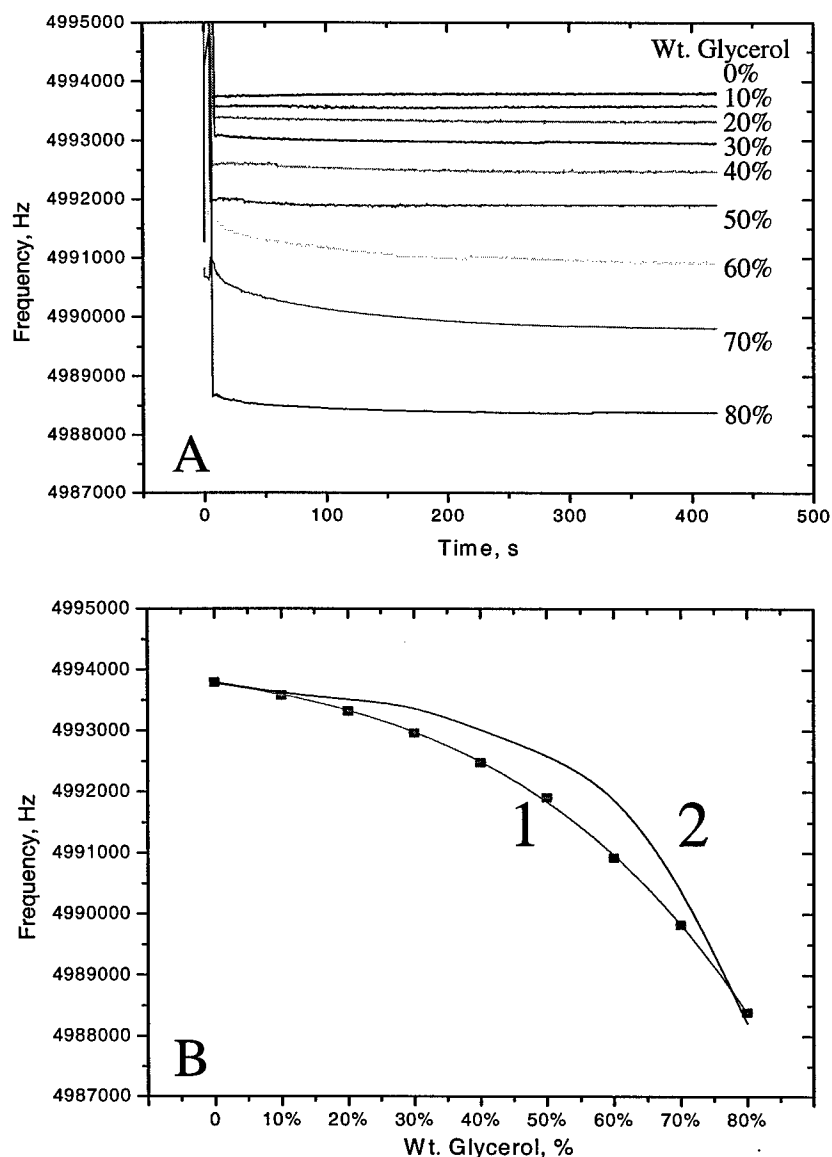


Fig. 5.23. Viscosity analysis using platform 1. (A) Frequency responses of clean QCR to differing concentrations of glycerol as a function of time. The resonator failed when a 90% solution of glycerol was assayed. (B) Dose-response relation of mean values ( $n = 954$ ) of steady-state voltage responses as a function of glycerol concentration. Fitted curve (1) is nonlinear sigmoidal fit of Boltzmann equation to experimental data points ( $R^2 = 0.999$ ). Bars are SD. Non-fitted curve (2) is B-spline fit to theory.

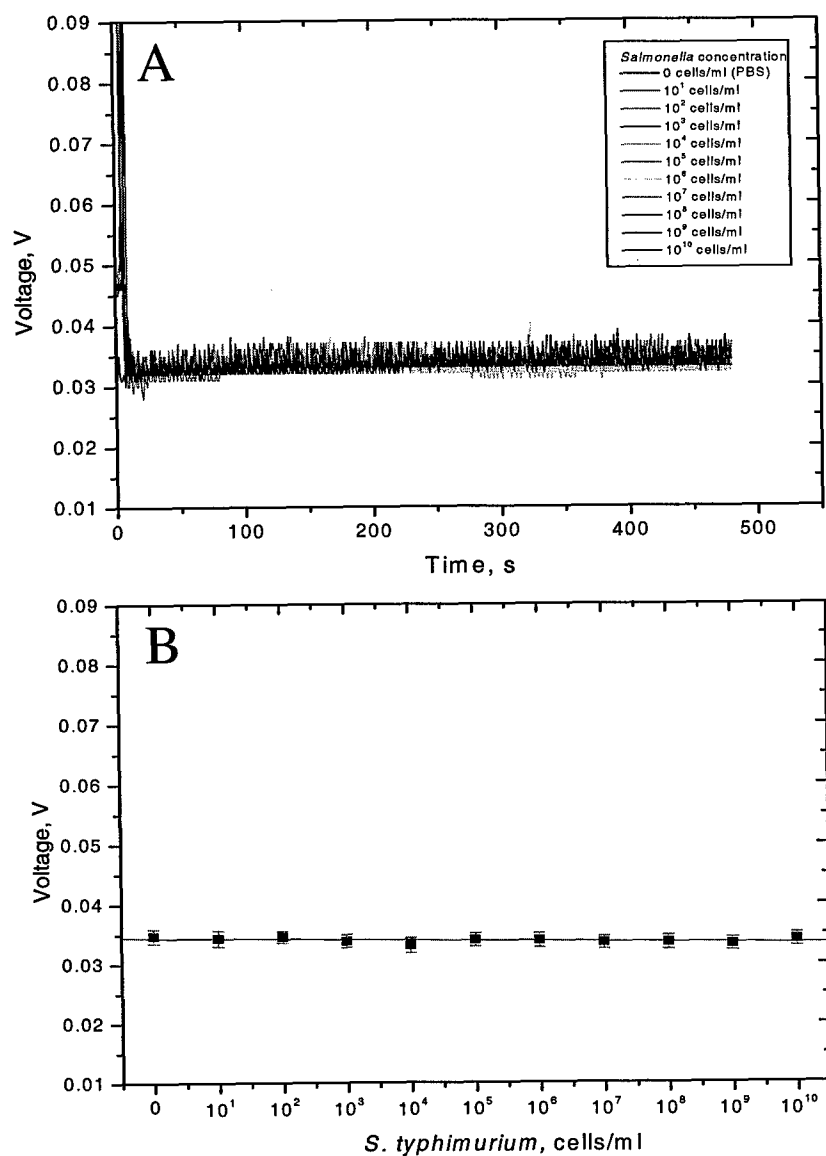


Fig. 5.24. Viscosity analysis and non-specific binding determination of *S. typhimurium* using platform 2. (A) Voltage responses of clean resonator to increasing concentrations of *S. typhimurium* as a function of time. (B) Dose-response relation of mean values ( $n = 431$ ) of steady-state output sensor voltages as a function of *S. typhimurium* concentration. Bars are SD. Line is linear least squares fit to experimental data points ( $R = -0.61$ , slope  $= -0.09$  mV,  $p < 0.05$ ).

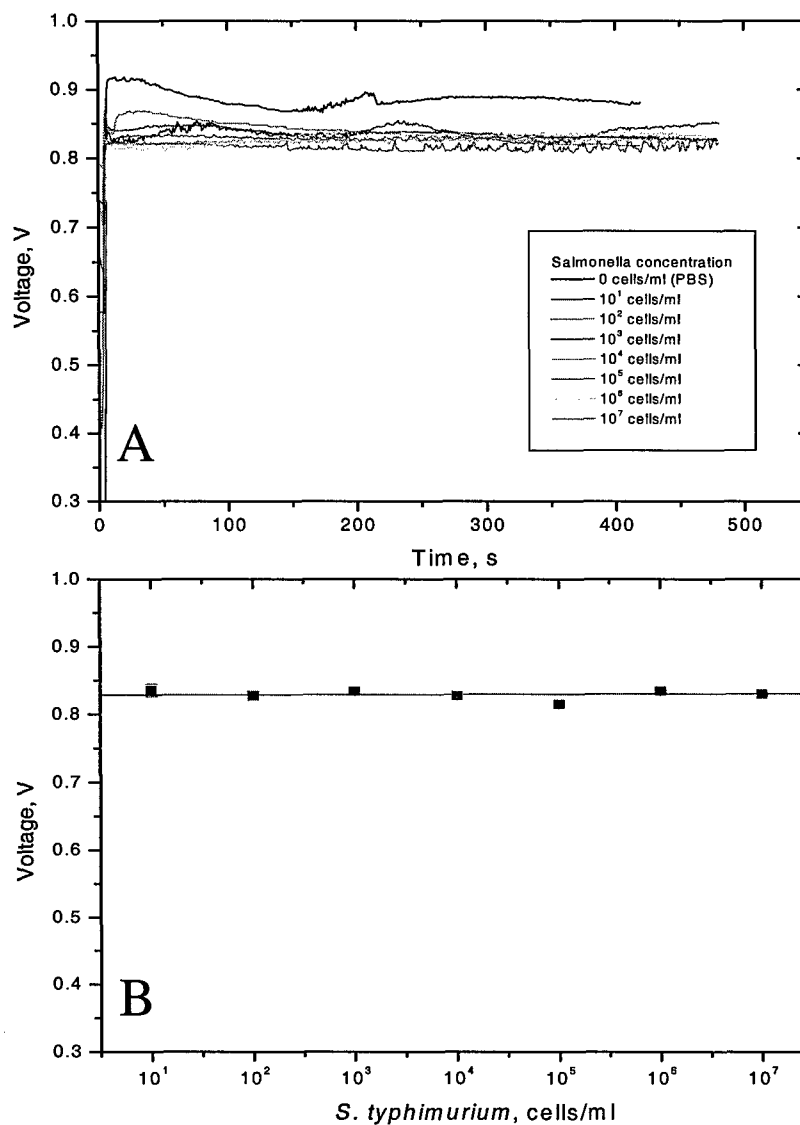


Fig. 5.25. Viscosity analysis and non-specific binding determination of *S. typhimurium* using platform 1. (A) Voltage responses of clean resonator to differing concentrations of *S. typhimurium* as a function of time. (B) Dose-response relation of mean values (n = 220) of steady-state output sensor voltages as a function of *S. typhimurium* concentration. Bars are SD. Line is linear fit least squares fit to experimental data points ( $R = 0.08$ , slope = 0.25 mV).

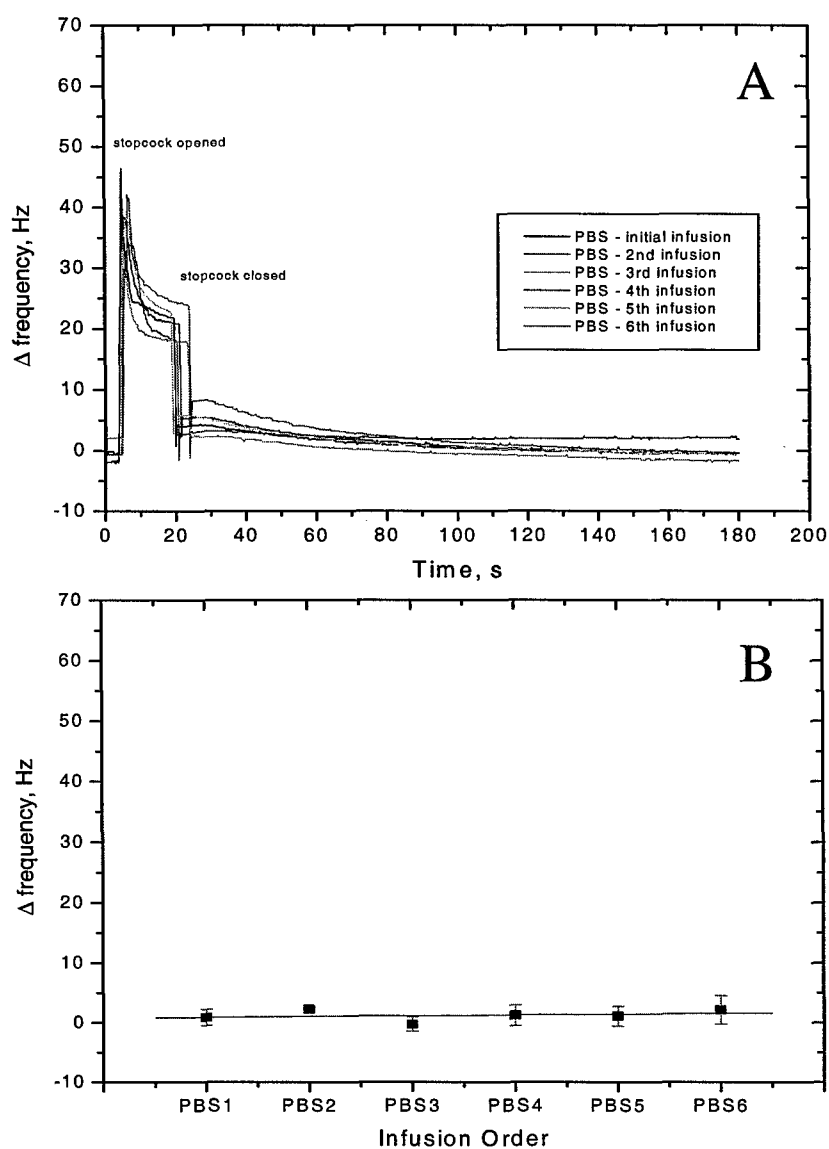


Fig. 5.26. Noise determination of platform 2. (A) Frequency responses of prepared phage biosensor assayed with PBS (all infusions are 1X concentration) as a function of time. (B) Dose response relation of the mean values ( $n = 1552 \pm 2$ ) of steady-state output sensor frequencies as a function of consecutive PBS infusions to the flow cell. Bars are  $SD = 0.3 - 2.1$  Hz. Line is linear least squares fit to experimental data ( $R = 0.25$ , slope =  $0.12$  Hz).

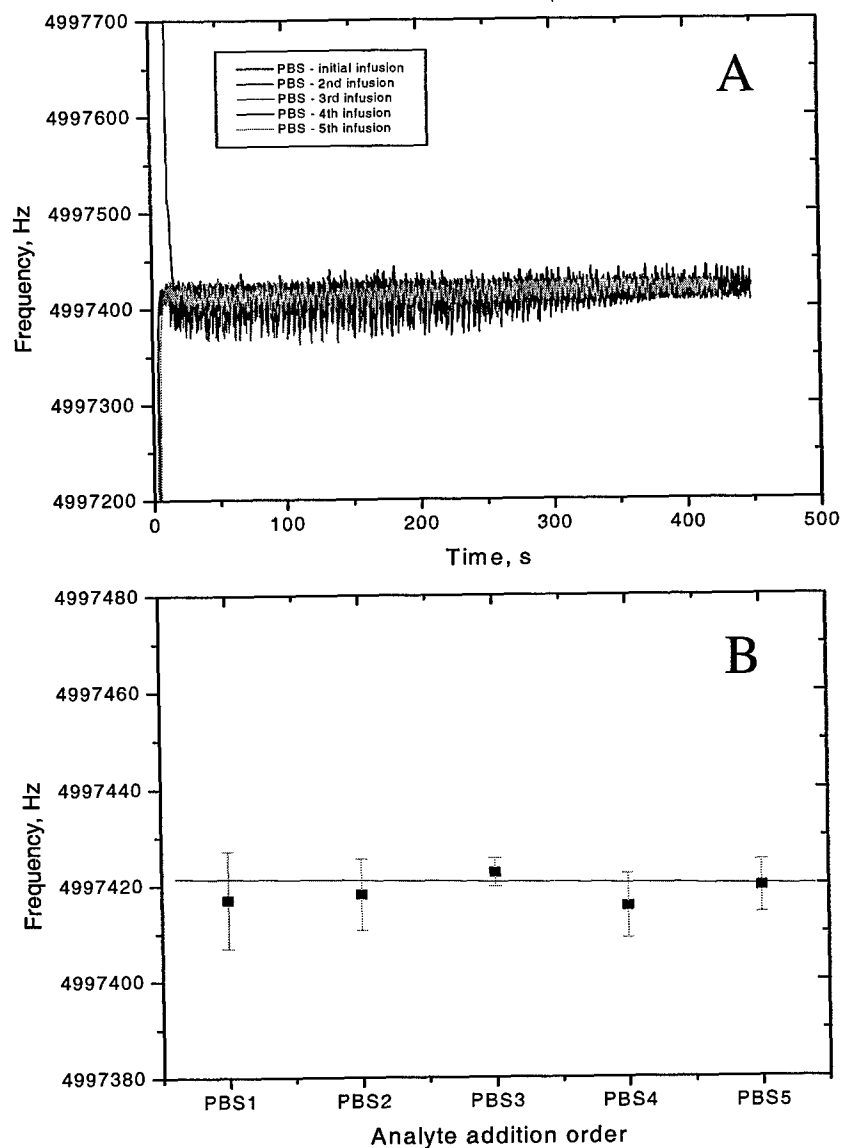


Fig. 5.27. Noise determination of platform 1. (A) Frequency responses of prepared phage biosensor assayed with PBS as a function of time. (B) Dose response relation of the mean values ( $n = 1500$ ) of steady-state output sensor frequencies as a function of consecutive PBS solutions. Bars are  $SD = 2.9 - 10.1$  Hz. Line is linear least squares fit to experimental data ( $R = -0.12$ , slope =  $-0.29$  Hz).

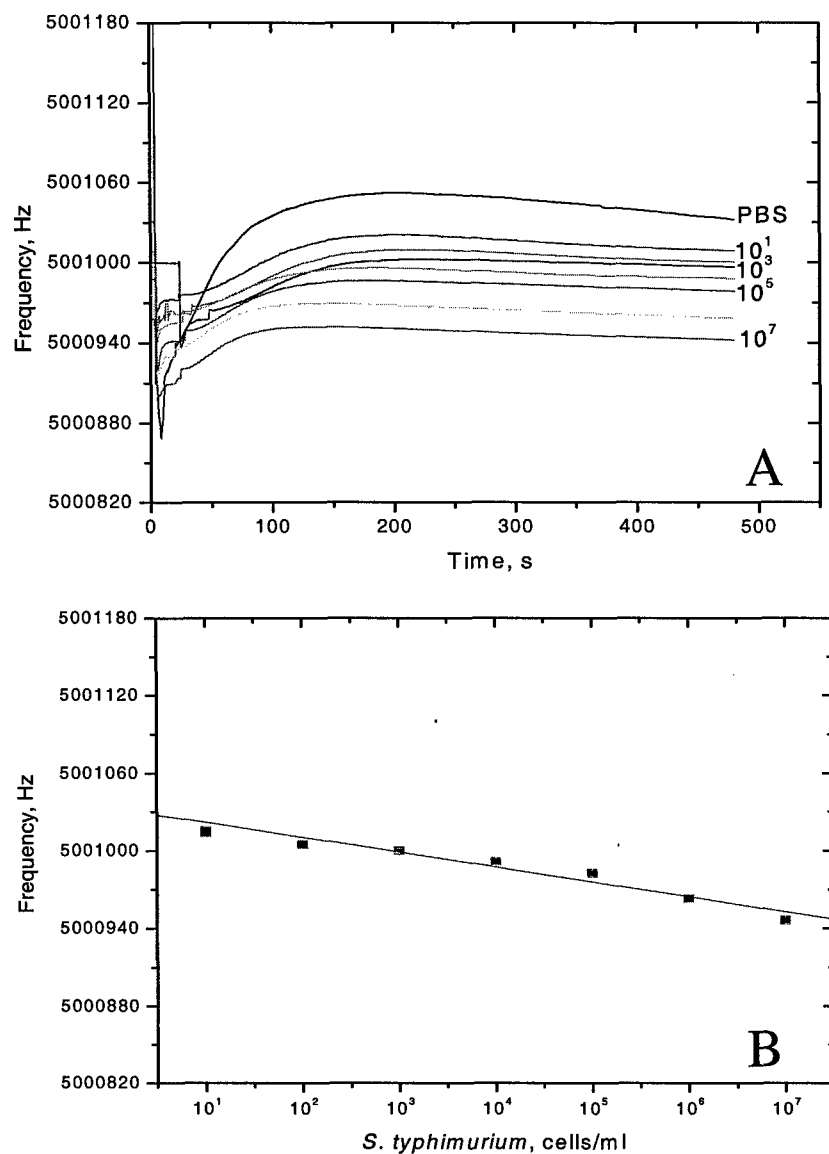


Fig. 5.28. (A) Frequency responses of phage biosensor to increasing concentrations of *S. typhimurium* as a function of time, using platform 2. (B) Dose-response relation of the mean values ( $n = 2800 \pm 2$ ) of steady-state output sensor frequencies as a function of *S. typhimurium* concentration. Gray bars are  $SD = 2.9 - 10.0$  Hz. Curve is linear least squares fit to experimental data ( $R = -0.98$ , slope =  $-10.9$  Hz,  $p < 0.001$ ).



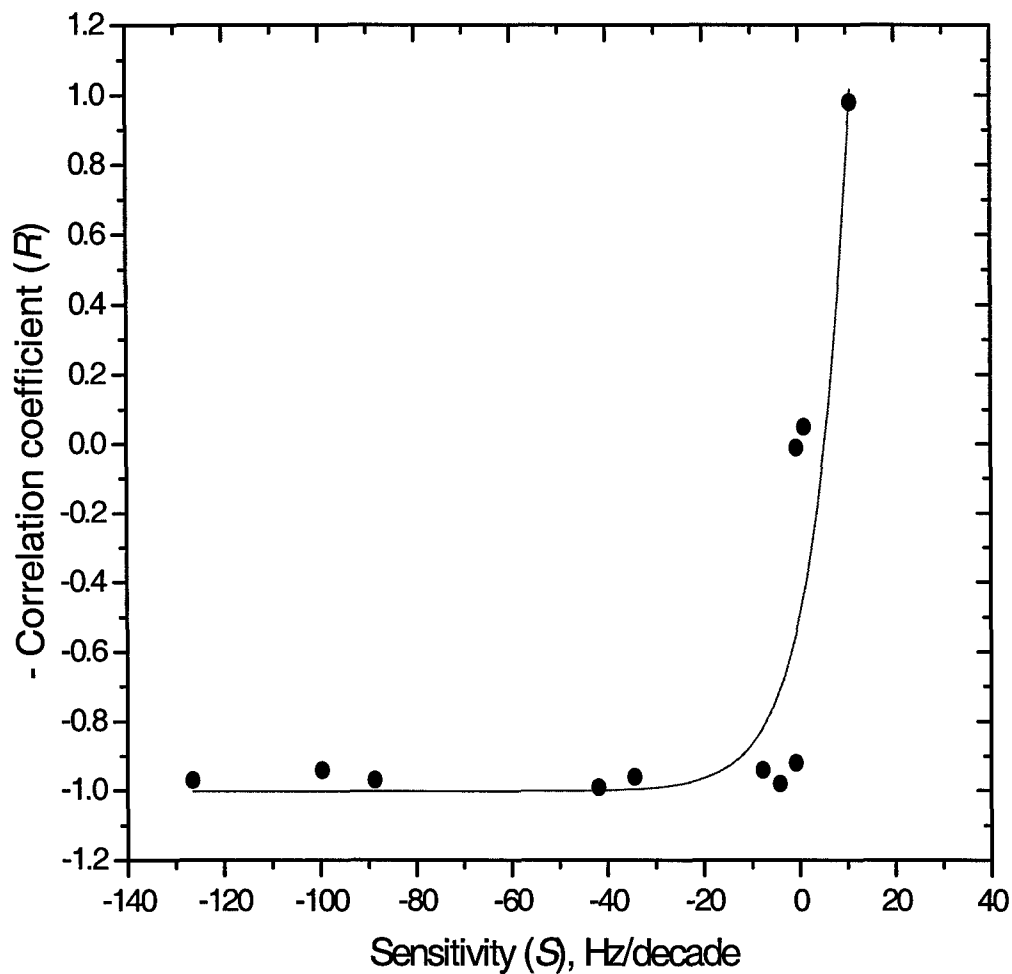


Fig. 5.29. Experimental correlation coefficient as a function of sensitivity for 12 filamentous phage (FPI) sensors prepared by physical adsorption and assayed with *S. typhimurium* using platform 2. Correlation coefficients,  $R$ , were derived from the linear fit to dose-response signals for each tested sensor; sensitivities,  $S$ , from the slope of the linear fit. Curve is nonlinear sigmoidal fit of Boltzmann equation to experimental data points ( $R^2 = 0.80$ ).

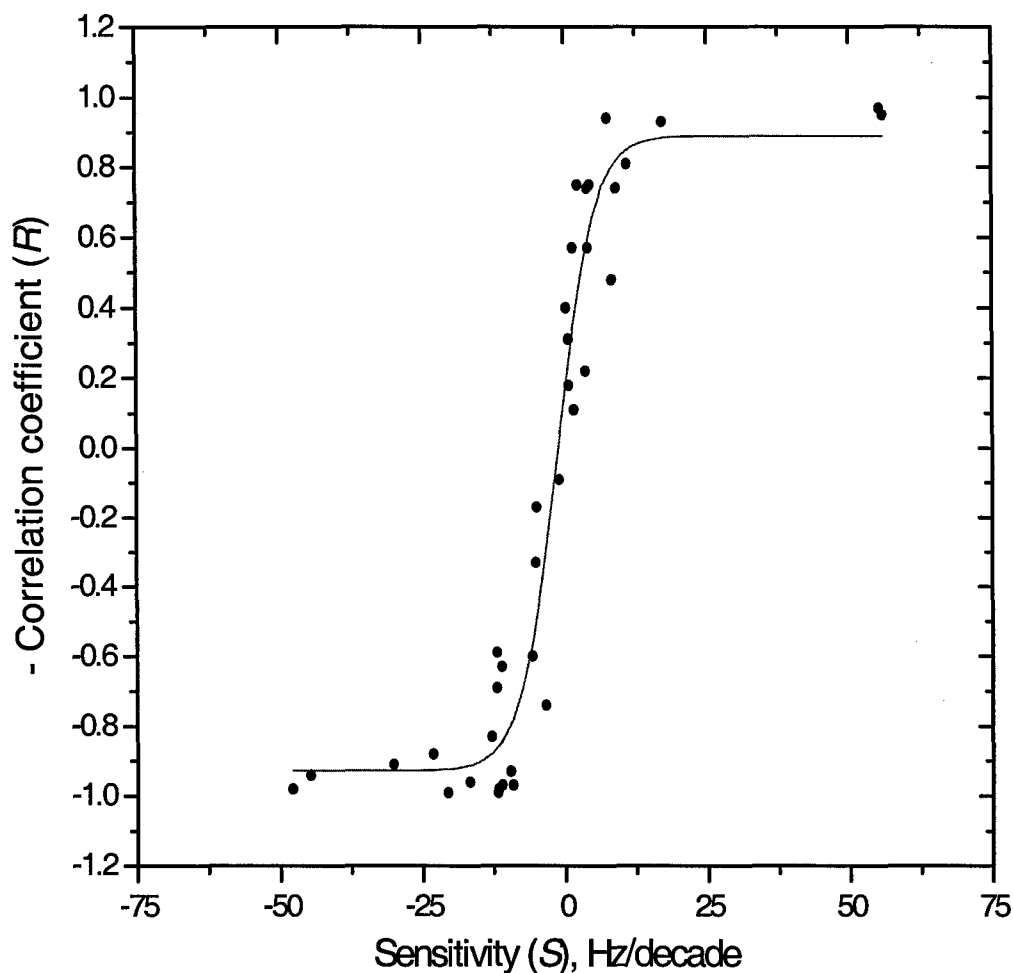


Fig. 5.30. Experimental correlation coefficient as a function of sensitivity for 37 filamentous phage (FPI) sensors prepared by physical adsorption and assayed with *S. typhimurium* using platform 1. Correlation coefficients,  $R$ , were derived from the linear fit to dose-response signals for each tested sensor; sensitivities,  $S$ , from the slope of the linear fit. Curve is nonlinear sigmoidal fit of Boltzmann equation to experimental data points ( $R^2 = 0.94$ ). Four of 37 sensors (11%) fit the acceptable performance criteria ( $R \geq 0.90$  and sensitivity greater than 1 Hz/decade bacteria concentration).

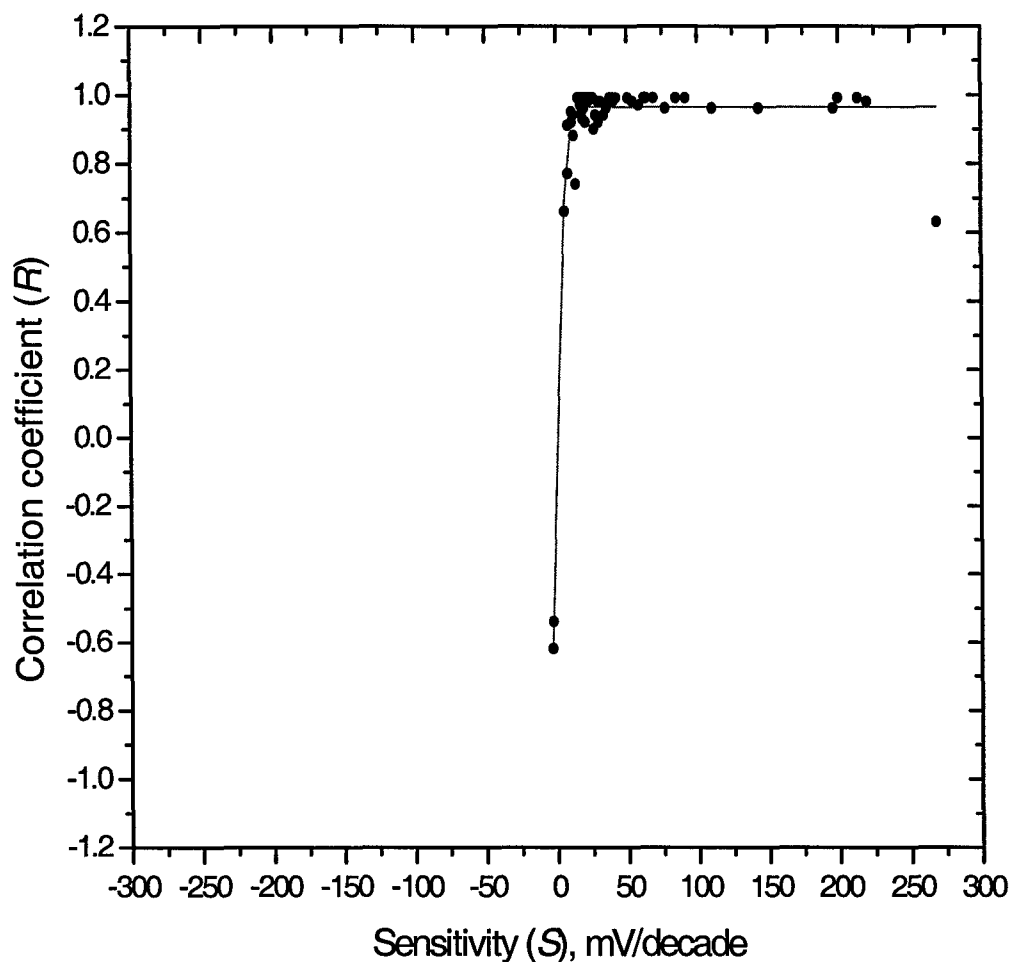


Fig. 5.31. Experimental correlation coefficient as a function of sensitivity for 59 biosensors (Sab) prepared from *Salmonella* antibodies against O-antigen (Sab) immobilized by Langmuir Blodgett method. Correlation coefficients,  $R$ , were derived from the linear fit to dose-response signals for each tested sensor; sensitivities,  $S$ , were derived from the slope of the linear fit. Curve is nonlinear sigmoidal fit of Boltzmann equation to experimental data points ( $R^2 = 0.96$ ). Fifty-three of 59 sensors (90%) fit the acceptable performance criteria ( $R \geq 0.90$  and sensitivity greater than 8 mV/decade bacterial concentration).

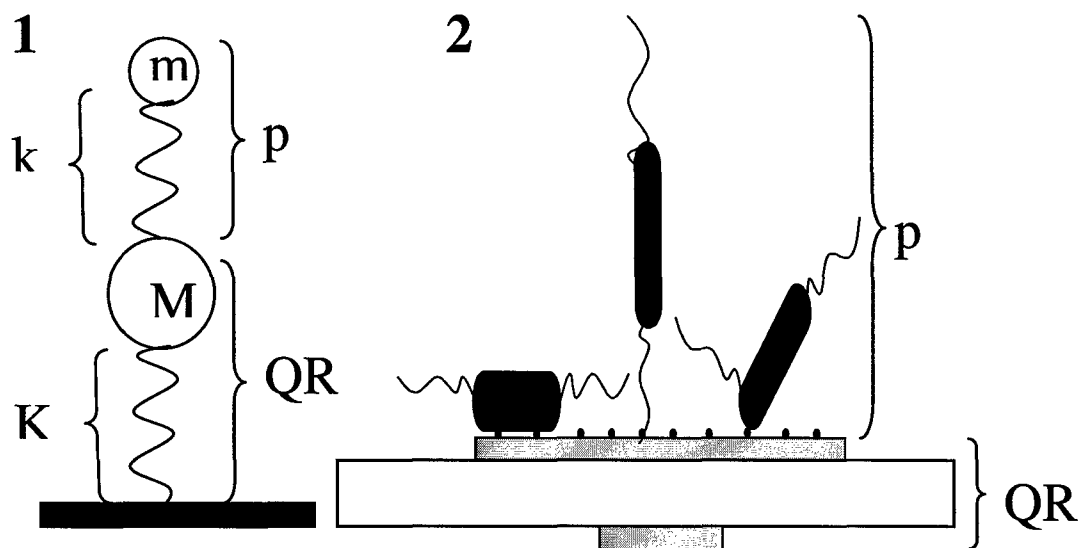


Fig. 5.32. Mechanical models of analyte-resonator interaction as composite and coupled oscillators (cf. Fig 5.58). (1) Reproduction of coupled oscillator model of Dybwad (1985, Fig. 2.) depicting quartz resonator (QR) as one mass ( $M$ ) spring ( $K$ ) system, and a loosely attached particle ( $p$ ) as a second mass ( $m$ ) spring ( $k$ ) system. Attachment of the loose particle causes QR to oscillate at a new, higher frequency when  $k < K$ . When  $k = K$ , a composite system is formed that produces expected mass loading effect with corresponding frequency decrease. (2) Corresponding model of Olsen et al. (2003, Fig. 9) that shows bacterial binding positions at the solid/liquid interface of the quartz resonator. When binding is firm between bacteria and receptor (left), the natural frequency of the cell as an independent mass-spring system equals the frequency of the resonator, forming a composite unit that produces expected mass loading effect with corresponding frequency decrease. When binding is loose between analyte and receptor (center and right), a coupled oscillator is formed whose frequency is dictated by the difference in the spring constants between the oscillator and bacteria.

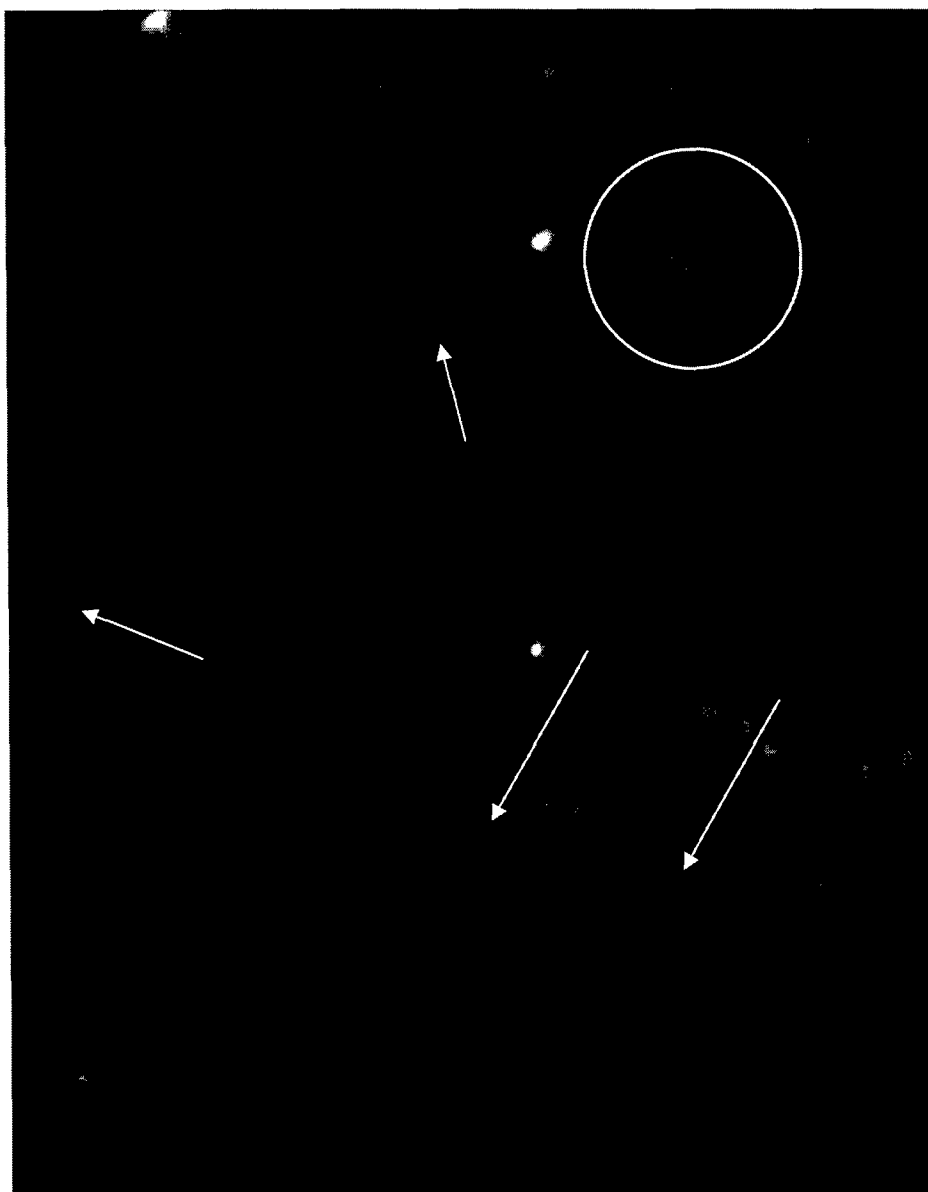


Fig. 5.33. Fluorescent microscopy image of *S. typhimurium* attached to the surface of a resonator previously coated with filamentous phage by physical adsorption. Numerous bacteria were visible; some were rigidly attached while others demonstrated flexible movement. The majority of bacteria demonstrated rigidly attached flagella (arrows). The pair of bacteria enclosed within the white circle is displayed in movement in Fig. 5.34. Magnification,  $\times 1000$ .

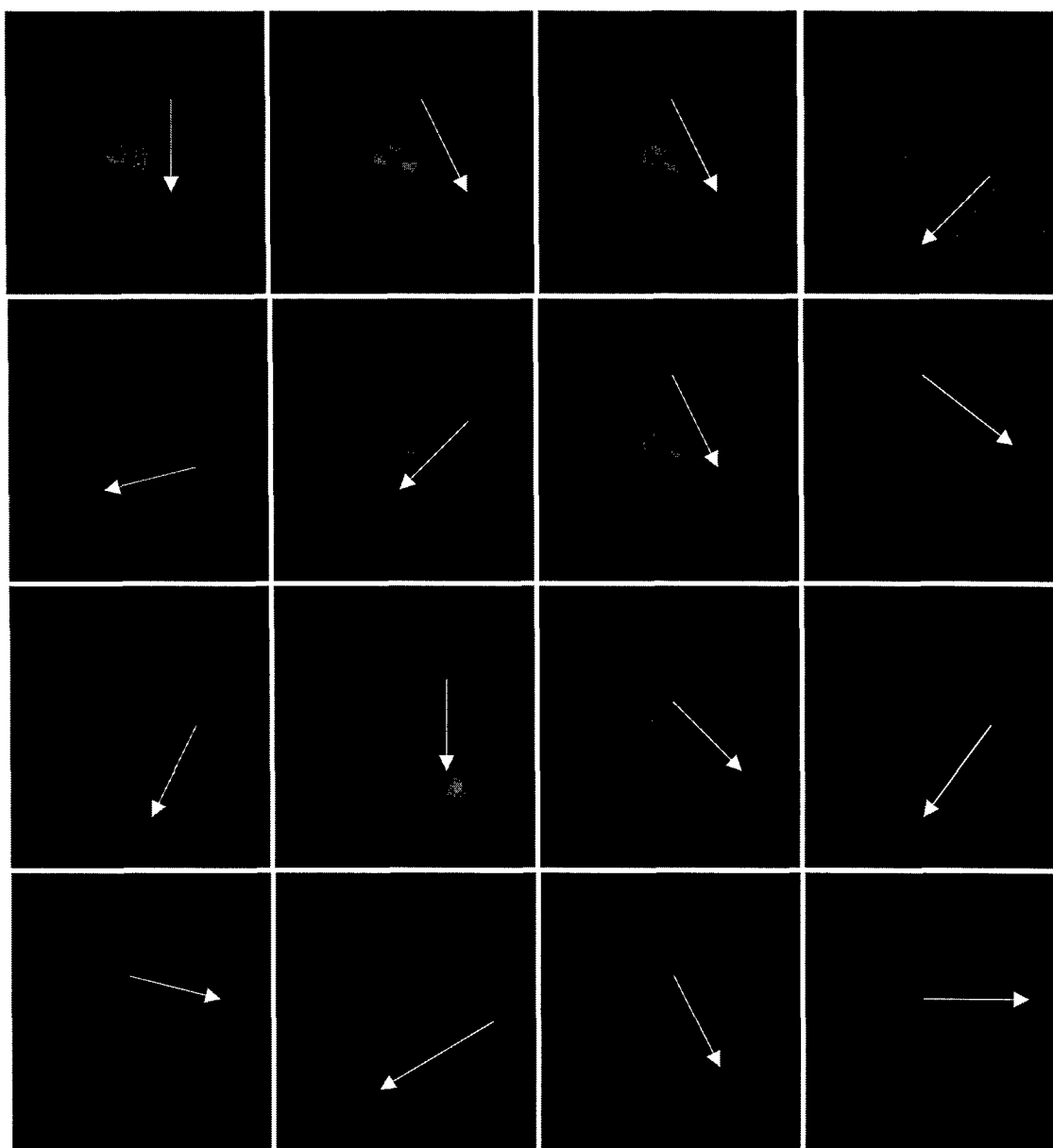


Fig. 5.34. Fluorescent microscopy images of two *S. typhimurium* cells attached to the surface of a QCM resonator coated with filamentous phage under operational conditions. Images are consecutive still frames (1 s intervals, top left to bottom right) showing two bacterium: one is rigidly attached to the sensor via phage (left) while the other (right) is flexibly attached, allowing oscillation and random directional movement (arrows) of the cell at the resonator surface. Magnification,  $\times 1000$ .

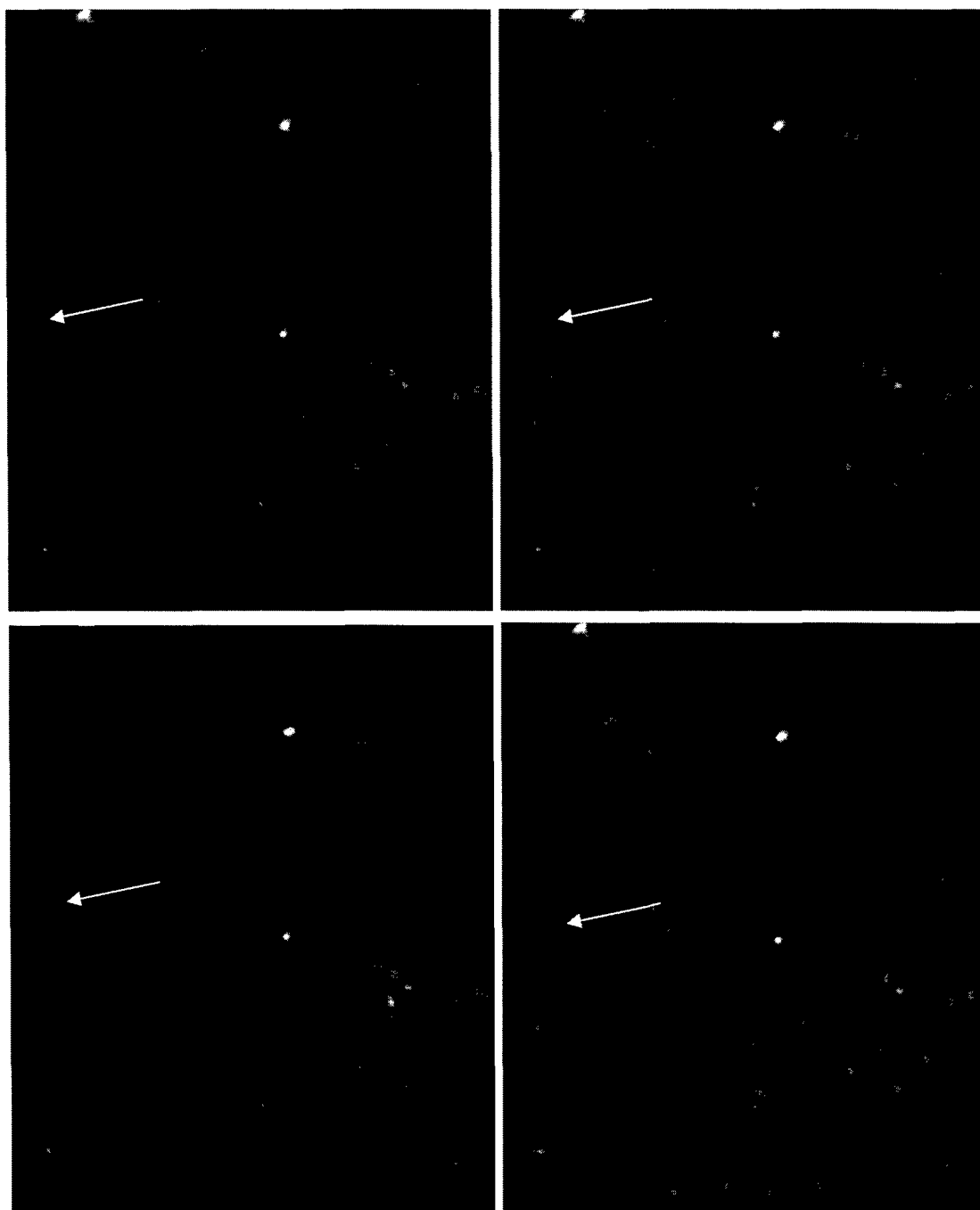


Fig. 5.35. Real-time observation of *S. typhimurium* attaching to QCM resonator (arrow) previously coated with filamentous phage by physical adsorption. Sequential fluorescent still frames (1 s intervals, top left to bottom right) show a bacterium rigidly attaching out of suspension. No further movement followed attachment. Flagella are evident and firmly “plastered” down to the surface of the sensor. Magnification,  $\times 1000$ .

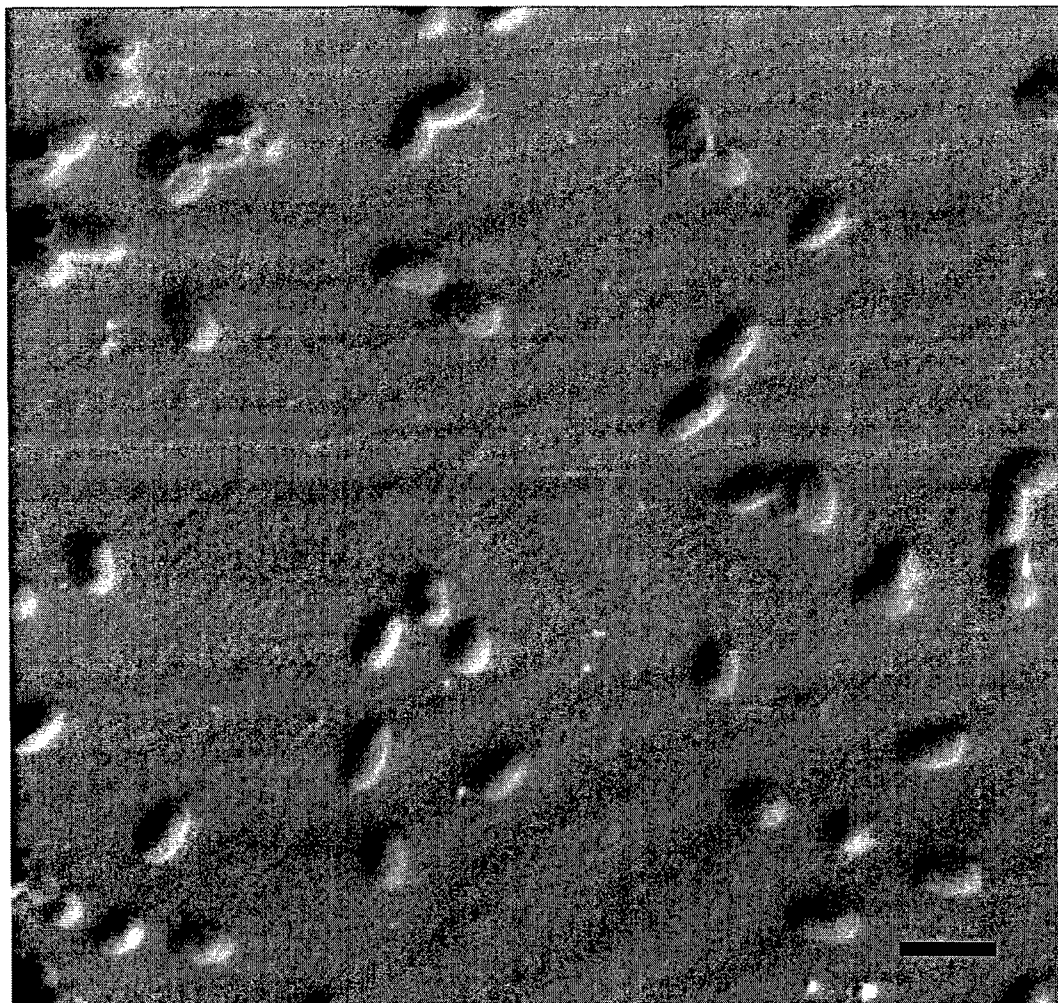


Fig. 5.36. Scanning electron micrograph demonstrating *S. typhimurium* binding to phage immobilized to the surface of a sensor by physical adsorption; *cf.* Fig. 5.37 (control).

Magnification,  $\times 3000$ ; bar = 5  $\mu\text{m}$ .



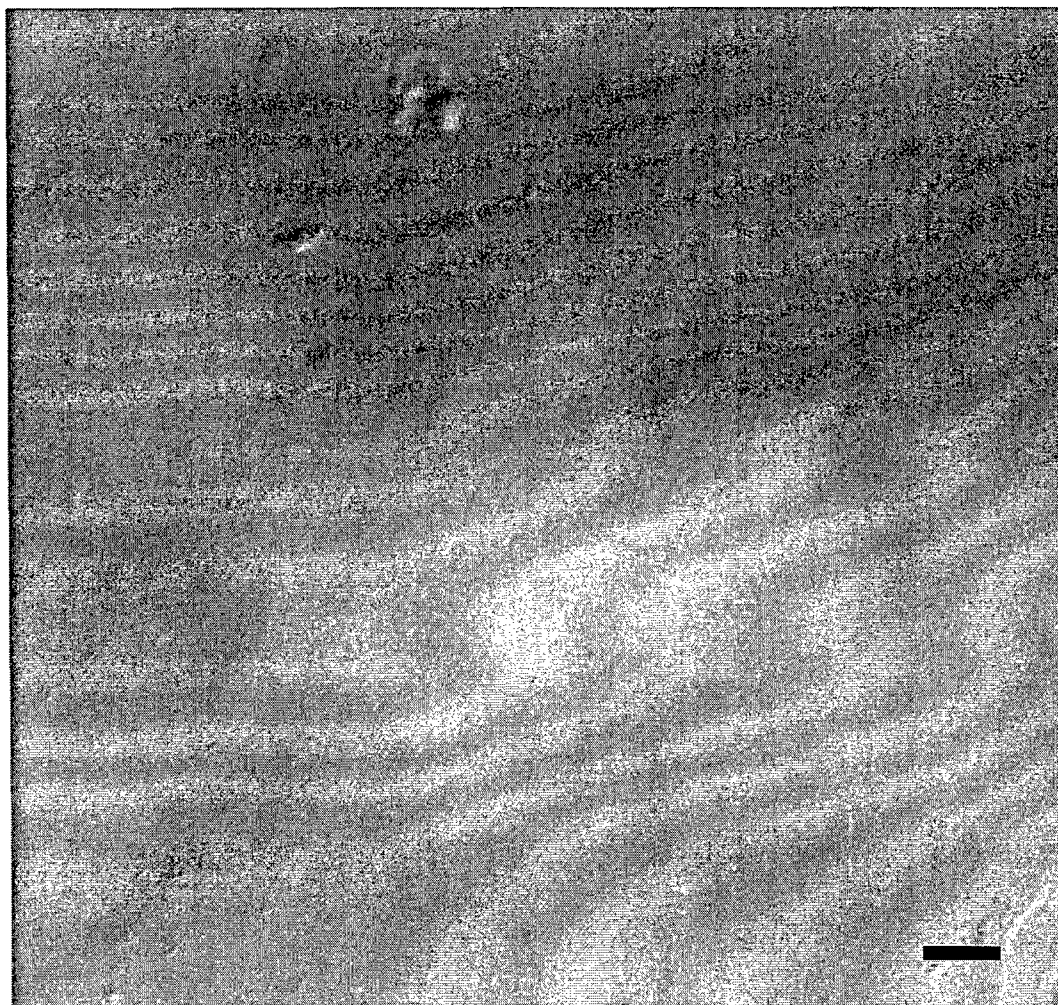


Fig. 5.37. Scanning electron micrograph depicting a sensor prepared with phage by physical adsorption. Acting as a control, the sensor was not exposed to *S. typhimurium*. The smooth surface is indicative of a polished resonator (*cf.* Fig. 3.1) and phage resolution was not possible. Magnification,  $\times 1000$ ; bar = 10  $\mu\text{m}$ .

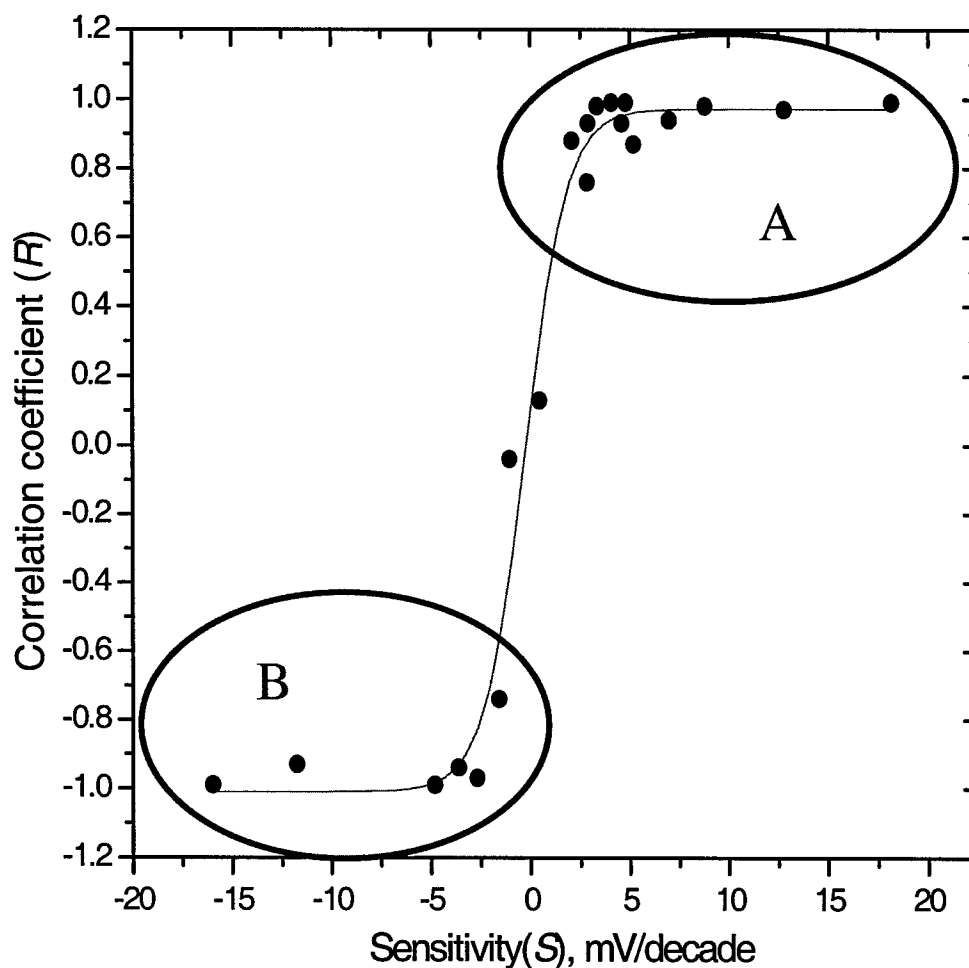


Fig. 5.38. Experimental correlation coefficient as a function of sensitivity for 20 FPB *S. typhimurium* biosensors prepared from biotinylated filamentous phage adsorbed to streptavidin activated resonators. Correlation coefficients,  $R$ , were derived from the linear fit to dose-response signals for each tested sensor; sensitivities,  $S$ , were derived from the slope of the linear fit. Curve is nonlinear sigmoidal fit of Boltzmann equation to experimental data points ( $R^2 = 0.98$ ). Eighteen of 20 sensors fall into two groupings shown in ovals (A) and (B), while 2 sensors are indifferent. Overall, 9 of 20 sensors (45%) fit the acceptable performance criteria ( $R \geq 0.90$  and  $S \geq 2$  mV/decade bacteria concentration).

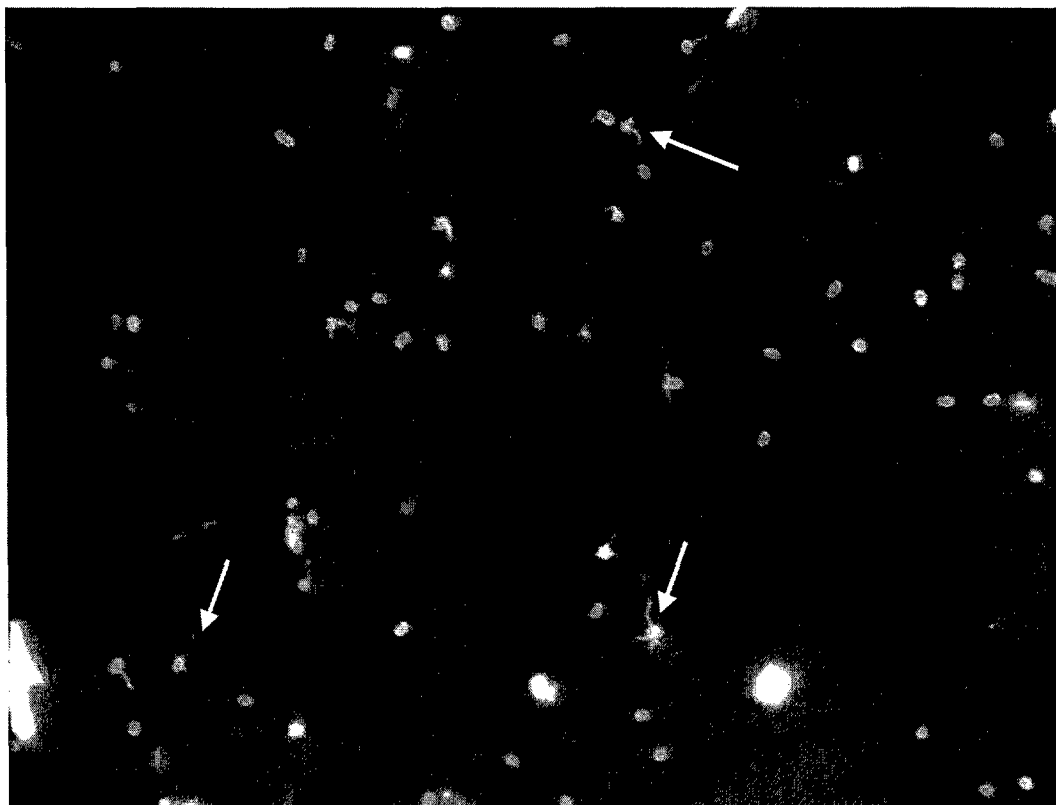


Fig. 5.39. Numerous *S. typhimurium* exhibiting flagella are clearly visible (arrows) in the foreground. Immobilized phage can be discerned in the background (*cf.* Figs. 5.17 and 5.19).

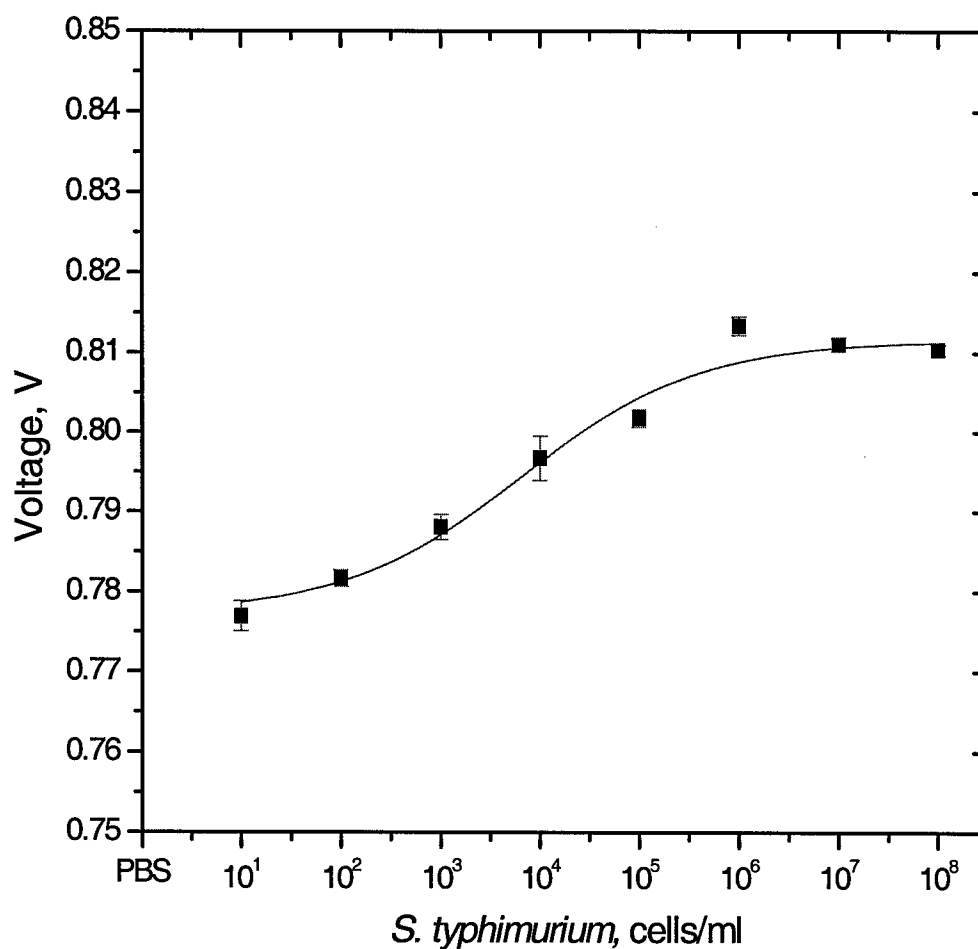


Fig. 5.40. Dose-response relation of the mean values ( $n = 300$ ) of steady-state output sensor frequencies for a FPB fluorescent sensor as a function of *S. typhimurium* concentration. Curve is nonlinear sigmoidal fit of Boltzmann equation to experimental data points ( $R^2 = 0.98$ ). Bars are SD.  $V_{\max} \approx 10^7$  cells/ml.

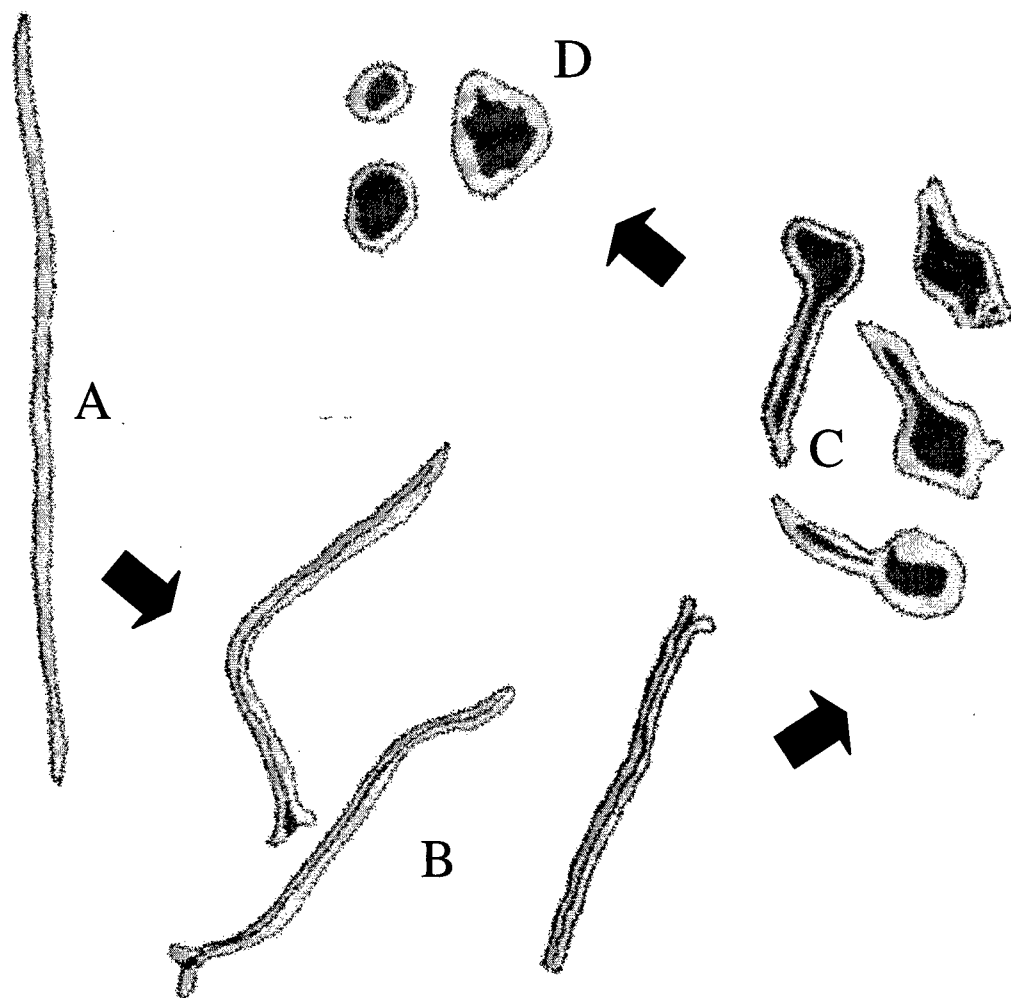


Fig. 5.41. Phage morphology induced by chloroform denaturation. Chloroform denaturation at room temperature contracts filamentous phage (A) to an intermediate (I) form (B), I-spheroid form (C) with subsequent DNA extrusion, and finally a spherical particle (spheroid) (D); *cf.* Figs. 5.43 and 5.44.

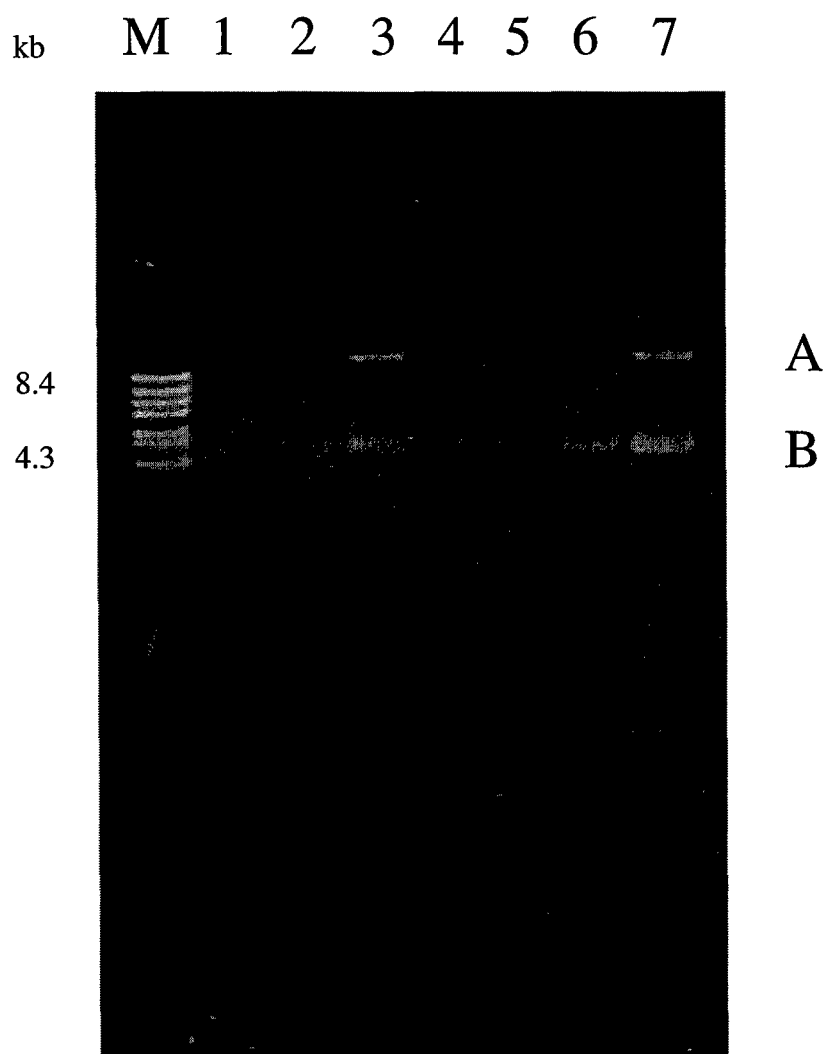


Fig. 5.42. Agarose (0.8%) gel electrophoresis analysis of spheroids as a function of chloroform exposure time and filamentous phage concentration. Lanes: M, *BstE* II  $\lambda$  DNA ladder; 1 – 3: 1 min vortex; 4 – 7: 3 min vortex; 1 and 4: neat phage; 2 and 5: 3 $\times$  dilution of neat phage; 3 and 6: 6 $\times$  dilution of neat phage; 7: solvent-phage interface from prep 1 (lane 1).

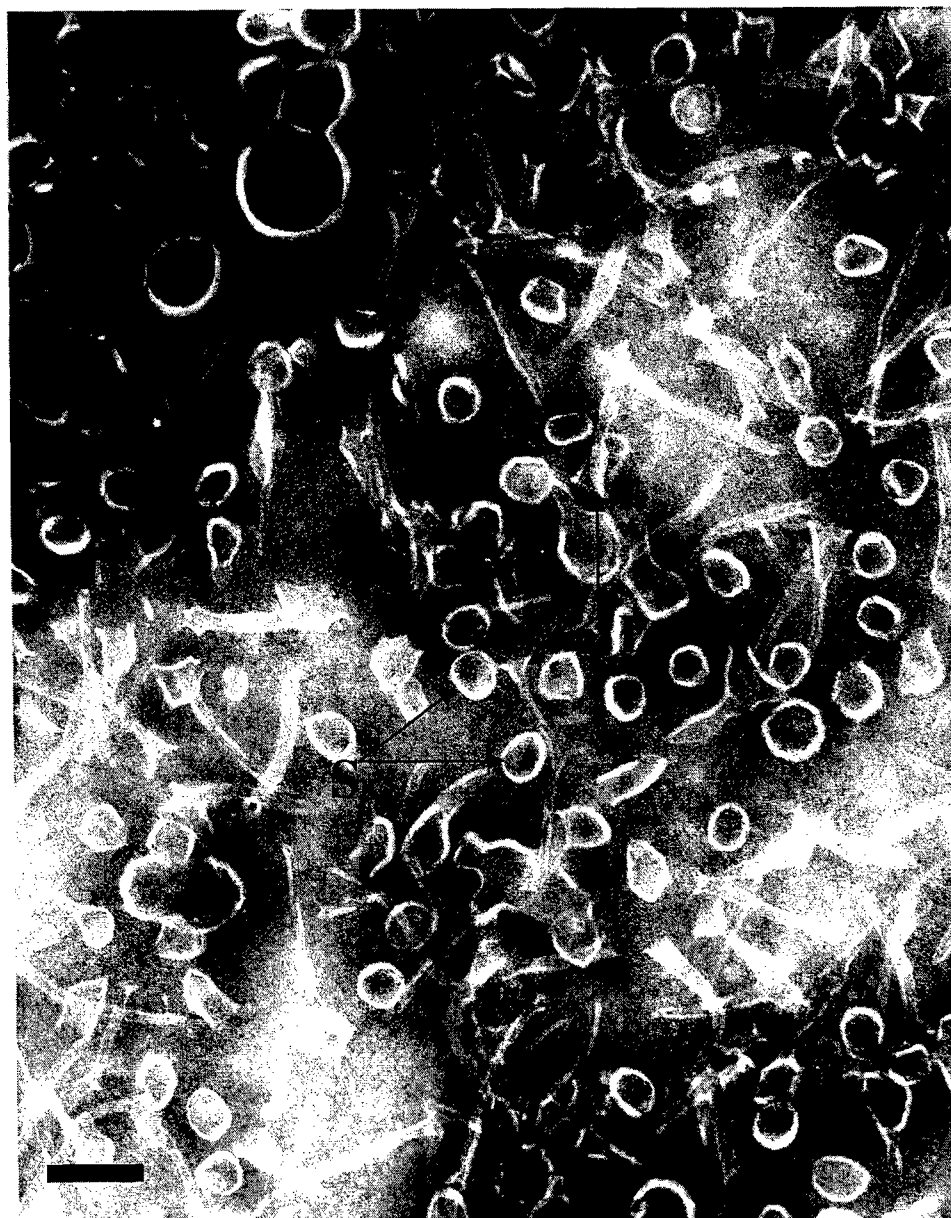


Fig. 5.43. Transmission electron micrograph of chloroform denatured filamentous phage E2. Examples of both I-forms (I) and spheroids (S) are evident following preparation at room temperature. Magnification,  $\times 195,300$ ; bar = 100 nm.

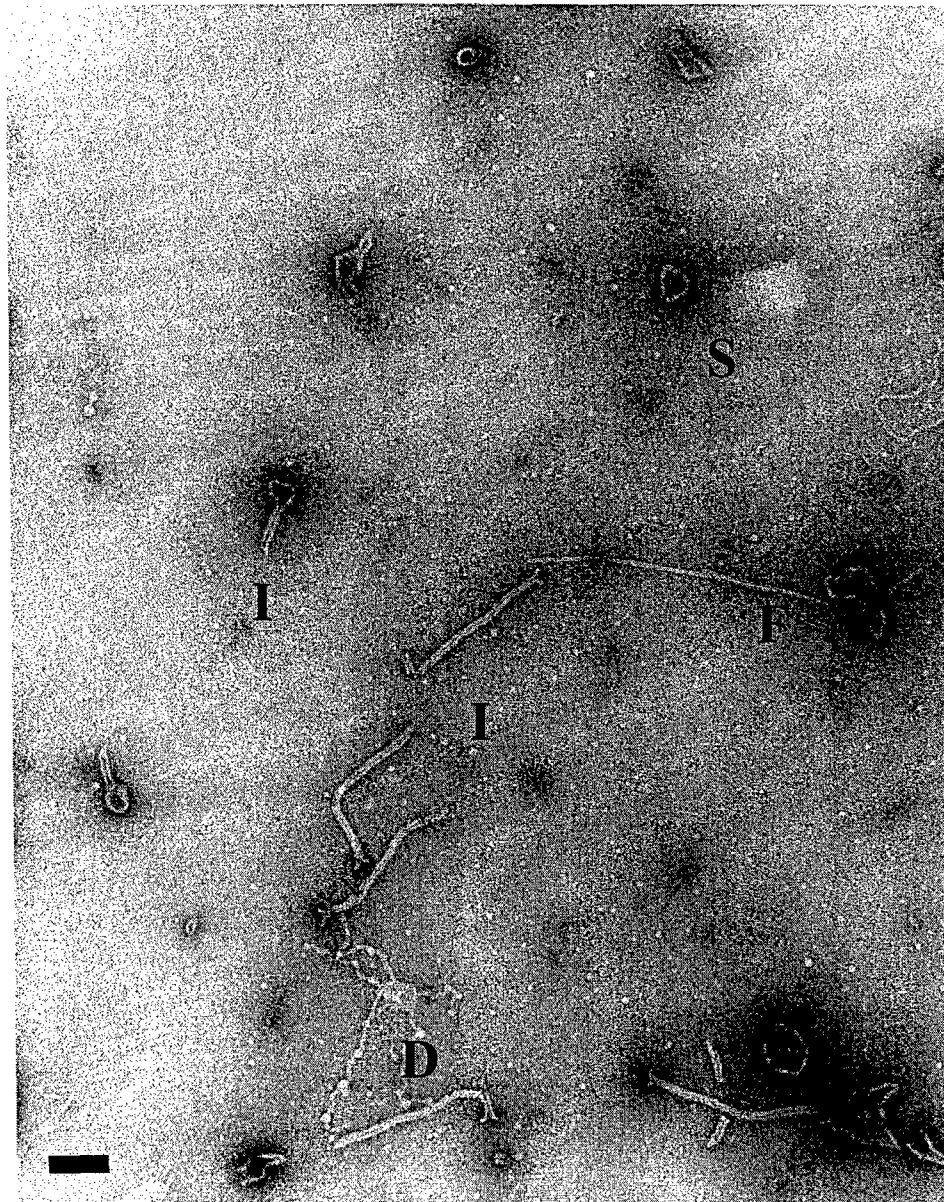


Fig. 5.44. Transmission electron micrograph of chloroform denatured filamentous phage E2. Filamentous phage (F), I-forms (I) and spheroids (S) are evident, as is spheroid DNA extrusion (D) in agreement with the finding of Manning et al., (1981). Magnification,  $\times 123,800$ ; bar = 100 nm.



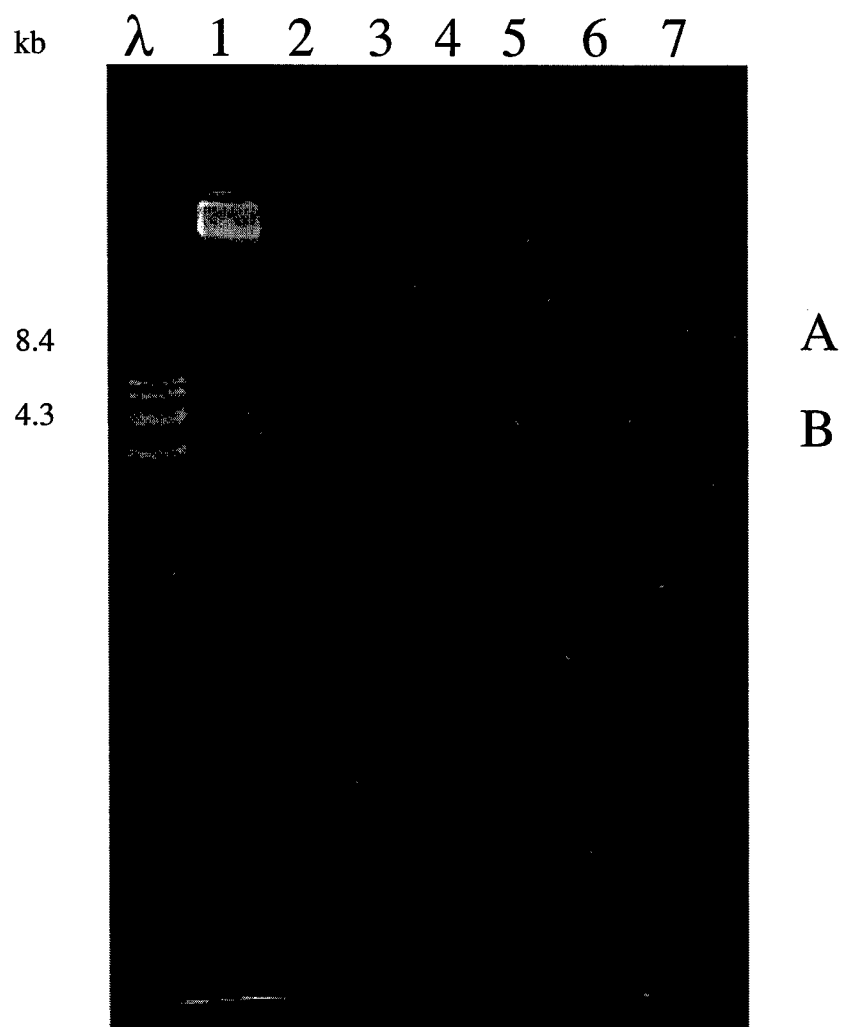


Fig. 5.45. Agarose (0.8%) gel analysis of spheroid conversion as a function of filamentous phage concentration. All vortex times 1 min. Lanes: M, *BstE* II  $\lambda$  DNA ladder; 2, neat phage E2 (not subjected to chloroform); 3: 3 $\times$  dilution of neat phage; 4: 9 $\times$  dilution of neat phage; 5: 27 $\times$  dilution of neat phage; 6: 81 $\times$  dilution of neat phage; 7: 243 $\times$  dilution of neat phage.



Fig. 5.46. Transmission electron micrograph of chloroform denatured filamentous phage E2. Phage bundles, as well as spheroids, are apparent in the interface phase between the solvent (chloroform) and aqueous phase that the phage is diluted in. This photo corresponds to Fig. 5.42, lane 7 - bands "A" and "B." No spheroids were noted in the aqueous phase of this sample (Lane 1, Fig. 5.42). Magnification,  $\times 30,300$ ; bar =  $1\mu\text{m}$ .

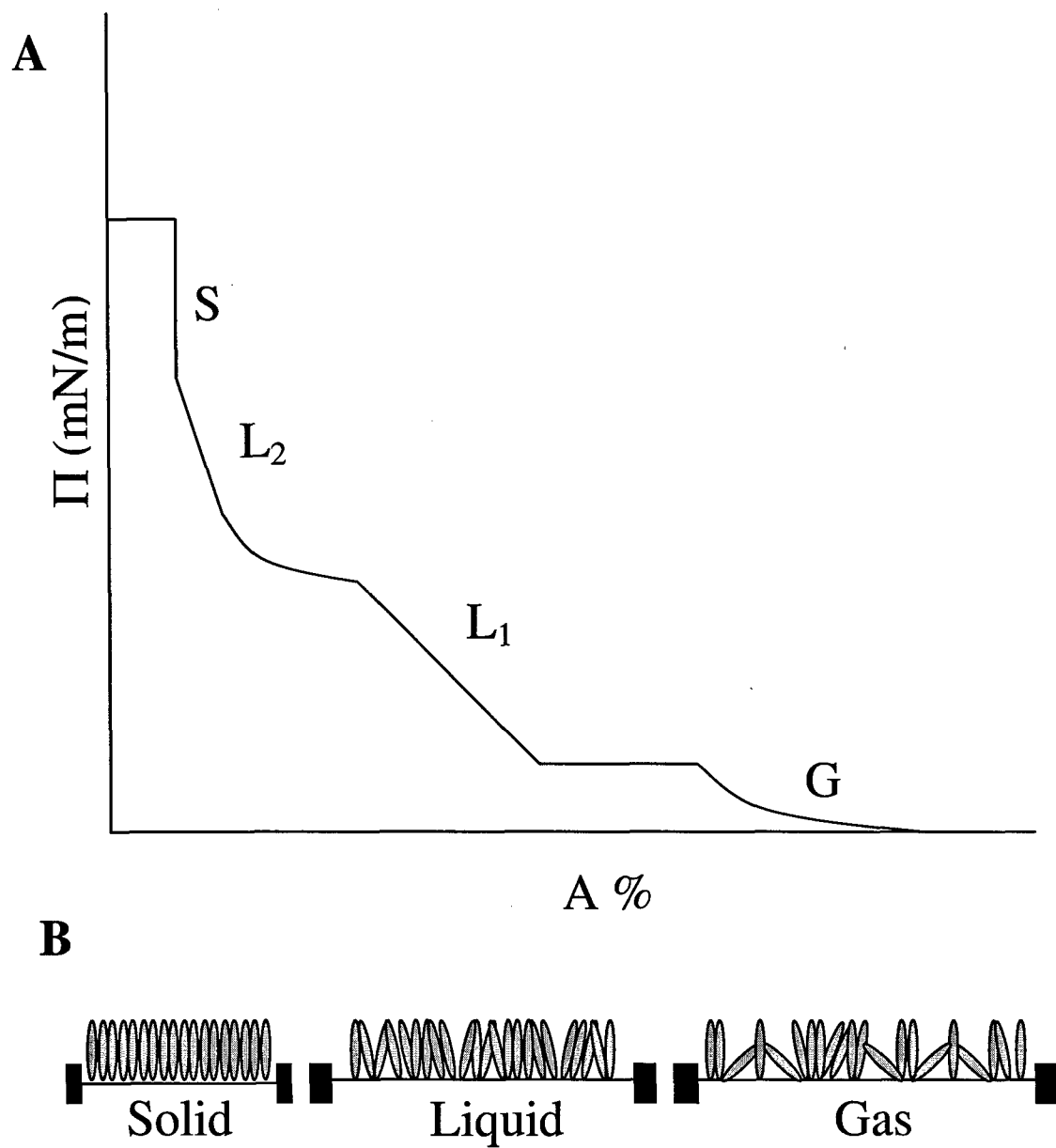


Fig. 5.47. (A) Schematic of  $\Pi$ - $A$  isotherm showing Gaseous (G), Liquid (L), and Solid (S) phases of "skinned phase." Depending upon the amphiphile, one or more liquid states ( $L_1$ ,  $L_2$ ) may exist. (B) Orientation of monolayer in the different phases.

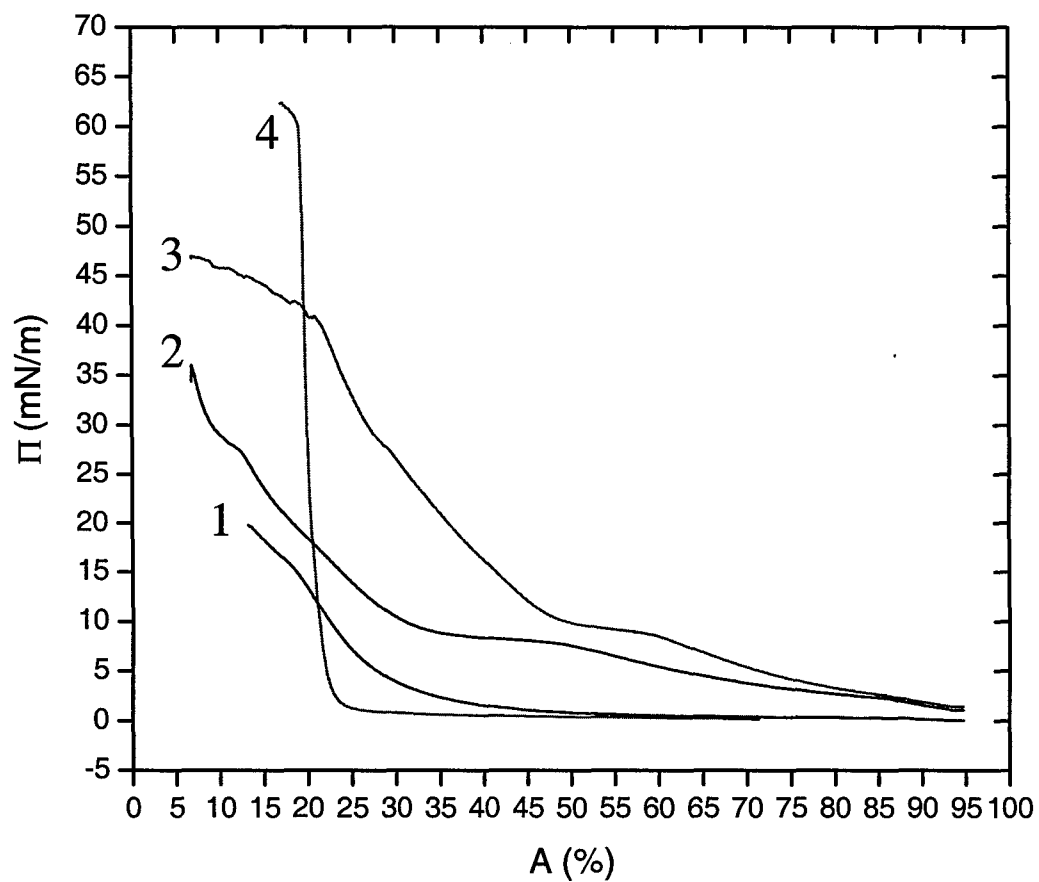


Fig. 5.48.  $\Pi$ -A isotherms of biopolymers as a function of compression at 20 °C. 1: *Salmonella* polyvalent O antibodies. 2: E2 spheroids. 3: E2 spheroids-PC. 4: Arachidic acid, courtesy Mark Hartell (Olsen, 2000).

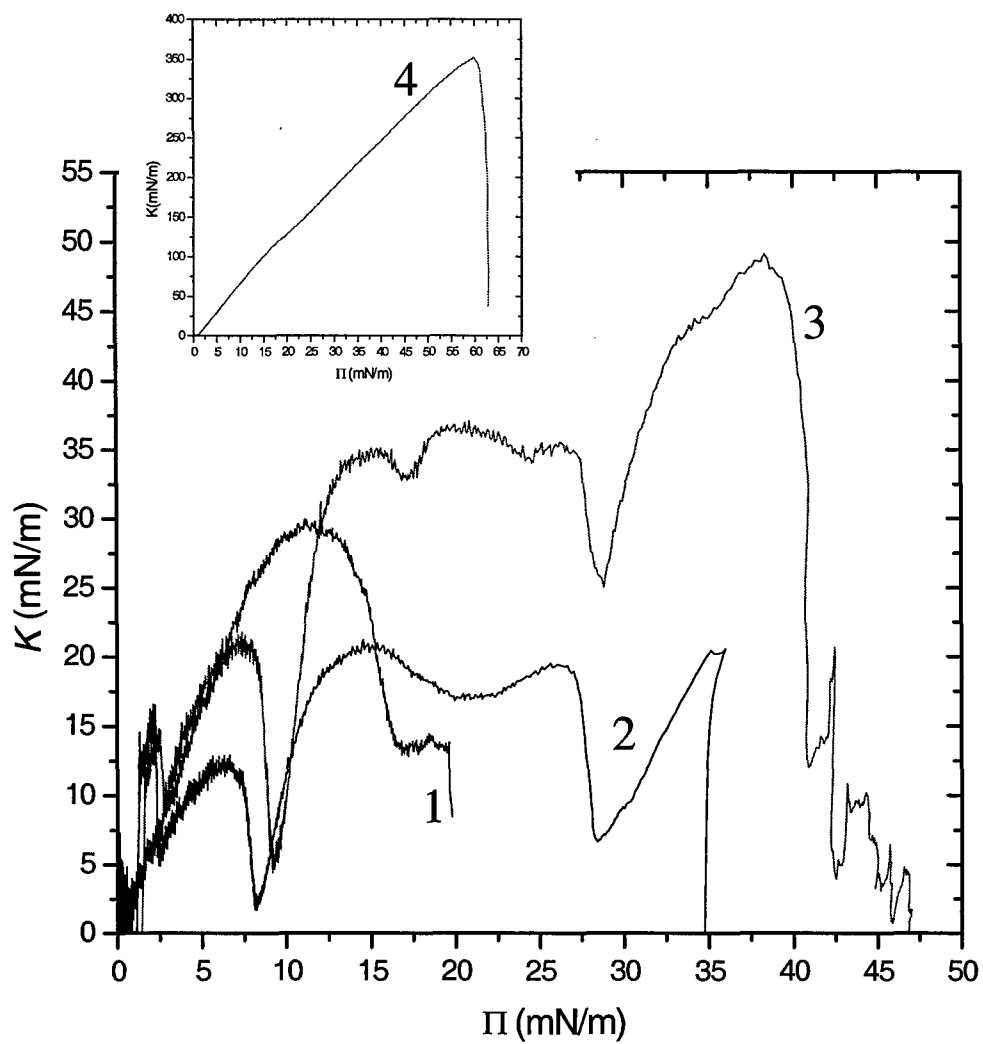


Fig. 5.49. Elasticity of monolayers as a function of surface pressure at 20 °C. 1: *Salmonella* polyvalent O antibodies. 2: E2 spheroids. 3: E2 spheroids-PC. 4: Arachidic acid, courtesy Mark Hartell (Olsen, 2000).

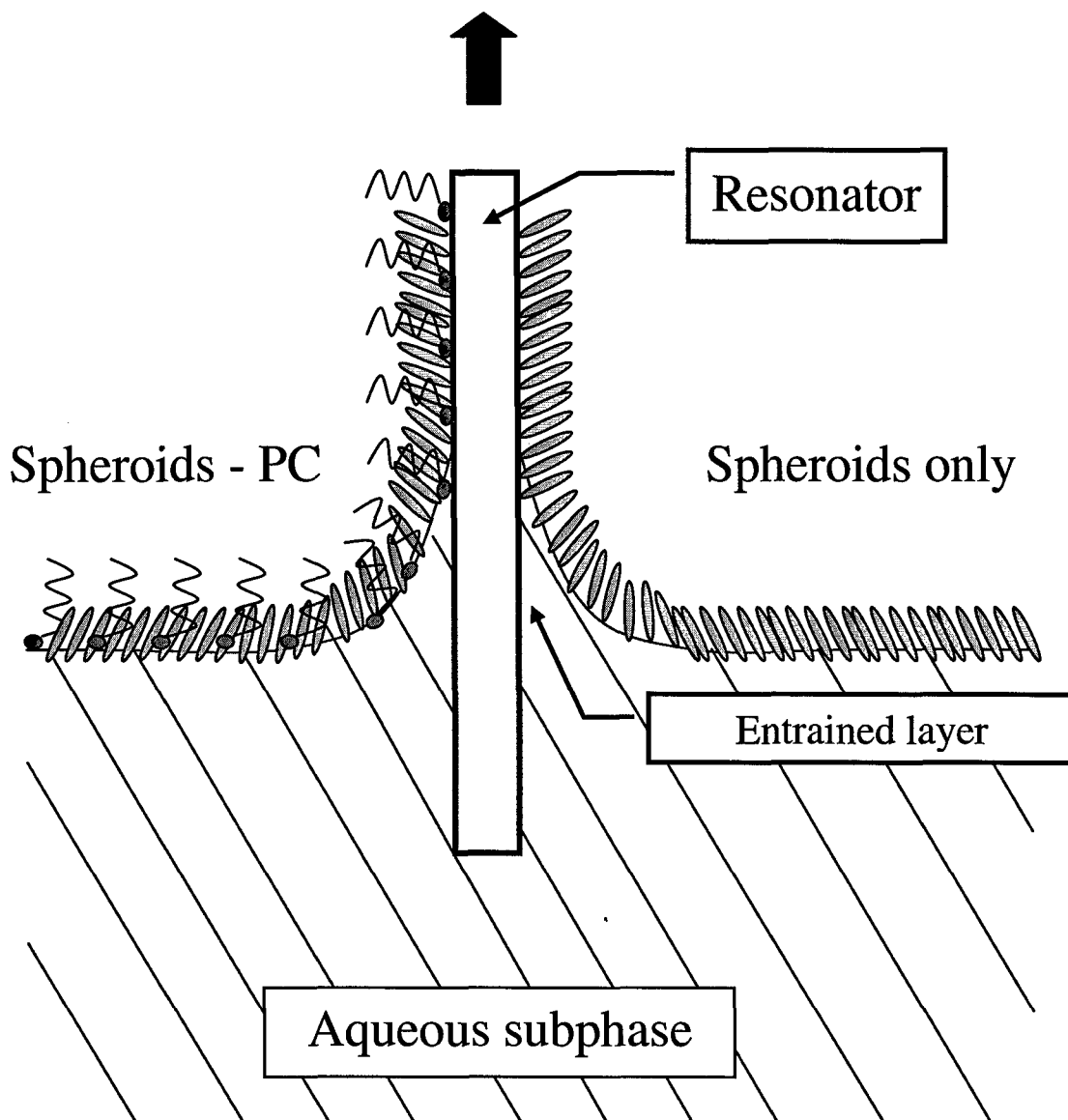


Fig. 5.50. Y-type deposition of a floating monolayer onto a hydrophilic substrate as described by Gaines (1966). Pure monolayers were prepared from either spheroids (right) or spheroids in phosphocholine (left) and are shown on either side of the substrate for illustrative purposes only (*cf.* Figs. 5.1 and 5.13).

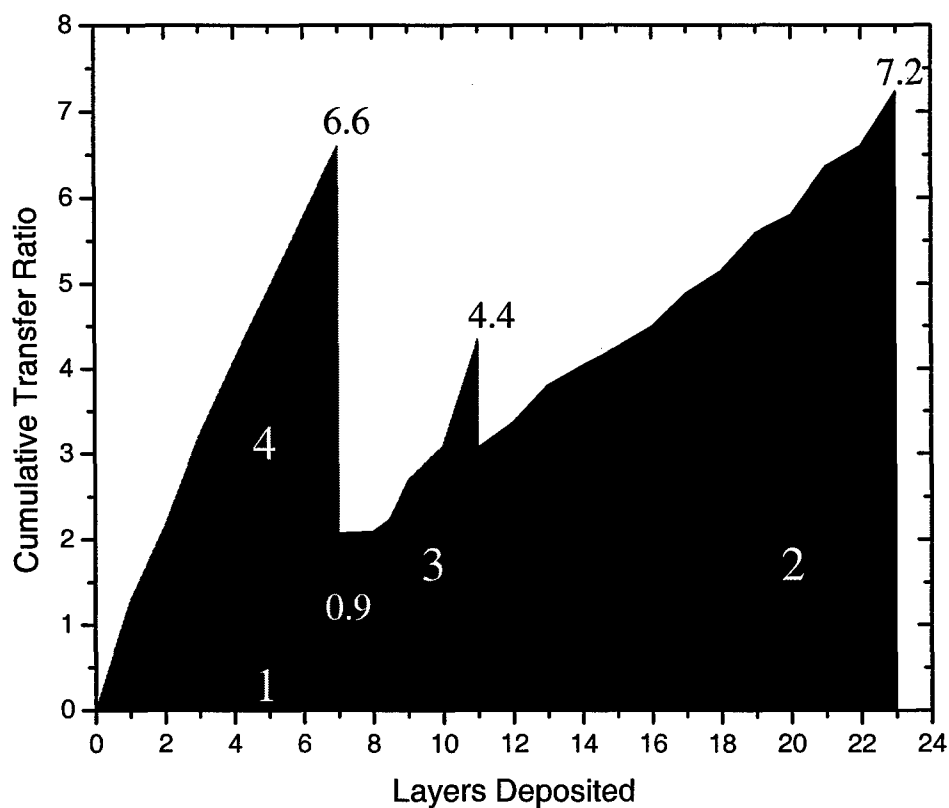


Fig. 5.51. Cumulative deposition of biopolymers onto quartz resonators as a function of transfer ratio at 20 °C. 1: *Salmonella* antibodies (Denka Seiken Co., LTD, Tokyo Japan). 2: Spheroids. 3: Spheroids-PC. 4: Arachidic acid, pH corrected to 10.0. Cumulative TR is shown numerically above curves for each respective material.

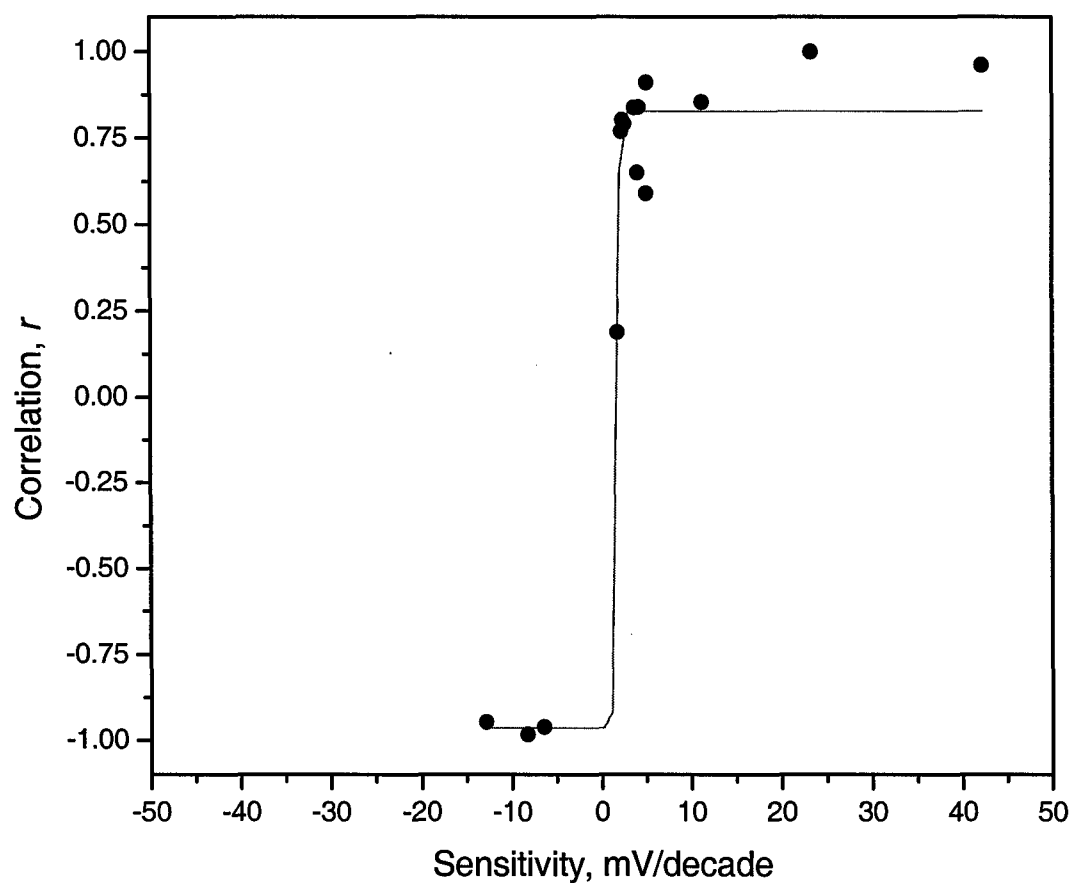


Fig. 5.52. Experimental correlation coefficient as a function of sensitivity for 15 *Salmonella* biosensors prepared with spheroids using LB method. Correlation coefficients,  $R$ , were derived from the linear fit to dose-response signals for each tested sensor; sensitivities,  $S$ , from the slope of the linear fit. Curve is nonlinear sigmoidal fit of Boltzmann equation to experimental data points ( $R^2 = 0.96$ ). Only 3 of 15 sensors (20%) fit the acceptable performance criteria ( $R \geq 0.90$  and  $S \geq 2.5$  mV/decade bacteria concentration).





Fig. 5.53. Transmission electron micrograph of *S. typhimurium* interacting with spheroids in aqueous solution. Cells appear to be "cemented" together by spheroids that are visible between adjoining cells. Flagella are also readily apparent. Magnification,  $\times 41,300$ ; bar =  $1\mu\text{m}$ .



Fig. 5.54. Transmission electron micrograph of *S. typhimurium* interacting with spheroids in aqueous solution. Cells appear to be “cemented” together by spheroids that are visibly apparent between adjoining cells. I-forms are also readily apparent. Magnification,  $\times 93,500$ ; bar = 100 nm.

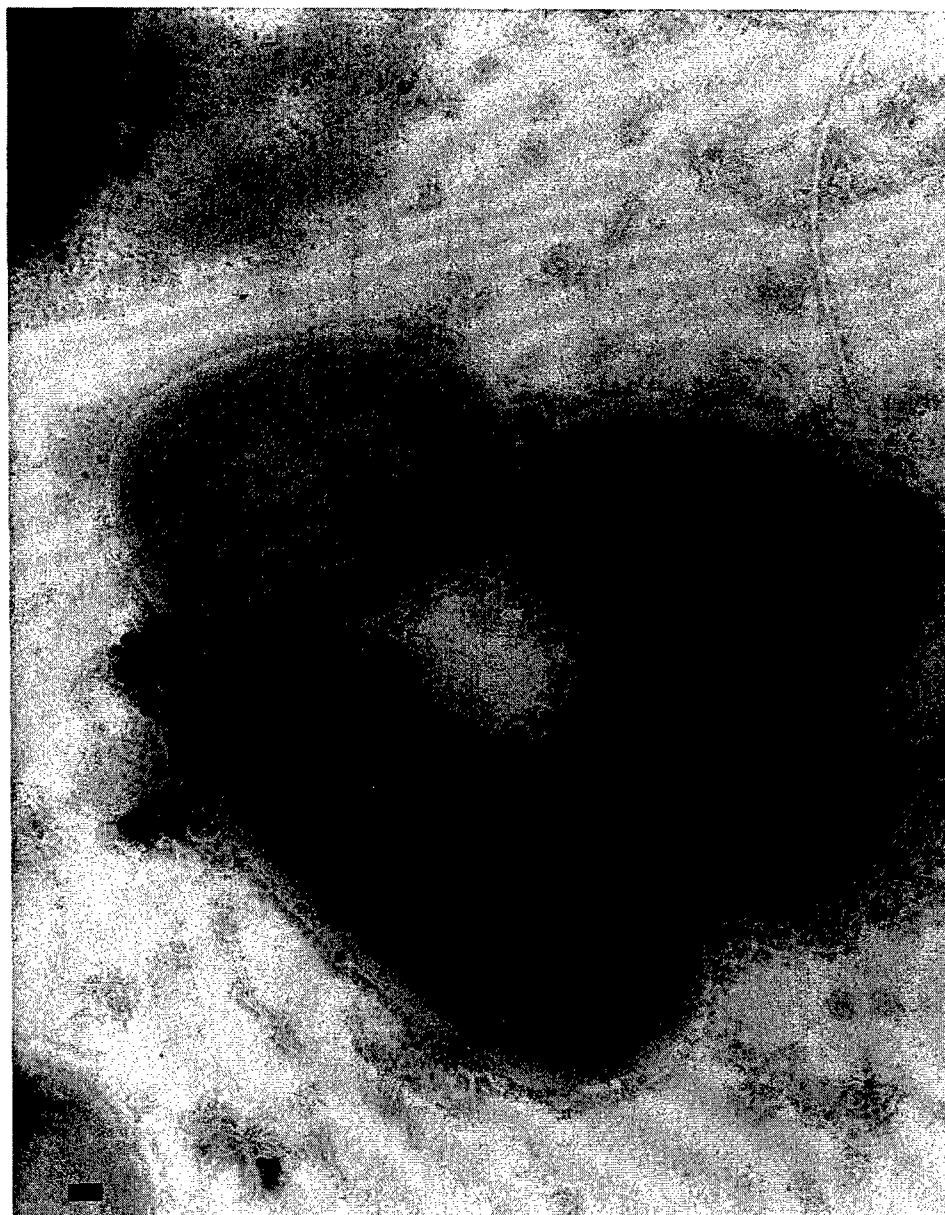


Fig. 5.55. Transmission electron micrograph of *S. typhimurium* interacting with spheroids in aqueous solution. Cells appear to be “cemented” together by spheroids that are visible between adjoining cells. I-forms and flagella are also readily apparent. Magnification,  $\times 68,800$ ; bar =  $1\mu\text{m}$  ( $100\text{ nm} = 4.13\text{ cm}$ ).

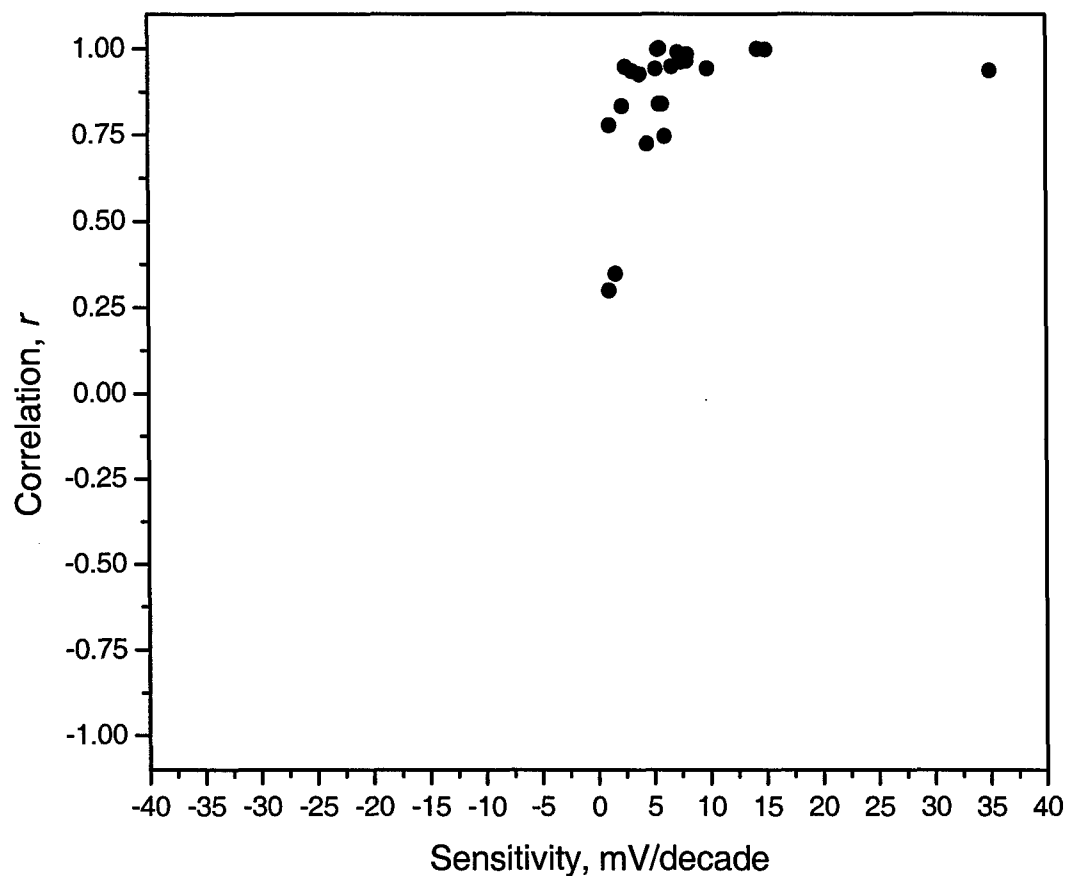


Fig. 5.56. Experimental correlation coefficient as a function of sensitivity for 24 biosensors prepared with spheroids in PC using LB method. Correlation coefficients,  $R$ , were derived from the linear fit to dose-response signals for each tested sensor; sensitivities,  $S$ , were derived from the slope of the linear fit. Overall, 15 of 24 sensors (63%) fit the acceptable performance criteria ( $R \geq 0.90$  and  $S \geq 2.5$  mV/decade bacteria concentration).

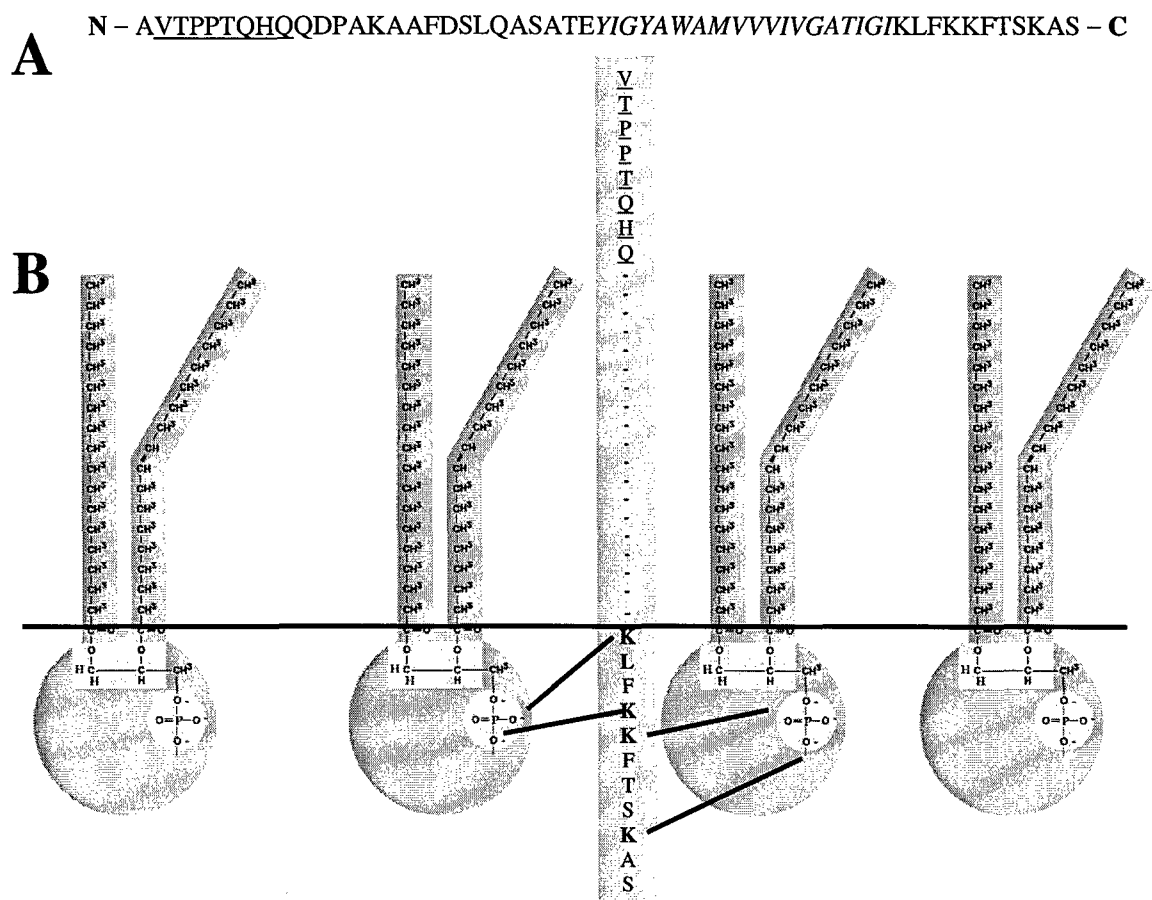


Fig 5.57. (A) Amino acid sequence of the pVIII protein of phage clone E2. The peptide insert displayed at the N-terminus is underlined. The hydrophobic region is italicized. Roughly half of the residues are exposed to the solvent, while the other half is buried within the capsid, where C-terminal residues interact with the phage DNA. (B) Hypothetical orientation and interaction of the rod-shaped pVIII protein with phospholipids as a result of phage skinning method. Following rupture of spheroids at the subphase surface in conjunction with phospholipids, the positively charged, basic amino acids of the C-terminus (bolded) may interact with negatively charged phosphate groups, resulting in a well-organized monolayer structure that facilitates the dynamic properties of the protein as a probe following deposition to substrates.

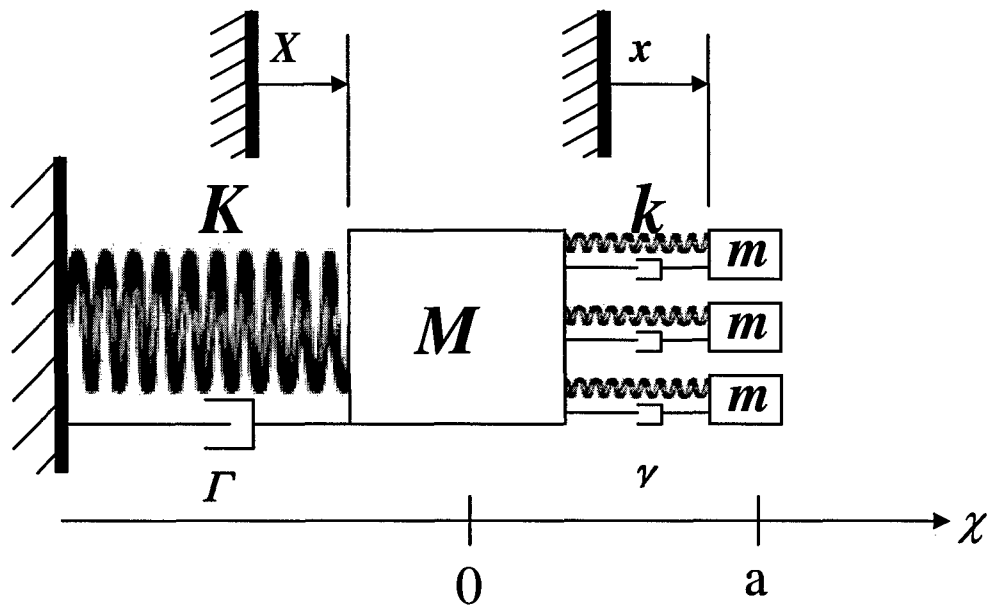


Fig 5.58. Externally driven, liquid-damped ( $\Gamma$ ,  $\gamma$ ), one-dimensional couple harmonic oscillator model with two different masses: bacteria of mass,  $m$ , and spring constant,  $k$ , attached to resonator of mass,  $M$ , and spring constant,  $K$ . Points “0” and “a” represent respective stable equilibrium points of resonator and bacteria along a one-dimensional line  $\chi$ .

## CHAPTER VI

### SUMMARY AND CONCLUSIONS

#### *Summary*

*Salmonella typhimurium* is a leading cause of gastrointestinal foodborne illness and a potential weapon for bioterrorism. The ability to rapidly identify this biological agent and other pathogens, regardless of their contamination origin, is an important consideration of any comprehensive strategic plan to maintain safety and security of the public food supply. Current research initiatives to replace traditional methods of food analysis that are slower, labor-intensive, and cost-inefficient include real-time, deployable threat agent detectors based on biosensors. The results of this research demonstrate the high specificity and selectivity of biosensors for the rapid detection of *S. typhimurium* in aqueous samples, based on piezoelectric transducers that utilize affinity-selected filamentous phage as biorecognition agents.

Biosensors prepared by immobilizing *Salmonella* polyclonal antibodies as a biorecognition layer yielded biosensors capable of detecting small quantities of *S. typhimurium*, with no specificity towards *E. coli* O157:H7. The analytical response was rapid,  $79 \pm 20$  s; the dose response of the antibody-based sensor was linear over 5

decades,  $10^2$  to  $10^7$  cells/ml, of bacterial concentration ( $R > 0.98$ ,  $p < 0.001$ ); sensor sensitivity, measured as a slope of the linear portion of the dose response, was  $18 \pm 5$  mV per decade of *S. typhimurium* concentration based on experiments from 112 sensors; and the detection limit, estimated at  $350 \pm 150$  cells/ml, was well below the reported infectious dosage for *Salmonella*-induced gastroenteritis. However, the antibody layer degraded quickly (36 h) under conditions of environmental aging in fluids from raw packaged poultry, resulting in loose binding between antibody and bacteria and subsequent non-functional performance of the sensors according to mass theory. As such, although antibodies demonstrated high specificity and selectivity in this application, their fragility to degradation processes demonstrates probable unsuitability for extended commercial deployment in enzymatically-rich, bacteria-laden consumables such as poultry. Additionally, antibodies possess numerous other general drawbacks including cost, lack of standardization, non-reusability, and the need for laborious immobilization methods.

Conversely, filamentous phage engineered as antibody substitutes possess distinct advantages in terms of affinity, cost, sensitivity, and resilience. Three multistage landscape phage selection procedures targeting immobilized or suspended *S. typhimurium* resulted in the discovery of five families of bacteria-binding peptides. Specificity of select phage clones for *S. typhimurium* was demonstrated using two variations of ELISA (phage capture and *Salmonella* capture) and confirmed by precipitation assay in reference to wild-type phage f8-5. Specificity of representative phage clone E2 for *S. typhimurium* – up to 22000 times greater than other clones and controls – was confirmed by fluorescence, optical and electron microscopy. The selectivity of E2 to *S. typhimurium*



was comparatively analyzed by precipitation assay and flow cytometry using a select panel of bacteria, primarily Enterobacteriaceae. Results revealed the phage clone to be 10 – 1000 times more selective in binding to the targeted bacterium in comparison to other panel bacteria. Affinity of E2 for *S. typhimurium* is as high as that reported for antibodies, with the  $K_d$  of the complex calculated at  $4.77 \times 10^7$  CFU/ml – corresponding to 1.6 pM phage, or 6.3 nM of the phage-borne peptide. This extraordinarily high affinity is speculated to be an avidity effect contributed by the multivalent interaction of phage, due to its 4,000 binding peptides, with multiply distributed bacterial surface receptors. This surface receptor was characterized by SDS-PAGE, western blot and protein sequencing, which revealed a single 60-70 kD band of protein. Phage recovery data shows that on average one phage particle interacts with one bacterial cell.

Phage clone E2 was immobilized to piezoelectric substrates using three methods (physical adsorption, biotin-streptavidin-phage self-assembly, and Langmuir-Blodgett technique) and two morphological phage forms (filamentous and spheroid) to prepare biosensors for the detection of *S. typhimurium* under aqueous conditions. Quantitative deposition studies indicated that  $\approx 10^{10}$  -  $10^{11}$  filamentous virions/ml incubated for 1 hour at room temperature was sufficient to prepare working biosensors by simple physical adsorption that were characterized by strong, non-reversible binding under aqueous conditions. The quality of phage deposition was confirmed by fluorescent microscopy.

As was seen previously in antibody-based sensors, specific bacterial binding resulted in resonance frequency changes of prepared sensors. All methods of phage immobilization and morphology resulted in the preparation of sensors capable of detecting *S. typhimurium* rapidly (< 3 min for steady state response) in aqueous solutions

ranging from  $10^1$  -  $10^7$  cells/ml. The best operational results were obtained when filamentous phage particles converted to phage coat proteins by chloroform denaturation were immobilized by Langmuir-Blodgett technique. Sixty-three percent of these sensors achieved acceptance criteria outlined ( $R \geq 0.90$ ,  $S \geq 2\text{mV}$ ) and possessed a high average  $R$  (0.90) of sensor groupings with acceptable sensitivity of 8.1 mV. *S. typhimurium*-filamentous phage binding on sensors prepared by physical adsorption was confirmed by scanning electron microscopy. Spheroid binding to *S. typhimurium* was confirmed by TEM. Transitional I-forms produced by chloroform denaturation at room temperature were revealed, countering the observations of previous researchers. Spheroids, prepared as pure protein phage coat monolayers and in combination with phosphocholine, were evaluated by isotherm, elasticity, and transfer ratio analysis for deposition to quartz resonators by LB method. Results showed that phage coat proteins combined with phospholipids produced a monolayer having higher elasticity and capable of higher transfer ratios than monolayers of phage coat proteins alone, resulting in spatially superior deposition to quartz resonators and subsequent firm binding of *S. typhimurium* that followed mass theory for quartz crystal resonators. Evaluation of a novel QCM flow cell configuration in comparison to the conventional standard revealed equivalence in dose responsiveness, and improvement in terms of signal stability, noise reduction, and biohazard reduction. Non-specific bacterial binding and viscosity-induced effects due to increasing cellular constituents of bacterial test suspensions were inconsequential to proper resonator functioning.

Normal mass loading theory was contradicted for the majority of sensors, with exception of sensors prepared with phage coat protein in phospholipids by LB method.

This contradiction has been noted in previous QCM studies by the author and other researchers working with non-uniform masses and is ground on less than firm phage-resonator-bacteria immobilization and/or binding, resulting in an elastic motion out of phase with resonance frequency. A model was formulated to compare this motion to an externally driven, liquid-damped, one-dimensional couple harmonic oscillator with two different masses.

### *Conclusions*

Overall, the results of this research demonstrate proof in concept development of biosensors for the rapid, specific, sensitive detection of *S. typhimurium*, based on recombinant phage probes immobilized to quartz crystal microbalance transducers. These phage-based sensors are comparable to antibody-based sensors in sensitivity, selectivity and speed, and incorporate the numerous advantages of phage. With further refining, this technology could be extended to nanoscale devices being developed by fellow food safety and detection team members, and evaluated through test beds. These envisioned miniature devices include biosensor tags (STags) molded into styrofoam meat-trays or attached to plastic wraps that measure not only bacterial count, but other parameters such as pH, temperature, and biochemical changes through human-in-the-loop, hand-held radio frequency interrogators, from processing to point-of-sale. Continuous monitoring of products from processing to consumption might allow preemptive disposal of tainted products prior to human consumption and could prevent thousands from incurring foodborne illness or death. If contamination has occurred,

traceability is enhanced, possibly leading to further food safety and security enhancements through identification of offenders. This enabling technology might also be applied as a rapid diagnostic method for research, industry, and clinical-based labs, eliminating outdated conventional culturing procedures that are costly and time-consuming. Furthermore, the nature of the methods used to derive phage probes for *Salmonella* hold potential utilization against any bacteria, virus or toxins to which a corresponding phage could be affinity-selected against.

### *Future Work*

The reproducibility of the sensor must be increased, possibly through the exploration of alternative immobilization schemes that complement the physical characteristics of filamentous phage. While the results of spheroids prepared with phospholipids are most promising, their preparation and immobilization require additional steps. The simplest, most straightforward approach using filamentous phage would be optimal. Possibly, the depletion of promising phage clones against gold (Au) surfaces would allow for the selection of phage as probes that are not only specific for *S. typhimurium*, but which also have a high affinity for gold surfaces. Additionally, the incorporation of a rigorous quality control process would allow exacting selection of only functional sensors from prepared batches.

While it is hypothesized that the flexibility of phage, analyte or possibly both at the solid/liquid interface of sensors causes loose binding with subsequent negative apparent mass (inverse linear correlation), it remains unclear which scenario is correct.

More research into the effect that tethered macromolecules have on resonator frequency is needed. The identity of the specific bacterial receptor targeted by the phage would also provide great insight in this regard.

Finally, inferior engineering design necessitated discontinuance of QCM platform 2 during sensor testing when air became trapped as a result of the infusion process.

While unsuitable for this study, future evaluation using a pulseless, low PSI pump may prove this configuration valuable in reducing sensor noise while increasing stability.

## CHAPTER VII

### BIBLIOGRAPHY

Ahluwalia, A., DeRossi, D., Monici, M., Schirone, A., 1991. Thermodynamic study of Langmuir antibody films for application to immunosensors. *Biosens. Bioelectron.* 6, 133–141.

Alberts, B., Bray, D., Lewis, J., Raff, M., Roberts, K., Watson, J.D., 1994. *Molecular Biology of the Cell*. Garland, New York, pp. 773–774.

Alocilja, E., Radke, S.M., 2003. Market analysis of biosensors for food safety. *Biosens. Bioelectron.* 18, 841–846.

Babacan, S., Pivarnik, P., Letcher, S., Rand, A., 2002. Piezoelectric flow injection analysis biosensor for the detection of *Salmonella typhimurium*. *J. Food Sci.* 67, 314–320.

Bailey, C.A., Fiebor, B., Yen, W., Vodyanoy, V., Cernosek, R.W., Chin, B.A., 2002.

Thickness shear mode (TSM) resonators used for biosensing. *Proc. SPIE Int. Soc. Opt. Eng.* 4575, 138–149.

Bandey, H.L., Martin, S.J., Cernosek, R.W., Hillman, A.R., 1999. Modeling the responses of thickness–shear mode resonators under various loading conditions. *Anal. Chem.* 71, 2205–2214.

Barraud, A., Perrot, H., Billard, V., Martelet, C., Therasse, J., 1993. Study of immunoglobulin-G thin-layers obtained by the Langmuir-Blodgett method: application to immunosensors. *Biosens. Bioelectron.* 8, 39–48.

Bennett, A.R., Davids, F.G., Vlahodimou, S., Banks, J.G., Betts, R.P., 1997. The use of bacteriophage-based systems for the separation and concentration of *Salmonella*. *J. Appl. Microbiol.* 83, 259–265.

Benz, R., Bauer, K., 1988. Permeation of hydrophilic molecules through the outer membrane of gram-negative bacteria. Review on bacterial porins. *Eur. J. Biochem.* 176, 1–19.

Berg, S., Johannsmann, D., Ruths, M., 2002. Frequency response of quartz crystal shear-resonator during an adhesive, elastic contact in a surface forces apparatus. *J. Appl. Phys.* 92, 6905–6910. Erratum in: *J. Appl. Phys.* 93, 3682.

Bishop-Hurley, S.L., Mounter, S.A., Laskey, J., Morris, R.O., Elder, J., Roop, P., Rouse, C., Schmidt, F.J., English, J.T., 2002. Phage-displayed peptides as developmental agonists for *Phytophthora capsici* zoospores. Appl. Environ. Microbiol. 68, 3315–3320.

Bonnycastle, L.L.C., Menendez, A. Scott, J.K., 2001. Filamentous phage biology. In: Barbas, C.F. III, Barton, D.R., Scott, J.K., Silverman, G.J (Eds.), Phage Display, A Laboratory Manual. Cold Spring Harbor Laboratory Press, Cold Spring Harbor, New York, pp. 1.1–1.37.

Borovsky, B., Krim, J., Syed Asif, S.A., Wahl, K.J., 2001. Measuring nanomechanical properties of a dynamic contact using an indenter probe and quartz crystal microbalance. J. Appl. Phys. 90, 6391–6396.

Boykin, M. “Re: Maxtek utilization in biological experiment.” e-mail communication. Maxtek technical service. 11 Aug 2003.

Brandenburg, K., Andra, J., Mueller, M., Koch, M.H., Garidel, P., 2003. Physicochemical properties of bacterial glycopolymers in relation to bioactivity. Carbohydr. Res. 338, 2477–2489.



Branigin, W., Allen, M., Mintz, J. "Tommy Thompson resigns from HHS." Bush administration. 3 Dec. 2004. The Washington Post. 5 Jan. 2005  
<[www.washingtonpost.com/wp-dyn/articles/A31377-2004Dec3.html](http://www.washingtonpost.com/wp-dyn/articles/A31377-2004Dec3.html)>.

Brigati, J., Williams, D.D., Sorokulova, I.B., Nanduri, V., Chen, I.H., Turnbough, C.L., Petrenko, V.A., 2004. Diagnostic probes for *Bacillus anthracis* spores selected from a landscape phage library. Clin. Chem. 50, 1899–1906.

Brigati, J.R., Petrenko, V.A., 2005. Thermostability of landscape phage probes. Anal. Bioanal. Chem. Submitted for publication.

Brooks J.L., Mirhabibollahi, B., Kroll, R.G., 1992. Experimental enzyme-linked amperometric immunosensors for the detection of Salmonellas in foods. J. Appl. Bacteriol. 73, 189–196.

Brown, C.W., Li, Y., Seelenbinder, J.A., Pivarnik, P., Rand, A.G., Letcher, S.V., Gregory, O.J., Platek, M.J., 1998. Immunoassays based on surface enhanced infrared absorption spectroscopy. Anal. Chem. 70, 2991–2996.

Bryan, F.L., 1982. Diseases transmitted by foods: a classification and summary. DHS publication no. 83-8237. U.S. Department of Health and Human Services, Centers for Disease Control, Center for Professional Development and Training, Atlanta, GA, pp. 1–101.

Brynda, E., Houska, M., Skvor, J., Ramsden, J.J., 1998. Immobilisation of multilayer bioreceptor assemblies on solid substrates. *Biosens. Bioelectron.* 13, 165–172.

Bunde, R.L., Jarvi, E.J., Jeffrey J., Rosentreter, J.J., 1998. Piezoelectric quartz crystal biosensors. *Talanta* 46, 1223–1236.

Buzby, J. C., Roberts. T., 1997. Economic costs and trade impacts of microbial food-borne illness. *World Health Stat. Q.* 50, 57–66.

Carinato, M.E., Collin-Osdoby, P., Yang, X., Knox, T.M., Conlin, C.A., Miller, C.G., 1998. The *apeE* gene of *Salmonella typhimurium* encodes an outer membrane esterase not present in *Escherichia coli*. *J. Bacteriol.* 180, 3517–3521.

Cavicacute, B.A., Hayward, G.L., Thompson, M., 1999. Acoustic waves and the study of biochemical macromolecules and cells at the sensor-liquid interface. *Analyst* 124, 1405–1420.

Clark, L.C., Jr., Lyons, C., 1962. Electrode systems for continuous monitoring in cardiovascular surgery. *Ann. N. Y. Acad. Sci.* 102, 29–45.

Connors, K.A, 1987. Binding Constants. The Measurement of Molecular Complex Stability. John Wiley and Sons Inc., New York, pp. 21–22.

Court rejects bacterial testing on processed meat – Supreme Beef Processors, Inc., v. United States Dept. of Agriculture, 275 F.3d 432 (5<sup>th</sup> Cir. 2001). Medical and Public Health Law Site – Food Law. 6 Dec. 2001. Louisiana State U. Law Center. 5 Jan. 2005 <biotech.law.lsu.edu/cases/food/supreme\_beef\_processors\_v\_DOA\_CA.htm>.

Cudic, M., Condie, B.A., Weiner, D.J., Lysenko, E.S., Xiang, Z.Q., Insug, O., Bulet, P., Otvos, L., Jr., 2002. Development of novel antibacterial peptides that kill resistant isolates. *Peptides* 23, 2071–2083.

Dahint, R., Bender, F., Morhard, F., 1999. Operation of acoustic plate mode immunosensors in complex biological media. *Anal. Chem.* 71, 3150–3156.

Davies, J. T., Rideal, E.K., 1963. *Interfacial Phenomena*, Academic Press, New York, pp. 1–480.

Developments in Hudson Foods *E. Coli* Outbreak, release no. 0284.97. 20 Aug. 1997. United States Department of Agriculture, Washington, DC. 7 Jan. 2005 <www.usda.gov/news/releases/1997/08/0284>.

Dill, K., Stanker, L.H., Young, C.R., 1999. Detection of *Salmonella* in poultry using a silicon chip-based biosensor. *J. Biochem. Bioph. Meth.* 41, 61–67.

Dickert, F.L., Hayden, O., Bindeus, R., Mann, K.J., Blaas, D., Waigmann, E., 2004.

Bioimprinted QCM sensors for virus detection–screening of plant sap. *Anal. Bioanal. Chem.* 378, 1929–1934.

Dickert, F., Hayden, O., Lieberzeit, P., Palfinger, C., Pickert, D., Wolff, U., Scholl, G., 2003a. Borderline applications of QCM-devices: synthetic antibodies for analytes in both nm- and  $\mu\text{m}$ -dimensions. *Sens. Actuat. B–Chem.* 95, 20–24.

Dickert, F., Lieberzeit, P., Hayden, O., 2003b. Sensor strategies for microorganism detection – from physical principles to imprinting procedures. *Anal. Bioanal. Chem.* 377, 540–549.

Donnelly, J.P., 1962. The secrets of Gram's stain. *Infect. Dis. Alert.* 15, 109–112.

D'Souza, S.F., 2001. Microbial biosensors. *Biosens. Bioelectron.* 16, 337–353.

Dultsev, F.N., Ostanin, V.P., Klenerman, D., 2000. “Hearing” bond breakage. Measurement of bond rupture forces using a quartz crystal microbalance. *Langmuir* 16, 5036–5040.

Dultsev, F.N., Speight, R.E., Fiorini, M.T., Blackburn, J.M., Abell, C., Ostanin, V.P., Klenerman, D., 2001. Direct and quantitative detection of bacteriophage by “hearing” surface detachment using a quartz crystal microbalance. *Anal. Chem.* 73, 3935–3939.

Dusch, H., Altwegg, M., 1995. Evaluation of 5 new plating media for isolation of *Salmonella* species. J. Clin. Microbiol. 33, 802–804.

Dybwad, G.L., 1985. A sensitive new method for the determination of adhesive bonding between a particle and a substrate. J. Appl. Phys. 58, 2789–2790

Dziadkowiec, D., Mansfield, L.P., Forsythe, S.J., 1995. The detection of *Salmonella* in skimmed milk powder enrichments using conventional methods and immunomagnetic separation. Lett. Appl. Microbiol. 20, 361–364.

Eppendorf technical service. Personal communication. 12 March 2004.

Fawcett, N.C., Craven, R.D., Zhang, P., Evans, J.A., 1998. QCM response to solvated, tethered molecules. Anal. Chem. 70, 2876–2880.

Fawcett, N.C., Craven, R.D., Zhang, P., Evans, J.A., 2004. Evidence for gravity's influence on molecules at a solid–solution interface. Langmuir 20, 6651–6657.

Foodborne diseases – possibly 350 times more frequent than reported. 1997 Press Releases. 13 Aug. 1997. World Health Organization. 7 Jan. 2005  
<[www.who.int/archives/inf-pr-1997/en/pr97-58.html](http://www.who.int/archives/inf-pr-1997/en/pr97-58.html)>.

Fries, R., Graw, C., 1999. Water and air in two poultry processing plant's chilling facilities—a bacteriological survey. *Br. Poult. Sci.* 1, 52–58.

FSIS sample collection guidelines and procedures for isolation and identification of *Salmonella* from raw meat and poultry products: testing, 1996. Federal Register Appendix E. 61, 38917–38925.

Fung, Y.S., Si, S.H., Zhu, D.R., 2000. Piezoelectric crystal for sensing bacteria by immobilizing antibodies on divinylsulphone activated poly-*m*-aminophenol film. *Talanta* 51, 151–158.

Fung, Y.S., Wong, Y.Y., 2001. Self-assembled monolayers as a coating in a quartz piezoelectric crystal immunosensor to detect *Salmonella* in aqueous solution. *Anal. Chem.* 73, 5302–5309.

Gaines, G. L., 1966. Transfer of monolayers to solids, multilayers. In: Prigogine, I. (Ed.), *Insoluble monolayers at liquid-gas interfaces*. Interscience Publishers, NY, pp. 327–346.

Gawande, P.V., Bhagwat, A.A., 2002. Inoculation onto solid surfaces protects *Salmonella* spp. during acid challenge: a model study using polyethersulfone membranes. *Appl. Environ. Microbiol.* 68, 86–92.

Ghafouri, S., Thompson, M., 1999. Interfacial properties of biotin conjugate–avidin

complexes studied by acoustic wave sensor. *Langmuir* 15, 564–572.

Goldman, E.R., Pazirandeh, M.P., Mauro, J.M., King, K.D., Frey, J.C., Anderson, G.P., 2000. Phage-displayed peptides as biosensor reagents. *J. Mol. Recognit.* 13, 382–387.

Green, N.M., 1990. Avidin and streptavidin. In: Wilchek, M., Bayer, E.A. (Eds.), *Methods in Enzymology*. Academic Press, San Diego, CA, pp. 55.

HACCP Guidelines, 1997. Food and Drug Administration 1997 Food Code. 7 Sep. 1999. United States Department of Health and Human Services, Public Health Service, 5 Jan. 2005 <[www.cfsan.fda.gov/~dms/fcannex5.html](http://www.cfsan.fda.gov/~dms/fcannex5.html)>.

Hamburger recall rises to 25 million pounds. U.S. News Story Page. 21 Aug. 1997. CNN News. 8 Jan. 2005 <[cnn.com/US/9708/21/beef.update/index.html](http://cnn.com/US/9708/21/beef.update/index.html)>.

Hamer, D.H., Gill., C.J., 2002. From the farm to the kitchen table: the negative impact of antimicrobial use in animals on humans. *Nutr. Rev.* 60, 261–264.

Hartman, N.F., Wyvill, J.C., Campbell, D.P., Edmonds, P., 1995. Rapid response biosensor for detection and identification of common foodborne pathogens. *Proc. SPIE Int. Soc. Opt. Eng.* 2345, 128–137.

- Hayden, O., Bindeus, R., Dickert, F.L., 2003. Combining atomic force microscope and quartz crystal microbalance studies for cell detection. *Meas. Sci. Tech.* 14, 1876–1881.
- He, X.Q., Pan, R.N., 1992. Bacteriophage lytic patterns for identification of salmonellae, shigellae, *Escherichia-coli*, *Citrobacter-freundii*, and *Enterobacter-cloacae*. *J. Clin. Microbiol.* 30, 590–594.
- Hengerer, A., Decker, J., Prohaska, E., Hauck, S., Kößlinger, C., Wolf, H., 1999a. Quartz crystal microbalance (QCM) as a device for the screening of phage libraries. *Biosens. Bioelectron.* 14, 139–144.
- Hengerer, A., Kößlinger, C., Decker, J., Hauck, S., Queitsch, I., Wolf, H., Dübel, S., 1999b. Determination of phage antibody affinities to antigen by a microbalance sensor system. *Biotechniques* 26, 956–960, 962, 964.
- Hermanson, G.T., Mallia, A.K., Smith, P.K., 1992. Immobilized affinity ligand techniques. Academic Press Inc., San Diego, CA, pp. 200–203.
- Hirsh, D.C., Martin, L.D., 1983a. Detection of *Salmonella* spp in milk by using Felix-O1 bacteriophage high-pressure liquid-chromatography. *Appl. Environ. Microbiol.* 46, 1243–1245.



Hirsh, D.C., Martin, L.D., 1983b. Rapid detection of *Salmonella* spp by using Felix-O1 bacteriophage and high-performance liquid-chromatography. Appl. Environ. Microbiol. 45, 260–264.

Hoppert, M., Holzenburg, A., 1998. Methods for scanning electron microscopy. In: Electron Microscopy in Microbiology. BIOS Scientific Publishers Ltd., Oxford, pp. 79–82.

Hseih, P. Written Communication. February 2000.

Ito, H., Morton, T.H., Vodyanoy, V., 1989. Small odorant molecules affect steady state properties of monolayers. Thin Solid Films 180, 1–13.

Ivanenkov, V., Felici, F., Menon, A.G., 1999a. Targeted delivery of multivalent phage display vectors into mammalian cells. Biochim. Biophys. Acta 1448, 463–472. Erratum in: Biochim. Biophys. Acta 1451, 364.

Ivanenkov, V., Felici, F., Menon, A.G., 1999b. Uptake and intracellular fate of phage display vectors in mammalian cells. Biochim. Biophys. Acta 1448, 450–462. Erratum in: Biochim. Biophys. Acta 1451, 364.

Ivnitski, D., Abdel-Hamid, I., Atanasov, P., Wilkins, E., 1999. Biosensors for detection of pathogenic bacteria. Biosens. Bioelectron. 14, 599–624.

Janshoff, A., Galla, H.J, Steinem, C., 2000. Piezoelectric mass-sensing devices as biosensors—an alternative to optical biosensors? *Angew. Chem. Int. Ed. Engl.* 39, 4004–4032.

Kanazawa, K.K., Gordon, J.G., 1985. Frequency of a quartz crystal microbalance in contact with liquid. *Anal. Chem.* 57, 1770–1771.

Kaspar, M., Stadler, H., Weiss, T., Ziegler, C., 2000. Thickness shear mode resonators (“mass sensitive devices”) in bioanalysis. *Fresenius’ J. Anal. Chem.* 366, 602–610.

Khan, A.S., Swerdlow, D.L., Juranek, D.D., 2001. Precautions against biological and chemical terrorism directed at food and water supplies. *Public Health Rep.* 116, 3–14.

King, W. H., 1964. Piezoelectric sorption detector. *Anal. Chem.* 36, 1735–1739.

Knirel, Y.A., Kocharova, N.A., Bystrova, O.V., Katzenellenbogen, E., Gamian, A., 2002. Structures and serology of the O-specific polysaccharides of bacteria of the genus *Citrobacter*. *Arch. Immunol. Ther. Exp. (Warsz)* 50, 379–391.

Knurr, J., Benedek, O., Heslop, J., Vinson, R.B., Boydston, J.A., McAndrew, J., Kearney, J.F., Turnbough, C.L., Jr., 2003. Peptide ligands that bind selectively to spores of *Bacillus subtilis* and closely related species. *Appl. Environ. Microbiol.* 69, 6841–6847.

König, B., Grätzel, M., 1994. A novel immunosensor for herpes viruses. *Anal. Chem.* 66, 341–344.

König, B., Grätzel, M., 1995. A piezoelectric immunosensor for hepatitis viruses. *Anal. Chim. Acta.* 309, 19–25.

Kothary, M.H., Babu, U.S., 2001. Infective dose of foodborne pathogens in volunteers: A review. *J. Food Safety* 21, 1–73.

Kouzmitcheva, G. Written communication. 17 Feb. 2005.

Krause, R., 1993. Process control for Ni/Au plating with QCM technology. *Circuitree* 6, 10–12.

Kuhn, J., Suissa, M., Wyse, J., Cohen, I., Weiser, I., Reznick, S., Lubinsky-Mink, S., Stewart, G., Ulitzur, S., 2002. Detection of bacteria using foreign DNA: the development of a bacteriophage reagent for *Salmonella*. *Int. J. Food Microbiol.* 74, 229–238.

Lee, D.R., Schnaitman, C.A., 1980. Comparison of outer membrane porin proteins produced by *Escherichia coli* and *Salmonella typhimurium*. *J. Bacteriol.* 142, 1019–1022.

Lee, R.V., Harbison, R.D., Draughon, F.A., 2003. Food as a Weapon. Food Prot. Trends 23, 664–674.

Legendre, D., Fastrez, J., 2002. Construction and exploitation in model experiments of functional selection of a landscape library expressed from a phagemid. Gene 290, 203–215.

Louie, A.S., Marenchic, I.G., Whelen, R.H., 1998. A fieldable modular biosensor for use in detection of foodborne pathogens. Field Anal. Chem. Tech. 2, 371–377.

Luong, J., Guilbault, G.G., 1994. Food biosensor analysis. In: Guilbault, G., and Wagner G. (Eds.), Food Science and Technology. Marcel Dekker, Inc., New York, pp. 151–233.

Luong, J.H., Prusak-Sochaczewski, E., Guilbault, G.G., 1990. Development of a piezoimmunosensor for the detection of *Salmonella typhimurium*. Ann. N. Y. Acad. Sci. 613, 439–43.

Madonna, A.J., Basile, F., Furlong, E., Voorhees, K.J., 2001. Detection of bacteria from biological mixtures using immunomagnetic separation combined with matrix-assisted laser desorption/ionization time-of-flight mass spectrometry. Rapid Commun. Mass Spectrom. 15, 1068–1074.

Manning, M., Chrysogelos, S., Griffith, J., 1981. Mechanism of coliphage M13 contraction: intermediate structures trapped at low temperatures. J. Virol. 40, 912–919.

Mansfield, L.P., Forsythe, S.J., 2000. The detection of *Salmonella* using a combined immunomagnetic separation and ELISA end-detection procedure. Lett. Appl. Microbiol. 31, 279–283.

Marriot, N.G., 1995a. Principles of Food Sanitation. Chapman & Hall, New York, pp. 11–50.

Marriot, N.G., 1995b. Principles of Food Sanitation. Chapman & Hall, New York, pp. 258–281.

Martin, S.J., Bandey, H.L., Cernosek, R.W., Hillman, A.R., Brown, M.J., 2000. Equivalent-circuit model for the thickness-shear mode resonator with a viscoelastic film near film resonance. Anal. Chem. 72, 141–149.

Martin, S.J., Granstaff, V.E., Frye, G.C., 1991. Characterization of quartz crystal microbalance with simultaneous mass and liquid loading. Anal. Chem. 63, 2272–2281.

Marxer, C.G., Coen, M.C., Greber, T., Greber, U.F., Schlapbach, L., 2003. Cell spreading on quartz crystal microbalance elicits positive frequency shifts indicative of viscosity changes. Anal. Bioanal. Chem. 377, 578–586.

Mead, P. S., Slutsker, L., Dietz, V., McCaig, L.F., Bresee, J.S., Shapiro, C., Griffin, P.M., Tauxe, R.V., 1999. Food-related illness and death in the United States. *Emerg. Infect. Dis.* 5, 607–625.

Meckes, M.C., MacDonald, J.A., 2003. Evaluation of a DNA probe test kit for detection of *Salmonellae* in biosolids. *J. Appl. Microbiol.* 94, 382–387.

Minunni, M., Mascini, M., Carter, R.M., Jacobs, M.B., Lubrano, G.J., Guilbault, G.G., 1996. A quartz crystal microbalance displacement assay for *Listeria monocytogenes*. *Anal. Chim. Acta.* 325, 169–174.

Miyamoto, T., Tian, H.Z., Okabe, T., Trevanich, S., Asoh, K., Tomoda, S., Honjoh, K., Hatano, S., 1998. Application of random amplified polymorphic DNA analysis for detection of *Salmonella* spp. in foods. *J. Food Protect.* 61, 785–791.

Mobley, J.A., 1995. Biological warfare in the twentieth century: lessons from the past, challenges for the future. *Mil. Med.* 160, 547–553.

Mosier-Boss, P.A., Lieberman, S.H., Andrews, J.M., Rohwer, F.L., Wegley, L.E., Breitbart, M., 2003. Use of fluorescently labeled phage in the detection and identification of bacterial species. *Appl. Spectrosc.* 57, 1138–1144.

Nastasi, A., Mammina, C., Mioni, R., 1999. Detection of *Salmonella* spp. in food by a rapid PCR-hybridization procedure. *New Microbiol.* 22, 195–202.

Naylor, J. M., 2002. Rapid and sensitive quartz crystal microbalance biosensor for the detection of *Legionella pneumophila*. MS Thesis, Auburn University, AL.

Neidhardt, F.C., 1987. Chemical composition of *E. coli*. In: Neidhardt, F.C. (Ed.), *Escherichia coli* and *Salmonella*. American Soc. For Microbiology, Washington, DC, pp. 3–6.

Nestle, M., 2003. Safe Food: Bacteria, Biotechnology, and Bioterrorism. University of California Press, Berkeley and Los Angeles, CA, pp. 211.

Nowotarska, M., Mulczyk, M., 1977. Serologic relationship of fimbriae among Enterobacteriaceae. *Arch. Immunol. Ther. Exp. (Warsz)* 25, 7–16.

O'Connell, P.J., Guilbault, G.G., 2001. Future trends in biosensor research. *Anal. Lett.* 34, 1063–1078.

Olsen, E.V., 2000. Functional durability of a quartz crystal microbalance sensor for the rapid detection of *Salmonella* in liquids from poultry packaging. MS Thesis, Auburn University, AL. <graduate.auburn.edu/auetd>.

- Olsen, E.V., Pathirana, S.T., Samoylov, A.M., Barbaree, J.M., Chin, B.A., Neely, W.C., Vodyanoy, V., 2003. Specific and selective biosensor for *Salmonella* and its detection in the environment. *J. Microbiol. Methods* 53, 273–285.
- Olsthoorn, M.M., Petersen, B.O., Duus, J., Haverkamp, J., Thomas-Oates, J.E., Bock, K., Holst, O., 2000. The structure of the linkage between the O-specific polysaccharide and the core region of the lipopolysaccharide from *Salmonella enterica* serovar Typhimurium revisited. *Eur. J. Biochem.* 267, 2014–2027.
- Osborn, M.J., Wu, H.C., 1980. Proteins of the outer membrane of gram-negative bacteria. *Annu. Rev. Microbiol.* 34, 369–422.
- O’Sullivan, C.K., Guilbault, G.G., 1999. Commercial quartz crystal microbalances—theory and applications. *Biosens. Bioelectron.* 14, 663–670.
- Overman, S.A., Kristensen, D.M., Bondre, P., Hewitt, B., Thomas, G.J., Jr., 2004. Effects of virion and salt concentrations on the raman signatures of filamentous phages fd, Pf1, Pf3, and PH75. *Biochemistry* 43, 13129–13136.
- Park, I.S., Kim, N., 1998. Thiolated *Salmonella* antibody immobilization onto the gold surface of piezoelectric quartz crystal. *Biosens. Bioelectron.* 13, 1091–1097.



- Park, I.S., Kim, W.Y., Kim N., 2000. Operational characteristics of an antibody-immobilized QCM system detecting *Salmonella* spp. Biosens. Bioelectron. 15, 167–172.
- Pathirana, S.T., Barbaree, J., Chin, B.A., Hartell, M.G., Neely, W.C., Vodyanoy V., 2000. Rapid and sensitive biosensor for *Salmonella*. Biosens. Bioelectron. 15, 135–141.
- Peng, H., Shelef, L.A., 2001. Automated simultaneous detection of low levels of *Listeriae* and *Salmonellae* in foods. Int. J. Food Microbiol. 63, 225–233.
- Pereira De Jesus, D.P., Neves, C.A., do Lago, C.L., 2002. Determination of boron by using a quartz crystal resonator coated with *N*-methyl-D-glucamine-modified poly(epichlorohydrin). Anal. Chem. 74, 3274–3280.
- Petrenko, V.A. Personal communication. 22 Mar. 2004.
- Petrenko, V.A., Smith, G.P., 2000. Phages from landscape libraries as substitute antibodies. Protein Eng. 13, 589–592.
- Petrenko, V.A., Smith, G.P., Gong, X., Quinn, T., 1996. A library of organic landscapes on filamentous phage. Protein Eng. 9, 797–801.

Petrenko, V.A., Smith, G.P., Mazooji, M.M., Quinn, T., 2002. Alpha-helically constrained phage display library. *Protein Eng.* 15, 943–950.

Petrenko, V.A., Sorokulova, I.B., 2004. Detection of biological threats. A challenge for directed molecular evolution. *J. Microbiol. Methods* 58, 147–168.

Petrenko, V.A., Vodyanoy, V.J., 2003. Phage display for detection of biological threats. *J. Microbiol. Methods* 53, 253–62.

PM-740 series operation and service manual, 1996. Detailed operation. Maxtek, Inc., Sante Fe Springs, CA, pp. 1–73.

Poultry and eggs. Briefing room. 8 Nov. 2004. United States Department of Agriculture Economic Research Service. 7 Jan. 2005 <[www.ers.usda.gov/briefing/poultry](http://www.ers.usda.gov/briefing/poultry)>.

Poultry meat production, 2004. FAO animal production and health factfiles archive. Food and Agriculture Organization of the United Nations, Rome, Italy. 7 Jan. 2005 <[www.fao.org/ag/againfo/resources/en/factfile.html](http://www.fao.org/ag/againfo/resources/en/factfile.html)>.

Poultry per capita consumption, 2002. Food consumption (per capita) data system. 20 July 2004. United States Department of Agriculture Economic Research Service. 7 Jan. 2005 <[www.ers.usda.gov/data/foodconsumption/datasystem.asp](http://www.ers.usda.gov/data/foodconsumption/datasystem.asp)>.

Powell, H.A., Gooding, C.M., Garrett, S.D., Lund, B.M., McKee, R.A., 1994. Proteinase inhibition of the detection of *Listeria-monocytogenes* in milk using polymerase chain reaction. Lett. Appl. Microbiol. 18, 59–61.

Preliminary foodnet data on the incidence of infection with pathogens transmitted commonly through food – selected sites, United States, 2003. Morbidity and Mortality Weekly Reports. 30 Apr. 2004. Centers for Disease Control and Prevention, Atlanta, GA. 7 Jan. 2005 <[www.cdc.gov/mmwr/preview/mmwrhtml/mm5316a2.htm](http://www.cdc.gov/mmwr/preview/mmwrhtml/mm5316a2.htm)>.

Program summary, program rational. National Research Programs, Food Safety (Animal and Plant Products). 14 May 2001. United States Department of Agriculture, Agricultural Research Service. 9 Nov. 2003  
<[www.ars.usda.gov/research/programs/programs.htm?np\\_code=108&docid=837](http://www.ars.usda.gov/research/programs/programs.htm?np_code=108&docid=837)>.

Progress report on *Salmonella* testing of raw meat and poultry products 1998-2002. Food Safety and Inspection Service, United States Department of Agriculture. Washington, DC. 5 Jan. 2005 <[www.fsis.usda.gov/ophs/haccp/salm5year.htm](http://www.fsis.usda.gov/ophs/haccp/salm5year.htm)>.

Progress report to Secretary Tommy G. Thompson: Ensuring the safety and security of the nation's food supply. National Food Safety Programs. 23 Jul. 2003. U.S. Food and Drug Administration, Department of Health and Human Services, Center for Food Safety and Applied Nutrition. 9 Nov. 2003. <[www.cfsan.fda.gov/~dms/fssrep.html](http://www.cfsan.fda.gov/~dms/fssrep.html)>.

Prusak-Sochaczewski, E., Luong, J.H.T, 1990. Development of a piezoelectric immunosensor for the detection of *Salmonella typhimurium*. Enzyme Microb. Tech. 12, 173–177.

Pyun, J.C., Beutel, H., Meyer, J.U., Ruf, H.H., 1998. Development of a biosensor for *E. coli* based on a flexural plate wave (FPW) transducer. Biosens. Bioelectron. 13, 839–845.

Recall cases, 1999. Recall information center. United States Department of Agriculture, Food Safety and Inspection Service, Washington, DC. 8 Jan. 2005  
<[www.fsis.usda.gov/oa/recalls/recdb/rec1999.htm](http://www.fsis.usda.gov/oa/recalls/recdb/rec1999.htm)>

Romanov, V.I., Durand, D.B., Petrenko, V.A., 2001. Phage display selection of peptides that affect prostate carcinoma cells attachment and invasion. Prostate 47, 239–251.

Romanowska, E., Lugowski, C., Mulczyk, M., 1976. Lipopolysaccharide immunoadsorbents and their application to affinity chromatography of O-antibodies and specific phages. FEBS Lett. 66, 82–85.

RQCM Operation and Service Manual, 2003. Maxtek, Inc., Sante Fe Springs, CA, pp. 1–55.

*Salmonella* Immune Sera “SEIKEN” package insert, 1996. In-vitro diagnostic reagents ref. (62E), no. 1438. Denka-Seiken Co. Ltd., Tokyo, pp. 1–4.

Salmonellosis. Disease information. 27 Sep. 2004. Centers for Disease Control and Prevention, Atlanta, GA. 7 Jan. 2005

<[www.cdc.gov/ncidod/dbmd/diseaseinfo/salmonellosis\\_g.htm](http://www.cdc.gov/ncidod/dbmd/diseaseinfo/salmonellosis_g.htm)>.

Salyers, A.A., Whitt, D.D., 2002. Bacterial pathogenesis: a molecular approach. ASM Press, Washington, DC, pp. 383–386.

Samoylov, A.M., Samoylova, T.I., Hartell, M.G., Pathirana, S.T., Smith, B.F., Vodyanoy, V.J., 2002a. Recognition of cell-specific binding of phage display derived peptides using an acoustic wave sensor. *Biomol. Eng.* 18, 269–272.

Samoylov, A.M., Samoylova, T.I., Pathirana, S.T., Globa, L.P., Vodyanoy, V.J., 2002b. Peptide biosensor for recognition of cross-species cell surface markers. *J. Mol. Recognit.* 15, 197–203.

Samoylova, T.I., Petrenko, V.A., Morrison, N.E., Globa, L.P., Bekker, H.J., Cox, N.R., 2003. Phage probes for molecular profiling of malignant glioma cells. *Mol. Cancer Pharm.* 2, 1–9.

Samuel, G., Reeves, P., 2003. Biosynthesis of O-antigens: genes and pathways involved in nucleotide sugar precursor synthesis and O-antigen assembly. *Carbohydr. Res.* 338, 2503–2519.

Sams, A.R., 2000a. First processing: slaughter through chilling. Poultry-borne pathogens: plant considerations. In: Sams, A.R. (Ed.), Poultry Meat Processing. CRC Press, Boca Raton, FL, pp. 22–23, 142.

Sams, A.R., 2000b. Preslaughter factors affecting poultry meat quality. In: Sams, A.R. (Ed.), Poultry Meat Processing. CRC Press, Boca Raton, FL, pp. 7–14.

Sanath Kumar, H., Sunil, R., Venugopal, M.N., Karunasagar, I., Karunasagar, I., 2003. Detection of *Salmonella* spp. in tropical seafood by polymerase chain reaction. Int. J. Food Microbiol. 88, 91–95.

Santos, A.F., 1994. Development of a piezoelectric biosensor for the determination of toxic amines in seafood. Ph.D. Dissertation, University of Rhode Island, RI.

Sauerbrey, G.Z.Z., 1959. Use of quartz vibrator for weighing thin films on a microbalance. Z. Phys. 155, 206–212.

Schumann, M.S., Schneid, T.D., Schumann, B.R., Fagel, M.J., 1997. Food Safety Law. John Wiley and Sons Ltd, New York, pp. 140–141.

Schuster, C.S., Khan, S., 1994. The bacterial flagellar motor. Annu. Rev. Biophys. Biomol. Struct. 23, 509–539.

Seo, K.H., Brackett, R.E., Hartman, N.F., Campbell, D.P., 1999. Development of a rapid response biosensor for detection of *Salmonella typhimurium*. J. Food Protect. 62, 431–437.

Shah, J., Wilkins, E., 2003. Electrochemical biosensors for detection of biological warfare agents. Electroanal. 15, 157–167.

Shons, A., Dorman, F., Najarian, J., 1972. An immunospecific microbalance. J. Biomed. Mater. Res. 6, 565–570.

Si, S., Li, X., Fung, Y., Zhu, D., 2001. Rapid detection of *Salmonella enteritidis* by piezoelectric immunosensor. Microchem. J. 68, 21–27.

Si, S., Ren, F., Cheng, W., Yao, S., 1997. Preparation of a piezoelectric immunosensor for the detection of *Salmonella paratyphi* A by immobilization of antibodies on electropolymerized films. Fresen. J. Anal. Chem. 357, 1101–1105.

Silverside, D., Jones, M., 1992. Small-scale poultry processing. FAO animal production and health paper 98. Food and Agriculture Organization of the United Nations, Rome, Italy. 7 Jan. 2005 <[www.fao.org/docrep/003/t0561e/t0561e00.htm](http://www.fao.org/docrep/003/t0561e/t0561e00.htm)>.

Skládal, P., 2003. Piezoelectric quartz crystal sensors applied for bioanalytical assays and

characterization of affinity interactions. J. Braz. Chem Soc. 14, 491–502.

Smith, G.P. Biotinylation of a receptor for use in affinity selection and binding assays.

1992. Phage-display vectors and libraries based on filamentous phage strain fd-tet. U.

Missouri. 13 Jan. 2005 <[www.biosci.missouri.edu:16080/smithgp/phagedisplaywebsite/phagedisplaywebsiteindex.html](http://www.biosci.missouri.edu:16080/smithgp/phagedisplaywebsite/phagedisplaywebsiteindex.html)>.

Smith, G.P., Petrenko, V.A., 1997. Phage display. Chem. Rev. 97, 391–410.

Smith, G.P., Petrenko, V.A., Matthews, L.J., 1998. Cross-linked filamentous phage as an affinity matrix. J. Immunol. Methods 215, 151–161.

Smith, G.P., Scott, J.K., 1993. Libraries of peptides and proteins displayed on filamentous phage. Methods Enzymol. 217, 228–257.

Sobel, J., Khan, A.S., Swerdlow, D.L., 2002. Threat of a biological terrorist attack on the US food supply: the CDC perspective. Lancet 359, 874–880.

Sofos, J.N., 1994. Microbial growth and its control in meat, poultry and fish. In: Pearson, A.M., Dutson, T.R. (Eds.), Advances in Meat Research, Quality Attributes and Their Measurement in Meat, Poultry and Fish Products. Blackie Academic & Professional, London, pp. 359–364.



Sorial, J., Lec, R., 2004. A piezoelectric interfacial phenomena biosensor. MS Thesis, Drexel University, PA <[dspace.library.drexel.edu/handle/1860/82](http://dspace.library.drexel.edu/handle/1860/82)>.

Sorokulova, I.B., Olsen, E.V., Chen, I., Fiebor, B., Barbaree, J.M., Vodyanoy, V.J., Chin, B.A., Petrenko, V.A., 2005. Landscape phage probes for *Salmonella typhimurium*. J. Microbiol. Methods. In Press.

Spake, A., 2001. Food fright. Terrorism spotlights the risks in the food supply. US News World Rep. 131, 48–50.

Stadler, H., Mondon, M., Ziegler, C., 2003. Protein adsorption on surfaces: dynamic contact angle (DCA) and quartz-crystal microbalance (QCM) measurements. Anal. Bioanal. Chem. 375, 53–61.

Starodub, N.F., Arenkov, P.Y., Starodub, A.N., Berezin, V.A., 1994. Immunosensors based on fiber optics and enhanced chemiluminescence: construction and biomedical application for determination of different antigens. Proc. SPIE Int. Soc. Opt. Eng. 2085, 44–52.

Storri, S., Santoni, T., Minunni, M., Mascini, M., 1998. Surface modifications for the development of piezoimmunosensors. Biosens. Bioelectron. 13, 347–357.

Strongin, R.J., 2002. How vulnerable is the nation's food supply? Linking food safety

and food security. NHPF Issue Brief 773, 1–22.

Su, X., Low, S., Kwang, J., Chew, V.H.T., Li, S.Y., 2001. Piezoelectric quartz crystal based veterinary diagnosis for *Salmonella enteritidis* infection in chicken and egg. Sensor. Actuat. B–Chem 75, 29–35.

Su, X.L., Li, Y.B., 2004. A self-assembled monolayer-based piezoelectric immunosensor for rapid detection of *Escherichia coli* O157:H7. Biosens. Bioelectron. 19, 563–574.

Summary of Notifiable Diseases – United States, 2002. Morbidity and Mortality Weekly Reports. 30 Apr. 2004. Centers for Disease Control and Prevention, Atlanta, GA. 7 Jan. 2005 <[www.cdc.gov/mmwr/preview/mmwrhtml/mm5153a1.html](http://www.cdc.gov/mmwr/preview/mmwrhtml/mm5153a1.html)>.

Sun, W., Brovko, L., Griffiths, M., 2001. Use of bioluminescent *Salmonella* for assessing the efficiency of constructed phage-based biosorbent. J. Ind. Microbiol. Biotechnol. 25, 273–275.

Sykora, J.C., 2003. Monolayers of biomolecules for recognition and transduction in biosensors. Ph.D. Dissertation, Auburn University, AL.

Tamblyn, K.C., Conner, D.E., Bilgili, S.F., 1997. Utilization of the skin attachment model to determine the antibacterial efficacy of potential carcass treatment. Poultry Sci. 76, 1318–1323.

Tapchaisri, P., Wangroongsarb, P., Panbangred, W., Kalambaheti, T., Chongsa-nguan, M., Srimanote, P., Kurazono, H., Hayashi, H., Chaicumpa, W., 1999. Detection of *Salmonella* contamination in food samples by dot-ELISA, DNA amplification and bacterial culture. Asian Pac. J. Allergy Immunol. 17, 41–51.

Tauxe, R.V., 1992. Gastroenteritis: infective and toxic. In: Berkow, R., Fletcher, A.J., (Eds.), The Merck manual of diagnosis and therapy. Merck Research Laboratories, Rahway, New Jersey, pp. 812–821.

Terrorist threats to foods – guidance for establishing and strengthening prevention and response systems, 2002. World Health Organization Food Safety. WHO, Geneva, Switzerland. 5 Jan. 2005  
<[www.who.int/foodsafety/publications/general/en/terrorists.pdf](http://www.who.int/foodsafety/publications/general/en/terrorists.pdf)>.

Testing for rapid detection of adulteration of food, 2003. National Food Safety Programs. U.S. Food and Drug Administration, Department of Health and Human Services, Center for Food Safety and Applied Nutrition. 9 Nov. 2003  
<[www.fda.gov/oc/bioterrorism/report\\_congress.html](http://www.fda.gov/oc/bioterrorism/report_congress.html)>.

Theis, M., 2002. Food and safety. Bioterrorism and our food supply. Health Care Food Nutr. Focus 19, 5–8.

Thompson, M., Arthur, C.L, Dhaliwal, G.K., 1986. Liquid-phase piezoelectric and acoustic transmission studies of interfacial immunochemistry. *Anal. Chem.* 58, 1206–1209.

Threlfall, E.J., 2000. Epidemic *Salmonella typhimurium* DT 104 – a truly international multiresistant clone. *J. Antimicrob. Chemother.* 46, 7–10.

Torok, T.J., Tauxe, R.V, Wise, R.P., Livengood, J.R., Sokolow, R., Mauvais, S., Birkness, K.A., Skeels, M.R., Horan, J.M., Foster, L.R., 1997. A large community outbreak of salmonellosis caused by intentional contamination of restaurant salad bars. *JAMA* 5, 389–395.

Tseng, S.Y., Macool, D., Elliott, V., Tice, G., Jackson, R., Barbour, M., Amorese, D., 1997. An homogeneous fluorescence polymerase chain reaction assay to identify *Salmonella*. *Anal. Biochem.* 245, 207–212.

USA Scientific technical service. Personal communication. 12 March 2004.

Uttenthaler, E., Schräml, M., Mandel, J., Drost, S., 2001. Ultrasensitive quartz crystal microbalance sensors for detection of M13-phages in liquids. *Biosens. Bioelectron.* 16, 735–743.

Vaughan, R.D., Carter, R.M., O'Sullivan, C.K., Guilbault, G.G., 2003. A quartz crystal microbalance (QCM) sensor for the detection of *Bacillus cereus*. Anal. Lett. 36, 731–747.

Vig, J.R., Ballato, A., 1998. Comments about the effects of nonuniform mass loading on a quartz crystal microbalance. IEEE Trans. Ultrason. Ferroelect. Freq. Contr. 45, 1123–1124.

Vodyanoy, V.J. Written communication. 25 Jan. 2005.

Vodyanoy, V.J., Neely, W.C., Chin, B.A., Barbaree, J.M. Detection of food-borne *Salmonella* contamination by polyclonal antibody assays. Patent-pending. 2000.

Vodyanoy, V., Pathirana, S., Neely, W.C., 1994. Stearic acid assisted complexation of  $K^+$  by valinomycin in monolayers. Langmuir 10, 1354–1357.

Wainwright, M., Lederberg, J., 1992. History of Microbiology. In: Lederberg, J. (Ed.), Encyclopedia of microbiology. Academic Press Inc., New York.

Weintraub, A., 2003. Immunology of bacterial polysaccharide antigens. Carbohydr Res. 338, 2539–2547.

- Welsch, W., Klein, C., vonSchickfus, M., Hunklinger, S., 1996. Development of a surface acoustic wave immunosensor. *Anal. Chem.* 68, 2000–2004.
- Wong, Y. Y., Ng, S.P., Ng, M.H., Si, S.H., Yao, S.Z., Fung, Y.S., 2002. Immunosensor for the differentiation and detection of *Salmonella* species based on a quartz crystal microbalance. *Biosens. Bioelectron.* 17, 676–684.
- Yang, Z.P, Li, Y.B., Slavik, M., 1998. Use of antimicrobial spray applied with an inside-outside birdwasher to reduce bacterial contamination on prechilled chicken carcasses. *J. Food. Protect.* 61, 829–832.
- Ye, J.M., Letcher, S.V., Rand, A.G., 1997. Piezoelectric biosensor for detection of *Salmonella typhimurium*. *J. Food Sci.* 62, 1067–1071, 1086.
- Yilma, S. Personal communication. Jan 2004.
- Yu, H., Bruno, J.G., 1996. Immunomagnetic-electrochemiluminescent detection of *Escherichia coli* O157 and *Salmonella typhimurium* in foods and environmental water samples. *Appl. Environ. Microbiol.* 62, 587–592.
- Yu, J., Smith, G.P., 1996. Affinity maturation of phage-displayed peptide ligands. *Methods Enzymol.* 267, 3–27.

Zhou, C., Pivarnik, P., Rand, A.G., Letcher, S.V., 1998. Acoustic standing-wave enhancement of a fiber-optic *Salmonella* biosensor. Biosens. Bioelectron. 13, 495–500.

Zhou, S., Datta, A.R., Ayers, S., Friedman, S., Walker, R.D., White, D.G., 2003. Antimicrobial-resistant *Salmonella* serovars isolated from imported foods. Int. J. Food Microbiol. 84, 87–92.